UNIVERSITY OF SOUTHAMPTON

Faculty of Engineering and Physical Sciences
School of Engineering

Design optimisation of mooring systems with load reduction devices for floating offshore wind

by

Oscar Festa

MEng

ORCiD: 0009-0003-8927-455X

A thesis for the degree of
Doctor of Philosophy

February 2025

University of Southampton

Abstract

Faculty of Engineering and Physical Sciences
School of Engineering

Doctor of Philosophy

Design optimisation of mooring systems with load reduction devices for floating offshore wind

by Oscar Festa

Floating offshore wind (FOW) has introduced new technical challenges to mooring system design including shallow waters and extreme wind loading relative to oil & gas installations, which contribute to high mooring stiffness and require expensive mooring and anchoring systems. Non-linear extensible mooring components known as load reduction devices (LRDs) enable significant cost reduction for FOW moorings, which introduce new design variables including a range of non-linear stiffness curves that must be optimised for each project. Current modelling and design methods are not adapted to rapidly screen these design variables, making it difficult for developers to understand the benefits of LRDs, leading to over-conservative design choices and reluctance to adopt innovative designs. For FOW, the financial risk associated with selecting an over-conservative design is higher than in hydrocarbon projects, as tens or hundreds of structures need to be moored for a single project. This thesis proposes a design optimisation framework for FOW mooring systems with LRDs, which can be applied to any project-specific location parameters, constraints and objectives. This was achieved by analytical modelling, numerical finite element modelling, surrogate modelling with neural networks, and optimisation using genetic algorithms. The output framework includes: 1) the development of a novel analytical model for catenary moorings with LRDs; 2) a parametric study of LRD design variables using dynamic analysis software; 3) the development of an optimisation methodology. The framework is applied to the design of taut moorings with 3-phase stiffness LRDs, and demonstrates reductions in peak loads by 58 %, fatigue damage by 74 %, nacelle accelerations by 59 % and seabed footprint by 78 % compared to traditional mooring designs. The analytical and optimisation models have been converted into free-to-use web applications, providing an efficient means for mooring designers to consider the benefits of innovative mooring systems.

Contents

List of Figures

List of Tables

Declaration of Authorship

I declare that this thesis and the work presented in it is my own and has been generated by me as the result of my own original research.

I confirm that:

1. This work was done wholly or mainly while in candidature for a research degree at this University;
2. Where any part of this thesis has previously been submitted for a degree or any other qualification at this University or any other institution, this has been clearly stated;
3. Where I have consulted the published work of others, this is always clearly attributed;
4. Where I have quoted from the work of others, the source is always given. With the exception of such quotations, this thesis is entirely my own work;
5. I have acknowledged all main sources of help;
6. Where the thesis is based on work done by myself jointly with others, I have made clear exactly what was done by others and what I have contributed myself;
7. Parts of this work have been published as: Festa, Oscar, Gourvenec, Susan and Sobey, Adam (2024) Comparative analysis of load reduction device stiffness curves for floating offshore wind moorings. Ocean Engineering, 250, Mar 2024. (DOI:10.1016/j.oceaneng.2024.117266), Festa, Oscar, Gourvenec, Susan and Sobey, Adam (2023) Analytical model of non-linear load reduction devices for catenary moorings. In Proceedings of the ASME 2023 42nd International Conference on Ocean, Offshore and Arctic Engineering (OMAE 23), (DOI:10.1115/omae2023-100845), Festa, Oscar, Gourvenec, Susan and Sobey, Adam (2024) A flexible neural network-based surrogate model for optimisation of floating wind moorings. Ocean Engineering. (under review)

Signed:..... Date:.....

Acknowledgements

First and foremost, I would like to express my deepest gratitude to my supervisor, Prof. Susan Gourvenec. Her technical insights were instrumental in completing this project, and her infectious enthusiasm and passion for engineering made the journey truly enjoyable. With her emotional support, guidance and good humour, she went above and beyond the duty of care that makes for exceptional PhD supervision.

I would like to thank all others with technical involvement in the project, including my co-supervisors, Dr. Jared Charles and Prof. Adam Sobey, and my industry connections Aengus Connolly, Danny Golden, Paul McEvoy and Hossam Ragheb for their invaluable insights and expertise.

I am also sincerely grateful to the Royal Academy of Engineering for their funding, which made this research possible.

Lastly, a heartfelt thank you to my family and friends for their support throughout these four years. I am particularly grateful to my research group friends, who made B178 such a great place to work, and to my housemates Elliot and Lydia for making Portswood feel like home. A special thanks also goes to my parents and grandparents for feeding and housing me during my rent-avoiding writing-up phase.

Chapter 1

Introduction

1.1 Background on floating offshore wind (FOW)

To reach net zero by 2050, the world may need up to 200,000 offshore wind turbines [1] [2]. Up to 80% of worldwide offshore wind resources are located in water depths greater than 50 m [3] where traditional fixed architectures such as monopiles or jackets become more technically challenging. In these deeper waters, offshore wind turbines must be deployed on floating platforms, which are connected to the seabed via mooring lines and anchors (Figure 1.1). These mooring systems are key to station-keeping of the floating structure, i.e. minimising the floating structure's offset from its designated location.

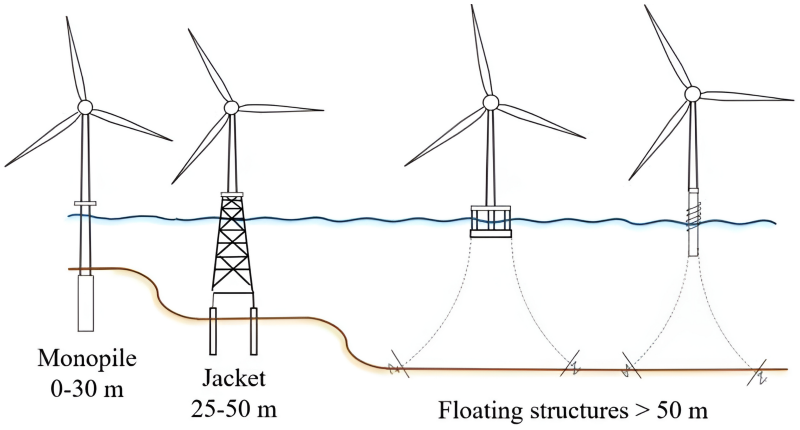

FIGURE 1.1: Fixed and floating offshore wind concepts.

Mooring systems have long been essential for the station-keeping of floating offshore structures, particularly within the offshore oil and gas (O&G) industry. In this sector, a single floating structure – requiring just one mooring system – can generate high energy yield, returning over 5 billion USD in a year [4]. Consequently, mooring systems for O&G have not posed a significant economic challenge, and have typically prioritised redundancy and proven technology above cost efficiency and innovation. In contrast, FOW will require hundreds of structures to be

moored to the seabed for the same energy yield as an O&G platform, and current mooring systems are not fit for this significant scale-up [5]. Innovation in mooring design is critical for improving cost-efficiency and enabling FOW to reach commercial viability. To achieve this, mooring systems must focus on overcoming a series of technical challenges and addressing design considerations unique to FOW.

1.2 Mooring design considerations for FOW

Current FOW mooring systems are derived from established practice for floating O&G moorings [6], as the basis of their design is similar: to ensure sufficient reliability and platform offsets below a specified threshold. However, FOW mooring design requirements have key technical differences:

1. FOW targets shallower water depths: 60 - 300 m, compared to often 300 m + for O&G. This results in stiffer mooring systems than deep waters for the same mooring configuration [7], i.e. a bigger increase in restoring force on the platform for a given offset from its reference position.
2. FOW structures are subjected to a unique set of loads, in particular high wind-induced horizontal loading, which increases mean platform offsets and further stiffens the mooring system response [8].
3. Platform offset thresholds are usually more lenient for FOW, and consequence of exceedance is lower [6]. Thus, stiff mooring systems which are highly resistant to platform motion are suitable for O&G, but can be over-conservative for FOW projects.

Points 1. and 2. combine to increase the stiffness of mooring systems, resulting in extreme loads on mooring lines and anchors [9]. Resisting these loads then requires large diameter lines and anchors: typical chain diameters currently considered for FOW mooring lines are up to triple those used in O&G, leading to nine times the mass per unit length (just under a ton per link of chain); similarly, drag anchors designs for FOW typically weigh 30 - 40 tons, compared to 10 - 12 tons for O&G [10]. These components are currently too expensive and carbon-intensive to manufacture, transport, and install at the scale required for FOW.

Crucially, point 3. suggests a route to reducing loads on FOW moorings, by reducing over-conservatism, and adjusting mooring system stiffness to mitigate the impact of environmental loads [9]. This means allowing as much compliance, i.e. extensibility, in the mooring as is permitted by platform motion constraints. The compliance is then available to reduce the impact of extreme waves, which can lower the dynamic tension in the mooring lines and anchors, leading to reduced material requirements. This can enable significant reductions in capital expenditure of a FOW project, whilst also reducing the carbon footprint, seabed disruption, and pressure on supply chains [11].

1.3 Challenges and advancements in compliant mooring design

Designing a mooring with optimal compliance is not always feasible if limited to traditional mooring systems. The stiffness of traditional mooring systems typically increases with the breaking strength of its chain or rope components, which can make it difficult to achieve sufficient compliance as it is not an independent variable. For instance, in rough and/or shallow water sites, a sufficiently strong mooring is often too stiff [7].

The recent development of load reduction devices (LRDs, see figure 1.2), which are in-line extensible components fitted in mooring lines, addresses this challenge by providing bespoke compliance to mooring systems. Typically located towards the upper extremity of the mooring line (the fairlead), LRDs can provide significant extension under tension (5 - 15 m), which does not compromise their breaking strength [12] [13]. LRDs have highly customisable non-linear stiffness curves, which can be tuned by varying the physical parameters of the device.

FIGURE 1.2: Load reduction device designed by TFI, formed of a compressive elastomeric spring, with a typical unstretched length of 7.5 m [12].

LRDs provide an additional source of compliance to mooring systems, but in doing so, extend the design space, as multiple LRD design variables (maximum extension, stiffness at design load) need to be considered alongside traditional mooring system variables (depth, line diameter, pretension etc.).

1.4 Design optimisation for FOW mooring systems

Current analysis methods for assessing the suitability of a mooring design require considerable computational resources and time to capture a large number of environmental load cases, typically achieved through dynamic finite-element (FE) or lumped-mass (LM) analyses [14]. These computational approaches are not well-suited for finding an optimal design at concept level, especially when considering a large design space. This results in engineers either: a) not performing optimisation, and settling for the first 'acceptable' design; or b) considering fewer design variables, i.e. restricting their design space. Both lead to convergence on a final solution which is sub-optimal.

Recent studies have addressed this challenge by employing surrogate models, which are mathematical models (e.g, artificial neural networks) that can accurately capture the input-output relationship of more complex physics-based models (in this case, dynamic FE or

LM models) in a fraction of the time [15] (e.g., [16], [17]). Once trained, these surrogate models are able to efficiently explore large and complex design spaces with multiple objectives (typically with the aid of search algorithms such as Genetic Algorithms), to find optimal mooring design solutions. However, these surrogate models are typically built for project-specific locations, constraints, and objectives, thus requiring re-training from project to project. This limits their applicability to concept design, where project-specific parameters may not yet be fixed.

1.5 Research aim & objectives

Existing methods make it difficult for FOW mooring designers to easily identify the benefits of using LRDs to optimise mooring system compliance at concept design level. This leads to detailed design being undertaken on base mooring configurations which may be sub-optimal, whilst more cost-effective areas of the design space remain unexplored. The overall aim of this PhD research is to develop a concept design optimisation framework for FOW mooring systems with LRDs, which can be applied to any project-specific location parameters, constraints and objectives. This will enable designers to rapidly screen mooring designs, and asess the benefits of optimised mooring systems using LRDs.

This aim will be achieved through the three objectives, O1-3. The output of objectives O1 and O2 inform the work undertaken in objectives O2 and O3 respectively, as depicted in Figure 1.3. As part of the PhD research, the outcomes of objectives O1 and O3 have also been converted into free-to-use web-based applications. The objectives are defined as follows :

- *O1*: Development of a quasi-static analytical model for initial sizing of mooring systems including non-linear load reduction devices.
- *O2*: Comparison of mooring configurations and non-linear LRD stiffness curves using commercial dynamic analysis software.
- *O3*: Development of a neural network surrogate model, based on dynamic analyses, for holistic optimisation of FOW mooring systems with LRDs according to project-specific platform motion constraints, loads, and water-depths.

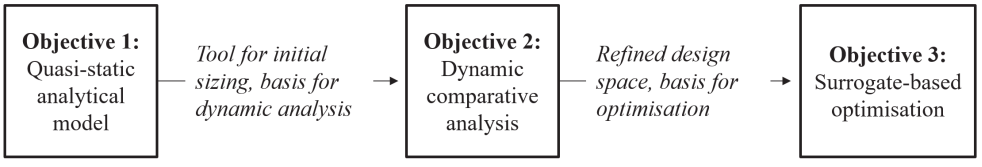

FIGURE 1.3: Flowchart of PhD research objectives. Outcomes of each objective (italics) are used to inform following objectives.

1.6 Novelty of PhD research

The novelty of this PhD research lies both in its technical findings, which involve modelling and analysis of FOW moorings with load reduction devices, and in the introduction of a novel machine-learning-based methodology for designing these mooring systems:

- *Technical novelty*: Although there are numerous derivations of analytical models for traditional mooring systems in the public domain, these have not yet been extended to accommodate the recent development of non-linear load reduction devices. This is addressed in objective O1, with the development of an analytical model which interfaces existing mooring equations with novel equations for non-linear load reduction devices. Moreover, no existing research proposes a comparison of load reduction device performance for FOW moorings, across a comprehensive set of environmental parameters and mooring configurations. This is addressed in objective O2, using traditional design and analysis techniques, as a basis for optimisation and innovation of the methodology.
- *Methodological novelty*: Traditional mooring design approaches involve running iterative simulations with varying mooring design input parameters until output parameters such as platform motions and mooring line tension meet the design requirements. The novelty of the methodology presented in this research resides in the reversal of this traditional design approach, with the development of an automated machine learning-based concept design approach (objective O3) which can take mooring requirements as an input and provide the optimal mooring design 'input' parameters as an output. This methodology is generaliseable for any pre-defined station-keeping requirements and project-specific variables such as water depth and environmental loads.

The of noverlty innto the novel framework is shown in figure Figure 1.4

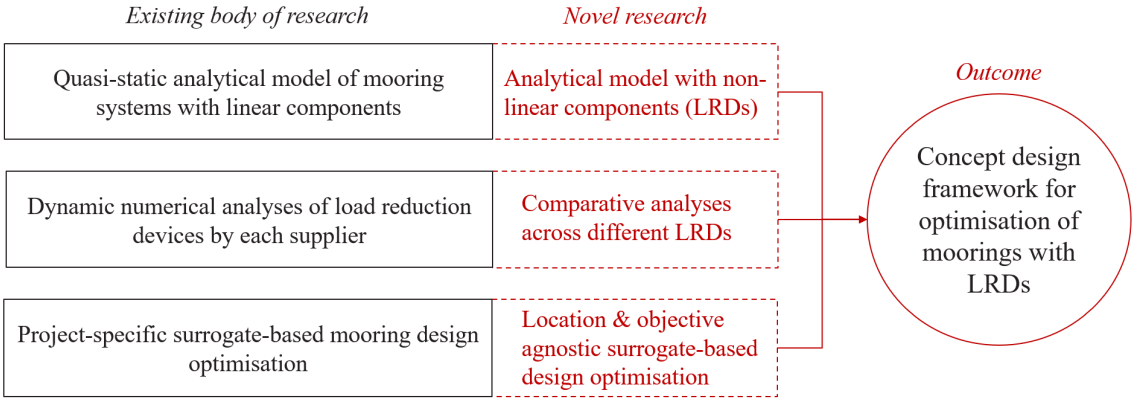

FIGURE 1.4: Visual summary of novelty with respect to existing bodies of research. Novel research in objectives O1, O2, and O3 combine to create the full concept design framework for optimisation of moorings with LRDs.

1.7 Outline of the thesis

The main body of this thesis comprises four chapters. The first chapter presents a literature review, which provides a technical background and critical analysis of existing research, for each of the four technical topics introduced in this chapter (sections 1.1, 1.2, 1.3 and 1.4). The following three chapters of the thesis, 4, 5 and 6, contain the main body of research, and address the three objectives O1, O2 and O3 outlined in section 1.6 respectively.

Chapter 4 presents an analytical model which enables initial sizing of LRDs, and analysis of the quasi-static stiffness of the resulting mooring system. This is the typical starting point for mooring design, which must be followed by dynamic analyses to provide insight on dynamic tensions. The following chapter, Chapter 5 addresses this, by providing a comparative analysis of the effect of LRDs on dynamically-induced mooring line tensions and platform motions, for various mooring arrangements. This comparative analysis enables refinement of the design space, and is used as a basis for the holistic optimisation performed in Chapter 6.

1.8 List of publications

Five conference papers and two journal papers, associated with the research presented in this thesis, are published or in review:

Journal papers:

- Festa, Oscar, Gourvenec, Susan and Sobey, Adam (2024) Comparative analysis of load reduction device stiffness curves for floating offshore wind moorings. Ocean Engineering, 250, Mar 2024. (doi:10.1016/j.oceaneng.2024.117266) (see section A.1 of appendix)
- Festa, Oscar, Gourvenec, Susan and Sobey, Adam (2024) A flexible neural network-based surrogate model for optimisation of floating wind moorings. Ocean Engineering. (under review)

Conference papers:

- Festa, Oscar, Gourvenec, Susan and Sobey, Adam (2023) Analytical model of non-linear load reduction devices for catenary moorings. In Proceedings of the ASME 2023 42nd International Conference on Ocean, Offshore and Arctic Engineering (OMAE 23). (doi:10.1115/omae2023-100845) (see section A.2 of appendix)
- Festa, Oscar, Gourvenec, Susan and Sobey, Adam (2022) Proxy model for the design of extensible floating offshore wind turbine mooring systems. In Proc. 32nd International Symposium on Ocean and Polar Engineering (ISOPE), June 5 – 10 (virtual). (doi:10.6863/ISOPE-I-22-030) (see section A.3 of appendix)

- Kwa, Katherine, Festa, Oscar, White, Dave, Sobey, Adam and Gourvenec, Susan (2023) Design benefits for plate anchors for floating offshore wind through coupling floater, mooring and geotechnical responses. 9th International SUT OSIG Conference "Innovative Geotechnologies for Energy Transition", Imperial College, London, United Kingdom. 12 - 14 Sep 2023. (doi:10.3723/xtom8787) (see section A.4 of appendix)
- Kwa, Katherine, White, Dave, Festa, Oscar and Gourvenec, Susan (2023) Dynamic seabed-anchor capacity enhancements for taut-moored floating offshore wind. In Symposium on Energy Geotechnics 2023. TU Delft OPEN Textbooks. (doi:10.59490/seg.2023.619). (see section A.5 of appendix)
- Kwa, Katherine, Festa, Oscar, White, Dave, Sobey, Adam and Gourvenec, Susan (2023) Integrated numerical modelling of soil-anchor-mooring line-floater response for floating offshore wind. Zdravkovic, Lidija, Kontoe, Stavroula, Tsiampousi, Katerina and Taborda, David (eds.) In Proceedings 10th NUMGE : 10th European Conference on Numerical Methods in Geotechnical Engineering. (doi:10.53243/NUMGE2023-129). (see section A.6 of appendix)

Chapter 2

Literature Review

2.1 Background on FOW

2.1.1 Introduction to FOW substructures

FOW turbines are reliant on a substructure to maintain station-keeping and stability in the offshore environment. FOW substructures can be divided into three systems [8]:

- Floating platform: maintains buoyancy and supports the turbine structure
- Mooring line: provides restoring force to the floating platform to keep it in place
- Anchor: fixes the mooring line to the seabed

Currently, there are over 80 different structural FOW concepts in various stages of development [18], which can be classified according to the platform, mooring, and anchoring concepts they employ. An overview of the aforementioned systems and their variations in the context of floating wind energy is given in sections 2.1.2 and 2.1.3. Section 2.1.4 offers a summary of completed and ongoing FOW projects in industry and the specific platform, mooring and anchoring configurations they employ.

2.1.2 Floating platform concepts for FOW

In contrast to fixed concrete or steel substructures which rely on their mass (self-weight) and resistance of the seabed to provide stability to the turbine, floating platforms rely on buoyancy, ballasting, and moorings for station-keeping and stability [8]. The substructure of a FOW turbine must be designed to withstand a range of operational and environmental loads: weight of the wind turbine structure, moments from the wind thrust on the rotor, dynamic wave loads, and tidal and current loads.

Of these loads, the overturning moment due to the wind on the rotor can be considered as the primary concern when designing the basic platform structure. The platform typically fits one of the basic concepts shown in Figure 2.1, which are distinguished by their different approaches to countering this moment [8]:

- Spar-buoy, i.e. ballast-stabilised: The platform is formed of a slender steel cylinder filled with ballast to maintain the centre of gravity below the centre of buoyancy, thus stabilising the structure in an upright position.
- Semi-submersible, i.e. buoyancy-stabilised: the platform is a large surface platform, typically constructed of three interconnected columns. The distributed buoyancy stabilises the platform, by providing a restoring force similar to that of the righting arm of a catamaran.
- Tension-leg, i.e. mooring-stabilised: a compact platform is entirely submerged, and tension-moored to the seabed using vertical taut mooring lines which provide the required stability.

Although many other platform concepts exist, they typically employ a combination of the three main approaches listed above. The barge type can be considered to behave similarly to a semi-submersible in that it uses distributed buoyancy to maintain stability, but is often mentioned as a distinct concept due to its wider water plane and shallower draft.

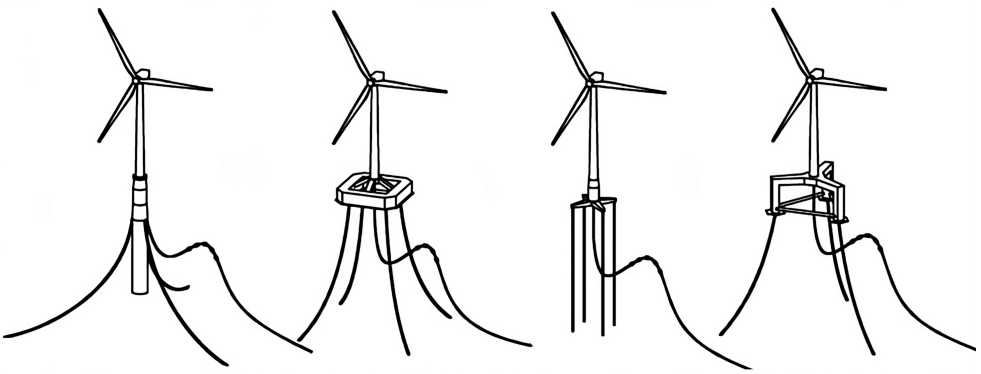

FIGURE 2.1: Basic concepts of FOW platforms [19]: (a) spar-buoy, (b) barge, (c) tension-leg, (d) semi-submersible

The various platform concepts have their own design, manufacturing and installation characteristics, and also respond differently to environmental laoding. Table 2.1 lists the main advantages and disadvantages of each design [9].

2.1.3 Mooring and anchoring

The principal objective of a mooring and anchoring system is to provide a connection to the seabed which ensures the platform stays within a set distance, i.e. offset, from its designated

TABLE 2.1: Advantages and disadvantages of main platform concepts [9]

Platform type	Semi-submersible	Spar-buoy	TLP
Advantages	Simple installation and maintenance Can be easily towed and disconnected Suitable for a range of water depths Versatile to different anchors	Good stability, adjustable with fluid ballast Small water plane surface reduces wave loads Simple to design and manufacture Versatile to different anchors	Highly stable in heave motion Minimal pitch during operation Compact structure Small seabed footprint
Disadvantages	Large surface and ballast increase motions Complex structure	Draft makes it unsuitable for shallow waters Offshore assembly requires a crane vessel	Cannot be easily disconnected Tether failure causes loss of stability Requires driven piles or suction caissons

position [9]. A wide range of mooring configurations exist, which are all typically derived from three fundamental concepts (see Figure 2.2):

- Catenary moorings: Typically characterized by significant amounts of chain on the seabed. The mooring lines then adopt a catenary curve between the platform and the seabed. The point of contact between the chain and seabed is well in advance of the anchor, thus subjecting the anchor to predominantly horizontal forces. Due to their reliability and simplicity (basic materials, straightforward installation) [8], catenary moorings are the most commonly used configuration for oil & gas applications in intermediate water depths (100 - 500m) [9], and by extension, have become the most common for FOW [20].
- Taut moorings: Fully suspended mooring lines under tension, which arrive at the seabed at an angle θ of typically 15-45 $^\circ$. The anchor is thus subjected to both horizontal and vertical forces. Taut lines typically employ synthetic rope which reduces their overall weight, thus making the configuration more suitable for deeper waters where the weight of a catenary configuration would be impractical.
- Vertical moorings: Taut steel lines which apply tension to the platform, specifically for the use of TLPs. The lines travel vertically down from the platform to the seabed, thus reducing the seabed footprint and subjecting the anchors to predominantly vertical forces.

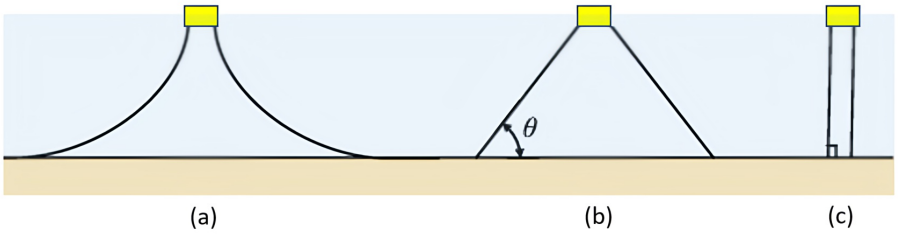

FIGURE 2.2: Three fundamental mooring configurations: (a) catenary, (b) taut and (c) vertical. [21]

The ratio of vertical to horizontal forces exerted on the anchor, along with the soil conditions, determines the most suitable anchor type. The most common types of anchors employed in the offshore industry can be divided into the following 5 categories (shown in Figure 2.3), based on their installation method [21]:

- Drag-embedded: can be either fixed fluke anchors (fluke is rigidly connected to shank) or plate anchors (the fluke/plate is held by wires, allowing the anchor to be rotated once embedded).
- Driven: hollow steel pipes (piles) that are driven and sometimes grouted into the seabed.
- Suction-installed: suction caisson anchors are large open-bottom cylinders with a valve in the sealed top cap. The self-weight of the anchor allows it to initially penetrate into the seabed. Full penetration is then achieved by pumping water out via the top cap valve.
- Dynamically penetrated: involves releasing a rocket-shaped anchor that freefalls through the water column under self weight to penetrate the seabed.
- Hybrid: some concepts have been more recently developed to get the best out of a combination of designs. For instance, the suction embedded plate anchor (SEPLA) combines a suction caisson with a plate in its lower end, where the caisson is retrieved after installation of the plate.

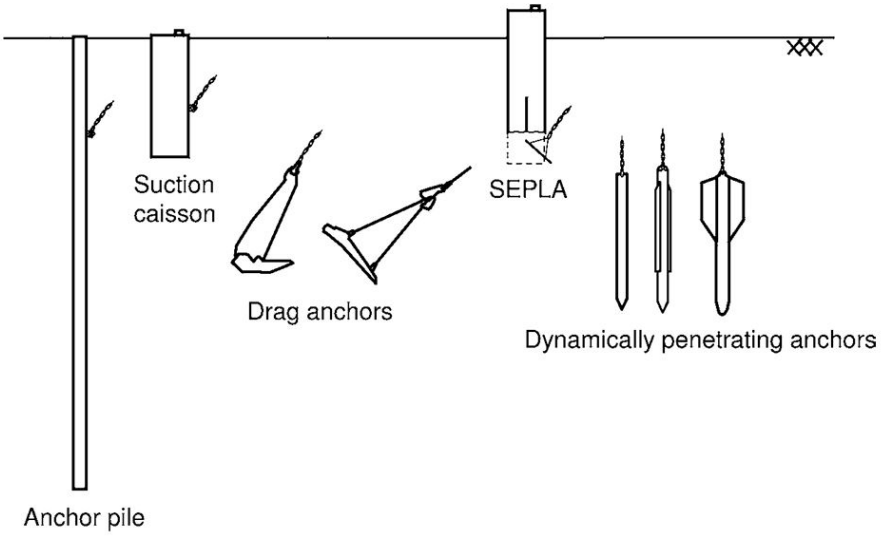

FIGURE 2.3: Types of embedded anchors
[21]

Catenary mooring configurations tend to employ traditional fixed fluke anchors as they are designed to resist horizontal loads. Taut moorings predominantly use deep pile anchors and suction caissons [22] to resist both vertical and horizontal loads. TLPs typically employ piles which provide sufficient shaft friction to resist the primarily vertical uplift loads.

2.1.4 FOW substructures in industry

The platform, mooring and anchoring concepts described in sections 2.1.2 and 2.1.3 convey the breadth of design options available to the FOW industry. As of 2024, the FOW industry counts

over 10 active projects: Table 2.2 lists all the projects with publicly available data, along with the platform and mooring concepts they employ. The data for this table has been obtained from two recent reviews of the industry [20] [23].

TABLE 2.2: Selection of active FOW projects along with the platform, mooring and anchor types employed.

Project	**Location**	**Installation**	**No. of turbines**	**Platform type**	**Water depth (m)**	**Mooring configuration**	**Mooring materials**
Unitech Zefyros	Norway	2010	1	Spar	186-204	Catenary	Steel chain
TetraSpar Demo	Norway	2021	1	'Semi-spar'	200	Catenary	Steel chain, synthetic rope
Hywind Tampen	Norway	2022	11	Spar	260	Catenary	Steel chain, synthetic rope
Hywind Scotland	UK	2017	5	Spar	100-120	Catenary	Steel chain
Kincardine Tranche 2	UK	2018	5	Semi-sub	70	Catenary	Steel chain
Floatgen	France	2019	1	Barge	33	Catenary	Steel chain, nylon
Provence Grand Large	France	2023	3	TLP	97	TLP	Steel wire
Windfloat	Portugal	2019	3	Semi-sub	92	Catenary	Steel chain, dyneema rope
Toda Haenkaze (Sakiyama)	Japan	2016	1	Spar	100	Catenary	Steel chain
Hibiki	Japan	2018	1	Barge	55	Catenary	Steel chain

Most of these projects have acted as 'demonstrator' or 'pilot' projects, providing proof-of-concepts of their relevant substructure technologies. In particular, as the challenge of building a floating platform capable of counteracting the wind thrust moments and forces generated by a wind turbine is new to offshore engineering, these projects have focused primarily on testing innovative platform concepts. As such, platform types can vary from one FOW project to another, including some combinations and variations of the fundamental concepts shown in Figure 2.1, such as the TetraSpar Demo 'Semi-spar', which features a tetrahedral tubular steel structure with a suspended keel, combining the properties of the semi-submersible and spar concepts.

In contrast, the mooring system designs currently employed in these projects have responded to 'standard' station-keeping criteria and established practice for offshore permanent mooring systems. This is manifested by all but one active project employing catenary mooring configurations. Some have employed synthetic rope on the upper end of the line (sometimes described as a semi-taut mooring), e.g. Floatgen, which uses sections of nylon [24] to reduce stiffness, or WindFloat which includes sections of high-modulus Dyneema rope to reduce weight [25].

2.1.5 Summary of FOW substructures

Designers of FOW substructures have a wide range of platforms, mooring and anchoring designs at their disposal. Current designs have pushed for innovation in platforms, but the the majority employ less innovative mooring systems, often composed of steel chains for the whole length of the mooring line. Although functional for reduced-scale projects, current mooring systems require large footprints, chain sizes, and anchors which will be difficult to upscale to much larger commercial arrays [26] [10], thus highlighting mooring design as a key avenue for optimisation.

2.2 Mooring design considerations for FOW

2.2.1 Overview of design considerations and standards

The objective of this section is to present an overview of the mooring design process and outline the main design considerations and the industry standards which accompany them, in view gaining a better understanding of the design variables for optimisation. The design methodology and criteria for FOW moorings are often a natural extension of those from the oil & gas industry, and as an emerging technology, the number of standards specific to the floating wind industry is limited. Most of the latest standards for offshore permanent moorings do not offer any specific guidance for the design of FOW moorings [8].

As mentioned in section 1.2, FOW presents a unique station-keeping challenge due to significant wind thrust loads and shallow water depths compared to oil & gas moorings. Mooring systems are generally designed with a focus on stiffness to resist motions of the floating structure [27], which in the case of FOW is heavily dependent on the selected platform configuration. Therefore, the starting point for designing a FOW turbine is usually the platform design (Figure 2.4). The first phase of design hence includes all considerations regarding the characteristics of the floating platform and its stability. Once the initial stability/motion analysis of the platform is completed, a typical second-phase design process involves refining the mooring design criteria until it satisfies given requirements [28].

Mooring system design requirements differ from project to project, in particular due to the high variability in environmental loads and water depths across different locations. Once all location-specific parameters are assessed, a suitable design must meet design criteria regarding three main considerations: 1. platform motions; 2. mooring line tensions; 3. anchor loading. These design considerations are interlinked: mooring line tension creates the restoring force that limits platform displacements, but also leads to loading at the anchor, thus governing the design of both mooring line and anchoring components. The following subsections review current guidance and standards relating to location-specific parameters and these three main design

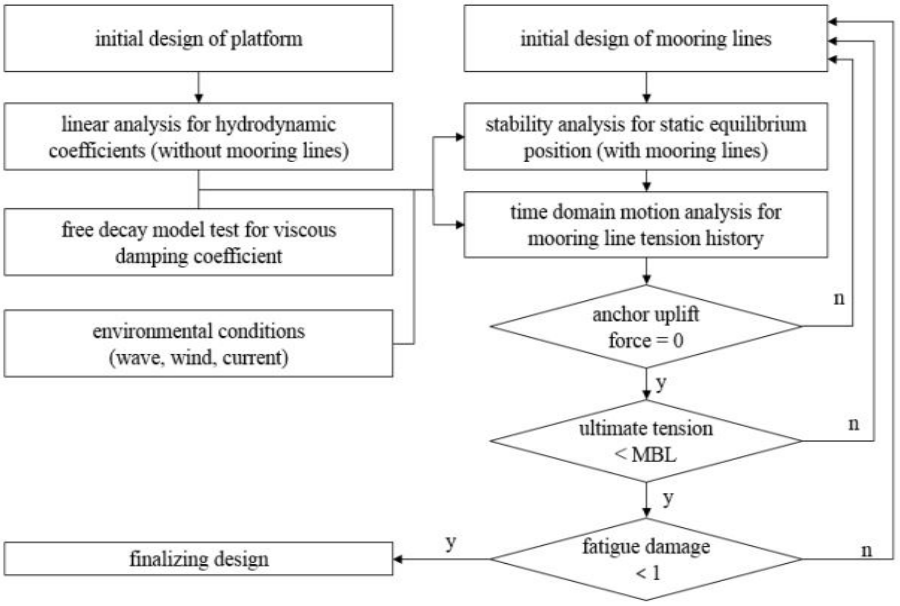

FIGURE 2.4: Typical iterative mooring design process [28]

considerations, in order to assess the significance of each in the overall system and determine which variables and metrics should be used to represent them.

2.2.2 Location-specific parameters

In this thesis, the terms 'location-specific parameters' refer to water depth and environmental loading parameters (e.g. wave height and period, wind speed, etc.), in other words, design parameters which are dependent on geographical location. The most critical location-specific parameter for FOW moorings is arguably water depth, which is typically one of the first considerations in a site assessment [20]. Current projects demonstrate high variability in this aspect, ranging from shallow waters (e.g. Floatgen, 33m [24]) to more intermediate depths (e.g. Hywind Tampen, 260m), with further projects in development in waters up to 500 m [29]. However, the majority of FOW projects in development will be on the shallower end of this spectrum, with many high potential sites identified between 50 and 150 m [23]. These shallower water depths for FOW present a significant design challenge, which will be discussed in more detail in Section 2.3.2.1.

Other critical location-specific parameters relate to environmental loads, which, along with the water depth, drive the sizing, configuration and cost of the mooring system. As shown in Figure 2.5, peak wave heights exhibit high-variability depending on the location, further justifying the importance of a method that enables project-specific optimisation for a range of locations. The most significant environmental loads affecting FOW turbines (and most other floating structures) belong to three categories, each characterised by specific parameters [9]:

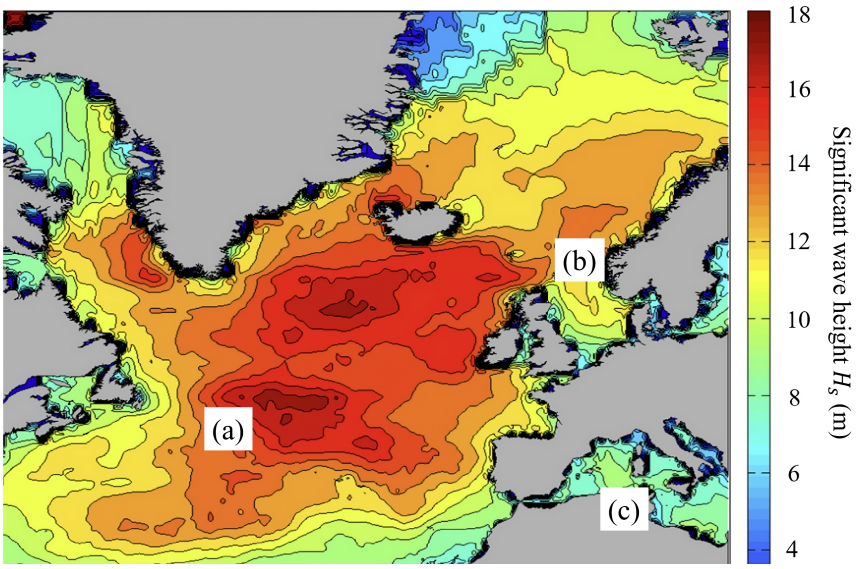

FIGURE 2.5: Variability in peak significant wave height (H_s) across: (a) the Atlantic, (b) the North Sea and (c) the Mediterranean [30]

1. Waves: significant wave height (H_s), peak period (T_p), spectral shape parameter (gamma), and direction. These parameters define the sea state and are crucial for determining wave-induced loads on the structure. The JONSWAP spectrum is commonly employed to model these conditions.

2. Wind: velocity, direction, velocity profile (magnitude as a function of height), and turbulence. Wind conditions directly impact both turbine performance and platform motions. The velocity profile is typically modeled using logarithmic or power law distributions, while turbulence is characterized by intensity and spectral properties.

3. Current: velocity, direction, and velocity profile. Currents contribute significantly to the static and dynamic loads on mooring systems. Current velocity profiles are typically approximated using empirical models such as the power law or logarithmic profile, as for wind.

These parameters form a complex, multivariate problem with no fewer than 10 parameters which must be considered in conjunction to accurately assess the total environmental loading on the FOW structure. These are typically simplified in initial analysis, by selecting 'worst cases' [31], but for detailed design, a full load matrix typically requires hundreds of combinations of these loads to be considered, and each combination must be modelled for a sufficient duration to obtain the worst-case scenario – typically 1 to 3 hours [31]. Additionally, when evaluating load cases, it is crucial to account for various turbine configurations, which can significantly influence the loads experienced by the turbine and its components. The two most common turbine configurations are: a) Normal operation, i.e. power production, where wind loads generate high thrust on the turbine, and b) Parked, or idling, where turbine blades are pitched to reduce the effect of wind loading. These cases are covered by the design load case (DLC) matrix,

DLC	Winds		Waves			Controls / Events	Load
	Model	Speed	Model	Height	Direction		Factor
1) Power Production							
1.1	NTM	$V_{in} < V_{hub} < V_{out}$	NSS	$H_s = E[H_s\|V_{hub}]$	β = 0°	Normal operation	1.25*1.2
1.3	ETM	$V_{in} < V_{hub} < V_{out}$	NSS	$H_s = E[H_s\|V_{hub}]$	β = 0°	Normal operation	1.35
1.4	ECD	$V_{hub} = V_r$, V_r±2m/s	NSS	$H_s = E[H_s\|V_{hub}]$	β = 0°	Normal operation; ±Δ wind dir'n.	1.35
1.5	EWS	$V_{in} < V_{hub} < V_{out}$	NSS	$H_s = E[H_s\|V_{hub}]$	β = 0°	Normal operation; ±Δ ver. & hor. shr.	1.35
1.6a	NTM	$V_{in} < V_{hub} < V_{out}$	ESS	$H_s = 1.09*H_{s50}$	β = 0°	Normal operation	1.35
2) Power Production Plus Occurrence of Fault							
2.1	NTM	$V_{hub} = V_r$, V_{out}	NSS	$H_s = E[H_s\|V_{hub}]$	β = 0°	Pitch runaway → Shutdown	1.35
2.3	EOG	$V_{hub} = V_r$, V_r±2m/s, V_{out}	NSS	$H_s = E[H_s\|V_{hub}]$	β = 0°	Loss of load → Shutdown	1.10
6) Parked (Idling)							
6.1a	EWM	$V_{hub} = 0.95*V_{50}$	ESS	$H_s = 1.09*H_{s50}$	β = 0°, ±30°	Yaw = 0°, ±8°	1.35
6.2a	EWM	$V_{hub} = 0.95*V_{50}$	ESS	$H_s = 1.09*H_{s50}$	β = 0°, ±30°	Loss of grid → -180° < Yaw < 180°	1.10
6.3a	EWM	$V_{hub} = 0.95*V_1$	ESS	$H_s = 1.09*H_{s1}$	β = 0°, ±30°	Yaw = 0°, ±20°	1.35
7) Parked (Idling) and Fault							
7.1a	EWM	$V_{hub} = 0.95*V_1$	ESS	$H_s = 1.09*H_{s1}$	β = 0°, ±30°	Seized blade; Yaw = 0°, ±8°	1.10

ECD - Extreme coherent gust with direction change
EDC - Extreme direction change
EOG - Extreme operating gust
EWM - Extreme wind speed
EWS - Extreme wind shear
NTM - Normal turbulence model
ETM - Extreme turbulence model
NWP - Normal wind profile model
NSS – Normal sea states
ESS – Extreme sea states

FIGURE 2.6: Selected cases from the IEC design load case (DLC) matrix [32] [14]

produced by the International electrotechnical commission (IEC), which are one of the main standards providers in the sector [14]. A selection of cases from the full matrix are shown in Figure 2.6. Usually, the key design driving cases for initial design are 1.6 (worst-case operational) and 6.1 (worst-case parked) [8]. For each of these scenarios, platform motions, and mooring and anchor loading must be assessed with respect to chosen criteria.

2.2.3 Platform motions

In the offshore environment, a floating platform exhibits motions in 6 degrees of freedom (DOF), as depicted in Figure 2.7. FOW projects typically have strict criteria regarding the maximum allowable displacements in these DOF, as they can cause undesirable effects to the system [27]: surge, i.e. horizontal platform offset, can damage the power cable if its allowable range is exceeded; pitch affects the aerodynamic performance of the turbine blades; heave can also affect the power output of the turbine by altering the angle of attack of the blades. In addition to displacements in these DOFs, accelerations at the nacelle of the turbine must be kept as low as possible, to avoid structural damage to the turbine [33].

As a general rule, mooring systems aim to keep the floating structure as close as possible to its reference location in the water plane, i.e., limiting maximum surge and sway motions [34]. These motions are highly sensitive to the mooring system stiffness, whereas rotational motions are more sensitive to platform buoyancy and hydrodynamics. Restricting water plane motions is especially important for oil & gas platforms, which are connected to the seabed by risers and

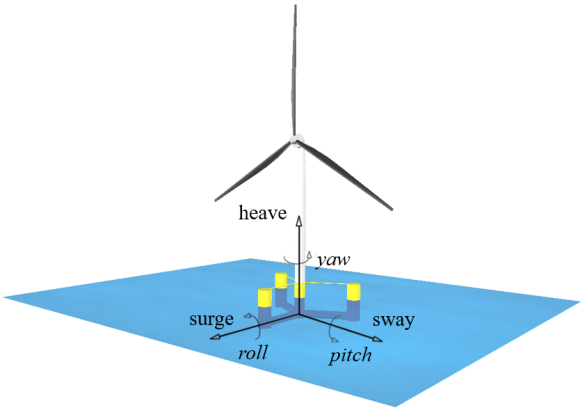

FIGURE 2.7: Visualisation of the 6 DOFs of the FOW platform. Rotational motions are shown in italics

drill pipes which offer limited compliance, especially in shallow waters [6]. The catastrophic consequences of riser failure, i.e. hydrocarbons spilling into the ocean, lead to high safety factors and strict station-keeping constraints. Designing FOW mooring systems to these requirements could lead to over-engineering and over-expenditure. There are two key factors to consider when comparing oil & gas and FOW mooring design criteria: 1) FOW moorings can be designed with lower reliability and do not have the same need for redundancy as oil & gas systems [35]; 2) Station-keeping requirements are not identical for both applications – whether higher displacements are tolerable for FOW is the subject of ongoing research, which is discussed hereafter.

For FOW, maximum allowable surge is primarily limited by the allowable offset of the power cable. Unlike fixed-bottom wind turbines which house power cables inside the tower, FOW turbines use dynamic power cables which are suspended between the platform and seabed and exposed to the marine environment. These cables are not designed to bear any load other than their self-weight, i.e., they must always be 'slack'. This can be achieved in various ways, but the most common approach involves using buoyancy modules installed along the line to create a 'lazy wave' which can extend as the floater is displaced (see Figure 2.8). Similar to mooring lines, these cable configurations can typically provide more extension in deeper waters than shallower waters, hence surge constraints are often given as a function of water depth. Fundamentally, allowable cable displacements are a design variable, rather than a hard constraint, i.e., these can typically be adjusted depending on the desired the complexity and cost [36].

Although updates are in progress to cover FOW, the ISO (ISO 19901-7:2013) [38] and API (API RP 2SK) [39] station-keeping standards for offshore engineering were developed for the oil & gas industry, and currently offer no FOW-specific station-keeping standards. In recent years, guidance has been made available for FOW mooring design, notably from ABS (E12PC00027) [40], DNV (DNV-OS-J103, DNVGL-ST-0119) [41], LR (LR-RP-003) [42] and BV (NI 572 DT R01 E) [43]. However, these guidance reports give limited insight into specific station-keeping criteria for FOWs: the DNV report only considers floating stability (i.e. no capsizing) as the general requirement of the system, while ABS and BV offer no guidance on maximum platform

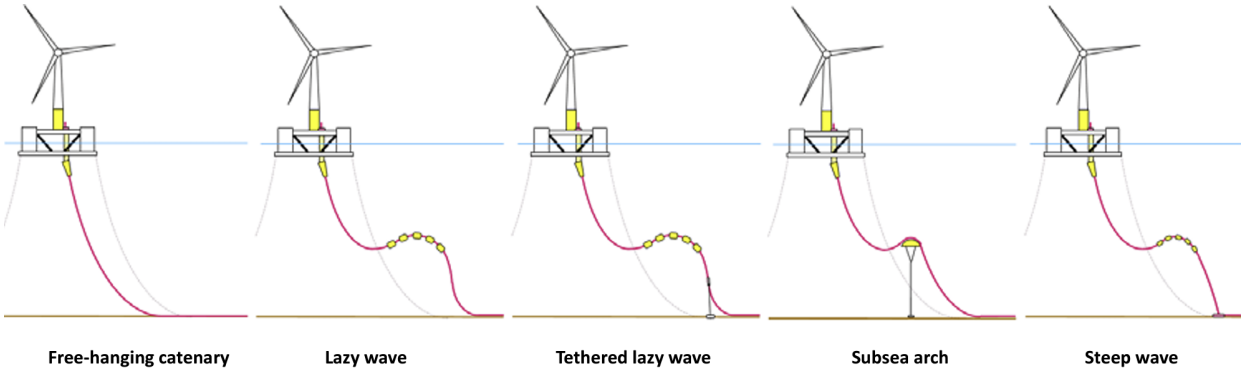

FIGURE 2.8: Dynamic cable configurations, in increasing order of complexity and cost [37]

motions, as these criteria are deemed highly project-specific, and must be determined based on the specific turbine, floater and cabling technologies used. More specific guidance is usually available in research publications and technical reports, but this typically varies highly across different projects, as shown in Table 2.3.

TABLE 2.3: Compilation of surge, pitch and nacelle acceleration limits mentioned in publicly available technical reports and research papers.

Ref.	Survival surge (% of water depth)	Operational pitch (deg)	Survival nacelle acc. (g)
[20]	50 - 25 ($< 250m$); 12 - 5 ($> 250m$)	no guidance	no guidance
[44]	30 - 35	no guidance	no guidance
[45]	30 - 12	+/- 5.5	0.45
[46]	33	+/- 5.0	0.3
[47]	no guidance	+/- 7.5	0.3
[17]	7.5	+/- 5.5	no guidance

The overall conclusion from existing literature is that although platform motions are undesirable as a whole, they may be more tolerable than in oil & gas systems, and can be specified on an individual basis depending on the project. This supports the purpose of this research, which aims to develop an efficient and versatile method to maximise the compliance in the mooring system whilst not exceeding the project-specific platform motion criteria.

2.2.4 Mooring line tension

2.2.4.1 Mooring line tension – ultimate limit state (ULS)

In offshore engineering, the ultimate limit state (ULS) is a failure criterion defined by the maximum load-carrying capacity. Criteria are typically well-established for ULS mooring line tension: the design tension T_d must stay below the characteristic strength S_c of the mooring line [8]:

$$S_c > T_d \tag{2.1}$$

where S_c is a function of the minimum breaking load, MBL, and its coefficient of variation, COV. For simplicity, S_c can be calculated by [41]:

$$S_c = 0.95 \cdot MBL \tag{2.2}$$

To define the maximum design tension T_d in the mooring line, ABS rules [40] require the mooring design to consider both operational and survival load cases. Although the typical ULS conditions are selected for a parked turbine with 50-year conditions, operating conditions should also be considered as the turbine thrust can cause loading comparable to those of survival conditions [27].

Once the ULS conditions are determined, the mooring line design tension T_d can be calculated such that it complies with the limiting technical design criteria. DNV guidance [41] suggests that T_d should be calculated as the sum of mean and dynamic tension terms, both arising from 50-year ULS conditions:

$$T_d = \gamma_{mean} \cdot T_{c,mean} + \gamma_{dyn} \cdot T_{c,dyn} \tag{2.3}$$

Where $T_{c,mean}$ is the characteristic mean tension, based on pretension and mean environmental loads, $T_{c,dyn}$ is the characteristic dynamic tension, which incorporates oscillatory wave effects, and γ_{mean} and γ_{dyn} are load factors which depend on the chosen safety class [41].

For a steel chain, the MBL is given in kN by:

$$MBL = cd^2(44 - 80d) \tag{2.4}$$

Where d is the chain diameter in mm and c is a coefficient based on the steel grade used. Both of these parameters directly influence the cost of the chain per metre (USD/m), which in turn can be estimated as a function of the MBL [48]:

$$Cost_{chain/m} = 0.0591 \cdot MBL - 89.69 \tag{2.5}$$

Equations similar to 2.5 exist for cost of synthetic ropes and steel wire, which can also be written as a function of MBL. Equation 2.6 gives the cost of polymer rope per metre as a function of the MBL [48]:

$$Cost_{poly/m} = 0.0138 \cdot MBL + 11.281 \tag{2.6}$$

Equations 2.3-6 convey the fact that the maximum mooring line tensions are crucial to the mooring line design, which in turn directly affects the cost of line. This justifies the need to reduce peak line tension, which would subsequently contribute to reducing the required MBL hence reducing the cost of the mooring lines themselves [20].

2.2.4.2 Mooring line tension – fatigue limit states (FLS)

Fatigue limit states (FLS) refer to the long-term damage caused by cyclic tensions due to repetition of wave, wind and current loading [43]. Statistics from the oil & gas industry suggest that fatigue damage is one of the main causes for mooring line breakage in floating offshore platforms [34].

The underlying principle of fatigue design is that individual mooring components should have fatigue lives that exceed the field life of the installation in question by a given safety factor. Rather than the ULS conditions based on 50-year storms (or 10,000-year storms for oil & gas), fatigue design conditions consist of a number of discrete conditions which represent the long term environment for a given location [27].

Fatigue life calculations for mooring components typically employ T-N or S-N curves, which characterise the relationship between number of cycles, N, and failure of a component as a function of constant normalised tension range (T for tension or S for stress), based on experimental data. An example T-N curve is shown in Figure 2.9 [49].

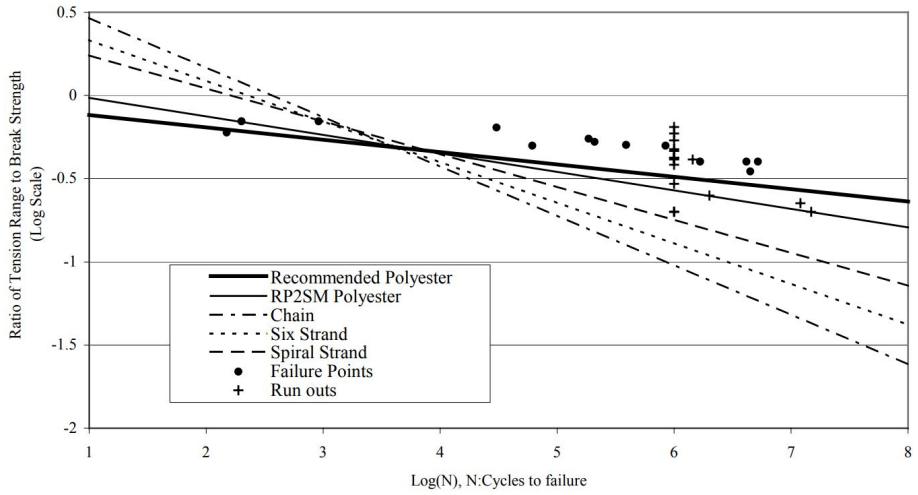

FIGURE 2.9: T-N curves for various mooring line materials, including polyester rope fatigue data [49]

API and ABS use similar criteria, both based on general format T-N curves [34]. The equation for a representative T-N curve is given by:

$$NR^M = K \tag{2.7}$$

where N is the number of allowable load cycles, R the ratio of cyclic tension amplitude to the breaking strength of the line, M is the slope of the T-N curve and K is a mean load dependent coefficient [40].

The total fatigue damage is then calculated by accumulating all the fatigue damage which has occurred in each of the sea states chosen to represent the long-term conditions. Both ABS and

DNV suggest the use of Miner's sum to predict cumulative damage (assumed to be linear) [40] [41], whereby the annual fatigue damage D_i for a design state i is given by:

$$D_i = \sum n_i / N_i \tag{2.8}$$

where n_i is the number of load cycles per year within the tension range interval i, and N_i is the corresponding number of cycles to failure according to the T-N curve. The total cumulative fatigue damage is then calculated as the sum of all D_i components over the chosen set of design states.

Overall, as can be noted from the presence of a tension range term in equations 2.6 and 2.7, higher tensions in the mooring line lead to more fatigue damage. A useful metric for assessing this is the Damage Equivalent Load (DEL), which represents a constant-amplitude load cycle that causes the same fatigue damage as the actual variable loads over a given period. DEL simplifies fatigue assessment by converting complex load histories into a single value, making it effective for both in normal operation sea states (DLCs 1.1, see Figure 2.6) and in more extreme sea states (DLCs 6.1 and 6.3) [50].

Alternative fatigue assessment methods offer varying advantages and drawbacks. Rainflow cycle counting, which is at the core of DEL, provides a detailed breakdown of stress cycles and forms the basis of many fatigue life prediction models. However, its direct application requires extensive data processing and post-analysis of stress cycles. DEL builds upon rainflow counting by aggregating the results into a single representative load, simplifying comparisons across different designs and loading conditions. Spectral fatigue analysis offers computational efficiency and is suitable for long-term fatigue estimation but may not fully capture non-linear effects in mooring dynamics. Probabilistic methods enhance fatigue life predictions by accounting for uncertainties, but their complexity and reliance on statistical distributions can limit their practicality in an optimisation context.

DEL remains the most suitable choice for mooring system optimisation. It ensures accuracy by directly capturing fatigue damage from time-domain simulations, without relying on statistical assumptions. While it requires full time series data, its single-value output makes it computationally feasible for optimisation workflows, where multiple design iterations must be evaluated efficiently. This balance between accuracy and practical implementation makes DEL a reliable and effective metric for fatigue assessment in offshore mooring systems [51], [52].

2.2.5 Anchor loads

Anchor design is influenced by a number of factors including anchor type, seabed conditions and loading conditions. Codes and standards offer in-depth guidance for anchor design depending on these considerations [27]. However, the principal concern for this research

regards the mooring loads on the anchor and the holding capacity required to resist the dynamic loading from the mooring lines.

DNV guidance defines an overall anchor design resistance R_d [41], given by:

$$R_d = R_c / \gamma_m \tag{2.9}$$

where R_c is the characteristic geotechnical anchor resistance and γ_m is a material factor which is dependent on soil properties and the anchor type, and type of loading. The design resistance is then expressed in the following design criterion:

$$T_d < R_d \tag{2.10}$$

Similarly, for drag-embedded anchors, BV defines the maximum holding power required as a function of the horizontal component of line tension at the anchor when the design tension is applied to the fairlead (i.e., the upper extremity of the mooring line) [43]. Thus, by reducing the design tension, the anchor design resistance can be reduced. In turn, this lowers the overall cost of the anchor system, which can be considered as directly related to the minimum breaking load (MBL) of the mooring line in kN by the following expression [20]:

$$Cost_{anchor} = 10.198 \cdot MBL \tag{2.11}$$

Equation 2.11 only applies to catenary lines and drag-embedded anchors, but the underlying principle that anchor cost is directly related to mooring line load would also be valid for other configurations. Overall, these simplified equations help to convey the importance of mooring line tension and anchor loading as a consideration of mooring system design. Reducing mooring line tensions not only leads to a reduction in the required material cost of mooring lines, it also contributes to reducing the cost of anchoring systems [20] .

2.2.6 Summary of design considerations

This section has presented the location-specific parameters, constraints, and objectives that must be considered for mooring design. In particular, several key design considerations were discussed, including fairlead tension, surge, pitch, and nacelle accelerations. The effect of these design considerations on the FOW system are summarised in Table 2.4.

Tension reduction was shown to be a key design objective for cost reduction, as it enables lower weight and cost of mooring lines and anchors, and increased reliability and longevity of these components. Although the benefit of minimising them is harder to quantify, platform motions were also discussed as both a constraint and an objective: developers may have limits regarding maximum motions, but these are often guidelines which can be accounted for in design. For

TABLE 2.4: Key outputs for FOW mooring design, along with the system benefits obtained from minimising these outputs.

Key outputs to minimise	Positive effects of minimisation on FOW system
Fairlead tension (T)	Reduced size of mooring line and anchor required (peak load), increased reliability and longevity of mooring (fatigue)
Surge (S)	Ensures safety of the power cable
Pitch (P)	Improves aerodynamic performance of the turbine
Nacelle accelerations (A)	Reduces structural damage to the turbine

instance, maximum allowable surge can be increased or reduced depending on the cost and feasibility of employing more complex dynamic cable configurations. Crucially, the literature discussed in this section indicates that identifying the optimal compliance on a project-specific basis is crucial to balance these trade-offs and finding the most cost-effective solution.

2.3 Challenges and advancements in compliant mooring design

2.3.1 Stiffness vs. compliance: a key trade-off for mooring design

As discussed in section 2.2, designing a mooring system should involve finding a balance between stiffness and compliance to fit project-specific station-keeping requirements [8]. A stiffer mooring system will maintain the floating structure closer to its reference position, at the expense of higher loads on the mooring lines and anchors. A compliant mooring system will allow more motion of the floating structure in response to environmental loads, reducing forces in the mooring line and anchor, in turn allowing for smaller, cheaper anchors and a reduced chance of mooring line failure (Table 2.5).

TABLE 2.5: Effect of compliance on FOW system

Mooring design:	stiff	compliant
Platform displacements	low	high
Mooring and anchor loads	high	low
Mooring and anchor cost	high	low

Ideally, mooring design optimisation would involve considering mooring system stiffness as a design variable, and platform motions and anchor and line tensions as conflicting objectives, to ensure the most cost-effective balance is found. However, traditional mooring configurations and materials often cannot deliver optimal mooring system stiffness when applied to FOW. Sections 2.3.2.1 and 2.3.2.2 discuss traditional approaches to delivering mooring system compliance, and their limitations within the context of FOW mooring design optimisation.

2.3.2 Compliance in traditional mooring systems

2.3.2.1 Geometric compliance

All taut and catenary mooring systems exhibit some form of compliance, which can be either geometric or elastic, allowing the platform to move under loading. Geometric compliance describes the ability of a mooring line to change its overall shape under loading, and generally refers to a catenary mooring line lifting off the seabed. This is shown in Figure 2.10, which depicts the change of profile of a catenary mooring line as the fairlead is subjected to an offset x_f of 20 m [53]. As the mooring line lifts of the seabed, its suspended weight creates a larger restoring force on the fairlead to bring it back to position. The initial configuration of the mooring line must be slack enough to allow some offset of the platform, but this must be balanced with enough initial suspended weight to provide sufficient 'pre-tension' stiffness to the mooring system.

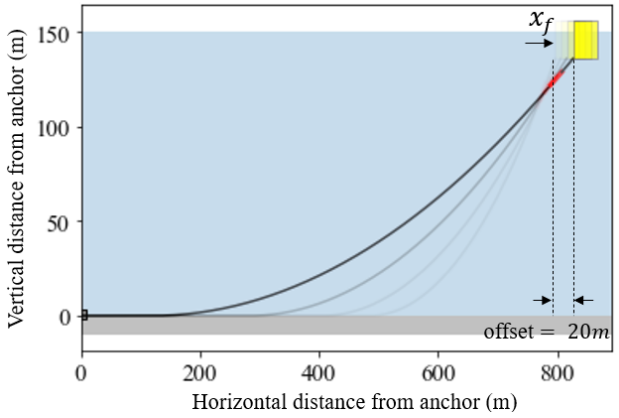

FIGURE 2.10: Change of shape of a catenary mooring line to accommodate a fairlead offset of 20m [53]

This balance is straightforward to achieve for catenary moorings in intermediate water depths (e.g. 200 m), but not in shallower waters, where the suspended length of line is much shorter. This is depicted in Figure 2.11, which shows 2D profile views of catenary mooring lines in 50 m and 200 m water depths. Both lines have the same top angle (i.e. ratio of horizontal to vertical forces), but the magnitude of this force will be lower in the 50 m depth case due to the lesser weight of suspended line, thus requiring clump weights (weighted modules connected to the line) or a larger chain to reach a suitable pretension [54].

When the platform is offset from its reference position, the shallow water configuration which lacked initial restoring force will then lift much more line off the seabed than the deeper water for the same offset, thus leading to much higher restoring force and high stiffness (i.e. high slope of tension-offset curves in Figure 2.11b). A smaller chain weight would reduce this, but this would require a very large seabed footprint, and would exacerbate the problem of lack of initial pretension. Crucially, adjusting the weight of chain (i.e., adjusting line diameter) also implicates

changing its breaking strength, making lighter chains unsuitable for the high-load scenarios where compliance is most critical.

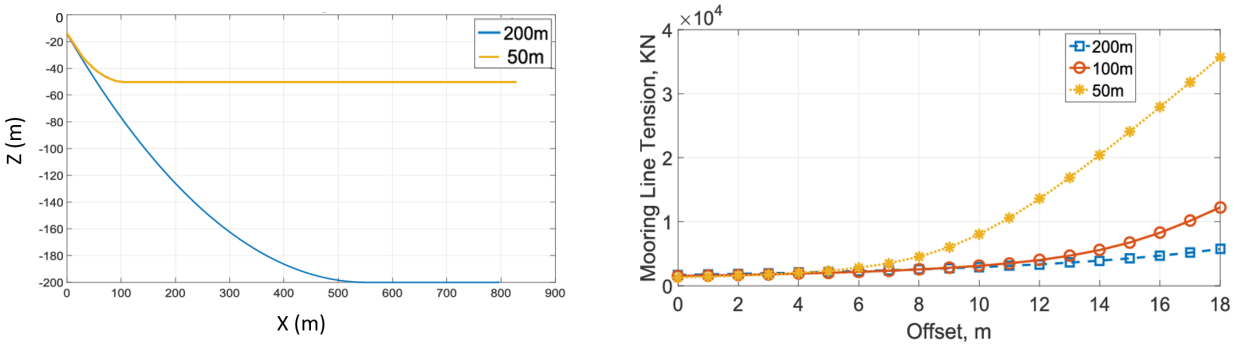

(a) Static catenary profiles

(b) Stiffness response to offset

FIGURE 2.11: Differences between catenary moorings in shallow and intermediate depths [54]

This challenge has significant implications for overall cost and feasibility of catenary moorings in shallow waters, and has been widely identified as a key area for innovation [36]. One approach to overcoming this challenge, which was employed by the Floatgen pilot FOW turbine, moored in 33m water depth, is to incorporate a section of nylon rope close to the fairlead to provide some extensibility, i.e., elastic compliance [24].

2.3.2.2 Elastic compliance

Elastic compliance describes the ability of a mooring system to extend axially under loading, and is typically obtained through the use of synthetic materials, in particular fibre ropes. In theory, steel chain does exhibit a minimal axial extension under tension, but this is usually negligible compared to that which can be obtained by polymers such as polyester or nylon [8] (Figure 2.12).

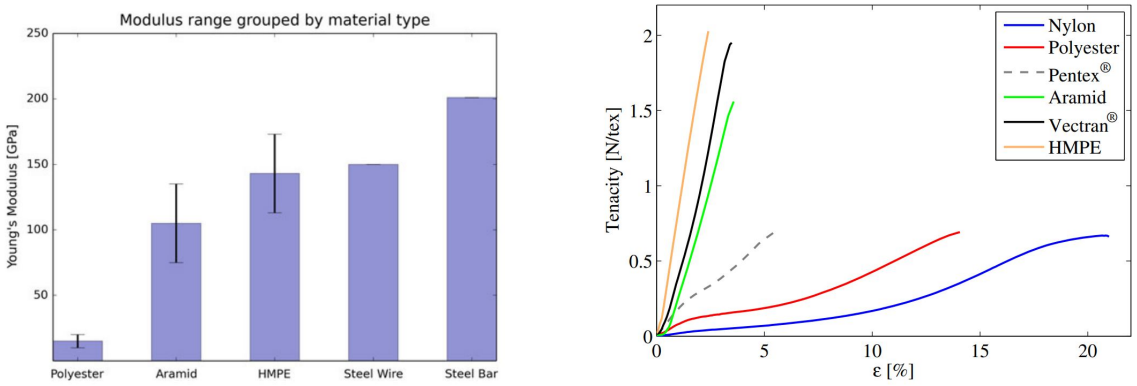

(a) Average Young's Modulus of typical mooring system materials [8]

(b) Stress-strain behaviour for typical synthetic fibre types [55]

FIGURE 2.12: Stiffness properties of various synthetic mooring materials [8] [55]

Over the last three decades, synthetic fibre ropes have proven to be a reliable and versatile option for permanent deep-water moorings [56]. This is mainly due to their near-neutral buoyancy, which keeps self-weight of the system at an acceptable level in water depths where a full-chain mooring would be too heavy [8]. However, when driven by weight-saving, synthetic rope designs usually employ the higher-modulus ropes due to their much their much higher breaking strength (Figure 2.12b). Although high-modulus synthetics provide some elasticity compared to inextensible chains, this does not to have a significant impact on reduction of anchor loads and mooring tensions [57] [58], and this impact is typically not accounted for in initial design [59].

However, low-modulus ropes such as Nylon and polyester can be employed to increase mooring system compliance. This elastic compliance is particularly crucial for taut moorings, which exhibit very little geometric compliance [55]. Research has shown that using low-modulus ropes in taut-compliant moorings can reduce the overall cost of the mooring system compared to standard catenary moorings [60] [61], and these cost savings are particularly significant in shallow waters [54]. Several studies have shown that these materials can provide additional compliance to catenary mooring systems for wave energy converters (WECs) [62] [63] [64]. Nylon ropes are shown to reduce peak loading from both computational and experimental data, at the expense of increased platform movements [62] [61]. This can lead to peak load reductions at the anchor of over 75%, when compared to a full-chain catenary for a typical operational sea-state. The weight of the anchor in question can then theoretically be reduced by 10 tons when incorporating nylon ropes to the mooring system, in turn leading to a 64% reduction of the overall anchoring cost [61].

Similar studies have been undertaken for FOW, where hybrid chain-polymer-chain catenary configurations have been shown to effectively reduce weight and add compliance to a mooring system [65]. Hybrid nylon lines, which have lower axial stiffness than polyester, enable significant mooring line tension reductions for both ULS and FLS [65] (Figure 2.13).

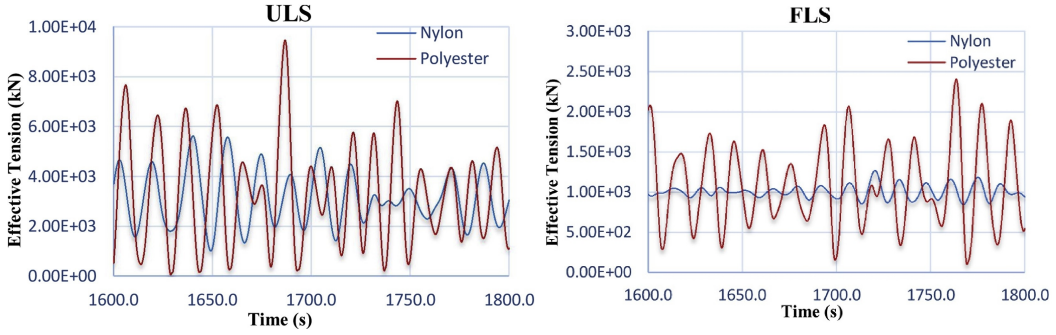

FIGURE 2.13: Modelled tension responses for nylon and polyester hybrid mooring lines in ULS (left) and FLS (right), for the Floatgen project [65].

However, the addition of elastic compliance through low-modulus ropes does not fully solve the shallow water mooring challenge. The total quantity of elastic extension available is determined by the length of synthetic rope, and in shallower waters, it can be difficult to obtain

sufficient length of rope [54]. For taut systems, more compliance can be obtained by using a line angle closer to horizontal, which increases the length of rope, however this leads to larger footprints and higher material costs.

In theory, this issue could be resolved by employing ropes with lower equivalent axial stiffness EA by using smaller cross sectional area A, i.e. smaller diameters, for the same modulus E [66]. However, using smaller diameters leads to lower minimum breaking load (MBL) of the rope [66], meaning lower stiffness ropes would not be applicable to locations with extreme environmental loading, which are those that may require the most compliance. In this sense, Nylon is the most promising material, as its low modulus E relative to the other rope fibres enables low stiffness EA without resorting to weaker diameters.

Using low-modulus ropes for compliance does come with another limitation however: their stiffness response is load-rate dependent, and stiffer in dynamic scenarios than under static tension. This is the case for most polymer ropes, but especially true for Nylon, where dynamic stiffness has been measured at up to 4 times the quasi-static stiffness [67]. Figure 2.14 shows the original working stiffness curve (OWC), the working stiffness curve (WC) which the material adopts when loaded below T_{max}, the dynamic stiffness about a given working point (WP), and the bi-linear stiffness which is a piecewise combination of the original working stiffness and the dynamic stiffness. This low static stiffness and high dynamic stiffness is counter-productive to finding the right balance in mooring system compliance, as it leads to high displacements under lower loads, but limits the extension available to reduce peak dynamic loads.

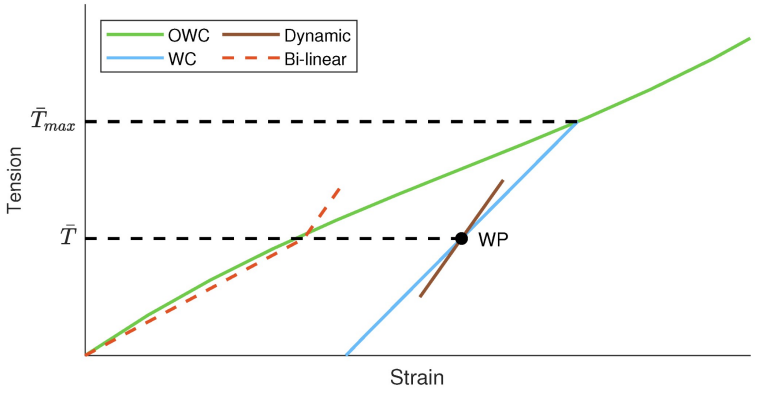

FIGURE 2.14: Stiffness curves of polymer ropes in different scenarios [67]

In summary, the elastic compliance provided by synthetic ropes is not fully independent as it is coupled to both strength and load rate. Although low-modulus ropes such as Nylon have shown promise for load reduction in some applications, a more customisable and reliable source of compliance would be advantageous.

2.3.3 Load reduction devices

2.3.3.1 Background on load reduction devices

Load reduction devices (LRDs) are a nascent technology which introduce targeted compliance into a mooring system, so that the mooring system stiffness is not constrained by its physical and geometric properties (weight of chain, angle of mooring line, MBL of rope, load-rate). Various load reduction device concepts exist, including ballasted pendulums [13], thermoplastic springs [68] and hydraulic dampers [69], all of which are designed to provide a low stiffness response under loading, without sacrificing strength.

Although interest and advancements in LRD technology has greatly accelerated due to their applicability for FOW, these respond to a challenge that has been identified in mooring design over 60 years ago [70]. Some early designs of elastic tethers date from the 1980s, where short rubber strands were grouped and connected to taut mooring systems for data measurement buoys [70]. A schematic of a buoy mooring incorporating an elastic tether is shown in Figure 2.15 [71].

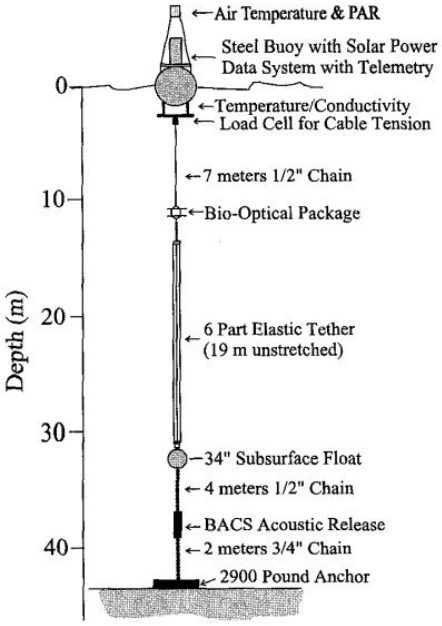

FIGURE 2.15: Configuration of GLOBEC test buoy incorporating an elastic tether, deployed in winter of 1994-1995 [71].

At the turn of the 21st century, the applications of elastic tethers gradually evolved from buoy moorings to more complex systems such as pontoons and yacht moorings. Companies such as Hazelett, Supflex and Seaflex have designed commercial devices for these marina-based applications, including novel mechanicsms which ensures low-stiffness in highly dynamic scenarios to effectively reduce mooring loads [72].

It is not until 2010, following research from both University of Exeter and TFI Marine, that extensible devices were seriously considered for load reduction in offshore renewable energy

applications. Initiatives have continued since then, with the development of four distinct yet comparable concepts : 1) The TFI Seaspring; 2) The Exeter tether; 3) The Intelligent Mooring System (IMS); 4) The Dublin Offshore LRD. The following subsections provide a brief overview of each of the four concepts along with publications that have accompanied them.

2.3.3.2 Technology for ideas (TFI) Seaspring

In 2012, TFI developed an extensible tether combining elastomeric and thermoplastic elements [68], as shown in Figure 2.16 [73].

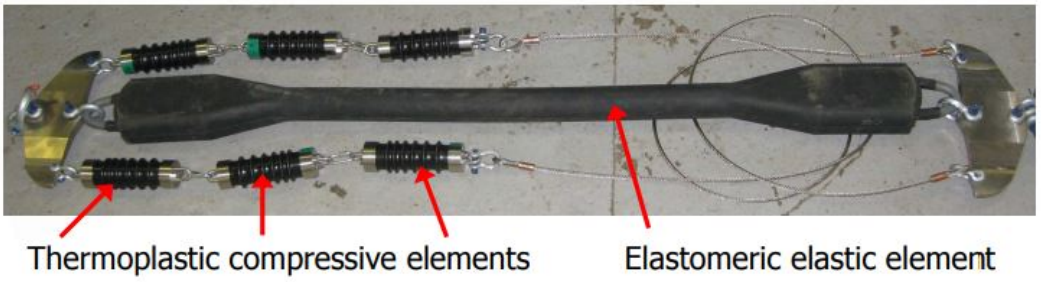

FIGURE 2.16: Prototype TFI Seaspring, composed of a central elastomeric load-bearing element combined with thermoplastic compressive elements[73].

As discussed in section 2.3.2.2, purely elastomeric materials have difficulty balancing the stiffness requirements for operational sea-states with those of extreme weather events. The size of elastomeric tether required to keep a floating structure on station during a storm would make it excessively stiff for normal operation [68]. Combining the high stiffness of an elastomeric element at maximum strain with the low-strain stiffness of a thermoplastic element addresses this challenge. The individual and combined stiffness responses are shown in Figure 2.17 [73].

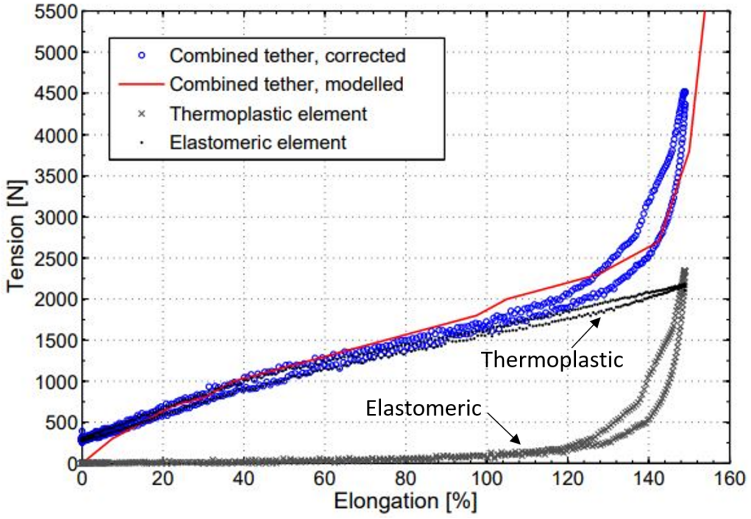

FIGURE 2.17: Stiffness curve of the TFI Seaspring, combining the elastomeric and thermoplastic responses. The 'corrected' terms refer to experimental results which have been corrected to exclude the disturbance in measurements caused by stiction forces in the bearings. [73].

From computational analyses, various stiffness responses have been compared in an attempt to determine the configuration which most effectively reduces mooring tensions. A 'sublinear' force-strain curve as shown in Figure 2.18 offered the largest mooring line tension reductions [12]. Further research from TFI [11] provided case studies of the component for the Maine Aqua Ventus 1 pilot FOW turbine. Cost saving analysis of the LRD showed it could reduce the levelised cost of energy (LCOE) by 17%.

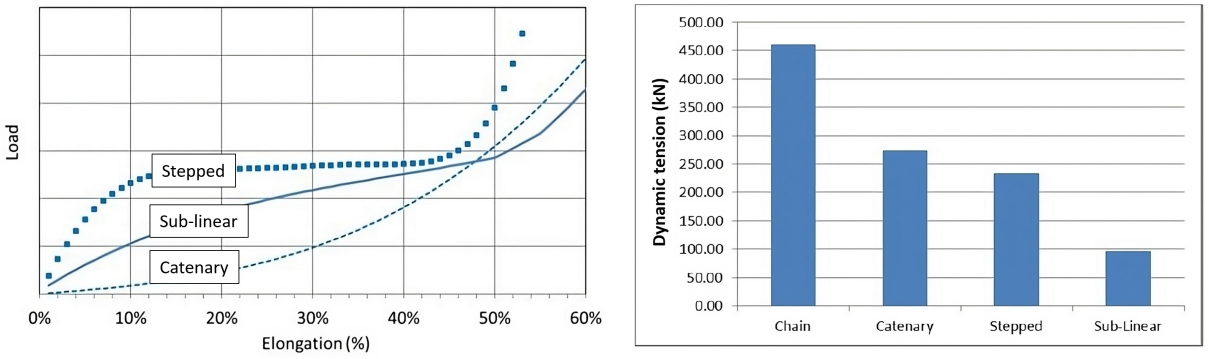

FIGURE 2.18: Three load-extension curves for the TFI tether (left) and the corresponding dynamic tension for each curve over the course of a simulation (right) [12].

2.3.3.3 Exeter tether

An alternative approach to achieving extensibility without sacrificing strength was provided by the 'Exeter tether', developed at University of Exeter [74] (Figure 2.19). The Exeter tether combines an elastomeric core with an outer layer of polyester rope, thus ensuring the high loads are carried through the rope rather than the core, whilst obtaining the low-stiffness benefits of the elastomer.

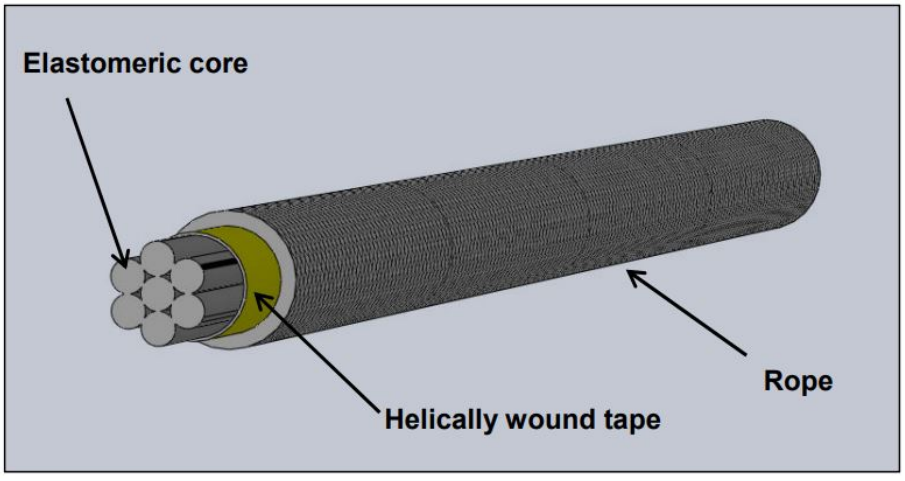

FIGURE 2.19: Cross-sectional view of the Exeter tether. The combination of materials enables decoupling of the tether's stiffness and strength [74].

Associated publications have discussed durability assessments and sub-component tests on the Exeter tether [75] [76]. It was tested on the South-West marine testing facility (SWMTF), and demonstrated reliability in operation and successful load reduction [74] [77].

2.3.3.4 Intelligent Mooring System (IMS)

As identified by the developers of the TFI SeaSpring [68], different environmental loads or operating conditions require different levels of compliance, and although the Exeter Tether decouples compliance and breaking strength, its stiffness curve shape is still constrained [78]. The IMS aims to solve this problem by employing a hydraulic system to provide an adjustable stiffness is response. The component is shown in Figure 2.20 [79].

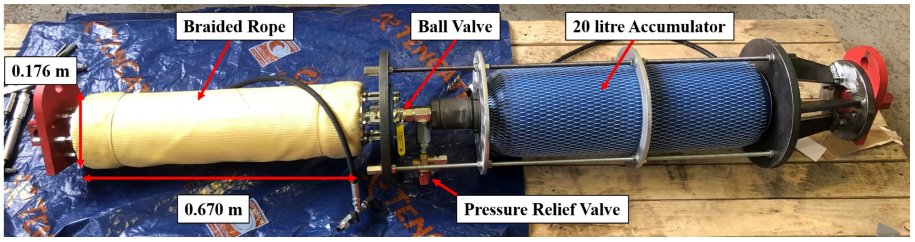

FIGURE 2.20: IMS configuration used for physical testing [79].

The braided rope holds a pressurised bladder filled with water, whilst the 20-litre accumulator on the other side is filled with gas. When tensile forces stretch the system, the braided rope extends, and the bladder is compressed. In the process, water is transferred to the accumulator, storing energy from the peak load and dissipating tension developed in the line. Pre-charge bladder pressure can be varied, allowing a multitude of possible stiffness responses [79]. Four different stiffness responses are plotted in Figure 2.21 , with nylon and wire rope responses also included for comparison [80].

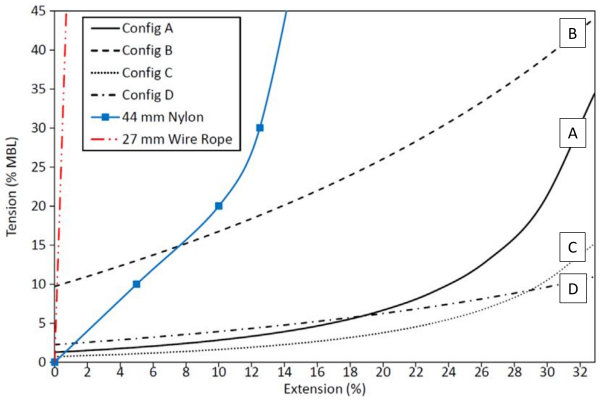

FIGURE 2.21: IMS stiffness curves for 4 different configurations [80].

These various curves were incorporated in an Orcaflex model, with simulations run for each curve to analyse its effect on surge and peak tension for two different wave heights (2.44 m and 6.51 m). Plots are shown on Figure 2.22, which convey an effective reduction in tension in taut

and catenary moorings for all except curve B which was hindered by its high stiffness at low extension.

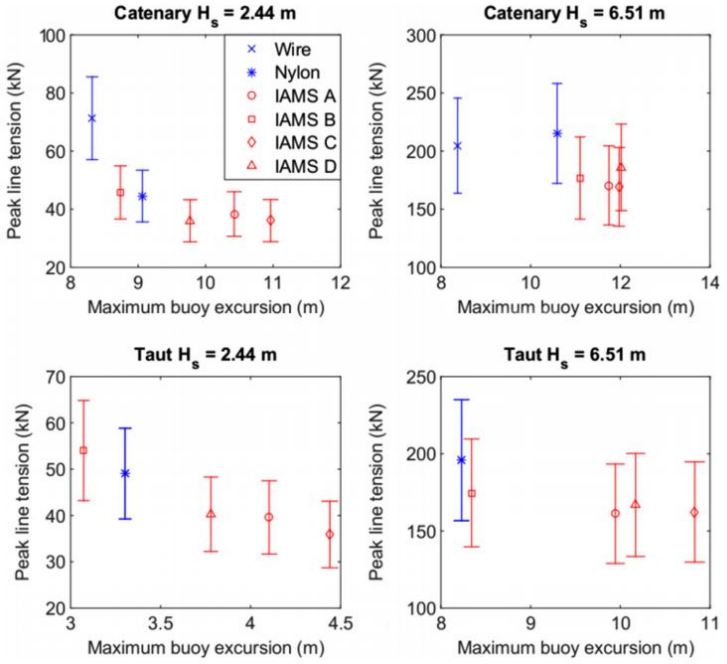

FIGURE 2.22: Amplitude plots of peak line tension vs maximum buoy excursion for various IMS configurations, for catenary and taut moorings, with 2 different wave heights [80].

Subsequent publications for the IMS have provided in-depth physical performance and reliability testing of the component [81], as well as computational analyses of its performance when included in a FOW mooring system [69] [79]. Computational parametric analyses have concluded that a longer component would further reduce peak tensions at the expense of additional surge motion [79].

2.3.3.5 Dublin Offshore (DO) load reduction device

The Dublin Offshore LRD (Figure 5.1b) is distinct from other LRD concepts, as it provides geometric compliance rather than elastic compliance. Thus, its stiffness response has the advantage of being unaffected by the load rate, load history and temperature induced variations which can affect thermoplastics and elastomers. The device provides compliance through a part-weighted, part-buoyant cylinder which rotates under axial load to extend the overall length of mooring line. The restoring force is created by counteracting weight and buoyancy moments Figure 2.23. By varying physical properties of the device such as position of hinges, density of ballast, and length of the device, a wide range of stiffness curves can be obtained, which are not dependent on the strength of the device (determined by the metalwork). Figure 2.23 shows a typical stiffness curve of the device, along with its safe working load, minimum breaking load (SWL, MBL) and serviceability, accidental and ultimate limit states (SLS, ALS, ULS). Similarly to the TFI SeaSpring, the resulting stiffness curve is composed of multiple phases, one initially stiff

phase when the LRD is near vertical, a lower-stiffness phase when the LRD rotates and the incident angle of the mooring line approaches 90 degrees (highest moment on the hinges) and a stiffer 3rd phase as the device approaches full extension.

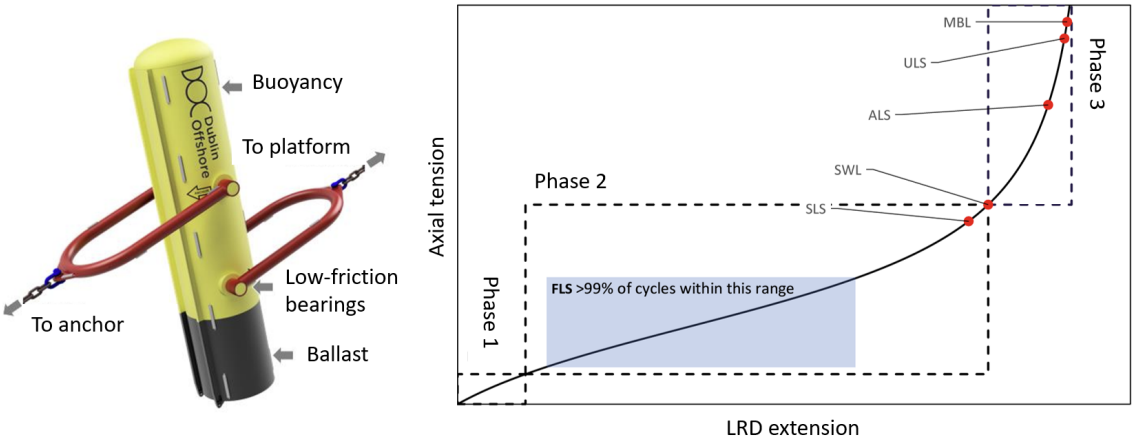

(a) LRD mechanism (b) Typical stiffness curve

FIGURE 2.23: Physical mechanism and stiffness curve of the Dublin Offshore LRD [82]

The Dublin offshore device has recently obtained DNV third-party certification status [83], and is due to be deployed in the Malin Sea project [84].

2.3.4 Summary of challenges and advancements in compliant mooring design

The challenge of delivering compliant mooring systems to FOW has been addressed in this section: the stiffness of traditional catenary or taut mooring systems is inherently coupled to key variables such as water depth or breaking strength of steel chain or polymer rope components. As FOW turbines are often located in shallow waters compared to other permanently moored structures, and are subjected to extreme horizontal wind loads which increase dynamic wave loading, it can be difficult for traditional mooring systems to achieve sufficient compliance as it is not an independent variable.

Load reduction devices provide a solution to this problem, by delivering independent, customisable compliance to mooring systems. These device offer a promising route to reducing anchor loads, mooring lines and overall cost of FOW mooring systems. However, the counterpart to having a customisable source of compliance with a wide range of stiffness curves is that this adds further complexity to an already highly multivariate design problem, and requires careful optimisation to ensure maximum benefit is obtained.

2.4 Design optimisation for FOW mooring systems

2.4.1 Introducing design optimisation in the context of FOW moorings

A traditional mooring design process involves iteratively assessing various combinations of design variables until a design that meets the constraints is found, as shown in Figure 2.24. This guarantees a safe solution, but not necessarily an optimal solution. For instance, in this case, many combinations of chain weight, line length, and anchor radius could satisfy ULS and FLS criteria, but these designs may not perform well with respect to the design objectives listed in Table 2.4. Design optimisation, by definition, is the process of identifying which combination(s) of design variables lead to the optimal solution(s), for one or more optimisation objectives [15].

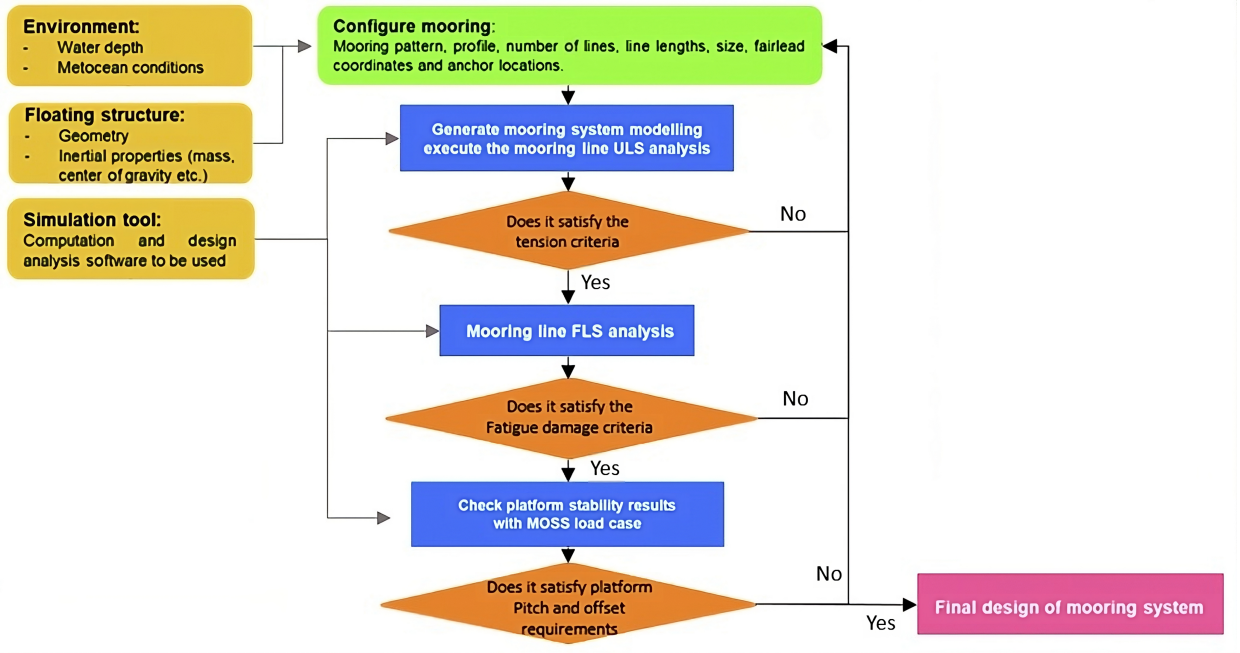

FIGURE 2.24: Traditional iterative mooring design process [85].

In the case of multiple optimisation objectives, which is common in mooring design, these can either be combined into one overall objective through a mathematical formulation, or 'cost function', or optimized separately using the concept of Pareto optimality. Pareto optimality involves finding solutions where no objective can be improved without worsening another, resulting in a set of optimal trade-offs known as the Pareto front [86]. This approach is depicted in Figure 2.25.

Overall, as shown in Figure 2.25, a design optimisation routine requires both a design space of all possible designs (i.e. combinations of design variables, such as (x_1, x_2)), and a model (i.e functions f_1, f_2), that map the designs to their performance in the objective space. In most cases, it is inefficient to model every possible design to generate a complete objective space from which to identify an optimal solution. Instead, an optimisation algorithm is usually employed

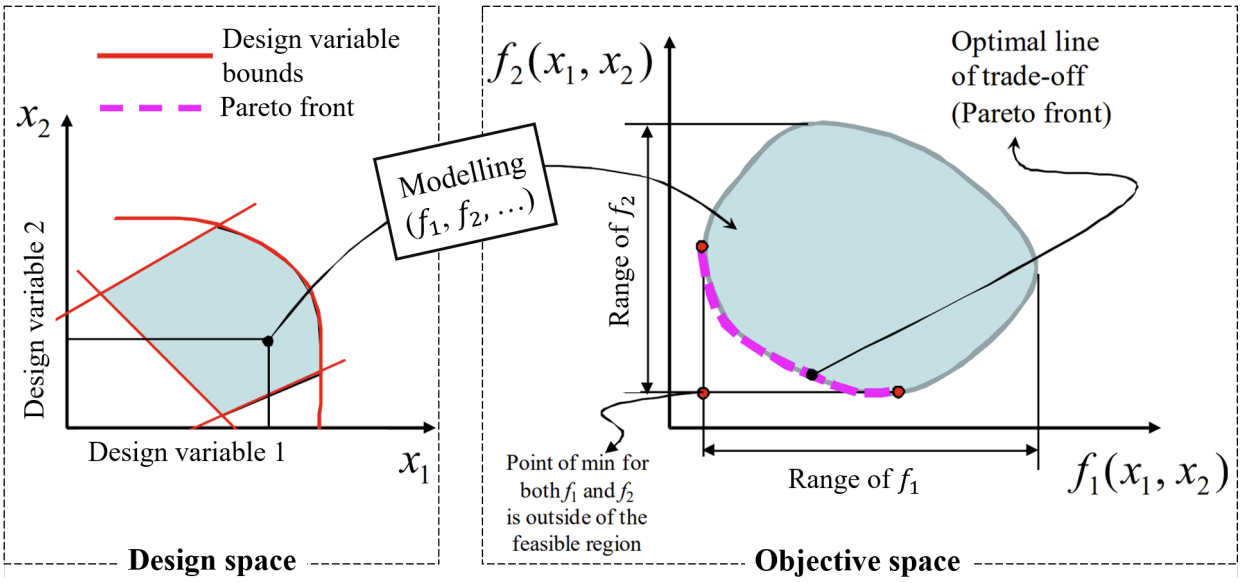

FIGURE 2.25: Overview of typical multi-objective optimisation problem, using the concept of pareto optimality [87] [88].

to identify which individual designs to model based on the performance of previous designs, thus finding an optimal from few points in the objective space.

The design space and objectives for FOW mooring system design have been discussed in sections 2.2 and 2.3 respectively. The next step is to establish a means of modelling designs, which, for mooring systems optimisation, implies finding an efficient and reliable way of assessing mooring line tensions and platform motions for a given design. Obtaining a valid model of the system can be considered the most important step of the optimisation process [86], as it then dictates which optimisation algorithms can be used, and influences the quality of the final result. Section 2.4.2.1 provides an overview of available modelling methods, and their prior applications to FOW mooring design optimisation. Section 2.4.2.5 then discusses optimisation algorithms.

2.4.2 Modelling and optimisation methods for FOW moorings

2.4.2.1 Static and quasi-static analysis

To simplify the analysis of a mooring system, dynamic loads (i.e. damping and inertial forces) on the mooring line can be ignored and environmental loads from wind, waves and current combined into a mean horizontal force acting at the fairlead. All the forces acting on the system are then constant, which means they can be resolved to find the equilibrium position of the mooring lines and platform and the tensions at each point of the mooring line independently of time. This constitutes a static analysis. The static equations can then be incorporated into a 'quasi-static' mooring model. This involves calculating the static equilibrium position of the platform for two or more time-steps, and assuming uniform and linear motion of the system

between consecutive time-steps, giving a simple relationship between axial displacement of the floater (i.e., surge, sway, or heave) and mooring line tension.

Although computationally efficient, the quasi-static modelling approach is limited due to its inability to account for damping and inertia of the mooring system. This is appropriate for slow varying loads and low-frequency platform motions, but is inaccurate when predicting the mooring line response to wave-frequency (WF) loads [34]. Under high-frequency wave excitation, the mooring line would not adopt the static catenary shape, as shown in Figure 2.26 [89]. In general, static and quasi-static analyses under-predict mooring tension due to their inability to capture these high-frequency oscillations, and studies of semi-submersible platforms in the oil & gas industry have shown this under-prediction can be significant during storm events [56]. Nonetheless, offshore engineering standards suggest static and quasi-static analyses as the first step of mooring system design, as long as greater safety factors are used to account for the added uncertainty [90] [91].

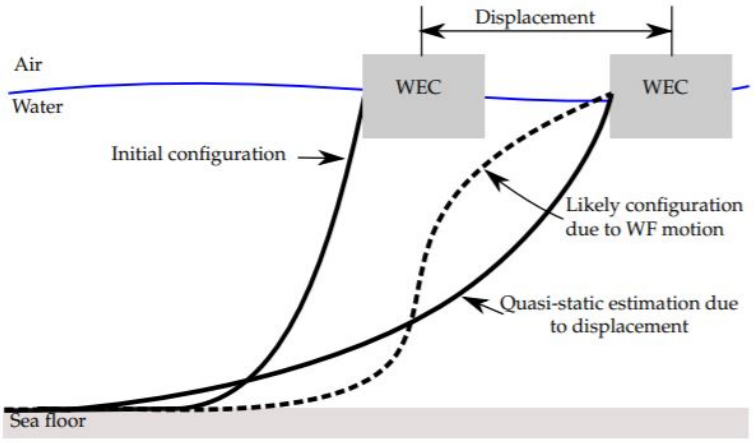

FIGURE 2.26: Comparison of quasi-static mooring profile vs.likely profile if wave-frequency (WF) motions are considered [89].

The computational efficiency of static and quasi-static calculations, which can be as simple as solving a closed-form set of non-linear equations, makes them a viable option for optimisation. Two existing studies have successfully employed quasi-static mooring system models as part of design optimisation routines for FOW moorings [92] [93]. However, these were mainly based on traditional full-chain catenary moorings, with an emphasis on number of lines and configuration rather than novel compliant designs to reduce loads. In fact, whereas quasi-static equations are well-established for traditional full-chain catenary moorings [32], these employ linear elastic stiffness terms, hence not capturing the non-linear extension of LRDs. To enable the use of quasi-static modelling for mooring design optimisation with load reduction devices, novel quasi-static mooring equations for LRDs are derived in Chapter 4, as part of objective O1 of this thesis (see section 1.5).

2.4.2.2 Dynamic modelling

Whereas the previously described methods calculate mooring forces at static equilibrium (Newton's 1st law), dynamic modeling of the mooring line in the time domain is formulated based on Newton's 2nd law of motion, which is inherently time-dependent as it relates acceleration to force and mass. This allows the model to incorporate inertial forces and the effects of fluid-drag, damping, and other nonlinear loads on the mooring line. This leads to complex equations of motion, which cannot be formulated in closed-form and solved analytically for the full system. To simplify the system, dynamic models discretise the line into a kinematic chain of distinct elements and employ numerical methods to approximate solutions to the governing differential equations. The typical format of discretisation is shown in Figure 2.27 [8].

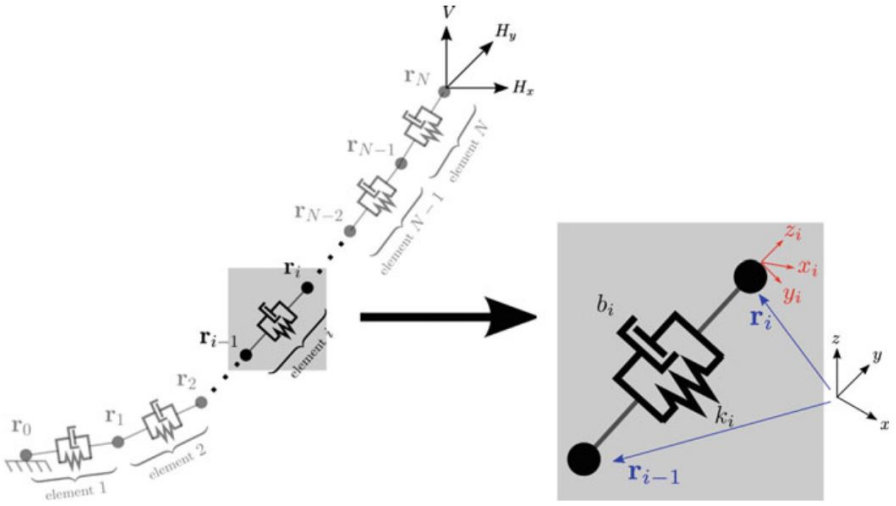

FIGURE 2.27: Representation of mooring line as discrete elastic elements, each with their own kinematic parameters and properties [8]

Figure 2.27 shows the general format of dynamic mooring line modelling. Based on these underlying principles, various models have been developed which employ slightly different techniques. These models can be classified into three main groups [8]:

- Lumped-mass (LM) : all effects of mass, external forces and internal reactions are lumped together at a finite number of nodes, modelling the mooring line as a series of individually concentrated masses linked together by massless springs. This produces a diagonal mass matrix, which typically makes lumped-mass model simulations less computationally-intensive than the two other variations [89].
- Finite-element (FE): whereas the LM model treats the mooring line as a fully discretised system from the start, the FE method uses a continuous formulation of the governing partial differential equations which are then discretised locally. Unlike the LM model, nonadjacent nodes can be coupled. This means the mass matrix can have off-diagonal terms, leading to longer simulation times than LM.

- Finite-difference (FD): uses a Taylor series expansion of the governing partial differential equations. Thus, where FE formulates exact derivatives locally, FD estimates gradients using first-order difference functions.

Several studies suggest that all three types of modelling should converge on identical solutions when given enough resolution [8] [94]. However, when considering lower resolution, the comparison is more nuanced. In terms of mooring line modelling, FE is considered as the most accurate and rigorous option at lower discretisation resolution [94]. Numerical stability is more difficult to achieve in FD methods [8], and the approach is therefore rarely used in commercial mooring software [94]. .

The drawback to these high-fidelity modelling methods is the computational requirement: a dynamic time-domain analysis of a FOW turbine usually requires a 1:1 ratio of computational time to simulated time. which means modelling a single design can take up to 3 hours per load case. For design optimisation, which can require modelling hundreds if not thousands of designs, sometimes for multiple load cases, this is often limiting. While some studies have run optimisation routines directly on time-domain models [95] [96], this limits the number of variables that can be realistically considered. More recent approaches have used low-complexity models to efficiently screen large parts of the design space and remove designs that are bound to perform poorly, using full time-domain simulations only to assess the best candidates [97].

2.4.2.3 Comparison of FOW modelling software

The state-of-the-art modelling methods currently used in the offshore engineering industry and required by certification standards use FE and LM models, usually as part of commercial dynamic analysis software such as Flexcom [98] or Orcaflex [99]. For FOW, these software typically provide full coupling with aerodynamic models of wind turbines, i.e., they integrate the aerodynamic forces and responses of the wind turbine with the hydrodynamic and structural dynamics of the floating platform, and mooring lines, allowing for comprehensive simulations of the entire system.

This subsection compares the capabilities of various codes currently used for FOWT simulations, as a means of assessing how the computational tool used in this research, Flexcom, places itself amongst other similar software.

The assessment of FOWT modelling codes has not been straightforward due to the lack of available physical data to validate against [8]. An international collaboration was initiated by the International Energy Agency (IEA) to establish code-to-code comparisons to examine accuracy and reliability of various models under a fixed set of load cases. This collaborative effort was undertaken in a number of iterations, which included studies on monopile, jacket and spar-buoy offshore wind turbine architectures. The iteration of interest to this research is the

OC4 Phase II, which involves a catenary-moored semi-submersible FOWT. The participants which took part in the numerical code comparison for Phase II are shown in table 2.6.

TABLE 2.6: List of participants in the OC4 phase II numerical code validation, along with the type of model employed for hydrodynamics and mooring. Adapted from [100].

Code	Code developer	OC4 Participant name	Main hydrodynamic approach	Mooring model
CHARM3D + FAST	TAMU + NREL	ABS	Potential flow + Morison	Dynamic (FE)
OPASS + FAST	CENER + NREL	CENER	Potential flow + Morison	Dynamic (LM)
UOU + FAST	UOU + NREL	University of Ulsan	Potential flow + quadratic drag	Quasi-static
Bladed 4.3	GH	GH, CGC, POSTECH	Morison	Quasi-static
OrcaFlex	Orcina	4Subsea	Potential flow + Morison	Dynamic (LM)
Hydro-GAST	NTUA	NTUA	Potential flow + Morison	Dynamic (FE)
Simo+Riflex+AeroDyn	MARINTEK + NREL	CESOS	Potential flow + Morison	Dynamic (FE)
Riflex-Coupled	MARINTEK	MARINTEK	Potential flow + Morison	Dynamic (FE)
3Dfloat	IFE-UMB	IFE	Morison	Dynamic (FE)
DeepLinesWT	PRINCIPIA-IFPEN	PRINCIPIA	Potential flow + Morison	Dynamic (FE)
Flexcom	*Wood group*	*n/a*	*Potential flow + Morison*	*Dynamic (FE)*

Flexcom did not take part in this code comparison, but is included at the end of table 2.6 to situate its modelling approach amongst others. As highlighted in the table, the majority of participants employed a dynamic mooring module, as well as both potential flow theory and Morison equations to model hydrodynamics. The results of the codes for a regular wave load case (no wind) are shown in figure 2.28.

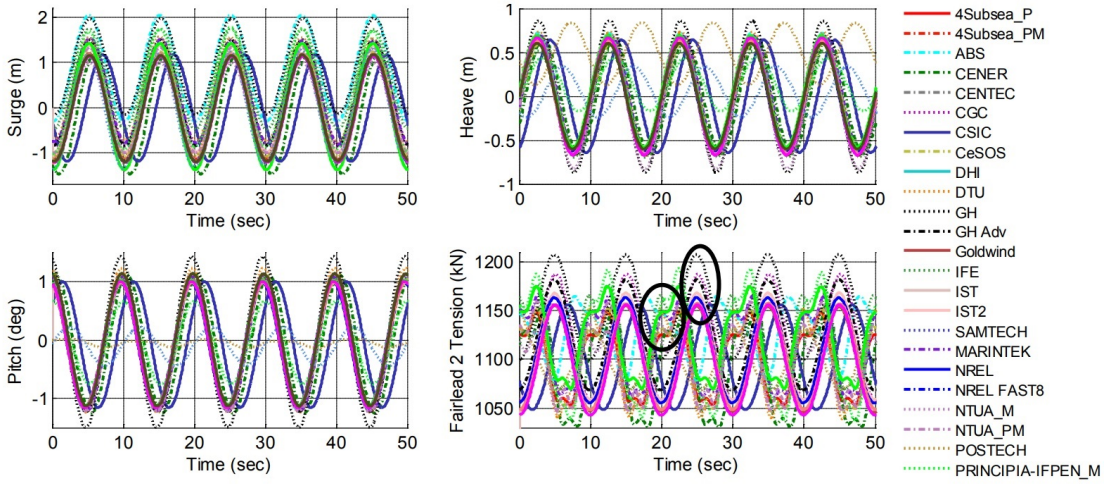

FIGURE 2.28: OC4 results for regular wave simulation, H = 6 m, T = 10 s [100]

Several inferences can be made from the graphs in figure 2.28, which are summarised in the points below. It should be noted that these trends were also apparent in other load cases and thus constitute valid outcomes for the code comparison as a whole [100]:

- *Surge*: significant differences in platform excursion. The codes that display an unrealistic zero-mean oscillation do not take wave drift forces into account .
- *Pitch*: Morison-only codes display an over-predicted pitch amplitude, with pitch frequency similar across all codes.

- *Heave*: Morison-only codes which are not augmented to calculate the dynamic pressure at the base of the columns (e.g. POSTECH) present inconsistent and under-predicted heave results.
- *Fairlead tension*: Clear disparities depending on the mooring model employed. Results from quasi-static models are out of phase and do not include any frequencies in the response beyond those of the waves. The two different responses are circled in black on the graph.

Overall, codes with a dynamic mooring model as well as a hydrodynamic approach consisting of both P.F. theory and Morison hydrodynamics, such as Flexcom, were generally in better agreement and provided more realistic results based on the findings from the OC4 study [100]. Flexom has since taken part in a later offshore code collaboration validation campaign also led by NREL, the OC6, in which it performed strongly, in agreement with other state-of-the-art modelling software such as FAST and Orcaflex [101].

2.4.2.4 Surrogate modelling

The high-fidelity dynamic modelling software described in section , although most accurate, is computationally intensive and unsuitable for concept design optimisation over a large design space. In general, employing physics-based approaches to modelling mooring lines, integrated directly into mooring design optimisation routines (as set out in Sections 2.4.2.1 and 2.4.2.2) involves compromising on either: (a) the complexity of the physics, e.g. by using quasi-static modelling, or (b) the complexity of the optimisation problem. e.g. reducing the number of design variables or objectives to enable dynamic time-domain analyses.

Surrogate modelling is an increasingly commonly used numerical technique which can capture maximum complexity of both the modelling and the optimisation problem, in feasible computational time [86]. Surrogate models serve as simplified approximations of complex systems, enabling efficient analysis of problems where direct computation is impractical. Fundamentally, the simplest forms of surrogate models could range from basic line fits through data points, capturing the underlying trend with minimal complexity, to more complex 3D polynomials or other mathematical functions [53]. However, machine learning provides an effective tool for creation of surrogate models with multiple and complex interacting variables. Machine learning based surrogate models are particularly useful when the relationship between inputs and outputs is not well understood or is computationally expensive to evaluate. Examples of surrogate modeling methods include:

- Random-forest (RF): many decision trees, i.e. simple models that make decisions based on input data, are trained from a dataset. When making a prediction, the method looks at the results from all the trees and chooses the most common answer (for classification tasks) or

the average result (for regression). Random forests are robust against errors that can occur from a single model, and can handle large datasets with higher dimensionality efficiently.

- Artificial Neural Networks (ANNs): ANNs are computational models inspired by the human brain, consisting of interconnected groups of artificial neurons. They are capable of capturing complex nonlinear relationships in data through layers of nodes, each applying a nonlinear transformation to its inputs.

Both of these surrogate modelling techniques have been employed for FOW mooring design optimisation ([102] and [17] respectively), and can replicate the results produced by dynamic time-domain modelling of the mooring system, at reduced computational cost.

2.4.2.5 Optimisation methods

If the modelling methods used in the optimisation routine are sufficiently fast, and the design and objective spaces are sufficiently small, the full design space can be mapped systematically to the full objective space, using discrete variables which makes finding an optimal solution trivial (e.g. [92]). This is an example of an exact optimisation method, often referred to 'brute-force' optimisation (BFO), which guarantees the solution is optimal over the full design space [103].

On the other hand, 'approximate' optimisation methods contrast with 'exact' methods by using random variables and probabilistic decisions to explore the design space, aiming to find a good solution without evaluating every possibility. In most cases, approximate methods are preferred over exact methods due to their efficiency. However, approximate optimisation algorithms are typically more complex to build, as they require careful selection of designs to assess from the design space, to get to the optimal regions of the objective space most efficiently. The main examples of approximate optimisation algorithms are:

- Heuristic: These methods use practical strategies to find good-enough solutions quickly without guaranteeing the best possible outcome. The Nelder-Mead (NM) algorithm is an example that adjusts a set of potential solutions to converge on a local minimum, making it useful for problems where precise calculations are difficult or unnecessary.
- Meta-heuristic: These are advanced strategies that guide other heuristics to explore complex search spaces effectively. Examples include: Genetic Algorithms (GA), which mimic natural selection by evolving solutions over time; Differential Evolution (DE), which optimises by iteratively improving candidate solutions based on the differences between them; and Particle Swarm Optimisation (PSO), which simulates social behaviors to collaboratively search for the best solution. Meta-heuristic methods are designed to efficiently navigate large and complicated problem spaces.

Both heuristic (e.g. Nelder-Mead [93]) and meta-heuristic (e.g. GAs [104] [16]) optimisation algorithms have been commonly used for mooring design optimisation. In theory, any of the

optimisation methods discussed in this section are suitable for mooring design optimisation. However, each method has particular strengths and weaknesses that are problem-dependent, making some more suitable depending on the problem formulation and the computational efficiency of the model used to evaluate the objective function. Table 2.7 summarises the optimisation methods and their performance across various problem characteristics, including multiple objectives, constraints, and computational intensity [15] [86].

In this research, computational intensity is not a limiting factor, as a key focus is the development of a highly efficient surrogate model capable of evaluating the objective function quasi-instantaneously. Consequently, methods with higher computational intensity were preferred, particularly because they are better suited for handling constraints and multiple objectives, which are central to this research. A grid search algorithm was used for single-objective constrained optimisation, while a genetic algorithm was used for multi-objective optimisation.

TABLE 2.7: Comparison of the strengths and weaknesses of various optimisation methods used in offshore engineering design, sorted from lowest to highest computationally intensity [15] [86].

Optimisation method	**Description**	**Handling of multiple objectives**	**Handling of constraints**	**Computational intensity**
Nelder-Mead (NM)	A simplex-based method for finding a local minimum of a function.	Poor	Poor	Low
Particle Swarm Optimisation (PSO)	Nature-inspired algorithm simulating social behavior of bird flocking or fish schooling.	Good	Good	Moderate
Differential Evolution (DE)	Population-based optimisation algorithm using vector differences for perturbation.	Good	Good	Moderate to High
Genetic Algorithm (GA)	Evolutionary algorithm inspired by natural selection and genetics.	Very Good	Very Good	Moderate to High
Grid Search Optimisation (GSO)	Exhaustive search evaluating every possible solution in the search space.	Very Good	Very Good	Extremely High

2.4.3 Summary of existing mooring design optimisation for FOW

All aforementioned studies on mooring system optimisation for FOW, which provide a comprehensive cover of the literature, are listed in Table 2.8, along with the mooring design variables and optimisation objectives considered.

From the existing literature, the following can be summarised:

- Existing studies have not considered load reduction devices as part of the design variables. Various mooring line materials have been considered [102], but these only included polymer ropes for weight-saving benefits rather than load reduction.

- Geometric mooring design variables have been considered by all studies. However, only design variables have been parameterised – location-specific variables such as environmental loads and water depth have been fixed, i.e. have not been made available as user inputs.

TABLE 2.8: Comprehensive summary of FOW mooring optimisation literature. Mooring models are either quasi-static (QS) or dynamic (Dyn), and sometimes assisted by a surrogate (S'gate). Optimisation algorithms used are Nelder-Mead (NM), Genetic Algorithms (GA), and differential evolution (DE).

	Mooring design variables				**Optmisation objectives**					**Mooring model**	**Opti. algorithm**
Ref.	Anchor position	Line length	Line angle	Line type	Cost	Mooring Footprint	Weight	Fatigue	Nacelle acc.		
[92]	x	x	x		x		x			QS	none
[93]	x	x	x			x				QS	NM
[104]	x	x			x				x	QS + Dyn	GA
[102]	x	x	x	x	x			x		Dyn	GA
[105]	x	x		x	x	x				Dyn + S'gate	GA
[17]	x	x		x			x			Dyn + S'gate	DE

2.5 Literature review summary

The conservatism in current mooring system designs, presented in section 2.1.4, combined with the importance of minimising mooring line and anchor loads, presented in section 2.2, forms a strong basis for optimisation of mooring system compliance. The new design space offered by LRDs, discussed in section 2.3, shows potential for enabling this optimisation, as sufficient compliance for FOW is not always possible with traditional mooring systems. Finally, existing approaches to mooring design optimisation were reviewed, discussing which are most suitable for this research (Section 2.4).

Overall, this review of the literature has identified three main gaps, which will be addressed by objectives O1, O2 and O3 in chapters 4, 5 and 6 respectively:

1. No quasi-static equations for moorings with LRDs exist in the public domain, even though quasi-static analysis is a key part of the early-stage design process.
2. No comprehensive comparison of LRD stiffness curves has been performed for FOW. Existing research has been mostly from LRD developers, and thus provide little opportunity for comparison across concepts and their characteristic curves.
3. No FOW optimisation studies have included LRDs in their design space. Additionally, their methodologies are not directly suited to LRDs, which, due to their configurability, could benefit from a more flexible approach to optimisation, with a wider range of objectives and constraints.

Further critical analysis on each of these gaps is given in each individual chapter, in sections 4.1.3, 5.1.2 and 6.1.2 respectively.

Chapter 3

Methods

3.1 Overview

The research work conducted for this thesis was entirely computational, and is based on a range of methods including mathematical and analytical modelling, numerical modelling and machine learning. This chapter outlines these computational methods, for both the physics-based modelling of FOW structures and the machine-learning models and algorithms for design optimisation. A full description of each method and how it was used is given in each individual chapter.

3.2 Physics-based computational modelling methods

3.2.1 Analytical model for quasi-static analysis

The analytical model presented in Chapter 4 was built in Python 3.8, using the following packages: Numpy for general mathematical operations and data pipelines [106], Scipy for symbolic equations and solvers [107], and Matplotlib for plotting and visualisation [108].

3.2.2 Commercial software for dynamic finite element analysis

The numerical modelling of the floater, turbine and mooring system was performed using Flexcom, a commercial finite element (FE) software. Flexcom offers fully-coupled aero-hydro-servo modelling using FAST plug-ins INFLOWWIND, AERODYN and SERVODYN, and has been validated against other commercial and academic software for a 5 MW turbine as part of an offshore code collaboration project [109]. The FOWT model used in this study is composed of the International Energy Agency (IEA) reference 15 MW wind turbine on the Volturn-US semi-submersible floating platform, and has been validated against the FAST

model in Flexcom documentation [98]. The full platform and turbine characteristics are described in detail in publications from the National Renewable Energy Laboratory (NREL) [110],[111]. All dynamic modelling was performed on an 18-core i9-10980 CPU.

3.3 Machine learning and optimisation methods

3.3.1 Artificial neural-network based surrogate modelling

The artificial neural networks (ANNs) used for surogate modelling were built and trained using the Keras Python toolbox [112], with GPU-accelerated TensorFlow support [113] on a NVIDIA 3080ti graphics GPU (laptop version).

3.3.2 Optimisation algorithms

All optimisation algorithms were also constructed in Python 3.8. The 3D surface optimisation plots were constructed using matplotlib, while the genetic algorithms were built using the python multi-objective opimisation toolbox PYMOO [114].

Chapter 4

Quasi-static modelling of mooring systems with load reduction devices

4.1 Background

4.1.1 Purpose of quasi-static modelling

Quasi-static modelling solves the static equilibrium of a mooring system at discrete time steps, neglecting inertial and hydrodynamic effects, to efficiently calculate mooring line tensions and positions. This constitutes a computationally efficient method for screening mooring concepts and visualising design options, and has been commonly used in the offshore industry for decades, to facilitate early-stage design iterations, supporting the comparison of mooring layouts, line properties, and anchor positions before progressing to detailed dynamic simulations. It enables rapid evaluation of key performance metrics such as maximum restoring forces and their horizontal and vertical components, surge limits, and tension-offset response (i.e. mooring stiffness). While it does not capture full dynamic behavior, quasi-static modelling offers a reasonable approximation of system response, balancing accuracy and computational efficiency.

4.1.2 Incorporating LRDs in a quasi-static model

Currently, no analytical quasi-static model in the public domain incorporate LRDs, and existing models cannot account for the highly non-linearity stiffness curves of LRDs. The highly non-linear stiffness curves of load reduction devices (LRDs), as shown in Figure 2.18, Figure 2.21, and Figure 2.23, can be tailored to fit specific loading conditions and mooring configurations (see section 2.3.3 for background). These non-linear stiffness curves have a compliant range over which the LRD is intended to operate to effectively reduce mooring line tension. For all LRD technologies, stiffness curves exhibit higher stiffness at high extension

when they reach their rated tension T_{rated}, which is defined in this study as an arbitrary design limit at which the compliance in the LRD has been exhausted. DO and TFI refer to the rated tension as the 'Safe Working Load' and 'Target Load' respectively. In practice, these different rated tensions are obtainable by changing the dimensions and/or material properties of the LRD. Higher rated tensions often apply to locations with more severe environmental loading, which typically require higher MBLs, but the LRD's MBL and rated tension are not inherently coupled. The MBL of the LRD can be can be adjusted to whichever value meets safety requirements, whereas the rated tension is a separate design variable which drives performance of the device. Graphical representation of the rated tension is shown for the IMS, DO and TFI LRDs in Figure 4.1.

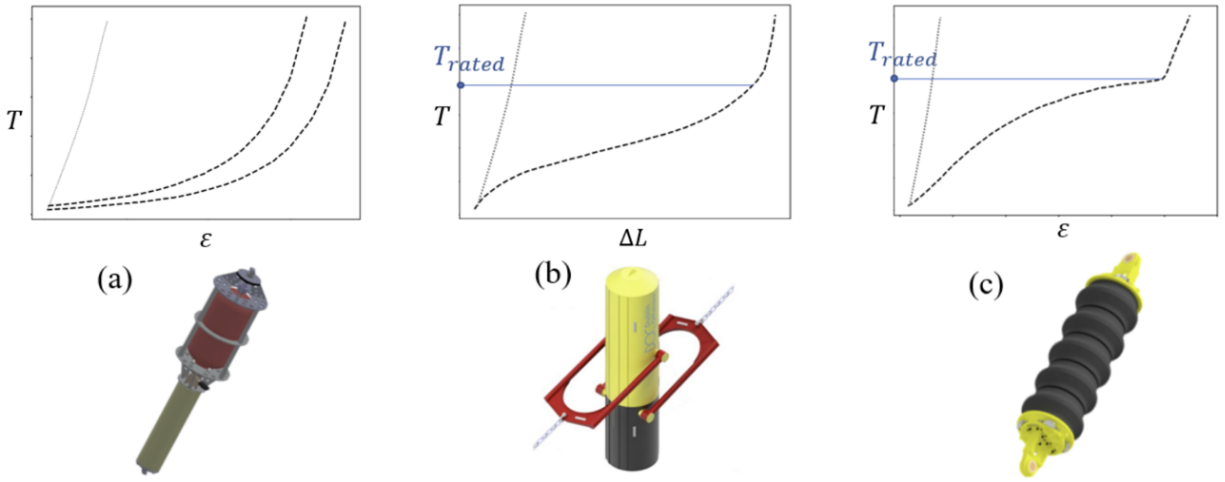

FIGURE 4.1: LRD technologies and associated stiffness curves: (a) IMS, (b) DO, (c) TFI. Stiffness of typical polymer rope is shown on dotted grey line for comparison [66].

The key to designing a mooring system with an LRD is to ensure the device operates in its compliant range as much as possible, i.e., to ensure the maximum tension in the device stays below T_{rated}. The optimal length of the LRD should then be determined to ensure the extension provided does not exceed station-keeping constraints. As discussed in section 2.4, this can form a complex design problem, which is currently solved with time consuming iterations of Finite Element (FE) analyses, as no quasi-static models support the non-linearity of the LRDs.

Current approaches to modelling moorings with LRDs include discretisation of the mooring lines and/or piece-wise linear interpolation of the non-linear stiffness curves. Commercial software such as Orcaflex is typically used for dynamic modelling of LRDs [11], which uses linear interpolation between consecutive points of the user-defined non-linear stiffness curve. LRDs have also been modelled with the open-source lumped-mass (LM) modelling software Moordyn, which also uses linear interpolation of the stiffness curve [50]. Although FE and LM these are reliable modeling solutions, these are computationally intensive to set-up and run. Incorporating LRDs in a quasi-static model would provide a cheaper and more efficient means of screening many LRD lengths, rated tensions and stiffness curve types at an early design stage.

4.1.3 Review of established quasi-static methods

If dynamic mooring effects, i.e. damping and inertia, are ignored, and the system is assumed to be static at a given instant t, the geometry of the mooring line can be solved analytically as a function of the fairlead coordinates (i.e. the position of the upper extremity of the mooring line) and the physical parameters of the mooring line.

For neutrally buoyant taut moorings, the relationship between fairlead coordinates and restoring forces is trivial: the mooring line adopts a straight line between the fairlead and anchor, and the tension-offset of the system corresponds directly to the material stiffness of the mooring line [115]. This relationship is more complex for catenary moorings, as the catenary shape (due to weight of suspended line) is controlled by tension, leading to a non-linear tension-offset profile. This is captured by the catenary mooring equations, which define the fairlead coordinates x_f and z_f as a function of the fairlead restoring forces H_f and V_f [116] and the mooring line length L, stiffness EA and unit weight w (Figure 4.4). For a line partially resting on a flat and friction-less seabed:

$$x_f(H_f, V_f) = L - \frac{V_f}{w} + \frac{H_f}{w} \cdot \ln\left[\frac{V_f}{H_f} + \sqrt{1 + \left(\frac{V_f}{H_f}\right)^2}\right] + \frac{H_f L}{EA} \tag{4.1a}$$

$$z_f(H_f, V_f) = \frac{H_f}{w} \cdot \left[\sqrt{1 + \left(\frac{V_f}{H_f}\right)^2} - 1\right] + \frac{V_f^2}{2EAw} \tag{4.1b}$$

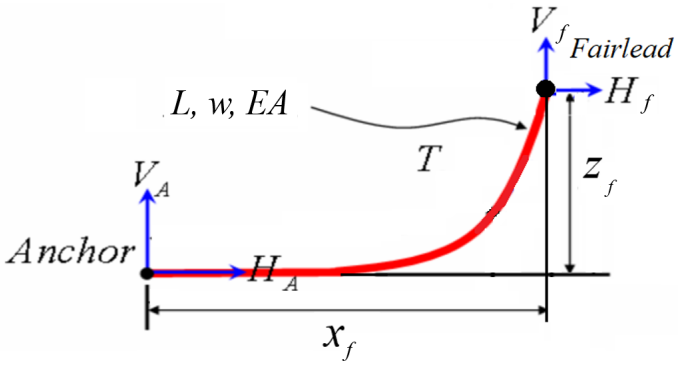

FIGURE 4.2: Profile view of simple catenary mooring line

The system of equations 4.1a & 4.1b can then be solved for any two unknowns. However, this is only valid for a homogeneous mooring line (i.e. full chain), and the stiffness term EA must be linear. As such, these equations cannot be used for analysis of a mooring system with a non-linear LRD. Other publications have presented equations for multi-segmented catenary mooring lines with a non-linear stiffness segment, in particular for polymer rope applications [115]. For this application, the non-linear stiffness is expressed in simple power law form, where the strain ε is given as a function of axial load T and constants p and q :

$$\varepsilon = pT^q \tag{4.2}$$

The power law form offers a good fit for material stiffness of typical synthetic polymer ropes, but this would not be suitable for the more complex stiffness curves shown in Figure 4.1.

4.1.4 Research objective

In line with objective O1 (see section 1.5), this chapter presents continuous functions which model the non-linear stiffness curves of the LRD devices shown in Figure 4.1. These functions are then combined with the existing equations for catenary moorings, to create a static analytical model of catenary moorings with LRDs. This requires no discretisation or stiffness interpolation, and as such provides a quicker approach to obtain the mooring geometry and restoring forces based on any input mooring properties and LRD parameters (rated tension, curve shape, LRD length). The analytical model can then be used to find optimal LRD parameters for any given water-depth, mean environmental load, and offset constraint.

4.2 Methodology

This research employs an analytical approach to mooring systems modelling. Firstly, a 2-segment formulation for a catenary mooring line with a linear-stiffness LRD at the fairlead is presented based on established equations. This formulation is then adapted with various non-linear stiffness functions, to form a set of equations for a chain catenary line with non-linear LRDs. These are solved using numerical root-finding methods, in particular the Newton-Raphson method [117], implemented in Python. Commercial FE software Flexcom is then used to validate the results obtained from the analytical equations. The validated analytical model is then applied to initial quasi-static design of an LRD. A structural overview of the methodology employed to develop the quasi-static model presented in this chapter is shown in Figure 4.3.

4.3 Development of quasi-static model

4.3.1 Catenary equations for 2-segment line

The static catenary equations 4.1a & 4.1b apply to a catenary line formed of a unique, homogeneous segment, with material properties defined by a single value of stiffness EA and apparent weight in water per unit length w. This section presents an adapted formulation for a mooring line with two distinct segments: one segment for the chain catenary line and one

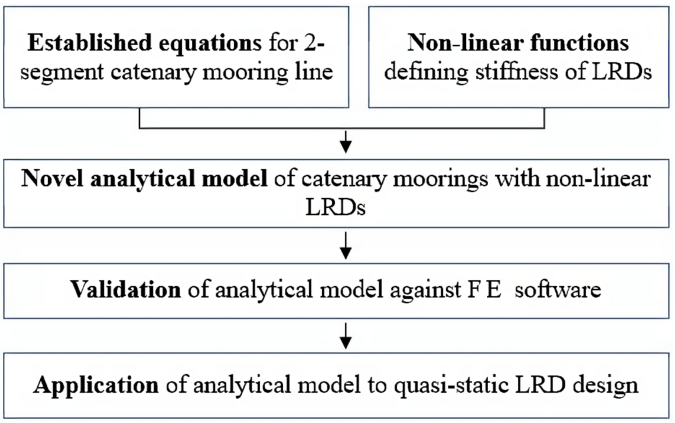

FIGURE 4.3: Methodology for the analytical solution

segment for a linear stiffness LRD at the fairlead (Fig. 4.4). This linear LRD formulation is then used as the starting point for the next section, which presents the equation for non-linear stiffness LRDs.

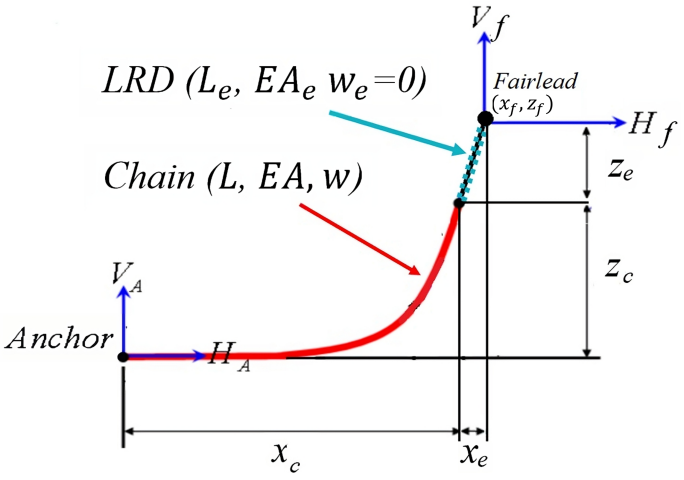

FIGURE 4.4: Profile view of the multisegment line

The static multi-segment mooring analysis approach is well-documented in literature [115]. For a catenary line composed of n segments of line, the fairlead coordinates (x_f, z_f) are given as a sum of the horizontal and vertical components of each segment:

$$x_f = \sum_{i=1}^{n} x_i \tag{4.3a}$$

$$z_f = \sum_{i=1}^{n} z_i \tag{4.3b}$$

Where the coordinates of the extremities of the i^{th} segment x_i and z_i are each defined by the catenary equations in their own coordinate system, with the origin at the start of the segment (starting from the anchor).

If the LRD is modelled as a simple non-linear spring segment, and assumed to be near-neutrally buoyant in water, which is typically the case of the IMS and DO technologies [69][13], this means the spring is subjected to constant tension throughout its length, thus adopting a straight line rather than a catenary shape. For a linear stiffness LRD, its extension ΔL_e is based on Hooke's law, where the tension-strain profile is a straight line passing through the origin and a single point EA. The coordinates of the horizontal and vertical extremities of the LRD segment (x_e, z_e) are then given by:

$$x_e = \frac{H_f l_e}{\sqrt{H_f^2 + V_f^2}} + \frac{H_f L_e}{EA_e} \tag{4.4a}$$

$$z_e = \frac{V_f l_e}{\sqrt{H_f^2 + V_f^2}} + \frac{V_f L_e}{EA_e} \tag{4.4b}$$

Where the first terms represent the horizontal (4.4a) or vertical (4.4b) projections of the unstretched length L_e of the LRD, and the second terms represent the elongation of the LRD, obeying Hooke's law.

According to the multisegment theory from equations 4.3a & 4.3b, equations 4.4a & 4.4b can be added to the chain catenary equations to give the coordinates of the fairlead (x_f, z_f) as a function of the restoring forces (H_f, V_f):

$$x_f(H_f, V_f) = L - \frac{V_f}{w} + \frac{H_f}{w} \cdot \ln\left[\frac{V_f}{H_f} + \sqrt{1 + \left(\frac{V_f}{H_f}\right)^2}\right] + \frac{H_f L}{EA} + \frac{H_f L_e}{\sqrt{H_f^2 + V_f^2}} + \frac{H_f L_e}{EA_e} \tag{4.5a}$$

$$z_f(H_f, V_f) = \frac{H_f}{w} \cdot \left[\sqrt{1 + \left(\frac{V_f}{H_f}\right)^2} - 1\right] + \frac{V_f^2}{2EAw} + \frac{V_f L_e}{\sqrt{H_f^2 + V_f^2}} + \frac{V_f L_e}{EA_e} \tag{4.5b}$$

4.3.2 Catenary equations for non-linear stiffness LRDs

To replace the Hookean extension term in equations 4.4a & 4.4b, the non-linear extension of the LRD must be defined as a function of the force applied at its extremities. This means determining the function ε which gives the LRD strain for any value of axial mooring line tension T, where T is the resultant of the horizontal and vertical mooring line forces H_f and V_f :

$$\varepsilon(T) = \varepsilon(\sqrt{H_f^2 + V_f^2}) = \frac{\Delta L_e}{L_e} \tag{4.6}$$

Equations analogous to 4.5a and 4.5b can be obtained by substituting the Hookean extension term (the final term in equations 4.5a & 4.5b) with the non-linear strain function ε, giving:

$$x_f(H_f, V_f) = L - \frac{V_f}{w} + \frac{H_f}{w} \cdot \ln\left[\frac{V_f}{H_f} + \sqrt{1 + \left(\frac{V_f}{H_f}\right)^2}\right] + \frac{H_f L}{EA} + \frac{H_f L_e}{\sqrt{H_f^2 + V_f^2}}(1 + \varepsilon(T)) \tag{4.7a}$$

$$z_f(H_f, V_f) = \frac{H_f}{w} \cdot \left[\sqrt{1 + \left(\frac{V_f}{H_f}\right)^2} - 1\right] + \frac{V_f^2}{2EAw} + \frac{V_f L_e}{\sqrt{H_f^2 + V_f^2}}(1 + \varepsilon(T)) \tag{4.7b}$$

These equations are valid for an extensible section located at the fairlead, attached to a homogeneous catenary mooring line with a portion resting on the seabed (i.e. no vertical loading on the anchor), where seabed friction is neglected. An analogous expression can also be derived for non-buoyant taut and semi-taut moorings where vertical anchor loading is non-zero, based on the equations for a fully-suspended line [116].

Equations 4.4a & 4.4b assume that the extensible section is neutrally buoyant in seawater. This is a valid assumption for the IMS and DO devices, but the TFI device has a non-negligible weight in water [50]. This means the upper extremity of the LRD is subjected to additional tension due to self-weight of the device, with a difference in vertical tension between the two extremities equal to $L_e w_e$ where L_e is the length of the device and w_e is its wet weight per unit length. Due to this difference in tension, the strain of the LRD is not constant along its length, and requires an integral to compute analytically. As a simpler approximation, the tension can be assumed to be constant throughout the LRD, taking the value of the tension at its midpoint, which is subjected to half of the self weight of the LRD: $\frac{1}{2} L_e w_e$. With this assumption, the strain in the device given by Equation 4.6 can be redefined as:

$$\varepsilon(T) = \varepsilon\left(\sqrt{H_f^2 + (V_f - \frac{1}{2} L_e w_e)^2}\right) \tag{4.8}$$

The chain section of the line, which is below the LRD, is not subjected to the additional vertical tension component. Thus, we define the component of vertical tension at the top chain as V_{tc} which does not include the self weight, and is given by $V_{tc} = V_f - L_e w_e$. The full expression is then given by:

$$x_f(H_f, V_f) = L - \frac{V_{tc}}{w} + \frac{H_f}{w} \cdot \ln\left[\frac{V_{tc}}{H_f} + \sqrt{1 + \left(\frac{V_{tc}}{H_f}\right)^2}\right] + \frac{H_f L}{EA} + \frac{H_f L_e}{\sqrt{H_f^2 + (V_f - \frac{1}{2}L_e w_e)^2}}(1 + \varepsilon(T)) \tag{4.9a}$$

$$z_f(H_f, V_f) = \frac{H_f}{w} \cdot \left[\sqrt{1 + \left(\frac{V_f}{H_f}\right)^2} - 1\right] + \frac{V_f^2}{2EAw} + \frac{(V_f - \frac{1}{2}L_e w_e)L_e}{\sqrt{H_f^2 + (V_f - \frac{1}{2}L_e w_e)^2}}(1 + \varepsilon(T)) \tag{4.9b}$$

4.3.3 Continuous functions for LRD stiffness curves

4.3.3.1 The Ramberg-Osgood model

Adapting the general-form equations 4.7a & 4.7b or 4.9a & 4.9b to a specific LRD technology requires determining the function $\varepsilon(T)$ which gives LRD strain as a function of axial tension T. In this section, functions have been derived for the three curve types shown in Figure 4.1. These functions are mostly based on the Ramberg-Osgood model, which is typically used to define non-linear stress-strain relationships. The original model defines stress as a function of strain and 3 parameters [118]. In this case, the model is used only in its mathematical sense, and the form is reversed to define strain ε as a function of axial tension T such that it can be incorporated into the catenary equations. This adaptation of the basic-form Ramberg-Osgood model can be given as:

$$\varepsilon(T) = \frac{aT}{(1 + (\frac{aT}{c})^n)^{\frac{1}{n}}} \tag{4.10}$$

Where a, c and define the shape of the curve (Figure 4.5).

The basic form equation of the Ramberg-Osgood model given in Equation 4.10, does not directly fit all of the LRD devices identified in Figure 4.1, in particular the TFI and DO LRDs which require additional terms and parameters. These variations of the basic form equation are described in the following subsections.

4.3.3.2 IMS stiffness expression

The curve of the IMS is the closest fit to the Ramberg-Osgood model, with the exception of the curve not passing through the origin due to variable pre-load in the device [69]. An additional

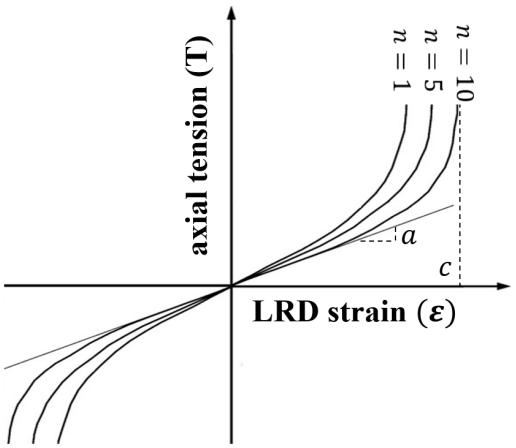

FIGURE 4.5: Basic-form Ramberg-Osgood curve

parameter b is introduced, which shifts the curve along the x-axis from the origin, such that the overall equation is given by:

$$\varepsilon_{IMS}(T) = \frac{aT - b}{(1 + (\frac{aT-b}{c})^n)^{\frac{1}{n}}} \tag{4.11}$$

Where b/a is the pre-tension, c is the asymptotic strain, and n is a parameter defining the rate at which the curve reaches its asymptotic strain, as shown in Figure 4.5. The value of n can be found if the rated tension required at a specific value of strain is known. The parameters of Equation 4.11 are fitted to two example supplier curves [69], using a simple linear regression algorithm, and the resulting curve fits are plotted in Figure 4.6. The values of each fitted parameter are given in Table 4.1, for curves A and B.

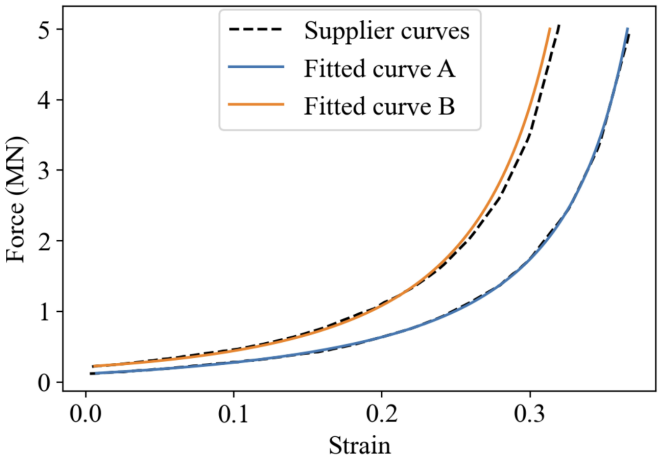

FIGURE 4.6: IMS stiffness curves from supplier publication [69], against fitted curve from Eq. 4.11

TABLE 4.1: IMS fitted parameters for Eq. 4.11

Parameter	fitted value (A)	fitted value (B)
a	0.958	0.837
b	0.113	0.183
c	0.426	0.396
n	0.834	0.728

4.3.3.3 DO stiffness expression

To obtain an expression of the DO curve, the base curve from Figure 4.5 is translated with an additional parameter b, as with the IMS fit. However, the DO curve must pass through the origin, which is not the case of the IMS curve in Eq. 4.11. To ensure that the DO curve passes through the origin, an additional term shown in Eq. 4.12 is subtracted from Eq. 4.11, giving the final expression of $\Delta L_{Dublin}(T)$ shown in Eq. 4.13.

$$\frac{-b}{(1+(\frac{b}{c})^n)^{\frac{1}{n}}} \tag{4.12}$$

$$\Delta L_{Dublin}(T) = \frac{aT-b}{(1+(\frac{aT-b}{c})^2)^{\frac{1}{2}}} + \frac{b}{(1+(\frac{b}{c})^2)^{\frac{1}{2}}} \tag{4.13}$$

The shape factor n, which defines the rate at at which the function reaches its asymptote, is fixed to $n = 2$. The parameters a, b and c of Equation 4.13 are fitted to the example curve from supplier documentation [13] using linear regression, resulting in the curve fit shown in Figure 4.7. The values of each fitted parameter for this curve are given in Table 4.2.

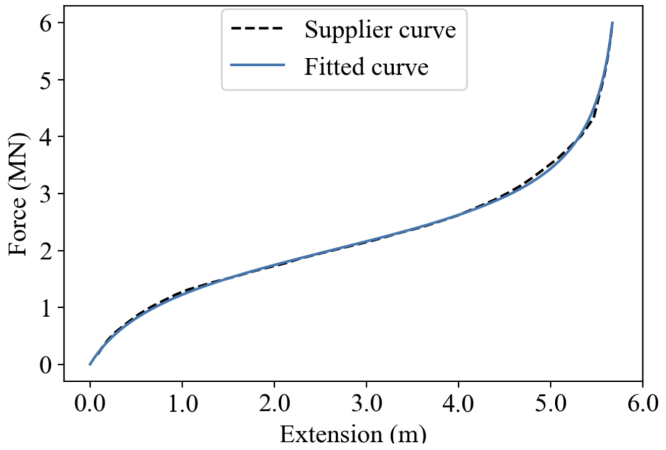

FIGURE 4.7: DO stiffness curve from supplier publication [13], against fitted curve from Eq. 4.13

In Eq. 4.13, parameter a is related to the rated tension of the device and c is related to the asymptotic extension of the device. These parameters can also be linked to physical dimensions of the device, based on supplier publications [13]. As opposed to the IMS and TFI devices which

TABLE 4.2: DO fitted parameters for EQ. 4.13

Parameter	fitted value
a	7.500
b	7.432
c	2.568

are spring-like, the DO LRD extends by rotating under loading (Figure 4.1b). Thus, extension $\Delta L(T)$ is used rather than the strain term $\varepsilon(T)$. When incorporated into the final system of static equations 4.7a & 4.7b, the length of device *Le* can then be based on the starting distance between the two hinge points. It should also be noted that Eq 4.13 is only valid for a fixed mooring line angle. The line angle affects the magnitude of the moment generated by the mooring line on the LRD hinges, in turn changing the shape of the stiffness curve

4.3.3.4 TFI stiffness expression

The TFI stiffness curve is complex to model with a continuous function due to the sudden stiffness increase at $T = T_{rated}$ (see Figure 4.1). The required function deviates more significantly from the base Ramberg-Osgood model, in three ways: 1. Parameter c is subtracted to the denominator of the first term to create the sudden gradient change; 2. An additional parameter k is introduced to factorise the whole expression, such that the rated strain of the curve can be directly adjusted without changing the other parameters; 3. An additional term is introduced, function of a new parameter d, in an attempt to better match the final phase stiffness. The resulting expression is given in Eq. 4.14, with the associated curve fit is shown in Figure 4.8, and the fitted parameter values given in Table 4.3.

$$\varepsilon_{TFI}(T) = k \cdot \left(\frac{a(eT-f)-b}{1+[a(eT-f)-b-c]^2} + \frac{af+b}{1+[-af-b-c]^2} + d\sqrt{a(eT-f)} - d\sqrt{-af} \right) \tag{4.14}$$

The fit is accurate up to, and including, the sudden increase in stiffness at $T = T_{rated}$. Accurate modelling of the response past this point is not crucial, as in practice the device should not be operating above T_{rated}. Although the expression is complex, only parameters k and e are required to parameterise the rated tension and strain. Any value of rated tension T_{rated} can be obtained by varying parameter e, and any value of rated strain $\varepsilon(T_{rated})$ can be obtained by varying parameter k.

For each LRD, the derived non-linear stiffness function is substituted for the $\varepsilon(T)$ term in the general form equations (4.7a & 4.7b, 4.9a & 4.9b), with the resulting systems of equations forming the analytical model. This model can be solved for the vertical and horizontal restoring

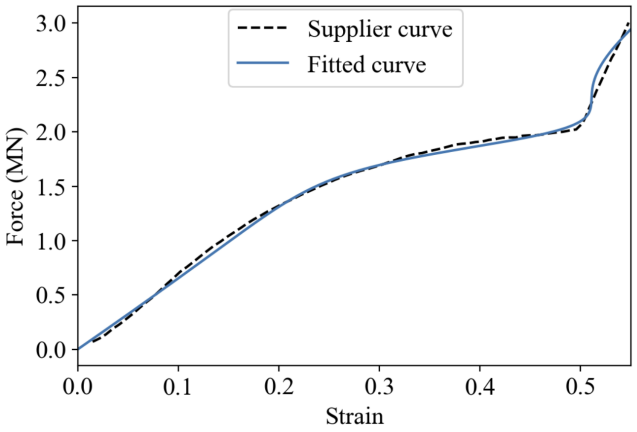

FIGURE 4.8: TFI stiffness curve from supplier publication [50], against fitted curve from Eq. 4.14

TABLE 4.3: TFI fitted parameters for eq. 4.14

Parameter	fitted value
a	1.238×10^{-2}
b	2.119×10^{2}
c	7.516×10^{-1}
d	1.149×10^{1}
e	2.405×10^{2}
f	-1.672×10^{5}
k	1.379×10^{-1}

forces H_f and V_f at the fairlead, for any fairlead coordinates x_f and z_f, by employing numerical root-finding methods. All LRD stiffness functions and resulting mooring equations are fully differentiable over their domain. This means the system can be solved with a Newton-Rhapson scheme with analytical Jacobians, providing fast and robust computation.

4.4 Validation of quasi-static model against commercial FE software

The analytical model was validated against results obtained from the commercial FE software Flexcom, which discretises the mooring line and interpolates the stiffness from a set of force-strain points. The validation was performed by comparing quasi-static tension-offset profiles for each of the LRD concepts. To obtain the quasi-static tension-offset profile, the horizontal fairlead coordinate x_t is gradually displaced along the horizontal axis parallel to the mooring line, and the analytical model is used to calculate the resultant fairlead tension T from the fairlead forces H_f and V_f at every step. This is depicted graphically in Figure 4.9. This figure was obtained using a graphical app built in Python, based on the analytical model, which enables visualisation of the geometry of a mooring system with any LRD parameters [119].

The properties of the mooring system used are identical to those of the OC4 Phase II mooring system [100], with the exception of the water depth which is set to 150 m rather than 200 m, to

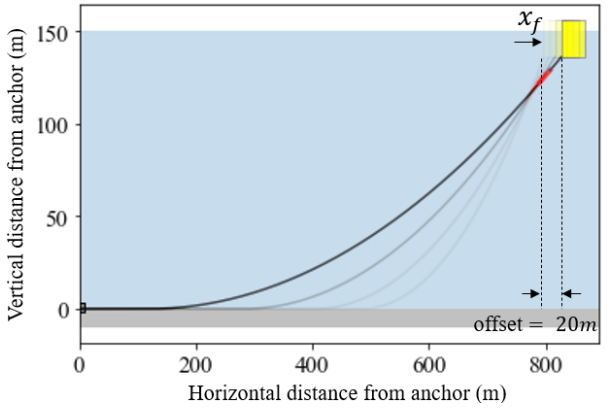

FIGURE 4.9: 2D plot of mooring line, with fairlead displaced along horizontal axis up to an offset of 20m

make the mooring system more sensitive to the LRD. These properties are summarised in Table 4.4. For each LRD concept, the stiffness curve parameters are taken from the curve fits shown in section 4.3.3 and the LRD lengths are set such that they all exhibit 5 m of extension at $T_{rated} = 2$ MN. This rated tension was chosen arbitrarily for this illustration, but the LRDs can be designed for any value of T_{rated}. The IMS and DO devices were modelled using Eq. 4.7a & 4.7b, which are valid for neutrally buoyant devices, whereas the TFI device was modelled using Eq. 4.9a & 4.9b. The wet weight of the TFI device was set to 8 kN/m, which corresponds to the weight of a 1m-diameter device with rated tension of 2 MN.

TABLE 4.4: Mooring system parameters, based on OC4 [100]

Mooring system parameter	Value
Fairlead-seabed vertical dist.	136 m
Unstretched mooring line length inc. LRD	825.35 m
Initial anchor-fairlead distance	796.7 m
Chain mass per unit length	145 kg/m
Chain EA	750 MN

The resulting tension-offset plots are shown in Figures 4.10, 4.11 and 4.12. These are displayed alongside the equivalent full-chain mooring system tension-offset, i.e. a catenary mooring with the same overall line length but no LRD. These show close alignment between the analytical and FE results, with a mean error $< 0.1\%$ and a maximum error across all curves of 0.4%. The maximum error occurs at the gradient change point of the TFI curve, where the fitted stiffness curve does not perfectly match the interpolated curve (Fig. 4.8). Other general take-away points from the tension-offset profiles are:

- All three LRD moorings show significantly more compliance than the full-chain catenary (i.e. lower gradient of tension-offset), especially at lower offsets where the LRDs operate in their low-stiffness regions. As a result of this increased compliance, the LRD moorings display higher horizontal offsets than the full-chain mooring for the same fairlead tension.

- All three LRDs have exhautsed all their extensibility once the fairlead tension is above the rated tension of the device. In practice, this would mean no extension is left to reduce dynamic loads. If these high loads/offsets are expected, an LRD with higher rated tension should be used.
- The extension of the LRDs under the weight of the chain at zero-offset leads to reduced pre-tension of the mooring system. In practice, this could be compensated for by reducing the overall length of line. Due to its self-weight, the TFI device (Fig. 4.12) shows higher pre-tension than the other LRDs for the same mooring line length.

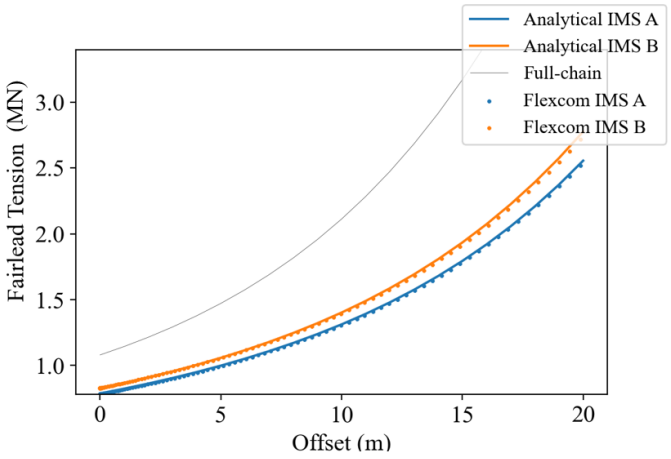

FIGURE 4.10: Tension-offset profile from analytical solution and FE software for IMS curves (configurations A & B)

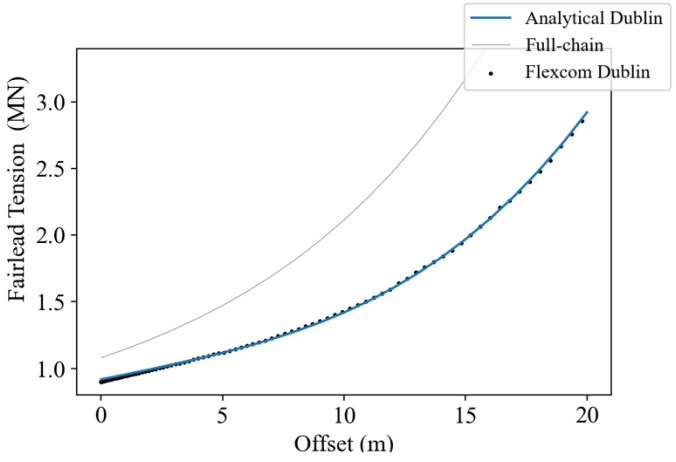

FIGURE 4.11: Tension-offset profile from analytical solution and FE software for DO curve

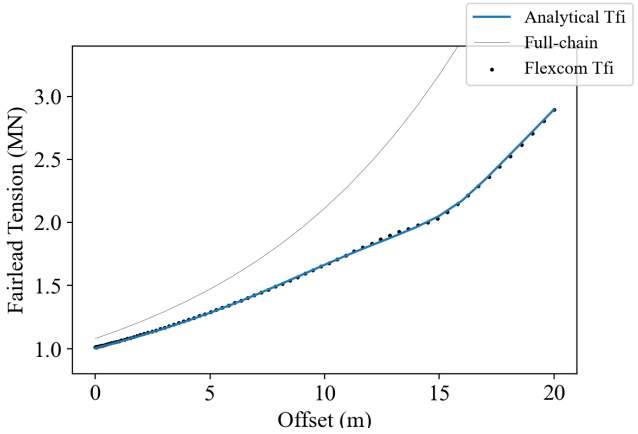

FIGURE 4.12: Tension-offset profile from analytical solution and FE software for TFI curve

4.5 Application of analytical model to LRD design problem

4.5.1 Quasi-static design scenario

Quasi-static design typically involves approximating a mean horizontal environmental force from met-ocean data [34]. This force is applied at the fairlead, and the analytical model can be used to find the fairlead tension and platform offset such that the system is in static equilibrium. For this example, the 50-year horizontal force was set as $F_{env} = 2$ MN. Knowing the horizontal fairlead force $H_f = F_{env}$, the vertical force V_f and resulting offset x_f were obtained from Eq. 4.9a & 4.9b. The 50-year quasi-static fairlead tension $T_{50yr,QS}$ was then calculated from the horizontal and vertical forces. The LRD design parameters could then be adjusted based on the quasi-static offset and fairlead tension.

In particular, two key LRD parameters should be determined at the initial design stage: 1. The rated tension of the device, determined based on the maximum expected load; 2. The maximum extension of the device (i.e., length of the device for spring-like LRDs), determined based on the maximum allowable offset. These parameters are typically found based on iterative dynamic analyses [50], which can be computationally-intensive. This section demonstrates how the analytical model can be used to find a fast initial approximation of the optimal LRD parameters at the quasi-static design stage. This example design scenario is applied to the TFI Seaspring LRD in a catenary mooring system with the physical properties listed in table 4.4.

4.5.2 Determining optimal LRD rated tension

The aim is to determine the suitable T_{rated} for the LRD such that it is not only above the 50-year quasi-static fairlead tension, but also above the 50-year dynamic tensions, to ensure the device can safely operate in the compliant range throughout its design life. Typical quasi-static mooring design approaches require application of a safety factor to the 50-year quasi-static tension to obtain the design tension, with values typically ranging from 1.4 to 2 in relevant

design codes [120]. As the LRD is expected to significantly reduce dynamic loads, a low safety factor of 1.4 is used for this example, such that:

$$T_{rated} \geq 1.4 * T_{50yr,QS} \tag{4.15}$$

To solve this, the analytical model was used to iterate through values of the TFI curve parameter e which is inversely related to T_{rated} (see Eq. 4.14), starting from a high value of e such that the starting rated tension T_{rated} is equal to the horizontal force F_{env}. All the other curve parameters were fixed to the values shown in Table 4.3. The fairlead tension, mooring configuration and resulting tension-offset profiles were then computed for each value of e, for the given environmental load until the value of T_{rated} that fits the criterion (Eq. 4.15) was reached. In this case, the 50-year quasi-static (QS) tension was found to be $T_{50yr,QS} = 2.217$ MN, which gives $T_{rated} \geq 3.10$ MN when including the safety factor (Eq. 4.15). This is depicted graphically in Figure 4.13. In this case, the value of $T_{50yr,QS}$ is only slightly above the horizontal environmental force F_{env}. This is due to the chain being relatively light, meaning the additional vertical restoring force component at the fairlead is small.

The curve with the lowest rated tension is operating above its rated tension when subjected to the 50-year horizontal load. This is visible on the tension-offset profile, with the dashed red line located above the 'kink' in the curve. The curve which satisfies the criterion is operating safely below its rated tension when subjected to the same load, meaning the LRD would be operating in its compliant range as intended. While an even higher rated tension would also be suitable in theory (e.g. 3.5 MN), the resulting tension-offset of the mooring system is stiffer overall, and less effective at reducing loads.

4.5.3 Determining optimal LRD length

In the case of a spring-like LRD (e.g. TFI), the length of the device determines its maximum extension, which in turn affects the resulting platform offset. In the study thus far, LRDs lengths were set such that they exhibit 5 m of extension at the rated strain, i.e. $L_e = 10m$ for the TFI device. For the curve with a rated tension of $T_{rated} = 3.25$ MN, the resulting 50-year quasi-static offset is of $T_{50yr,X} = 13.35m$ (can be deduced graphically from Fig. 4.13). If this is below the maximum quasi-static offset criterion, a longer LRD could be used, for added compliance. As an example, the maximum allowable quasi-static offset is set to 20m. The model was then used to iterate values of L_e, and resulting tension-offset plots were generated. The optimal length of the LRD is selected by finding the tension-offset profile which is just below the maximum offset for the 50-year tension. This process is depicted in Figure 4.14, and yields $L_e = 15m$.

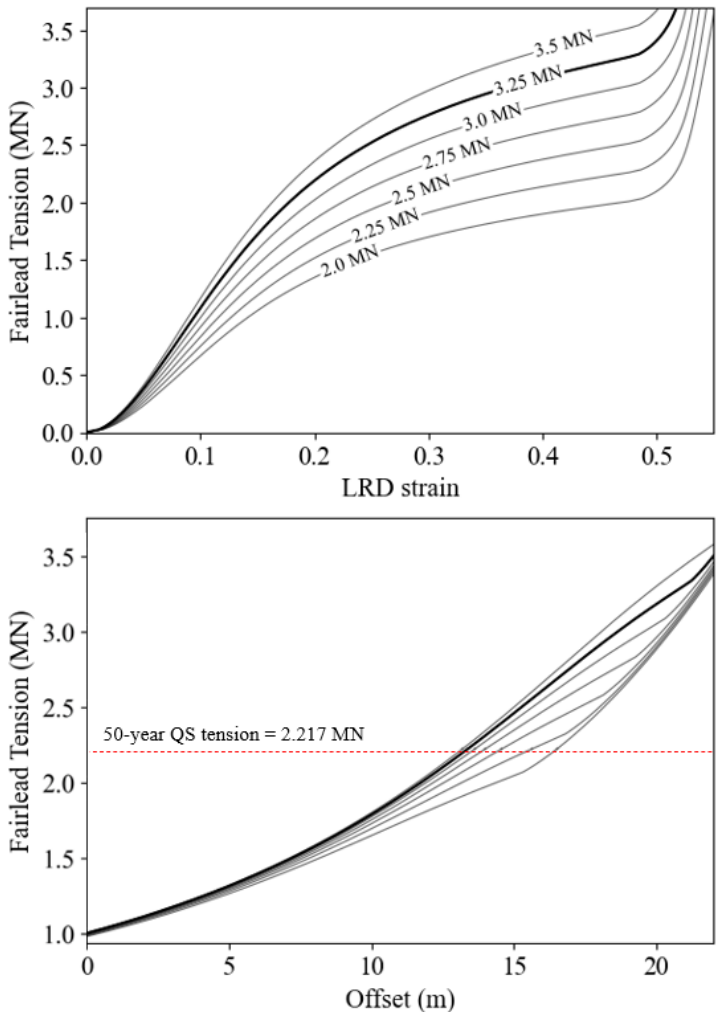

FIGURE 4.13: Top: LRD tension-strain curves for 7 values of T_{rated}; Bottom: Resulting mooring system tension-offset profile for each curve. The curve satisfying the design criterion is shown in bold.

4.6 Conclusions

4.6.1 An efficient analytical model for quasi-static design

This chapter presented an analytical quasi-static model of catenary moorings with LRDs with three different non-linear stiffness curves. Continuous parameterised equations, defined for the stiffness curves of three different LRDs, were incorporated into the static equations for a multi-segmented catenary mooring. Results from the analytical model, using the continuous equations for the LRD stiffness, match closely with results of a commercial FE model, which uses piece-wise interpolation of user-defined LRD stiffness curves. The analytical model has been packaged into an executable function as well as an associated web application, which enables visualisation of the mooring geometry and tension-offset profiles for any input LRD and mooring design parameters [119]. The effectiveness of the analytical model has also been demonstrated here through an example quasi-static design scenario, and was used to find an

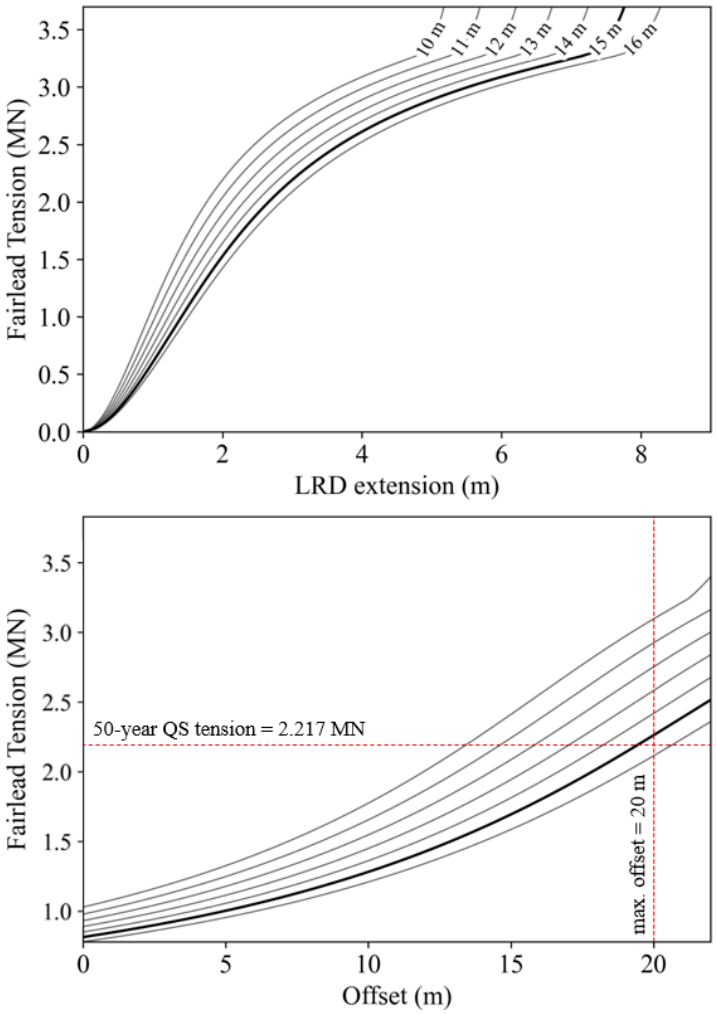

FIGURE 4.14: Top: LRD tension-extension curves for 7 values of L_e; Bottom: Resulting mooring system tension-offset profile for each curve. The curve satisfying the maximum offset criterion is shown in bold.

initial LRD design for a given 50-year environmental load. By determining the optimal stiffness curve, the LRD was ensured to operate below its rated tension, and by finding the optimal LRD length, it satisfied the maximum offset criterion while maintaining maximum compliance. This design approach yields quasi-instantaneous results, and thus provides an efficient means of screening the complex design space of mooring systems with LRDs.

4.6.2 A basis for dynamic analyses

The quasi-static design approach presented here has taken dynamic forces into account using a factor of safety, which was assumed constant regardless of the stiffness curve rated tension or length. Although this approach provides useful insight for basic initial sizing, it does not provide information on the dynamic tension reduction, or the increase in dynamically-induced platform motions provided by each LRD stiffness curve and LRD length. In theory, this would be expected to drive LRD and mooring system design at later stages. The following chapter,

Chapter 5 addresses this, by providing a comprehensive comparative analysis of LRD stiffness curves and their effect on dynamically-induced mooring line tensions and platform motions.

Chapter 5

Comparative dynamic analysis of load reduction device stiffness curves

5.1 Background

5.1.1 Motivation

While the quasi-static model established in Chapter 4 provides an efficient method for initial sizing of LRDs, it does not account for dynamic tension reductions or the influence of LRD properties on platform motions. In this chapter, the analysis is extended by directly evaluating the effects of different LRD stiffness curves and lengths on dynamically-induced mooring line tensions and platform movements. Through a comparative analysis, these dynamic effects are quantified, providing a comprehensive basis for LRD and mooring system design.

As discussed in Section 2.3.3, each LRD concept has its own characteristic non-linear stiffness curve shape. These curves can be divided into two categories, a shown in Figure 5.1: '3-phase' curves (TFI, DO), or 'single-phase' curves (two different curves chosen to represent different stiffness profiles achievable with the IMS device: IMS 1, IMS 2). 3-phase curves have a high initial stiffness, then a low stiffness range over which the LRD is intended to operate, and a high third phase stiffness once compliance is exhausted. The single-phase curves have a gradually increasing stiffness throughout.

The range of curve shapes enables considerable freedom in compliant mooring design for FOW, as each curve shape can be altered to further vary the overall mooring stiffness response : via the device's rated tension Figure 4.13, and length Figure 4.14. This provides a solution to the limitations of traditional moorings outlined in sections 2.3.2.1 and 2.3.2.2, but from a design optimisation point of view, this means adding variables to an already complex design space. Dynamic numerical modelling is required, to provide a thorough assessment of load reduction

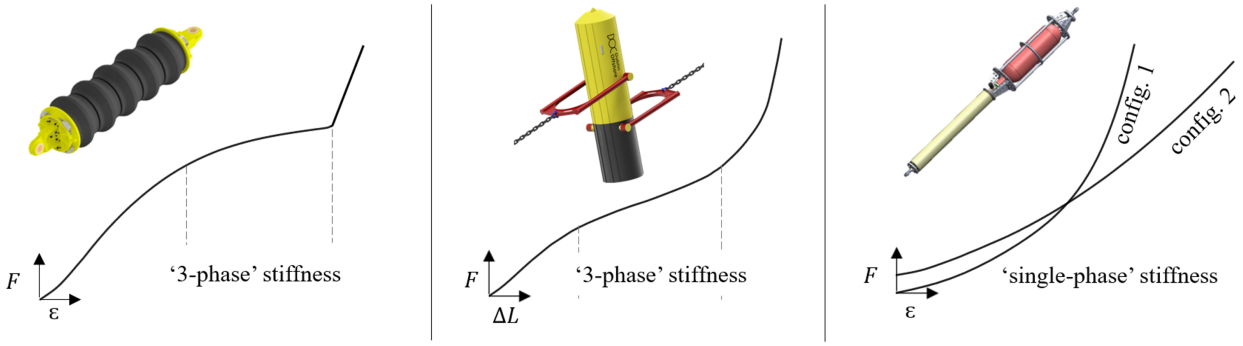

(a) TFI Seaspring (TFI) (b) Dublin Offshore LRD (DO) (c) Intelligent Mooring System (IMS)

FIGURE 5.1: The three different LRD concepts along with their characteristic stiffness curves: (a) TFI Seaspring (TFI), (b) Dublin Offshore LRD (DO), (c) Intelligent Mooring System (IMS)

performance of the various stiffness curves with respect to the design considerations outlined in 2.2.

5.1.2 Review of existing comparative analyses on LRDs

Dynamic numerical modelling of the whole FOW turbine and mooring system is key to capture the dynamic load reduction performance of LRDs. Various studies, from the LRD developers, have provided such numerical modelling and assessed the performance of their LRD for a specific set of mooring and environmental input conditions. These studies provide little opportunity for comparison across LRDs, as variations in input conditions lead to vastly different results, ranging from 10% peak load reduction for the IMS [79] to 59% reduction in peak load for the TFI [50]. Some further studies from the developers of the IMS have compared the performance of a specific LRD in different water depths, showing that tension reductions can be up to three times higher in 100 m water depth compared to 200 m [121]. Research by TFI developers has provided parametric analyses on LRD length, showing that longer LRDs provide increased tension reduction up to a certain point, with diminishing returns once sufficient compliance is reached [11]. The effect of various stiffness curve shapes for the TFI device has been compared [12], but for a tidal energy converter application rather than a FOW turbine. No existing study in the public domain has compared the stiffness curves for each of these devices, across constant sets of input conditions, for catenary and taut FOW moorings. A summary of all numerical studies on LRDs for FOW, wave energy converters (WECs), and tidal energy converters (TECs) is given in Table 5.1. Although studies have considered 1 or in cases 2 variables, this study has created a generalised approach allowing all variables to be parameterised simultaneously.

5.1.3 Research objective and workflow

In line with objective O2 (see section 1.5), this chapter presents a comparative analysis on the effect of different non-linear LRD stiffness curve shapes, each representative of a specific LRD

TABLE 5.1: Summary of publicly available numerical studies on LRDs, categorised by the parameterised variable(s)

Parameterised variable	Load case	Water depth	LRD length	Mooring configuration	LRD stiffness curve shape
Studies for WECs/TECs	[80]	[80]	[12]	[80]	[12]
Studies for FOW	[50], [121], [53]	[121]	[11], [79], [53]	[122], [123]	*no studies in public domain*

concept, on tension reduction and platform motions for FOW. To provide a comprehensive assessment with a broad range of applicability, the LRD stiffness curves were considered across a matrix of 8 different mooring scenarios and load cases:

- 4 mooring scenarios: 150 m depth catenary, 150 m depth taut, 75 m depth catenary, 75 m depth taut
- 2 load cases: parked 50-year extreme, operational 50-year extreme

The results were obtained from numerical modelling on a reference 15 MW wind turbine and semi-submersible platform. The model, mooring system, LRD modelling approach and load cases are described in section 5.2. The results are then divided into four sections. The first three sections consider a fixed LRD length, and study the effect of the LRD curve shape on mooring stiffness, fairlead tension reduction and FOW motions respectively. The third section compares the effect of varying the LRD length on fairlead tension and platform motions, for different LRD curve shapes.

5.2 Methodology of comparative analysis

5.2.1 Base mooring description

Two conventional symmetric mooring configurations were studied, both composed of three evenly-spaced lines: a full-chain catenary mooring and a taut mooring composed of polyester rope with chain ends. Each mooring configuration was modelled in two water depths, 75 m and 150 m, resulting in a total of 4 mooring scenarios. Each scenario is shown in Figure 5.2, annotated with the direction of wind and wave loading. All mooring components for both configurations (i.e. chain, polyester, and chain links) were given the same MBL of 15 MN for consistency in the comparative analysis. This corresponds to an R3 Studlink chain with a diameter of 143 mm, and Brydon-Bekaert MoorLine polyester rope diameter of 234 mm [66]. Pretension was also kept constant across all configurations and water depths, at 12.5% of MBL. The taut mooring was set at an inclined angle of 35 degrees with respect to horizontal, for both

the shallow and intermediate water depth moorings, based on a previous study for taut FOW systems [124]. The mooring parameters are summarised for both mooring configurations in Table 5.2:

TABLE 5.2: Mooring parameters of the base mooring system

Mooring config.	**Taut inclined (35 deg)**	**Catenary**
Pretension	1.875 MN	1.875 MN
Material type	Brydon Moorline Polyester	R3 Studlink Chain
MBL	15 MN	15 MN
Diameter	234 mm	143 mm
Stiffness (EA)	100 MN	3750 MN
Mooring radius (m)	252 (150 m depth); 145 (75 m depth)	640

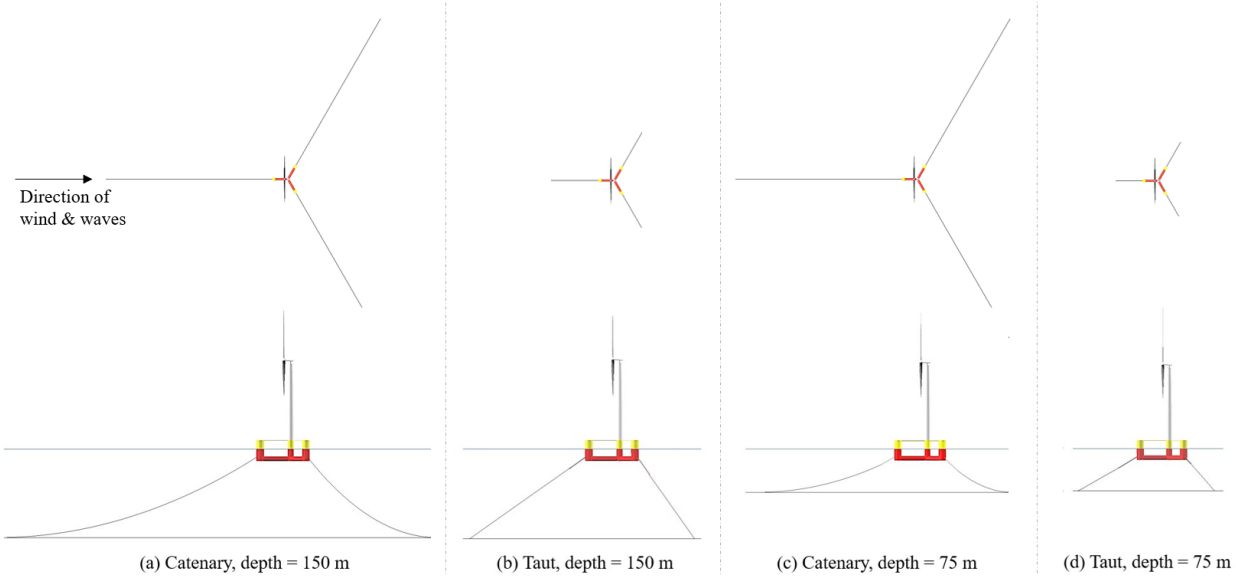

FIGURE 5.2: Top-down and side views of the 3D Flexcom model of the IEA 15 MW wind turbine on the Volturn US platform, for the four mooring scenarios considered in this chapter.

5.2.2 LRD modelling

To model the LRD mooring systems, the base mooring configurations were modified by substituting a non-linear spring element representing the LRD for a section of the line at each fairlead. This approach is in keeping with the numerical modelling from the various studies listed in Table 5.1. As the aim of this study is to compare different non-linear LRD stiffness curves, physical properties such as diameter, linear mass and LRD length were equalised to provide a meaningful comparison. In practice, these parameters vary across the three concepts considered: for the two spring-like devices, typical values of diameter and dry linear mass quoted in literature range from 0.3 m and 71 kg/m for IMS [121], to up to 1.43 m and 1759 kg/m for TFI [50]. These properties make the IMS device neutrally buoyant in seawater, and the TFI device slightly heavier. The diameter of the ballasted cylinder of the DO device, Figure 5.1(b), can range from 2.9 - 5.1 m, and the buoyant section is designed such that the full device is

neutrally buoyant in water [13]. For this study, the LRD line sections were all given a diameter of 1 m, and the dry linear mass was then set to 785 kg/m for neutral buoyancy in seawater. The lengths of LRDs considered also vary across different studies, ranging from 4 m [79] to 30 m [11]. A length of 20 m was taken as the reference length for this study, with subsequent comparison of additional lengths from 10 m to 30 m. By using standardised non-linear spring elements for all LRD concepts, the impact of the LRD stiffness curve on the system was isolated, which is key for this study. For more advanced studies on a specific LRD, a detailed, geometrically accurate LRD model could be employed to capture additional hydrodynamic or mechanical characteristics.

Non-linear stiffness curves for each LRD concept were reproduced from developer documentation, and normalised such that all LRDs exhibit the same tension at 0.5 strain, with 10 m extension for the 20 m LRDs considered. For each of the 4 curve shapes, shown in Figure 1 for the 3 devices, the stiffness is scaled depending on its 'rated tension' (see discussion in 4.1.2). In this chapter, selected rated tensions range from 2.5 MN, which is just above the mooring pretension, to 7 MN, which is just below the maximum expected tension with no LRD, determined from an analysis on the base-case mooring system. The 10 rated tensions considered in this study are shown for each of the 4 stiffness curve shapes in Figure 5.3.

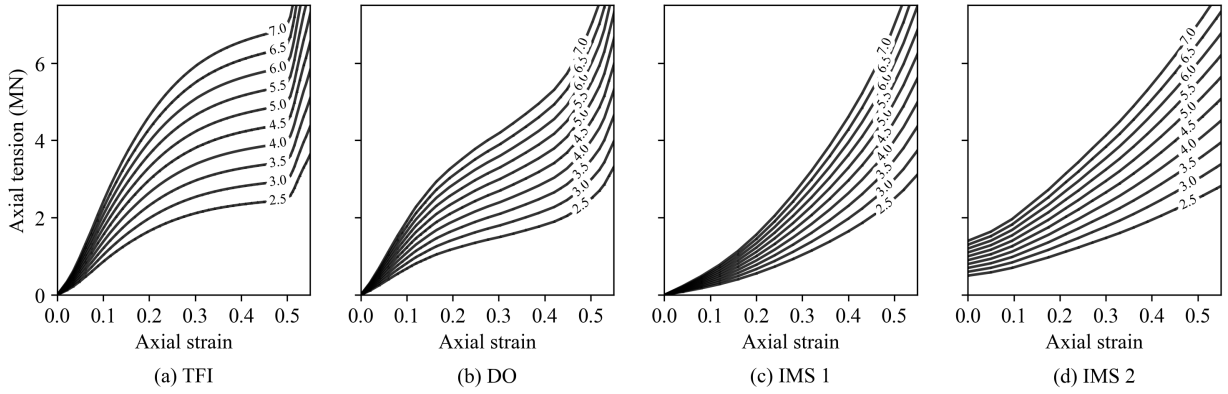

FIGURE 5.3: : Tension-strain plots for the 4 non-linear stiffness curve shapes considered in this chapter. 10 different rated tensions are modelled for each curve shape, from 2.5 MN to 7 MN

5.2.3 Design load cases

The load cases applied in the model are representative of the New York Bight area, which is a moderate-intensity location that has been used to assess LRDs in existing literature [50]. The choice of location was not critical for this chapter, the primary focus being on comparing various mooring system designs against a set of fixed load cases. Two load cases were considered: a 50-year return period load case for an operational wind turbine, and a 50-year return period load case for a parked turbine, i.e., with feathered blades to reduce wind loading. For the operational load case, the wind speed equals the turbine's rated wind speed of 10.59 m/s, generating the highest amount of wind thrust on the system [110]. This scenario can sometimes cause higher tensions on the mooring system than more extreme conditions with a parked

turbine, hence both load cases require consideration as potential design driving scenarios. The parameters of each load case are summarised in Table 5.3.

TABLE 5.3: Operational and parked load cases used in this study [50].

Load case	**50-yr operational**	**50-yr parked**
IEC load case reference	IEC 1.6	IEC 6.1
Wind speed (m/s)	10.59	41.10
Turbulence intensity	0.085	0.154
Significant wave height (m)	4.72	8.70
Peak wave period (s)	10.03	12.73
Peak shape parameter	2.02	2.03
Current	not considered	not considered

The two load cases were run on all 4 base mooring scenarios for the IEC-recommended duration of 3600s [14], with wind and waves acting in the direction shown in Figure 5.2. For the irregular wind and wave seeds considered, the highest loads on the windward mooring line occurred in the first 1200s of the simulation. The resulting time-series of fairlead tension and surge (i.e. horizontal platform offset), were cropped to the first 1200s and are shown in Figure 5.4.

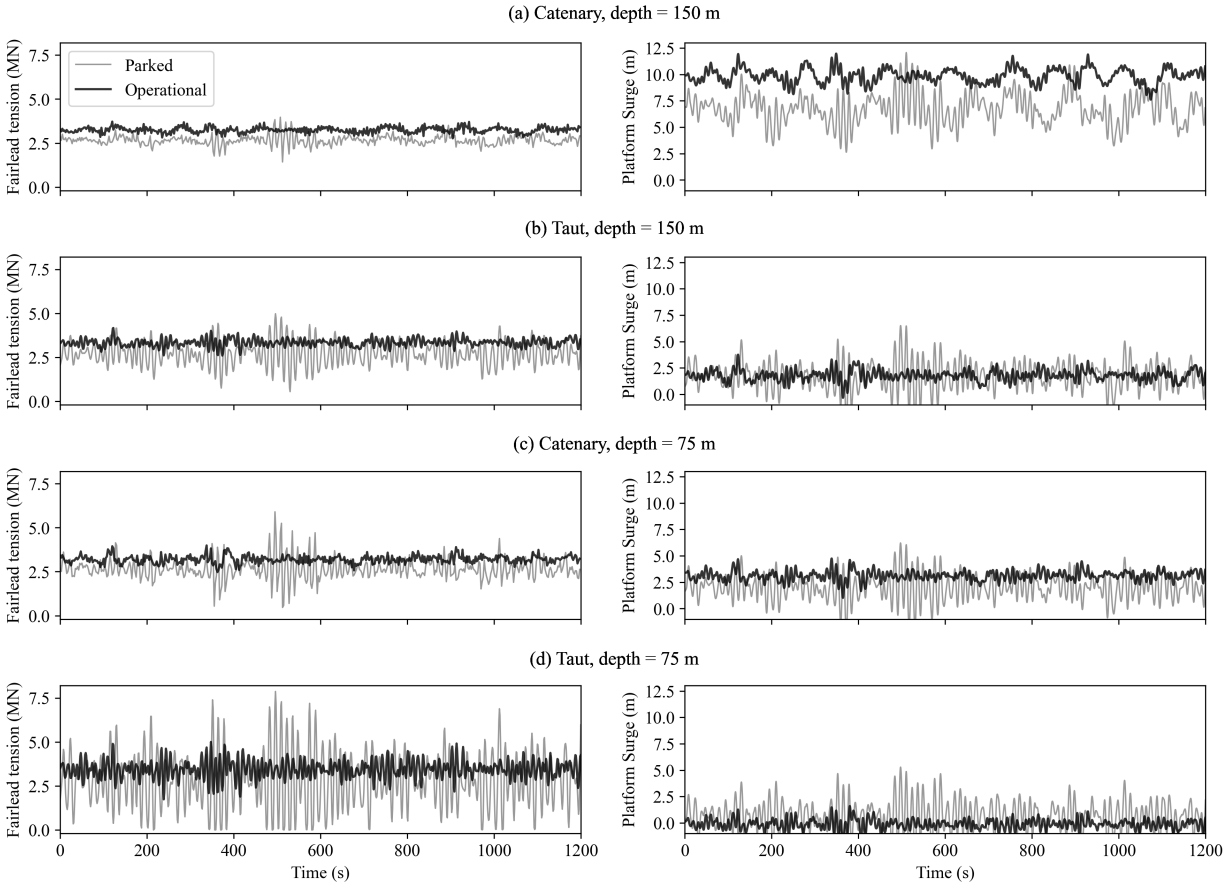

FIGURE 5.4: Time-series of fairlead tensions and platform surge for the four base-case mooring scenarios, for 50-year parked (IEC 6.1) and 50-year operational (IEC 1.6) load cases.

The fairlead tensions are highest for the taut moorings in 75 m water depth (Figure 5.4d), due to the lowest compliance in the mooring system. These high fairlead tensions, which are essentially restoring forces maintaining the platform in position, translate to much lower surge of the platform (see Figure 5.5). Conversely, the catenary mooring in 150 m depth (Figure 5.4c), is the most compliant and shows the highest surge and lowest tensions at the fairlead. Under the 50-year parked load case, the shallow taut configuration also exhibits numerous 'slack' events, where the fairlead tension momentarily reaches zero. These events can potentially be damaging to the mooring system. In practice, this mooring system would not be viable without an LRD for the given conditions, and a line angle much closer to horizontal would have to be considered to increase the line length and deliver more compliance. Alternatively, pretension at the fairlead could be increased in the no-LRD shallow water taut mooring case, to reduce the occurence of slack events by increasing the mean tension in the line. For this study, the line angle and pretension were kept constant across all mooring arrangements and water depths, to isolate the effect of LRDs and study their impact on slack events.

5.3 Effect of LRD stiffness curves on mooring system stiffness

Each combination of LRD stiffness curve shape, rated tension and mooring scenario leads to a different stiffness curve of the mooring system as a whole. Full mooring stiffness curves are obtained from tension-offset analyses for each combination, and presented in Figure 5.5.

The stiffness of a full mooring system, including all of its components (in this case, LRD and rope or chain) is defined as the relationship between the position of the platform and the subsequent restoring force imparted on the platform (i.e. fairlead tension). The mooring stiffness dictates the equilibrium position of the platform for a given mean load, and the slope of the stiffness curve about this mean load then affects the dynamic response of the mooring.

The full mooring system stiffness is highly dependent on the stiffness of the LRD, but is also driven by the response of the catenary chain or taut rope which forms the rest of the mooring line. To obtain the stiffness profile of the full system, the platform was slowly displaced along the surge axis, and the fairlead tension required for static equilibrium was calculated at every step. Resulting plots of fairlead tension against surge (i.e. horizontal plaftorm offset) are shown in Figure 5.5 . These plots illustrate some useful concepts:

- The shallower and taut mooring systems exhibit higher stiffness, which translates to lower surge (i.e. horizontal platform offset) for the same value of fairlead tension.
- The taut moorings are generally less compliant than the catenary mooring, and their stiffness is more dominated by the stiffness of the LRD. In other words, the stiffness curve of the taut mooring system is very similar to that of the LRD, as the rope does not contribute much to the compliance.

- In the case of a 3-phase LRD stiffness curve (TFI, DO), low rated tensions can actually lead to much stiffer mooring systems once a certain value of surge is reached, as the LRD compliance is rapidly exhausted, leading to operation in the stiff, third-phase of the curve.

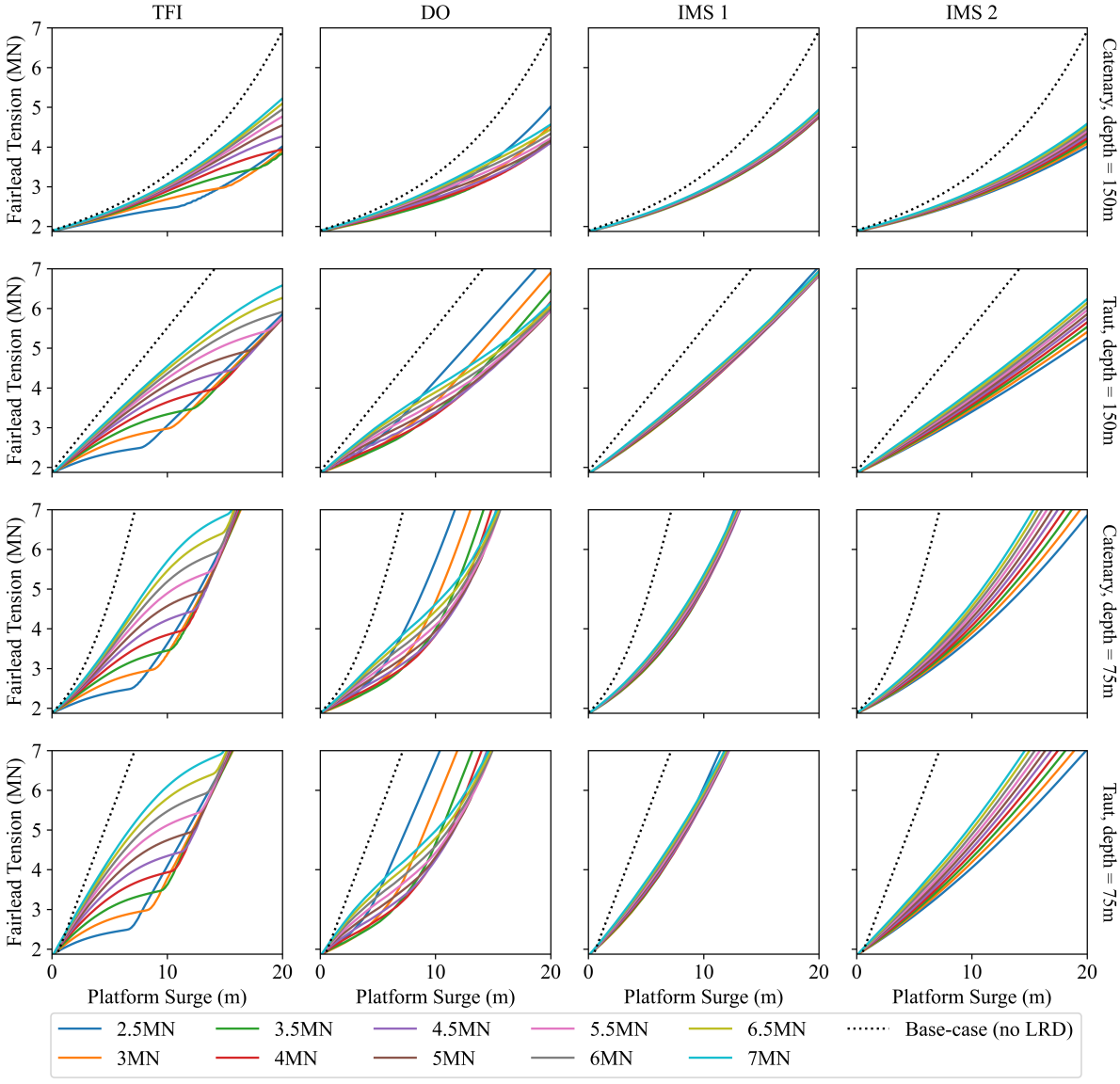

FIGURE 5.5: Stiffness curves of the full mooring system (i.e., mooring line + LRD) for all combinations of mooring scenarios, LRD curve shapes, and LRD rated tensions.

5.4 Effect of the LRD stiffness curves on tension reduction

5.4.1 Significance of the LRD rated tension in stiffness curve comparison

To compare the LRD stiffness curves, the loading time-series shown in Figure 5.4 are applied to the LRD mooring system, for each of the 4 different stiffness curve shapes and 10 rated tensions shown in Figure 5.3. For the 3-phase curves, the rated tension defines the point at which the LRD enters its third-phase stiffness. However, in a more general sense, the rated tension defines the overall steepness of the non-linear stiffness curve, i.e. its slope $dT/d\varepsilon$. This impacts the performance of the LRD, by affecting the phase of the stiffness curve over which it operates and is effective in reducing tension. This is depicted in Figure 5.6, which shows the span between the mean LRD strain and the maximum LRD strain over the course of the time-series, defined as the 'operating strain region'. For brevity, the operating strain regions are shown only for the most severe load conditions, i.e. 75 m water depth and parked load case.

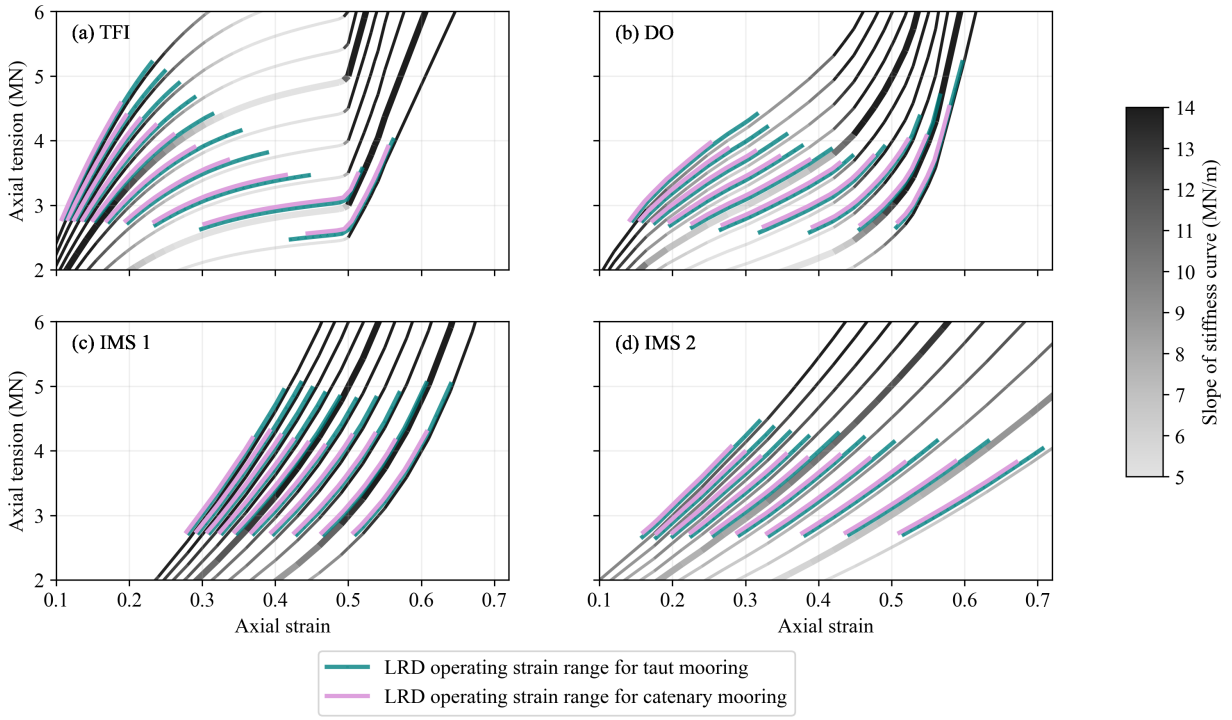

FIGURE 5.6: Stiffness curves plotted for each rated tension and curve type, and color graded according to the slope of the stiffness curve. The operating strain region of the LRD, for the 75 m water depth and parked load case, is plotted on top of each curve. The 3 MN and 5 MN rated tension curves are shown with bold lines.

For all 4 stiffness curve shapes, the lower rated tensions lead the LRD to operate in higher strain regions. For the two single-phase curve shapes (Figures 5.6c & 5.6d) this has limited significance, as the slope of the stiffness curve is similar regardless of the operating strain region. However, for the 3-phase curve shapes (Figures 5.6a & 5.6b), the slope of the stiffness curves varies considerably depending on the operating strain region. The lowest maximum tensions, i.e. tension at maximum strain, are found when the LRD operates in the second phase

stiffness, which has the lowest stiffness curve slope. Thus, to obtain the full benefit of the LRD in extreme 50-year conditions, the rated tension of 3-phase curves must be low enough for the LRD to stretch past its first-phase stiffness, but high enough such that it doesn't exceed its rated tension and operate in its stiff, third phase.

To visualise the effect of different LRD stiffness curve shapes and rated tensions on the system, Figure 5.7 shows a time-series of fairlead tension for the LRD moorings plotted against the base-case mooring, for all 4 mooring scenarios in the parked load case. For each of the stiffness curve shapes, 2 rated tensions are considered, 3 MN and 5 MN. The time-series are cropped to capture the peak loading events, which occur between 450 and 550 s in the parked load case, for the wind and wave seeds considered (see Figure 5.4). All LRDs (coloured lines) reduce the peaks in fairlead tension compared to the base-case mooring (grey lines). Additionally, LRDs eliminate slack line events in taut mooring configurations (5.4 d), i.e., they maintain tension in the mooring line when it would otherwise reach zero during troughs in dynamic load response.

Greater tension reduction is apparent in mooring scenarios with less inherent compliance in the base case mooring configuration, i.e., in the taut line and shallow-water moorings (Figure 5.7 d).

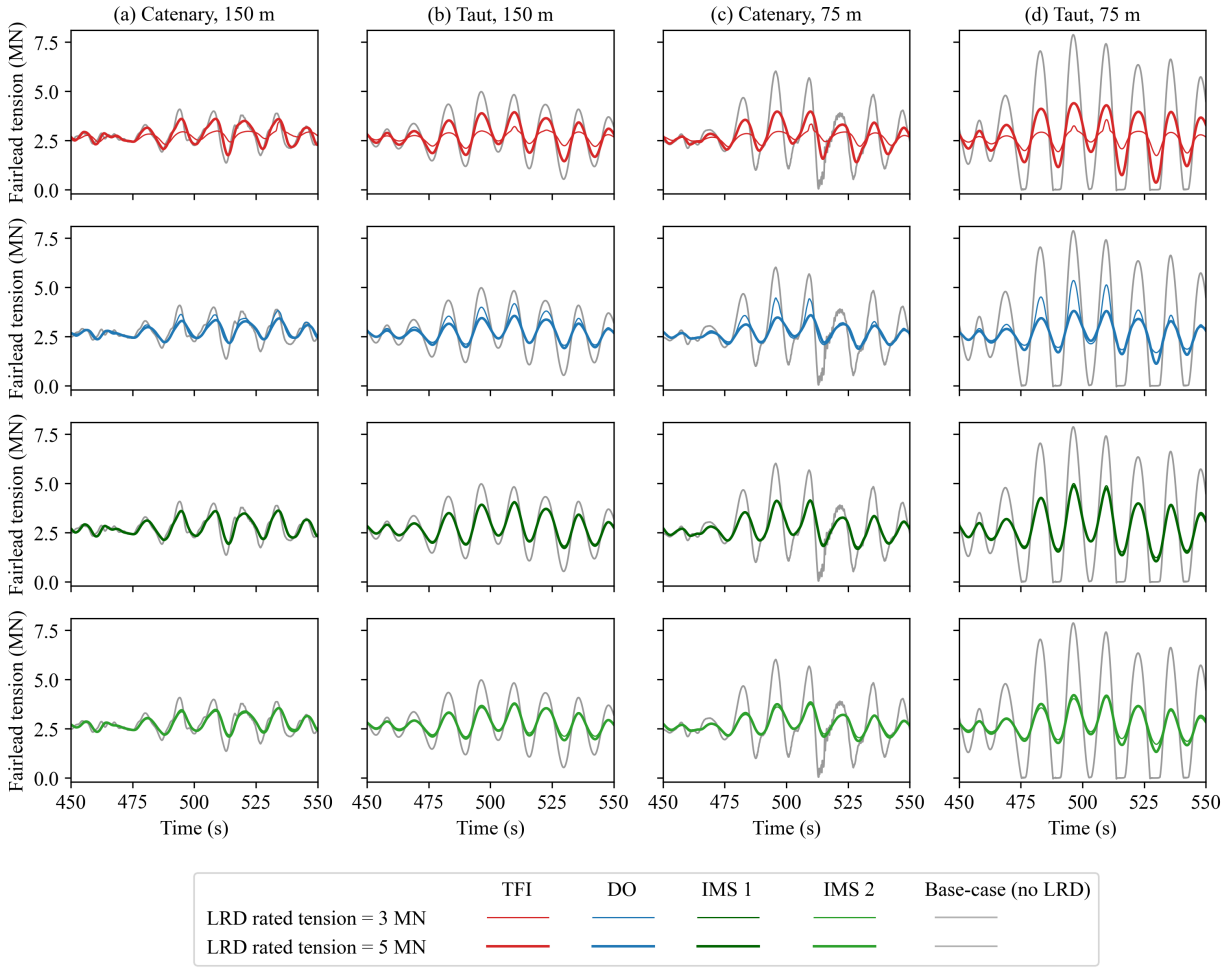

FIGURE 5.7: Peak fairlead tension event in parked turbine load case. time-series for each LRD is plotted against no LRD case, for two values of rated tension.

As expected, LRDs with 3-phase stiffness curves, TFI and DO, show different fairlead tension responses depending on their rated tension, whereas the single-phase stiffness curve LRDs show similar responses for the two rated tensions considered. For the DO device, the 3 MN rated tension LRD is too soft, thus operating in the third phase stiffness and not reducing tension as much as the stiffer 5 MN LRD which operates in the second phase as intended. Conversely, the 5 MN TFI device is too stiff, thus operating in the first phase of its stiffness curve and not reducing tension as much as the 3 MN device. However, as shown by the operating strain region of the 3 MN TFI curve (Figure 5.6a) the device momentarily exceeds its rated tension and enters its third phase stiffness at the maximum load for the 75 m water depth case. This is visible in the time-series of the TFI device (Figure 5.7d, at 490s and 510s), where a secondary peak in tension appears, caused by the device 'locking-out' at 50% strain as it suddenly enters the high-stiffness third phase.

5.4.2 Maximum fairlead tension reduction

In the following results, the maximum fairlead tension reduction provided by different LRD curve shapes is compared across all rated tensions, to ensure the optimal rated tension is captured for each curve shape. Maximum fairlead tension is recorded over the full time-series for each LRD curve shape, and compared to the tensions in the base mooring for the same conditions (Figure 5.8).

Across all 8 sets of input conditions, the 3-phase stiffness curves (TFI, DO) show better maximum tension reduction than the single-phase curves (IMS 1, IMS 2), as long as a suitable rated tension is selected. The window of suitable rated tensions, which allow the LRDs to operate in their second phase stiffness, is smaller for the TFI curve (3 - 4 MN) than for the DO curve (4 - 6.5 MN). This is due to the low, regressive slope of the TFI stiffness curve in its second phase (less than 5 MN/m), which is highly effective at reducing tension, but also translates to rapid extension of the device as it approaches its rated tension. The DO curve has a stiffer second-phase response, leading to slightly lower tension reduction, but enabling a greater range of rated tensions to operate within the second phase.

In the scenario where peak loads are design-driving, the rated tension which provides the highest tension reduction would theoretically be the most advantageous. However, in some cases, selecting this rated tension could lead to the LRD exhausting its compliance and exceeding its rated tension. For instance, with the TFI LRD in the taut 150 m case (Figure 5.8 b), a rated tension of 3 MN provides the highest tension reduction. However, the maximum fairlead tension when using this device is of 3.2 MN, meaning the LRD has exceeded its rated tension and entered its third-phase stiffness. If the 'optimal' rated tension for the specific application is defined as that which provides the highest tension reduction without the LRD exceeding its rated tension, a rated tension of 3.5 MN should be chosen for the TFI curve. Similarly, the 'optimal' rated tensions for this application would be taken as 4.5 MN for the IMS and DO LRDs.

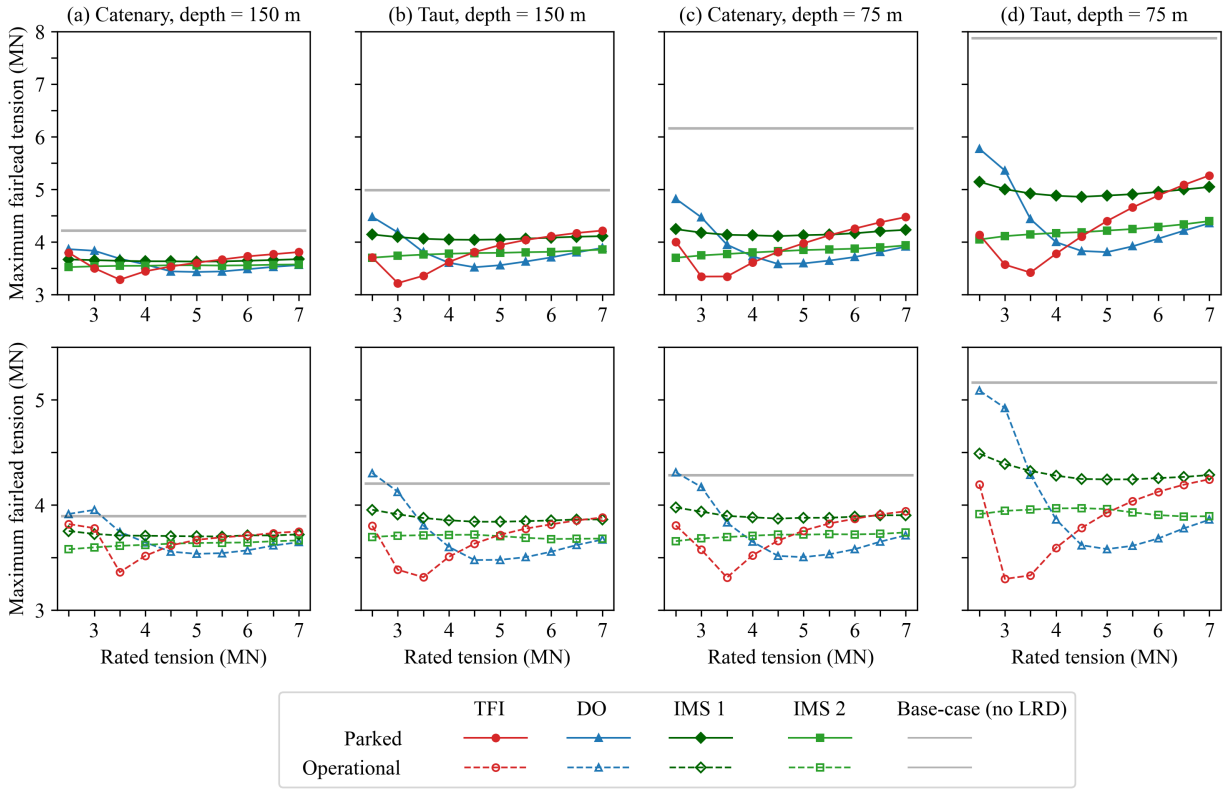

FIGURE 5.8: Maximum fairlead tension for each of the 4 LRD curve types across a range of rated tensions. Each of the 8 subplots represents a same set of input conditions, covering all 4 mooring scenarios and 2 load cases

In general, all curves offer better tension reduction in the parked load case than in the operational load case. This can be put down to two factors: 1. The higher waves in the parked case create more dynamic tension, which in turn increases the effectiveness of the LRDs [53]; 2. the lower wind thrust in the parked case leads to a lower effective strain range in the LRD, meaning more compliance is left to reduce the peak wave-induced loading. The wind thrust in the operating case causes a constant, 'background' load, which displaces the floater from its reference position, stiffening the mooring system in the process. This offset increases the mean strain of the LRD, meaning less compliance is available to reduce peak dynamic wave loads. This is especially apparent with lower rated tensions on the 3-phase curves, where the LRD has exhausted its compliance under the background load, leading to an increase in maximum tension.

5.4.3 Fatigue damage reduction

In addition to reducing the tension caused by the maximum loading event, which can lower the required material cost of a FOW mooring system, LRDs also reduce the tension on the mooring system caused by other, lesser, loading events. As detailed in Section 2.2.4.2, the damage caused by these lesser loads can accumulate over the structure's lifetime, causing fatigue in the mooring components which constitutes the leading cause of chain failure for permanent moorings [125].

The reduction in lower-amplitude loads is apparent in the time-series shown in Figure 5.7, where 'smaller' peaks in tension occurring at 450s and 475s are reduced by the LRDs. This tension reduction reduces the overall damage caused on the chains, ropes, and mooring components, which can extend their fatigue life and reduce the risk of failure. To portray this, the magnitude and timestamp of every fairlead tension peak were measured from the original time-series of the base-case moorings, for each of the time-series shown in Figure 5.4. For each peak, the resulting tension reduction for the LRD moorings is measured and scattered against the magnitude of the original peaks (Figure 5.9), using the optimal rated tensions determined in section 5.4.2.

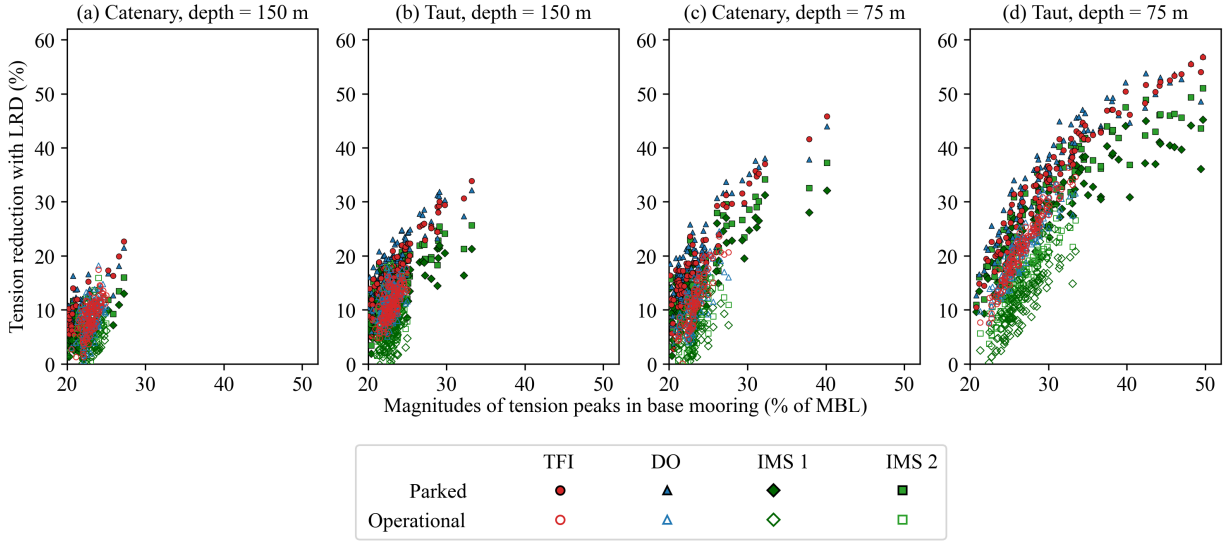

FIGURE 5.9: Reduction in tension provided by each LRD for individual fairlead tension peaks across the time series, plotted against magnitude of the peak in the base-case mooring scenario, i.e. without LRD.

These results show a strong correlation between peak load magnitude in the base-case mooring, and the resulting tension reduction provided by the LRD. The moorings with more inherent compliance (Figure 5.9 a & b) do not experience loads above 35 % MBL, thus do not obtain the full benefit of the LRDs. Peak load reductions in the operational load case follows the same correlation, albeit with slightly lower reductions due to more of the LRD compliance being consumed by the background wind load. The 3-phase stiffness curves, TFI and DO, are shown to offer the best tension reduction across all load magnitudes above 20% MBL, regardless of the mooring scenario or load case, which suggests they provide the highest damage reduction.

The total fatigue damage caused over a specific duration can be estimated by a metric known as the damage equivalent load (DEL). For a given irregular loading time-series, the DEL represents the amplitude of a constant cyclic load that results in the same cumulative fatigue damage as the irregular loading time-series itself [126] (see section 2.2.4.2 for more details). This was calculated using a rainflow counting algorithm, with a fatigue slope of 5 [50], for each full time-series. The resulting DEL is shown in Figure 5.10 for each rated tension and stiffness curve type.

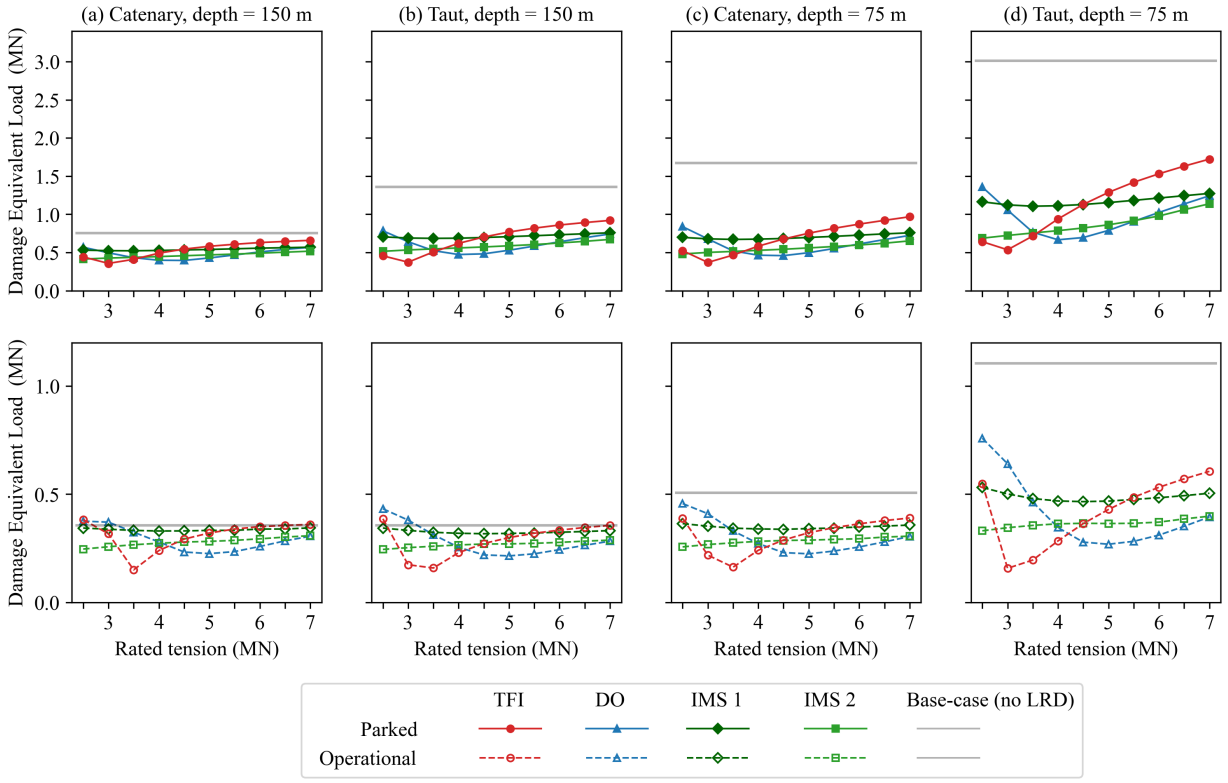

FIGURE 5.10: Damage equivalent load over the full time-series for each of the 4 LRD curve types and 10 rated tensions considered. Each of the 8 subplots represents a same set of input conditions, covering all 4 mooring scenarios and 2 load cases.

As with maximum load reduction, the DEL reduction is highest in the taut moorings and shallower waters, where there is less inherent compliance in the base-case mooring system. The effect of the LRD stiffness curve shape on the DEL follows a similar pattern to its effect on the maximum tension, with the 3-phase stiffness curves offering the most DEL reduction, as long as suitable rated tensions are selected. However, the rated tensions which provide highest DEL reduction are slightly lower than the rated tensions which provide highest maximum load reduction, as the lower stiffness can better reduce the impact of lesser loads. In the taut 75 m case for instance (Figure 5.10d), the 3 MN TFI and 4 MN DO curves provide highest DEL reduction, whereas the 3.5 MN and 4.5 - 5 MN curves provide highest maximum load reduction (see Figure 5.8d). In the scenario where fatigue is design driving, the lower rated tension could be considered, at the cost of the device potentially exceeding its rated tension and entering its third phase stiffness under the maximum load. Whether this trade-off is acceptable would depend on the type of LRD and developer guidance.

5.5 Effect of LRD stiffness curves on platform motions

5.5.1 Significance of platform motions

When altering the stiffness response of a mooring system, such as by introducing an LRD, it is crucial to consider the subsequent impact on the motions of the platform. Since the wind and wave loads considered in this study are acting along the same axis (surge axis in Figure 2.7), only the DOFs in the plane parallel to this axis are considered, i.e. only the surge, pitch and heave DOFs (see Figure 2.7). More background discussion on platform motions is provided in section 2.2 of the literature review.

Mooring designs for FOW must allow the system to safely operate within the maximum motion criteria. This is particularly important for surge, as the maximum surge under a given set of environmental loads is directly dependent on the stiffness of the mooring system (see Figure 5.5). Motions and accelerations outside of the water plane such as heave and pitch are typically more influenced by the hydrodynamics of the platform than by the mooring system, but must be considered in mooring design nonetheless. This section presents an assessment of the effect of LRD stiffness curves on platform motions and nacelle accelerations. For brevity, IMS 1 is omitted, and one rated tension is selected for the 3 other LRDs, which correspond to the 'optimal' rated tensions described in section 5.4.2: 3.5 MN for TFI and 4.5 MN for DO and IMS 2.

5.5.2 Wave-induced motions

To isolate the effect of the LRDs on wave-induced motions of the structure, the full FOW and mooring system were subjected to a set of regular Airy waves with varying frequency and fixed amplitude. The amplitude of motion is measured, normalised with respect to the wave amplitude, and plotted against the frequency of the waves. The resulting statistic forms the Response Amplitude Operator (RAO). RAOs for the 4 key motions are shown in Figure 5.11, for each mooring scenario and LRD stiffness curve type.

For the catenary configurations, the RAOs of the LRD moorings are near identical to those of the base moorings. The taut shallow water mooring has very little compliance without the LRD, hence its stiffness is primarily driven by the stiffness of the LRD (see Figure 5.5 for further discussion), in turn leading to a more visible effect of the LRD on the RAO curve. This effect is reduced in deeper waters, where the base mooring system is less stiff and therefore less sensitive to the LRDs.

These results show that the addition of the LRDs does not introduce problematic frequencies for wave-induced motions, irrespective of the LRD stiffness curve shape. In fact, for the taut moorings, surge, heave and pitch motions are slightly reduced across key wave periods, 10-15s. This reduction is higher in the shallow water scenario. Heave response is increased by LRDs at

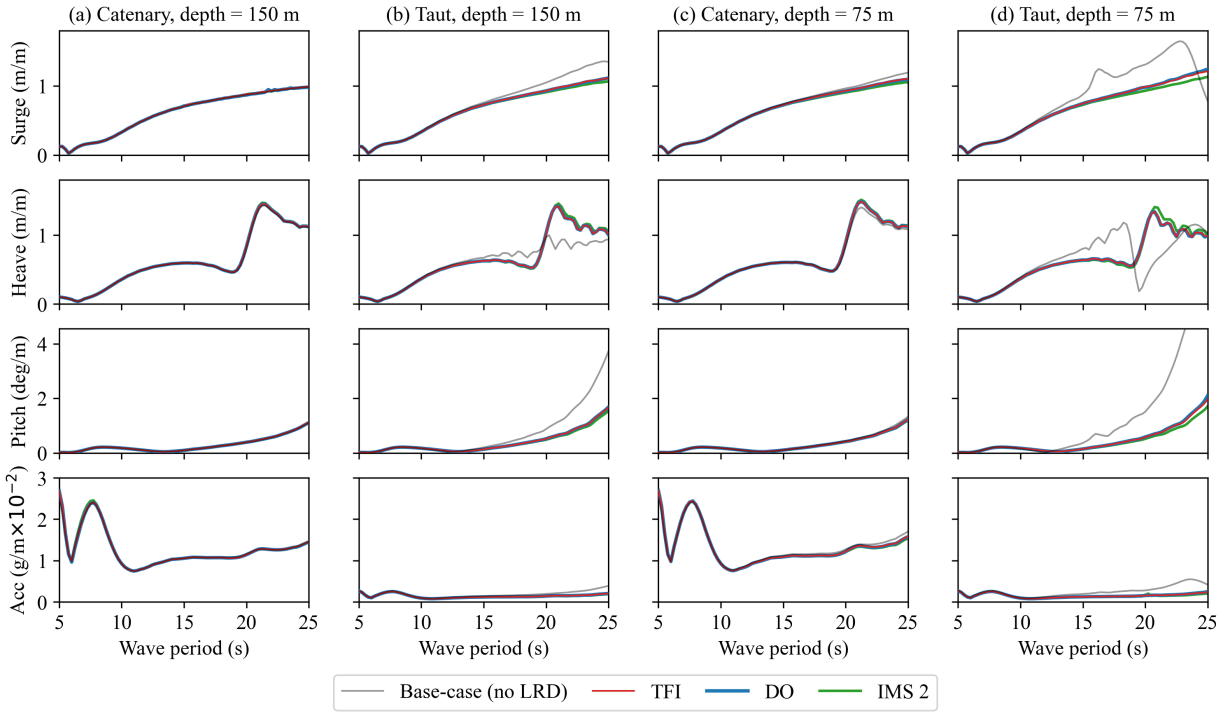

FIGURE 5.11: Effect of regular wave-only loading on platform surge, heave, pitch and nacelle accelerations.

very high wave periods, 20-25s, but these are typically not experienced in realistic sea states so should not be of concern.

5.5.3 Wind-induced motions

To isolate the effect of the LRDs on wind-induced motions of the structure, the full FOW turbine and mooring system were subjected to the same irregular wind conditions used in section 5.2.3, but without waves. Resulting time-series of surge (i.e. horizontal platform offset), heave, and horizontal nacelle accelerations are shown in Figure 5.12, cropped to show the peak loading event, which occurs at different timestamps for the parked and operational cases. Only 75 m water depth mooring scenarios are displayed, as these are most sensitive to LRDs as shown in Figure 5.11. The vertical degrees of freedom (heave and vertical acceleration) are omitted as the absence of waves means loading is purely horizontal.

The wind generates a constant 'background' load on the structure, especially in the operational case where the thrust on the turbine is at its highest. The subsequent moment on the turbine also leads to high mean pitch (Figure 5.12 c & d). During the parked case (Figure 5.12 a & b), the blades are feathered to shed load, but the wind speed is much higher (41.10 m/s for parked vs. 10.59 m/s for operational) and less regular, leading to a greater variation in response for both surge and pitch. In both parked and operational cases, the negligible dynamic loading means nacelle accelerations are low.

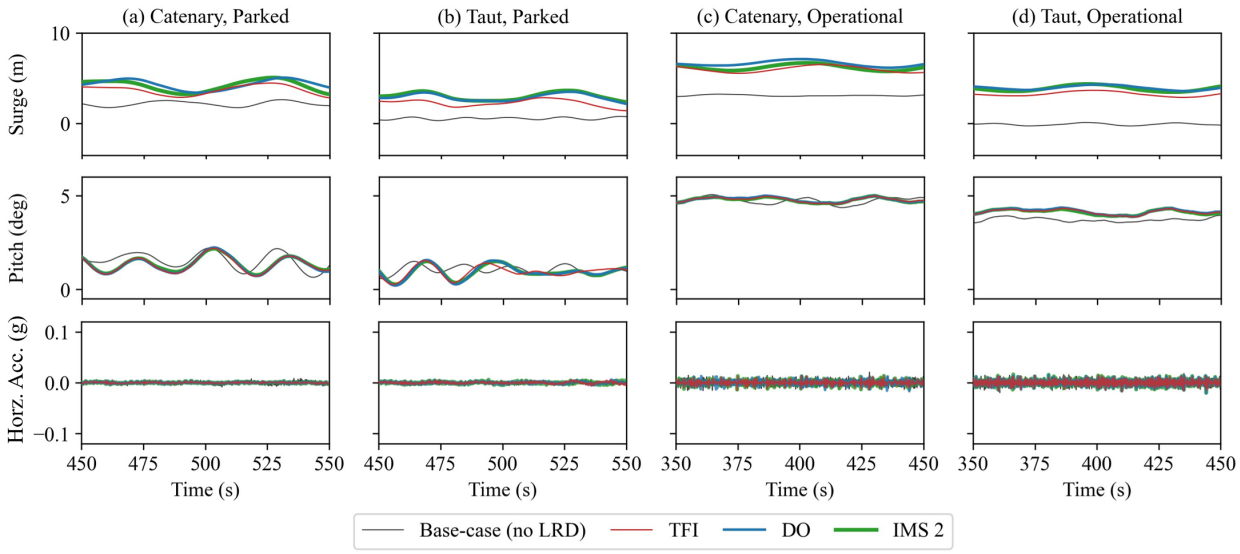

FIGURE 5.12: Effect of wind-only loading on platform surge, pitch and horizontal nacelle accelerations, for 75 m water depth.

In both cases, with the absence of waves, the relationship between fairlead tension and platform surge is essentially quasi-static: the platform finds an equilibrium position, which is determined by the stiffness of the mooring system. Hence, the presence of an LRD, which reduces the mooring stiffness, increases the mean surge (or horizontal offset) of the platform. However, the mean pitch, which is mostly influenced by platform design rather than mooring stiffness, is not increased by the LRD. Overall, when similar rated tensions are considered, these trends do not depend on the shape of the LRD stiffness curve.

5.5.4 Combined wave and wind motions

Having studied the effect of LRDs on the motion response to wind and wave loading individually, the next step is to analyse the response to combined wind and wave loading. The same design load cases as described in section 5.2.3 are considered, and time-series of the relevant platform motions in the wind/wave plane are recorded for each LRD curve type. Resulting time-series of platform motions are shown in Figure 5.13, cropped to show the peak event. For brevity, only the 75 m water depth mooring scenarios are displayed, as these are the most sensitive to LRDs.

The general effect of the LRDs on platform motions and nacelle accelerations, regardless of stiffness curve shape, can be summarised as follows:

- The damping effect from the LRDs results in a lower wave-induced dynamic surge response, in contrast to the increased wind-induced surge component induced by LRDs (as shown in section 5.5.3, Figure 5.12). This leads to a higher increase in surge in the operational case with higher wind loading (Figure 5.13 b and c) than in the parked case

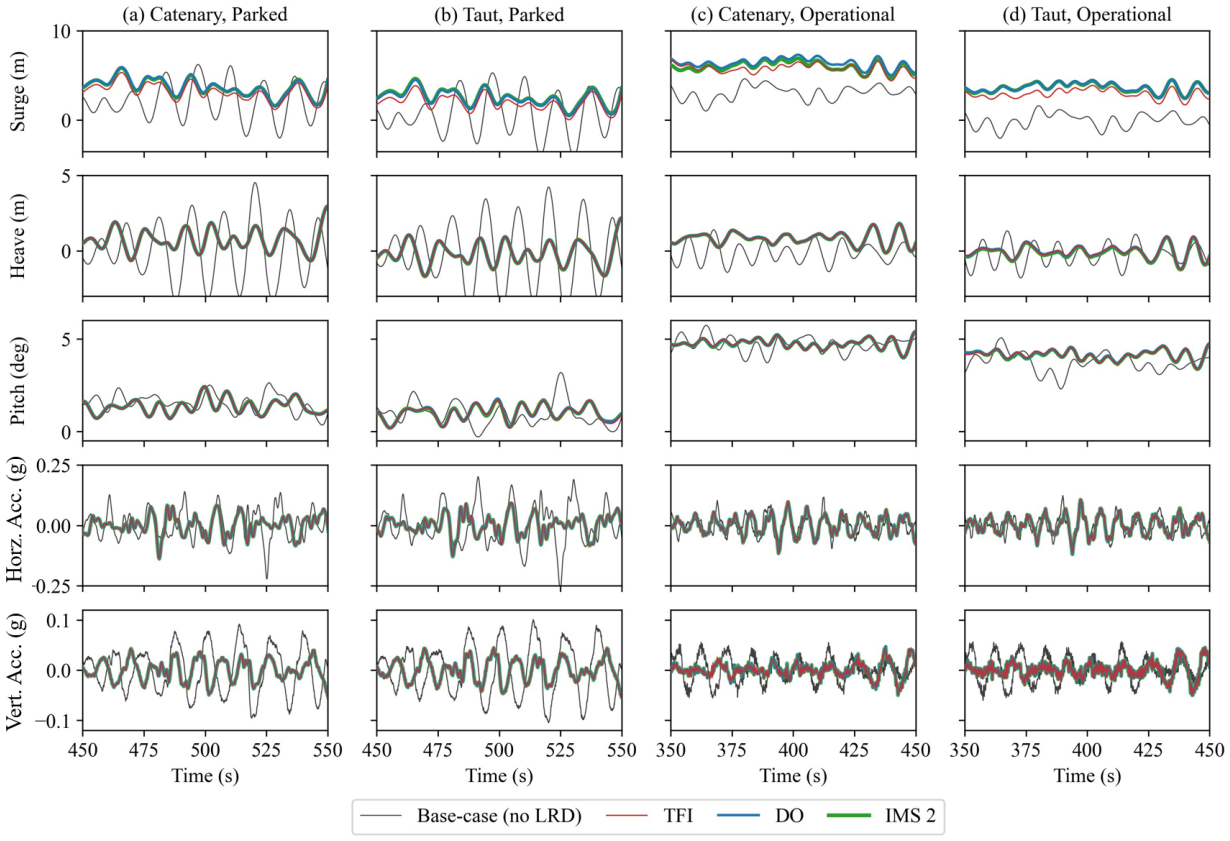

FIGURE 5.13: Effect of combined wind and waves on platform motions in 3 DOF and nacelle accelerations in 2 DOF (vertical and horizontal), for 75 m water depths.

with higher wave loading (Figure 5.13 a and b). Thus, the governing design case, i.e. case of maximum surge, can become the operational case when incorporating an LRD.

- Heave motions caused by the lower frequency waves, occurring at 500s in the parked condition, are reduced by the LRDs, which is consistent with the RAO results. As the heave motion is driven by wave height, amplitudes are higher in parked condition with a higher significant wave height.
- Pitch oscillations are due to wave loads, whereas the mean pitch is caused by the moment from the wind thrust on the rotor, leading to much higher mean pitch in the operational load cases compared to the parked load cases. The wave-induced pitch oscillations are reduced by the LRDs, but the mean pitch is not affected, as was shown in section 5.5.3.
- Wave-induced accelerations at the nacelle are reduced by LRDs for both the horizontal and vertical components, especially in the parked load case.

Overall, as was shown in the RAOs, the variation in stiffness curve shape of an LRD has very little effect on the motion response of the platform when compared to the response with the base-case mooring, i.e. without the LRD. All LRD curve shapes reduce oscillatory motions for pitch, heave and nacelle accelerations, but increase maximum surge (i.e. horizontal platform offset) of the platform. The surge motion is the only case where slight differences could be noted

between the three LRD curve shapes. This is due to differences in the extension of the LRDs, which are minimal as the rated tensions considered across the 3 devices (3.5 MN, 4.5 MN, 4.5 MN) were similar.

5.6 Sensitivity analysis of LRD length

5.6.1 Significance of LRD length in stiffness curve comparison

Previous analyses in this chapter have considered two LRD design parameters: stiffness curve shape and rated tension. Another key design parameter is the maximum extension of the LRD, which is defined by the length of the LRD section in the FE model. LRD extension determines the amount of compliance introduced by the LRD, and can make a significant difference to the overall stiffness profile of the mooring system, as was discussed in Chapter 4 (see Figure 4.14) and section 5.3 (see Figure 5.5). The LRD length has been fixed at 20 m in the results presented so far, i.e., a maximum extension of 10 m when the LRD reaches its rated tension at 50% strain. In practice, the 'length' of the LRD section, or its maximum extension, would be increased by combining multiple devices in series, or in the case of the mechanical DO device, by increasing the distance between the its hinge points.

5.6.2 Influence of LRD length on tension reduction

Figure 5.14 shows the effect of varying the length of the LRD section on the maximum tension reduction, in the parked load case, for two rated tensions. For each curve shape, one rated tension is set 0.5 MN below the 'optimal' rated tension defined in section 5.4.2, the other is set 0.5 MN above. For all stiffness curve shapes, increase in LRD length leads to higher reductions in maximum tension. The gains in tension reduction tend to be greater in the scenarios where the base-case mooring has little compliance (Figure5.14d). However, these benefits are regressive: once sufficient compliance is reached, increasing the length of the LRD has less effect on the tension reduction.

These trends also vary across the three curve shapes considered. In particular, for the 3-phase stiffness curves, i.e. TFI and DO, varying the LRD lengths can change the optimal rated tension of the LRD. This is especially true for the TFI curves, and is visible from the full red line (tension reduction for 3 MN rated tension) going above the dashed red line (tension reduction for 4 MN rated tension) as the LRD length is increased. This has significant implications for LRD design: using shorter LRDs, which provide less compliance, requires higher rated tensions to avoid extending into the third-phase stiffness. Conversely, with longer LRDs, the lower rated tensions can provide greater tension reduction. This benefit is especially significant for the 3 MN TFI curve, which is operating in its stiff, third phase stiffness when the LRD is too short, thus not

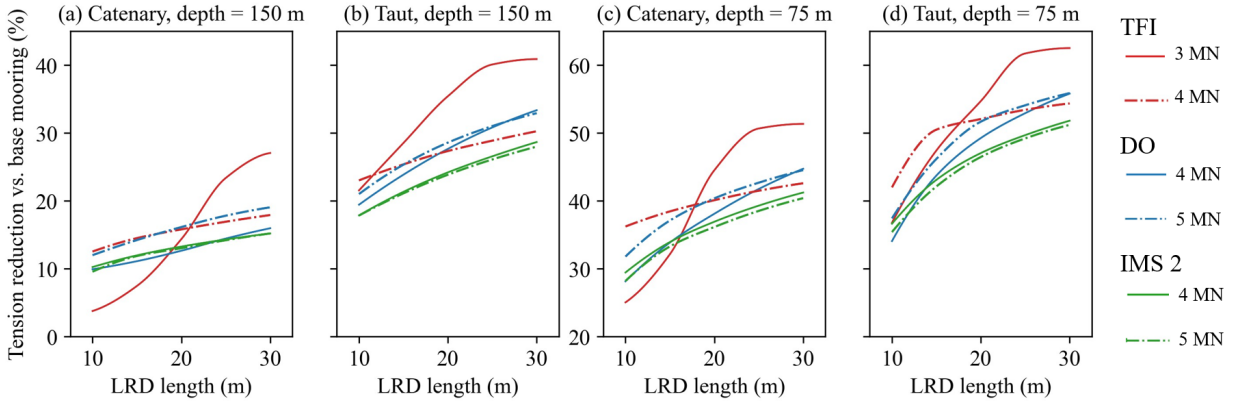

FIGURE 5.14: Effect of varying the LRD length on maximum tension reduction compared to the base-case mooring, for the parked load case. Two rated tensions are considered, either side of the optimal rated tensions defined in section 5.4.2.

providing adequate compliance, but can provide much higher tension reduction when the length of the device is increased.

5.6.3 Influence of LRD length on maximum platform surge

The wind-induced surge (i.e. horizontal platform offset) increase introduced by LRDs, which constitutes additional 'quasi-static' platform offset along the axis of loading, is expected to be driven by the extension of the LRD (see Figure 5.12). The extension of the LRD, as shown in Figure 5.15, is itself dependent on both its length and rated tension. Thus, to get a better idea of the effect of the LRD stiffness curves on surge, multiple combinations of lengths and rated tensions should be considered. Figure 14 shows the effect of varying the length of the LRD section on the added surge, in the operational load case, for two rated tensions. For each curve shape, one rated tension is set 0.5 MN below the 'optimal' rated tension defined in section 5.4.2, the other is set 0.5 MN above.

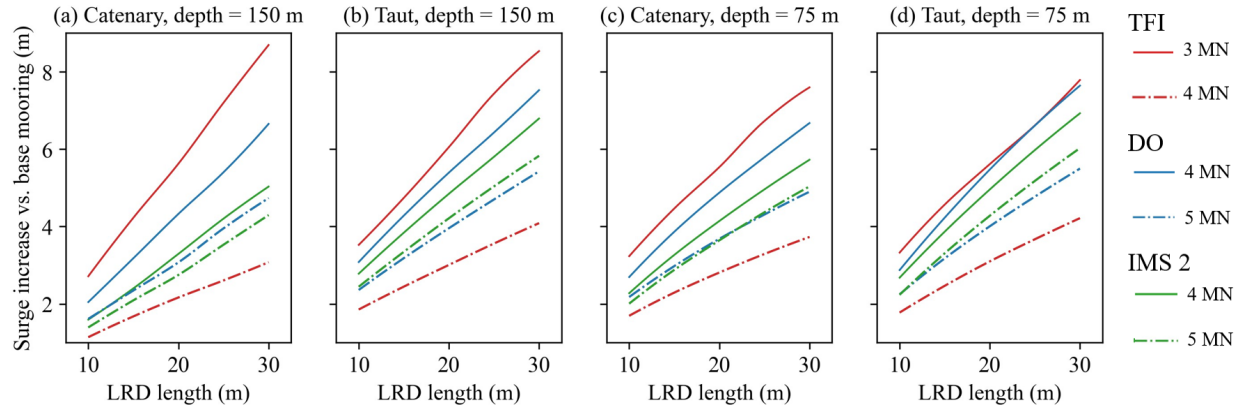

FIGURE 5.15: Effect of varying the LRD length on surge increase (i.e. horizontal platform offset difference) compared to the base-case mooring, for the operational load case. Two rated tensions are considered, either side of the optimal rated tensions defined in section 5.4.2.

As expected, the increased length of LRDs leads to more surge of the operational turbine, across all 4 mooring scenarios. However, Figure 5.15 also shows that the increased surge can be mitigated by using a stiffer LRD, i.e., with a higher rated tension. This is especially true for the 3-phase stiffness curves, where a 1 MN higher rated load can lead to over 60% reduction in additional surge. This is due to the slightly stiffer LRD not fully entering its second phase stiffness when in operation, and consequently extending much less, which can come at the cost of sightly lower tension reduction (see Figure 5.14). For the 3-phase stiffness curves, this trade off is not linear, and using the stiffer LRDs can be beneficial as it significantly reduces surge for only small increase in tension. For instance, in the taut 75 m depth case with a 20 m TFI device, using a 4 MN curve instead of 3 MN leads to 45% less surge increase (Figure 5.15d), at the cost of only 5% less tension reduction benefit (Figure 5.14d).

The underlying principle here is the coupling between variables: the rated tensions which provide optimal tension reduction for a 20 m LRD, as defined in section 5.4.2, may not be optimal for other LRD lengths. Similarly, the LRD lengths which provide acceptable surge (i.e. horizontal platform offset) increase for a given rated tension and stiffness curve shape, may not be acceptable for other rated tensions. Hence, LRD design should be attempted holistically, where different combinations of LRD length, stiffness curve shape, and rated tension are assessed in parallel, to obtain the required reduction in fairlead tension which fits platform motion constraints.

5.7 Conclusions

5.7.1 A refined design space

This chapter has shown that the combination of 3-phase stiffness LRDs, such as the TFI Seaspring and Dublin Offshore LRD, with high-modulus taut moorings can be considered a strong choice of design space for FOW mooring system optimisation.

The LRDs with 3-phase non-linear stiffness curves, featuring a high initial and final stiffness with a low-stiffness second phase, performed better than single-phase curves both in terms of maximum tension and DEL reduction. This was true regardless of the water depth, mooring configuration, and load case. However, tension reduction performance for 3-phase curves LRDs relied on finding the optimal window of rated tension, whereas the single-phase curves (i.e. IMS) provided more consistent tension reduction across all rated tensions.

The 3-phase curve shapes did not lead to worse effects on motions of the system than single-phase stiffness curves: the increases in mean surge (i.e. offset) caused by the LRDs were shown to be mainly affected by LRD length rather than curve shape. Compared to the moorings without LRDs, all LRDs lead to reduced amplitudes of wave-induced surge (i.e. horizontal platform offset), heave, pitch and nacelle accelerations.

In all scenarios, tension reductions were shown to be higher in taut moorings than catenary moorings, as the higher stiffness in the base taut moorings allowed the LRD to drive the compliance of the full system, thus maximising its benefits. These taut moorings are highly efficient in terms of materials usage, weight, and footprint size, but they typically lead to extreme loads in highly dynamic situations, and slack load events which are damaging to the mooring lines 5.4. The taut moorings with correctly designed LRDs produce no slack events, thus making the mooring systems viable, even with steep inclination angles such as the one considered in this chapter (35 deg).

5.7.2 A basis for holistic design optimisation

This chapter established the importance of finding the optimal rated tension of the LRD, to ensure it operates in the second phase of its stiffness curve, for LRDs with 3-phase stiffness curves. However, finding this optimal rated tension is not straightforward, as it is dependent on the stiffness curve shape, the length of the LRD, as well as the type of mooring system. Thus, the LRD should be optimised holistically, i.e., varying LRD parameters simultaneously alongside other mooring parameters in a multivariate analysis, to ensure a global rather than local solution is found.

The optimal LRD design was also shown to be dependent on project-specific parameters, such as water depth, load case or even objective considered: optimal fatigue reduction required a lower rated tension, whilst maximum tension reduction benefited from a higher rated tension. In other words, the ideal LRD design optimisation framework should enable as much flexibility as possible in the selection of project-specific parameters. This means covering a broader design space and objective space than previous studies (see section 2.4), and as such, is well suited to the machine learning techniques outlined in sections 2.4.2.4 and 2.4.2.5.

Chapter 6

Surrogate-based optimisation of mooring systems with load reduction devices

6.1 Background

6.1.1 Motivation

Chapter 5 identified a promising design space for FOW mooring design: taut moorings with 3-phase stiffness load reduction devices (LRDs). This design space is illustrated in Figure 6.1, and shows the two 3-phase stiffness LRDs (TFI and DO), along with the set of design parameters for the full taut-LRD system. The taut-LRD system was shown to be particularly effective as the LRD can deliver all the required compliance, enabling the usage of higher-modulus rope and smaller seabed footprints, whilst reducing loads on moorings and anchors in extreme conditions.

Three LRD parameters are considered in this design space: 1) the rated tension T_{rated}, which is the design limit for tension in the device, and corresponds to the point at which compliance is exhausted; 2) the maximum extension ΔL_{max}, which determines the extension of the LRD at the rated tension (ΔL_{max} is driven by the length of the spring in the FE model); 3) the shape of stiffness curve, which is either based on the DO or TFI LRD for this chapter. Determining the optimal combination of LRD parameters for load reduction depends on location-specific variables, such as water depth and environmental loads; but also on the other mooring design variables shown in Figure 6.1b, which affect the tension in the LRD. Thus, to provide most benefit, an optimisation framework should consider all LRD and mooring design variables simultaneously, to find the combinations of variables resulting in the lowest possible design tensions. Additionally, for a holistic design approach, other objectives apart from load reduction

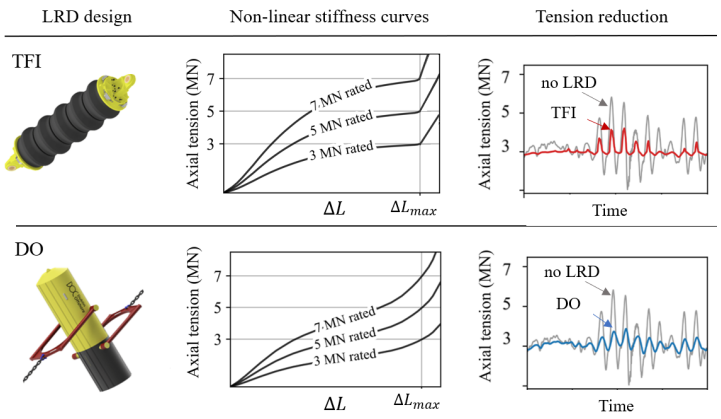

(a) TFI Seaspring and Dublin Offshore (DO) LRDs, along with typical non-linear stiffness curves and tension reduction capability.

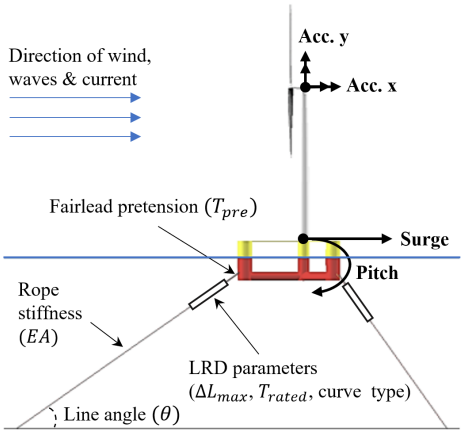

(b) Profile view of FOW model used in this chapter, annotated with mooring design variables and platform motions considered.

FIGURE 6.1: Novel design space for FOW moorings, which combines LRDs with a taut mooring configuration.

should also be considered. In particular, FOW projects typically have strict criteria regarding the maximum allowable motions which can cause undesirable effects to the system if exceeded. In the case of loading parallel to the primary line, these motions include pitch, surge, and acceleration of the nacelle.

Including all of these considerations means covering a broad design space, and formulating a complex optimisation problem with multiple objectives. Furthermore, to adequately capture the dynamic tension reduction provided by LRDs, time-dynamic modelling must be used to assess performance of designs with respect to objectives. As discussed in section 2.4.2.4, combining high-complexity optimisation and high-fidelity modelling is a challenge well-suited to surrogate-based optimisation.

6.1.2 Review of existing surrogate-based FOW mooring optimisation

Two recent studies used machine-learning techniques to train surrogate models based on data from time-domain dynamic modelling, for FOW mooring optimisation [16] [17]. Both studies employ a two-step process to reduce the number of designs which need to be fully assessed: the first step employs a simple classification model which filters out initial designs if constraints are violated, and the second step employs a more complex regression model which then assesses the filtered designs with respect to the optimisation objectives. These studies were shown to provide effective optimisation results using surrogate models trained for specific water depths, load cases, and pre-defined objectives and constraints. However, if a new location and/or new optimisation objectives were to be considered, the full training dataset would need to be regenerated and the surrogate models retrained. This is not necessarily an issue for detailed

design once project specifics are fully determined, but at concept design level, more flexibility would be advantageous.

6.1.3 Research objective

In line with objective O3 of the thesis, this chapter proposes a flexible design methodology to optimise a taut mooring with LRDs for any water depth, load case, and optimisation objectives and constraints (see section 1.5). The method is enabled through the development of a surrogate model that takes time-domain wave elevation inputs, and predicts quasi-instantaneous time-domain outputs of fairlead tension and platform motions. The surrogate model can then be applied to single or multi-objective optimisation routines with a variety of objectives. A full list of design outputs that were included in the optimisation design space for this chapter are shown in Table 6.1 (replica of Table 2.4 in chapter 2), along with the system benefits which can be obtained from minimising each output: tensions, both fatigue and (T), surge (S), pitch (P), Nacelle accelerations (A). For illustration, this method is applied to two example locations, and two example optimisation approaches at the end of this chapter.

TABLE 6.1: Key outputs for FOW mooring design, along with the system benefits obtained from minimising these outputs.

Key outputs to minimise	**Positive effects of minimisation on FOW system**
Fairlead tension (T)	Reduced size of mooring line and anchor required (peak load), increased reliability and longevity of mooring (fatigue)
Surge (S)	Ensures safety of the power cable
Pitch (P)	Improves aerodynamic performance of the turbine
Nacelle accelerations (A)	Reduces structural damage to the turbine

The surrogate model developed and presented in this chapter is specific to the design space it was trained for, i.e., taut rope moorings with LRDs – albeit for any water depth, load case, and optimization objectives and constraints. However, the framework of the method presented is applicable to other design spaces, including alternative mooring configurations, with or without LRDs, or other design problems altogether (e.g. for the platform or controller).

6.2 Methodology

6.2.1 Workflow

The overall workflow for the surrogate-based optimisation approach developed in this chapter can be divided into two distinct steps. The first step was to create the surrogate model, which involved setting the design space boundaries, generating the full FEA model dataset within these boundaries, and training neural networks from the resulting dataset. This process was the most time-consuming and computationally intensive, but only needed to be performed once for

the chosen design space. Once the surrogate model was obtained, its computational efficiency offered a significant advantage, enabling the generation of time domain outputs 100,000 times faster than the original FEA (Figure 6.2).

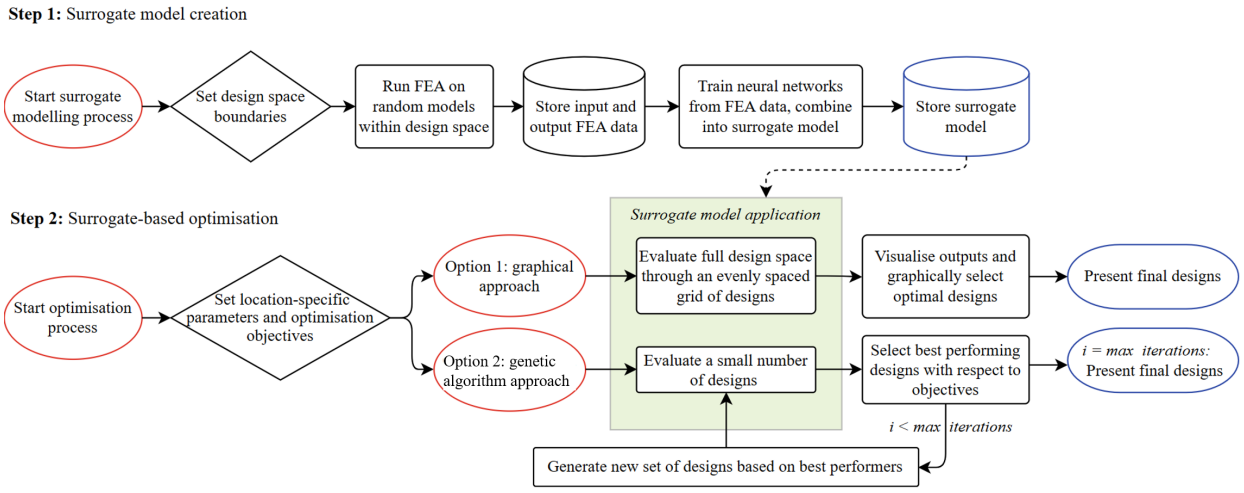

FIGURE 6.2: Overall workflow for creating the surrogate model (step 1) and applying it to the optimisation problem (step 2). Start of self-contained processes are outlined in red, process terminators are outlined in blue, and actions are outlined in black.

The second step involved applying the trained surrogate model to the optimisation problem. This step was flexible and repeatable, as the trained surrogate models could be applied to any modelling problem within the design space. The surrogate models created for this research were applied to two optimisation approaches : a graphical approach, and a numerical approach. The graphical approach consisted of using the surrogate models to model grid-spaced combinations of mooring design variables, using the resulting multivariate plots to graphically determine optimal designs based on a required single objective and constraints. For multi-objective optimisation, numerical optimisation was required, using a genetic algorithm (GA). The GA-based optimisation involved generating a set of designs, called 'individuals', evaluating them with respect to pre-defined objectives, and selecting the best sets to iteratively create the next generation of designs. After a certain number of generations, the best individuals were extracted and formed the 'final' designs.

6.2.2 Generating the dataset

The training dataset was generated from dynamic time-domain analyses with a commercial FE software package, Flexcom. Flexcom offers fully-coupled aero-hydro-servo modelling using FAST plug-ins INFLOWWIND, AERODYN and SERVODYN, and has been validated against other commercial and academic software for a 5 MW turbine as part of an offshore code collaboration project (OC4 - OC6) [109]. To generate the training dataset, a total of 40,000 Flexcom simulations were run in an automated manner, with a uniformly-distributed set of random input parameters, storing time series outputs of every run to form the dataset.

The simulations were run with full aero-hydro-servo coupling, with irregular JONSWAP waves, constant uniform wind, and constant current in a co-linear direction to the incident waves. Constant uniform wind was chosen to simplify the overall problem and resulting surrogate model. The main limitations of using constant uniform wind, rather than a full 3D wind field, or even uniform but time-varying, are the resulting under-estimates of drift motions of the platform and accelerations at the nacelle [127]. This limitation was deemed acceptable in the context of this concept design tool, as in extreme load cases the LRD design is expected to be driven by the wave heights rather wind turbulence [11] [128]. For more detailed design, the methodology and framework can be easily scaled to generate a surrogate model with a time-varying wind input, where instead of saving a scalar input value of mean wind speed at the hub, the whole input time series is stored for each simulation. The neural networks can then be trained with the same structure, with an additional time series input channel for wind speed alongside the wave elevation time series input.

The first step in running the simulations involved defining the boundaries of the design space of the FEA model. The design space is defined by two key components, which affect the range of applicability of the resulting surrogate model:

1. Fixed inputs: these were fixed across all FEA simulations. Consequently, the trained surrogate model cannot be run for a different value of these inputs, and they cannot be used as design variables for the optimisation routine.

2. Variable inputs: these were varied within a set of bounds for each FEA simulation. The trained surrogate model can then produce accurate outputs for any new input values, as long as they are within the set bounds.

In theory, the training dataset can be generated for as many variable inputs as necessary, but each added variable requires more training data, thus more computational time, and adds a potential source of error to the trained surrogate model. For the surrogate model presented in this chapter, the fixed inputs included all the model components which are not related to the mooring system. These were based on the reference models of the International Energy Agency (IEA) 15 MW wind turbine and the Volturn-US semi-submersible platform, which are available as pre-built Flexcom models (validated against the FAST model [98]). The full model specifications are detailed in publications from the National Renewable Energy Laboratory (NREL) [110],[111]. The only modification made to the base model was the mooring system, which was changed to a 3-line taut system with an LRD at each fairlead, as shown in Figure 6.1b. The LRDs were modelled as single spring elements with the non-linear stiffness curves shown in Figure 6.1a, and a length of spring determined by the maximum extension parameter ΔL_{max}. The ΔL_{max} is achieved at 50% strain for TFI and 100% 'strain' for DO, thus the spring sections were given a length of $2\Delta L_{max}$ for TFI and ΔL_{max} for DO. The DO spring section was made neutrally buoyant, and the wet weight of the TFI spring section was scaled to its rated tension as recommended in supplier guidance [82].

The variable inputs were then divided into two categories: the mooring and LRD design variables, which are subjected to optimisation, and the location-specific parameters (i.e. water depth, load case parameters), which are fixed for each load case used to optimise the mooring system. Crucially, these location-specific parameters were included in the variable inputs, making the surrogate model applicable to any location which falls within the bounds of the dataset. The full list of fixed and variable inputs, along with their values or bounds, is shown in Table 6.2.

TABLE 6.2: Fixed and variable inputs to the FE model, used to generate the training dataset.

	Fixed inputs	**Values**
	Wind turbine model	IEA 15 MW reference turbine
	Platform model	Volturn-US semi-submersible
	Mooring configuration	3-line taut with LRDs
	Variable inputs	**Bounds**
Mooring & LRD design variables	Mooring line angle w.r.t. horizontal θ (deg)	15 - 42.5
	Fairlead pretension T_{pre} (MN)	0.75 - 2.5
	Rope stiffness EA (MN)	25 - 125
	LRD type	Dublin Offshore, TFI SeaSpring
	LRD rated tension T_{rated} (MN)	3 - 8
	LRD extension at rated tension ΔL_{max} (m)	5 - 15
Location-specific parameters	Water depth h (m)	50 - 175
	Mean wind speed at hub height V_{hub} (m/s)	5 - 55
	Wind-induced current U_c (m/s)	0 - 1.60
	Significant wave height H_s (m)	1 - 16
	Peak wave period T_p (s)	6 - 18
	Jonswap peakedness factor γ	1 - 4

Before running the simulations to generate the dataset, a list of stored outputs from the FEA simulations needed to be determined. The surrogate model is able to produce the same outputs as were stored from the FEA, provided that they were all included in the training. For this chapter, five outputs were requested from the FEA, corresponding to the key outputs identified in Table 2.4: fairlead tension, surge, pitch, and horizontal and vertical accelerations of the nacelle. All FEA simulations were then run for 3600s for each combination of input variables, and the resulting output time series were combined with the inputs of the run and stored to form the dataset. Once trained, the surrogate model could then be run iteratively with longer wave elevation input time series to generate outputs of any required duration.

6.2.3 Creating the surrogate model

The FEA dataset was used to train a set of five recurrent neural networks, one for each of the required outputs. Of the 40,000 time series forming the original FEA dataset, 5,000 were used for validation, 5,000 for testing, and the remaining 30,000 for training (all randomly assigned). The neural network architecture included one layer of dense inputs, one hidden layer or recurrent cells, and a single-cell final output layer, as shown in Figure 6.3. The recurrent cells, unlike

classic feed-forward neurons used in scalar-to-scalar neural networks, are specialised for handling sequential data rather than individual scalar values. In this case, they retain a memory of previous input waves and previous tension and platform motion outputs, which influences the processing of current inputs, and enables sequence-to-sequence regression. Thus, the full wave elevation time series used in the FEA simulations can be used as an input variable, rather than the JONSWAP parameters Hs, Tp, γ. This allows the neural networks to generalise for any wave seed, meaning they can be run iteratively with new random wave seeds to provide outputs of any duration. Additionally, the sequence-sequence regression provides full flexibility of output metrics without re-training the neural network, allowing an output time series to be characterised by its maximum value, mean value, RMS, or rainflow counted (for tension time series only) depending on the objective required. A scalar-scalar, or sequence-to-scalar model would require re-training for each output metric, and would not be able to accurately reproduce time history-reliant metrics such as the damage equivalent load (DEL).

With a sequence-to-sequence model, the full wave elevation time series used in the FEA simulations can be used as an input variable, rather than the JONSWAP parameters H_s, T_p, γ. This allows the neural networks to generalise for any wave seed, meaning they can be run iteratively with new random wave seeds to provide outputs of any duration. Once trained, the neural networks were then combined to form the surrogate model, as per the structure shown in Figure 6.3.

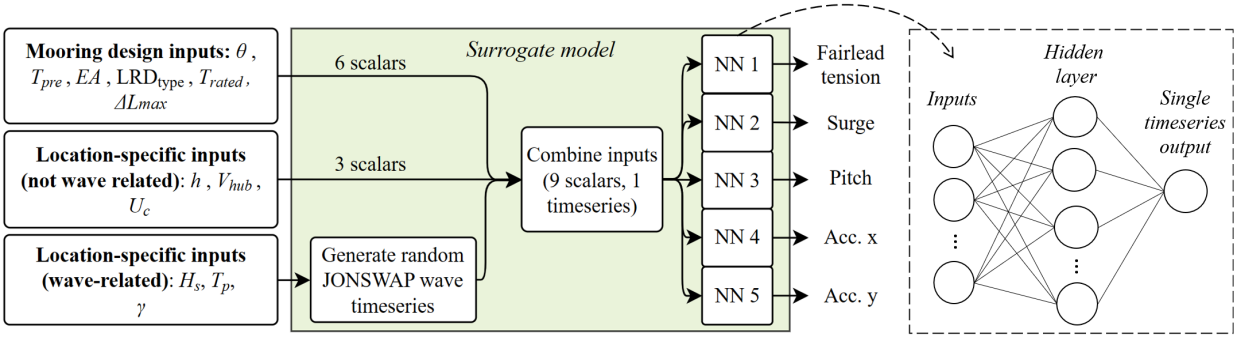

FIGURE 6.3: Overview of surrogate model, which takes both location-specific parameters and mooring design variables as inputs, and produces 5 output time series of any required length. All neural networks which constitute the surrogate model contain similar general architectures, as shown in the dashed section on the right of the figure.

6.2.4 Applying the surrogate model

The first step in applying the surrogate model involved fixing values for the location-specific parameters, leaving only the design variables to be determined by the optimisation process. Two sets of example locations were selected, which are representative of offshore Maine (East coast USA, North Atlantic) and Fos (South coast France, Mediterranean) [46]. For a given location, any representative load case could theoretically be modelled, as long as it is within the bounds outlined in Table 6.2. For this chapter, each location was attributed three sets of design

load cases (DLCs), defined according to IEC guidance (more background on DLC selection and the IEC load case matrix is given in section 2.2.2):

1. Extreme load cases (DLCs 6.1): parked turbine and 50-year wind and wave conditions, typically used to assess maximum loads and platform motions in parked turbine states.
2. Severe load cases (DLCs 1.6): operational turbine at rated wind speed and 1-year wave conditions, typically used to assess maximum loads and platform motions in operational turbine states.
3. Normal load cases (DLCs 1.1): operational turbine and normal wind and wave conditions, typically used to assess cumulative fatigue damage on the structure.

The location-specific parameters of these three sets of DLCs are outlined in Table 6.3, for each example location: Location 1, representative of offshore Maine, USA, in the North Atlantic, rated as a 'medium-intensity' location; Location 2, representative of offshore Fos, France, in the Mediterranean, which is rated as a 'low-intensity' location. For both locations, extreme and severe load cases (DLCs 6.1 and 1.6) were defined with fixed values for all parameters except for the peak wave period T_p, which was defined as a range. Unlike the other parameters, where the higher values usually generate higher loads, the highest value of T_p does not always lead to the maximum loads or platform motions. Thus, all T_p values within the possible range were considered to the nearest full second to ensure maximum events were captured, representing 4 to 7 different sea states for DLCs 6.1 and 1.6. The normal load cases (DLCs 1.1), which were used for fatigue analysis, were composed of 15 different sea states which capture the most common weather loading for each location. For brevity, Table 6.3 only shows the parameter bounds of these 15 sea states, and these are described in full in appendix A. For each group of DLCs, all sea states were run for 3600s of simulation time (i.e. 3600s of time series outputs).

TABLE 6.3: Description of the three groups of design load cases (DLCs) used for mooring design optimisation in this chapter, based on data from the COREWIND report for two example locations [46].

	Location 1: water depth = 130 m			**Location 2:** water depth = 70 m		
	DLCs 6.1	**DLCs 1.6**	**DLCs 1.1**	**DLCs 6.1**	**DLCs 1.6**	**DLCs 1.1**
Vhub (m/s)	44.00	10.59	5.81 - 29.05	37.00	10.59	5.11 - 29.93
Uc (cm/s)	66.00	15.89	8.71 - 43.57	55.50	15.89	7.66 - 44.89
Hs (m)	10.90	7.70	1.59 - 5.09	7.50	4.00	1.00 - 3.69
Tp (s)	11.00 - 16.00	9.00 - 16.00	7.57 - 10.34	8.00 - 12.00	8.00 - 12.00	5.16 - 9.34
Gamma	2.75	2.75	1.00	2.75	2.75	1.00

Once the location-specific parameters were defined, these could be set as fixed inputs to the surrogate model, and various combinations of mooring design variables could be assessed for optimisation. Two optimisation approaches were demonstrated, as described in Figure 6.2: a graphical approach, which was applied to a single-objective optimisation problem with constraints, and a numerical approach, which was applied for multi-objective optimisation problem.

6.3 Surrogate model validation

6.3.1 Neural network architecture selection and training

The most critical components of the surrogate-based optimisation are the 5 recurrent neural networks (RNNs) which produce the time series outputs. Unlike simple feed-forward networks, RNNs can retain memory of previous inputs, making them well-suited for sequential data. Each RNN contains a single, wide hidden layer, which is defined by two main parameters: the type of recurrent cell used, and the number of cells in the layer. Various types of recurrent cells are available, but the two most commonly used types for sequence-to-sequence modelling are Long Short-Term Memory (LSTM) [129] and Gated Recurrent Unit (GRU) [130]. LSTM units are a type of RNN cell which can capture long-term dependencies, using mechanisms called gates to regulate the flow of information. These gates include input, output, and forget gates, allowing LSTMs to selectively remember and forget patterns over time. GRUs are a newer, simpler variant with fewer parameters, combining the input and forget gates into a single update gate for a more computationally efficient structure.

Once the type of cell is determined, the second key parameter of the hidden layer is its width, i.e. the number of cells it contains. A large number of cells can capture more patterns and inter-dependencies between input variables, but can cause over-fitting if the problem is not sufficiently complex and the amount of training data is too small. To find the best combinations of layer types and width, a grid search was performed. This is a commonly used process to tune neural networks, which involves training multiple variants with different combinations of parameters, usually for a reduced number of epochs to limit computational time, and assessing performance of each combination using the test data. Using this approach, a set of 6 different RNNs (3 layer widths, 2 layer types) were trained for each output, for 6 epochs.

These were then tested using the set of 5,000 testing data 'packages' which had been set aside after the data generation step. Each testing data 'package' corresponds to one original FEA simulation, and contains the output time series of that FEA simulation, along with the unique set of input model and load case parameters used to run that simulation. Using these input parameters, predicted output series were generated using the neural network, and added to each test package. Thereby, for each of the 5,000 test packages, the original FEA time series and RNN-predicted time series could be compared according to any required error metrics. In time series regression, prediction accuracy can be measured with specialised error metrics such as cumulative error index (CEI), which sums accumulated errors at every time step, capturing long-term forecasting stability and error drift (i.e. gradual worsening of errors throughout a sequence). In this case, as the RNNs are used for sequence-to-sequence with a short fixed input-output window (3600 seconds) rather than long-term forecasting, no significant drift was expected. Thus, standard error metrics were considered for each of the test packages: 1) mean absolute error, which was taken as the mean difference between all RNN-predicted outputs and original FEA outputs across all time series points, capturing the performance of the RNN over a

full time series ; 2) maximum absolute error, which was taken as the largest difference between NN-predicted outputs and original FEA outputs across all time series points, capturing the performance of the RNN for peak values. For the neural network architecture selection, two commonly-used error metrics were averaged across all 5,000 test packages, and resulting statistics for both error metrics are shown in Figure 6.4.

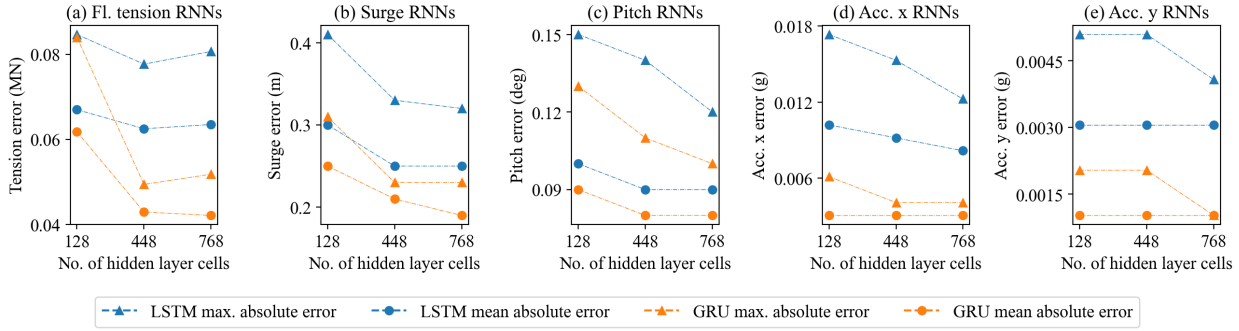

FIGURE 6.4: Grid search for optimal hidden layer architecture, considering two types of RNN cell (LSTM and GRU) and three widths of hidden layer. The grid search was performed for each output independently, and the neural networks were assessed according to maximum absolute error and mean absolute error over each test time series.

The GRU layer displays better performance than the LSTM across all outputs, for both error metrics. This can be explained by the more complex structure of the LSTM, which may attempt to model longer term relationships which are not relevant for this scenario: for FOW response, outputs depend on a small number of previous wave elevation points, but not on waves encountered much earlier in the time series. In particular, for the nacelle accelerations, where small oscillations occur about zero and little memory is required, the GRU performs significantly better.

In general, larger numbers of hidden layer cells display better performance for both maximum and mean error metrics. The largest performance benefits are shown when increasing the layer width from 128 to 448 cells, which suggests that the 128-cell architecture was not providing enough complexity to model some key relationships between input variables. Increasing from 448 to 768 generally provided smaller gains in accuracy, and in the case of output (a), resulted in poorer performance for the maximum error metric, which is a typical symptom of overfitting. As per the results of the grid search, the optimal hidden layer architectures were selected as 448-cell GRU for output (a), fairlead tension, and 768-cell GRU for outputs (b) to (e), representing the platform motions.

Once this architecture was selected, the RNNs were trained for a greater number of epochs (10 epochs). The loss function, i.e. the error function used to adjust hidden layer weightings during training, was the mean absolute error, which ensured equal error weighting for all points in the output time series. Training data were processed individually, which involved feeding individual training points to the neural network and updating weights after each training point. The resulting loss, calculated at every epoch for both the training and validation data, is shown in Figure 6.5.

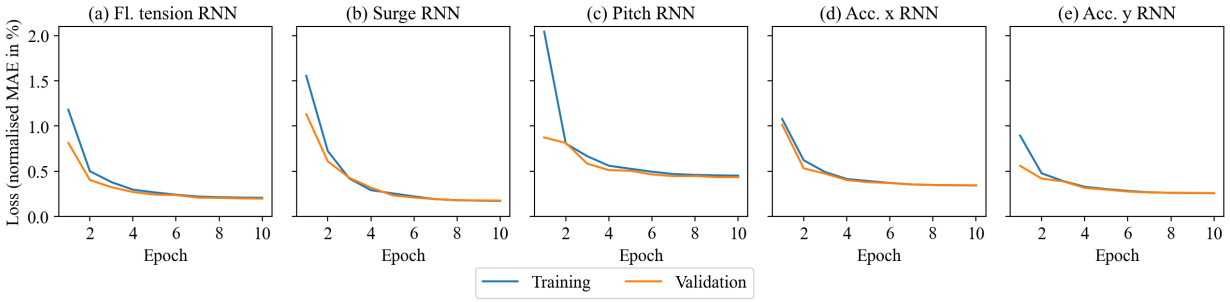

FIGURE 6.5: Training and validation loss over full training routine, for each time series output.

All loss curves evidence a successful training routine, with convergence to low mean absolute error (0.5%) and no overfitting, i.e. no differences between test and validation loss. In the initial 1 to 2 epochs, all RNNs exhibit lower validation loss compared to training loss. This occurs because the validation loss is computed at the end of the epoch, reflecting a more trained state of the RNN. Conversely, the training loss, which is averaged over each epoch, includes poor predictions made early in the epoch after little training has been completed.

6.3.2 Neural network error analysis

The mean absolute error values achieved by the RNNs at the final training epoch (i.e. epoch 10 loss, shown in Figure 6.5) indicate that mean absolute error across all time steps in all the validation time series is below 0.5%. This error metric is effective for training, as it weights all errors evenly throughout the time series, thus enabling the neural network to learn relationships evenly and reducing the risk of over-fitting to local maxima. However, in the context of FOW design, errors are not equally important at all points in the time series. In particular, errors at the maximum values of the time series may be design-driving and thus require more attention. To validate the neural networks, a new error metric $error_{@max}$ is introduced, which represents the absolute error between the predicted and target time series at the maximum point in the original FEA time series (not to be confused with the maximum absolute error discussed in section 6.3.1, which can happen anywhere in the time series). The $error_{@max}$ values were calculated for each of the 5,000 test data packages, for each of the 5 RNNs, and the resulting frequency distribution of errors is shown in Figure 6.6.

The histograms show that the majority of $error_{@max}$ are close to zero, for all 5 RNNs. However, the single maximum $error_{@max}$ values from the whole test dataset can be high. For instance, the maximum fairlead tension $error_{@max}$ value across all test data for RNN (a) is close to 1 MN, which could be problematic if the specific case at the source of this error is design driving. The sources of these error values are investigated in more detail in Figure 6.7, which displays the worst prediction along with the associated input variables at the source of the error.

For all outputs, the $error_{@max}$ occur for combinations of input variables that are close to the boundaries of the training dataset, in particular with high values of current and wind speed

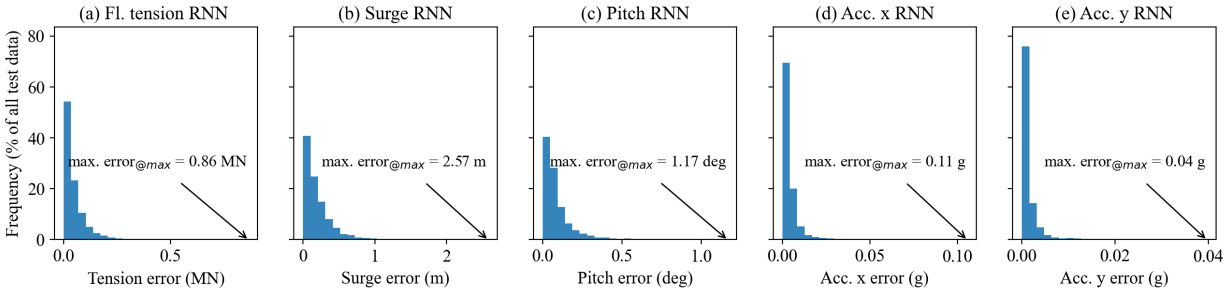

FIGURE 6.6: Distribution of errors at the maximum point in the target time series ($error_{@max}$). Maximum $error_{@max}$ values across the entire test dataset are labelled for each output.

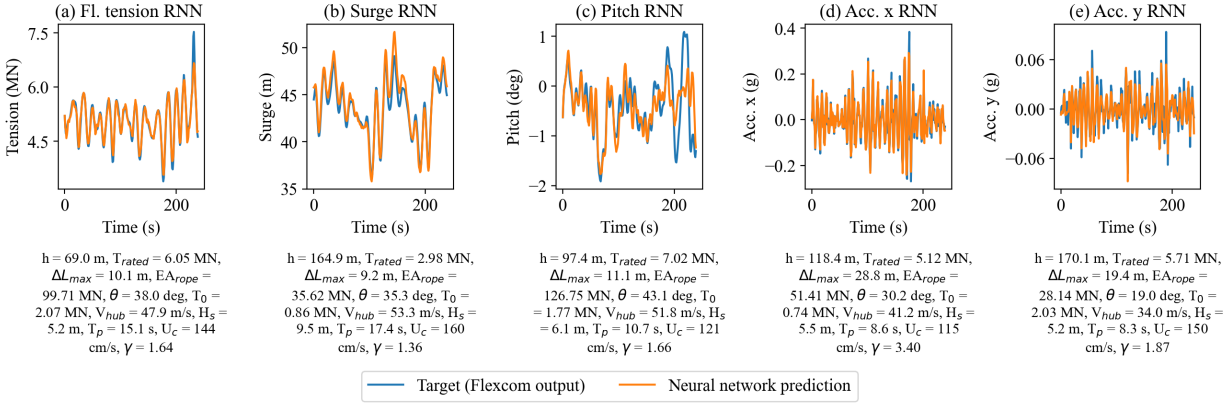

FIGURE 6.7: Time series with worst $error_{@max}$ from the full set of 5000 test data, for each RNN, along with the associated set of inputs that generated the time series.

(RNN (a), (b) and (c)) and low values of wave period (RNN (d) and (e)), which means they will have limited impact on the design load cases chosen for the optimisation case study (Table 6.3).

One of the advantages of using RNNs trained for any random wave elevation seed is that errors can be mitigated by considering multiple wave seeds for the same set of inputs, and averaging the outputs. For each set of inputs that generated the maximum $error_{@max}$ value (i.e. the sets of inputs shown in Figure 6.7), the RNNs were run with 14 additional random wave seeds, and mean and median values of the maximum outputs were taken across multiple seeds. Figure 6.8 shows the resulting reduction in $error_{@max}$ for each additional random wave seed considered, starting from the original seed which was the source of the high error.

These results show that if five or more seeds are considered for each output, and the median of the results is taken across all seeds considered, the maximum $error_{@max}$ can be significantly reduced for all 5 RNNs. For all further results in this chapter, all surrogate model runs were performed using 6 different wave seeds for each set of inputs, and all metrics calculated from the output time series were taken as the median value across all 6 seeds. Using this approach, the maximum $error_{@max}$ values can be considered satisfactory for concept design.

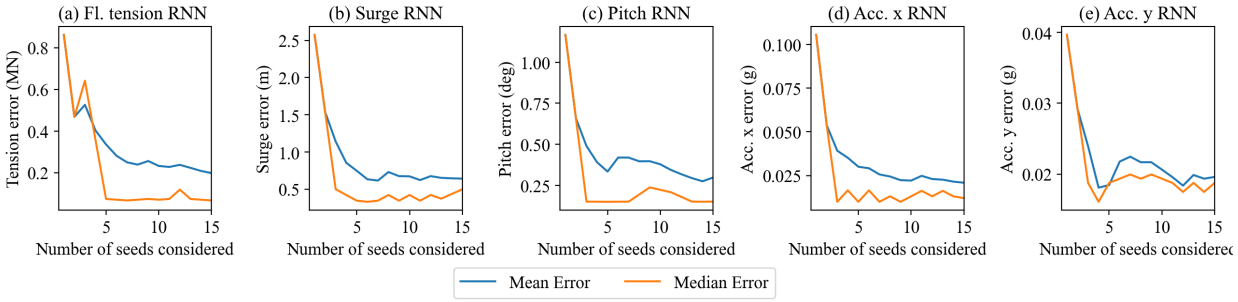

FIGURE 6.8: Reduction of the extreme $error_{@max}$ values shown in Figure 6.7 by considering additional wave seeds, and taking the mean or median of the output.

6.4 Optimisation case studies

6.4.1 Capabilities of surrogate model for optimisation

Holistic design optimisation is made possible by the efficiency of the final surrogate model, which takes less than one second to run all DLCs shown in Table 6.3 for 3600s, including the use of 6 seeds per sea-state to reduce error as discussed in Section 6.3.2. The time series outputs then allow full flexibility in the selection of objectives, constraints, and metrics to assess the outputs. As discussed in section 6.3.2, the maximum point of the time series is a key metric, especially for surge and tension, as these maximum values are typically design-driving [8]. For pitch, although maximum values are important, high values sustained over long durations are a particular concern for energy production [33], thus the root-mean-squared (RMS) of the output time series is a suitable metric. For assessment of fatigue damage on the mooring line caused by irregular loading, a specific metric exists, known as the damage equivalent load (DEL). For a given irregular time series of mooring line tension, the DEL represents the amplitude of a constant cyclic load that results in the same cumulative fatigue damage as the irregular tension time series itself [126]. In this section, the applicability of the surrogate model is demonstrated for select objectives and constraints formulated using the aforementioned metrics, using the graphical and numerical approaches described in Figure 6.2. The graphical approach was applied to single-objective optimisation with constraints, and the numerical approach was applied to unconstrained multi-objective optimisation. For both approaches, the two example locations described in Table 6.3 were considered, each with a different LRD, resulting in two scenarios: scenario A using the TFI Seaspring (TFI LRD) for location 1, and scenario B using the Dublin Offshore device (DO LRD) for location 2. Neither location necessarily suits one LRD technology over the other, and although contrasts between the two scenarios are briefly discussed, the main intention is to demonstrate the flexibility of the surrogate model rather than to compare LRDs and locations.

6.4.2 Graphical single-objective optimisation

6.4.2.1 Motivation

The choice of method for optimisation is motivated by the characteristics of the optimisation problem, as well as the efficiency of the underlying model. Since the surrogate model developed in this chapter can evaluate hundreds of designs in seconds, it enables the use of highly computationally-intensive optimisation methods. In Table 2.7, a range of methods were explored, each with different computational intensity and aptitude at handling constraints and multiple objectives. The grid search optimisation is the most computationally intensive, as it evaluates every possible solution in the search space, but has the benefits of: 1) being highly reliable, as the exhaustive search means it cannot get stuck in local minima or maxima; 2) providing insightful results over the whole design space, which can be interpreted graphically to gather more understanding of the problem. This section explores the application of a grid search approach to a single-objective problem, and provides a graphical interpretation of results which can be used as a basis, or as an alternative to the genetic algorithm-based optimisation.

6.4.2.2 Optimisation problem definition

To perform holistic design optimisation, all design variables shown in Figure 6.1b must be considered simultaneously. For the specific scenario, the optimal set of design variables $\mathbf{x}$ must be found, where $\mathbf{x} = [\theta, T_{pre}, EA_{rope}, T_{rated}, \Delta L_{max}]$, within a set of bounds $\mathcal{X}$ as defined by the limits of the design space shown in Table 6.2. This constitutes a 5-dimensional optimisation problem, which is complex to visualise graphically. To do so, the design space can be split into grid-spaced combinations of variables, to obtain a set of multivariate plots which adequately covers the design space. For this analysis, particular emphasis was placed on the LRD design variables as these require detailed consideration [128], and a grid-spaced combination of 20 T_{rated} and 20 ΔL_{max} values were considered within the design space bounds. For each of the three other design variables, only two values were considered for brevity and ease of visualisation. This resulted in a total of $20 \times 20 \times 2 \times 2 \times 2 = 3200$ combinations of mooring design variables to be assessed for every load case, which would not be practical with full FEA model, but could be completed in less than one hour using the surrogate model.

In this section, two example single-objective optimisation problems are considered: sop_1, with the objective of reducing maximum fairlead tension in the extreme 50-year condition (DLC 6.1), and sop_2, with the objective of reducing fatigue damage on the mooring line in normal sea states (DLC 1.1). These objectives are commonly used in mooring design optimisation [41], as both can offer significant cost and reliability benefits (Table 2.4). However, optimising for these objectives generally involves reducing the mooring system stiffness, and this must be considered alongside increased platform motions. For this example, constraints are applied to two key platform motions: surge (S) and pitch (P). As maximum surge is limited by the displacement

range of the power cable, the designs were assessed using DLC 6.1 (50-year parked) to obtain the highest expected values of surge in the FOW turbine's design life. For pitch constraints, which are usually determined by performance requirements in operation, most severe operational load case with 1-year return (DLC 1.6) was used. For this case study, indicative constraint values were selected based on existing literature [46], and are displayed in Table 6.4. The two single-objective optimisation problems sop_1 and sop_2 are then defined mathematically, giving Equations 6.1 and 6.2 respectively:

$$
\begin{aligned}
& sop_1 : \\
& \min_{\mathbf{x}} \quad T_{\text{max, 6.1}}(\mathbf{x}) \\
& \text{s.t.} \quad S_{\text{max, 6.1}}(\mathbf{x}) \leq S_{\text{lim}} \\
& \qquad P_{\text{RMS, 1.6}}(\mathbf{x}) \leq P_{\text{lim}} \\
& \qquad \mathbf{x} \in \mathcal{X}
\end{aligned}
\tag{6.1}
$$

$$
\begin{aligned}
& sop_2 : \\
& \min_{\mathbf{x}} \quad T_{\text{DEL, 1.1}}(\mathbf{x}) \\
& \text{s.t.} \quad S_{\text{max, 6.1}}(\mathbf{x}) \leq S_{\text{lim}} \\
& \qquad P_{\text{RMS, 1.6}}(\mathbf{x}) \leq P_{\text{lim}} \\
& \qquad \mathbf{x} \in \mathcal{X}
\end{aligned}
\tag{6.2}
$$

where $T_{\text{max, 6.1}}$ is the maximum fairlead tension from all DLCs 6.1, $T_{\text{DEL, 1.1}}$ is the overall damage equivalent load for all DLCs 1.1, $S_{\text{max, 6.1}}$ is the maximum surge from all DLCs 6.1, and $P_{\text{RMS, 1.6}}$ is the root-mean squared pitch from all DLCs 6.1. $S_{\text{max, 6.1}}$ and and $P_{\text{RMS, 1.6}}$ are subject to constraints S_{lim} and P_{lim} respectively.

TABLE 6.4: Chosen values of constraints, for the two example locations described in Table 6.3. The surge constraint is defined as 20% of the water depth, and the pitch limit is fixed at the same value for both locations, based on values used in previous studies 2.3.

Constraint metric	**Location 1**	**Location 2**
Maximum surge from DLCs 6.1 ($S_{\text{max, 6.1}}$)	$S_{\text{lim}} = 14$ m	$S_{\text{lim}} = 26$ m
Root-mean-squared pitch from DLCs 1.6 ($P_{\text{RMS, 1.6}}$)	$P_{\text{lim}} = 5.5$ deg	$P_{\text{lim}} = 5.5$ deg

6.4.2.3 Graphical visualisation of constraints

To graphically find the solutions satisfying the surge and pitch constraints, all 3200 combinations of design variables were assessed using the surrogate model, for DLCs 6.1 and 1.6

respectively. The results for scenario A, i.e. location 1 and TFI LRD, are shown in Figure 6.9, which covers the full design space using a separate surface plot for each combination of θ, T_{pre}, and EA_{rope}, (see Table 6.2) where each surface plot covers all combinations of LRD design variables T_{rated} and ΔL_{max}.

Lower stiffness combinations of mooring variables in the top left of the grid (lower pretension T_{pre}, lower rope stiffness EA_{rope}, and lower mooring line angle θ) result in higher surge (or horizontal offset) of the floating platform. Similarly, reducing the stiffness of the LRD by increasing its maximum extension ΔL_{max} or reducing its rated tension T_{rated} also increases surge. Thus, most of the combinations of low stiffness design variables do not adhere to the surge constraint. All design variables show strong correlations to surge, and differences of up to 300% can be noted between the lowest stiffness designs (top left surface) and highest stiffness designs (bottom right surface). For pitch (Figure6.9 (b)), this trend is different: most design variables are shown to have little correlation with the output, and only a 20% difference in pitch can be noted between the lowest stiffness designs and highest stiffness designs. In fact, the pitch value is shown to be mainly driven by mooring line angle, which affects the magnitude of the vertical restoring force counteracting the rotational motion of the platform. Hence, for all combinations of other design variables, the lower mooring line angle is shown to exceed the pitch constraint.

Results for scenario B (location 2, DO LRD) are shown in Figure 6.10. The overall trends are similar to scenario A, with lower-stiffness combinations of variables causing higher surge, and the lower values of mooring line angle causing pitch to exceed the specified constraint. However, the magnitude of the maximum surge values is significantly lower, which is due to the lower water depth and lower overall intensity of the environmental loading in DLC 6.1 for location 2 (see Table 6.3). The difference in location-specific parameters is less influential for pitch, and the magnitude of the RMS pitch values is overall comparable to those obtained for scenario A. This is due to the wind-thrust on the turbine, which drives the pitch, being equal for both scenarios A & B as their respective DLCs 1.6 both employ the same operational wind speed (10.59 m/s, as shown in Table 6.3).

6.4.2.4 Graphical visualisation of objectives

Having removed portions of the design space which exceed the platform motion constraints, the optimal designs for the single-objective problems sop_1 and sop_2 can then be determined graphically, using the same format as the constraint visualisation plots in Figures 6.9 and 6.10. The resulting surface plots are shown in Figure 6.11, for scenario A (Location 1, TFI LRD), with the hatched areas from both pitch and surge constraints combined to illustrate the remaining available areas of the design space.

As expected, the low-stiffness combinations of mooring design variables (top left of grids (a) and (b)) led to the lowest fairlead tensions, for both maximum tensions and fatigue (DEL). However, the design space for the LRD design variables is more non-linear, and LRDs with

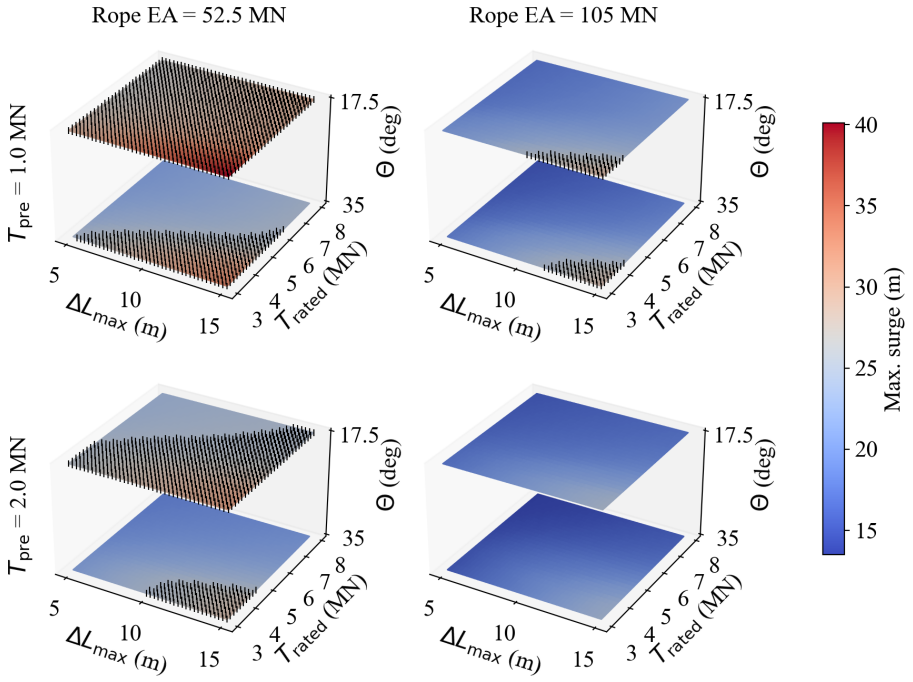

(a) Max. surge DLCs 6.1

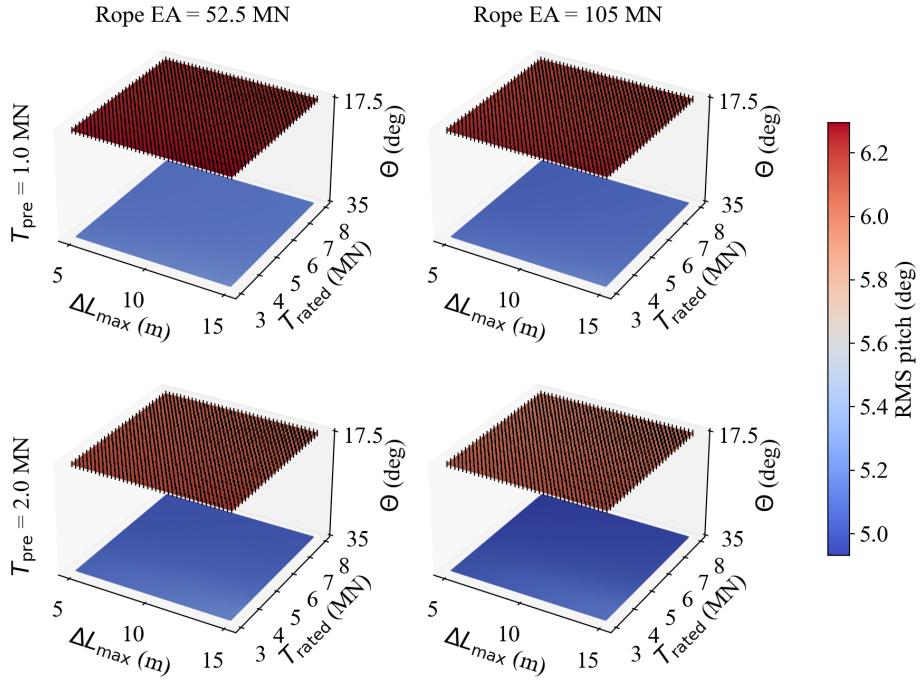

(b) RMS pitch DLCs 1.6

FIGURE 6.9: Mooring performance with respect to (a) surge constraint and (b) pitch constraint, for scenario A (Location 1, TFI LRD). Each surface shows the output value for all combinations of T_{rated} and ΔL_{max}, and these surfaces are positioned in the grid based on the value of the other variables θ, T_{pre}, and EA_{rope}. Portions of the design space exceeding the constraints are hatched.

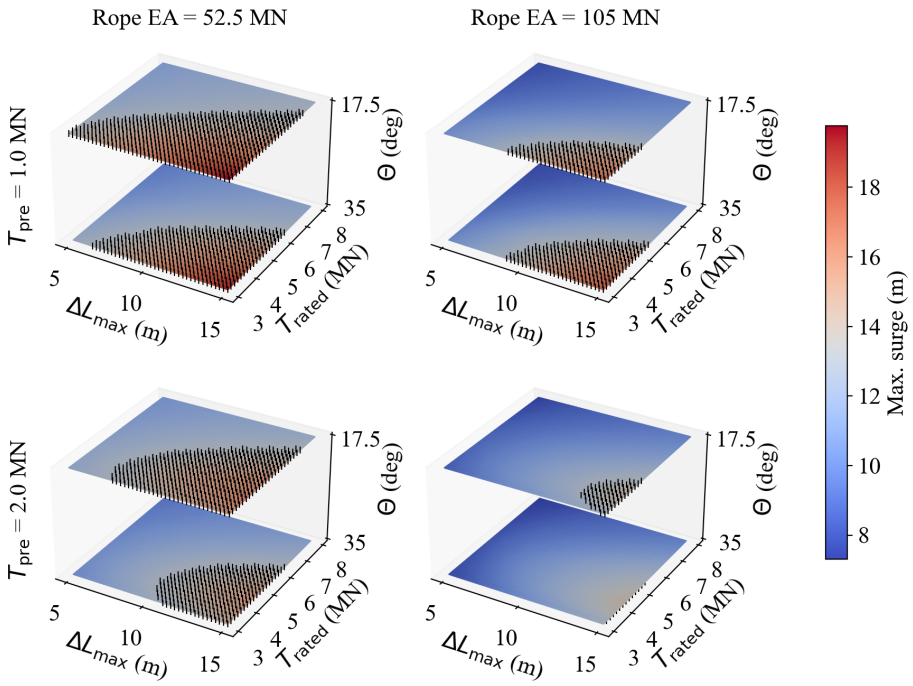

(a) Max. surge DLCs 6.1

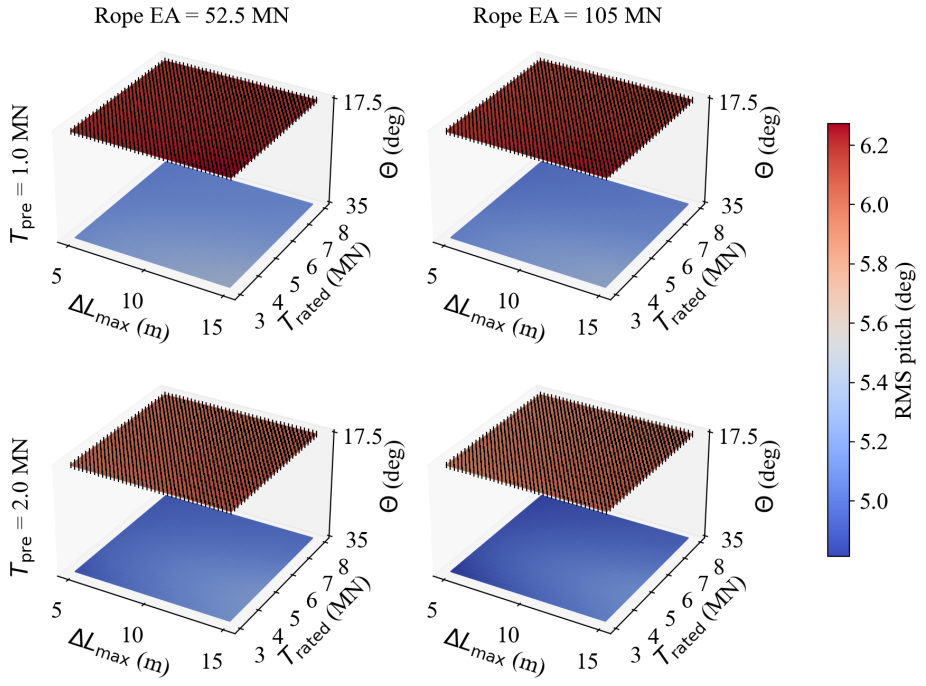

(b) RMS pitch DLCs 1.6

FIGURE 6.10: Mooring performance with respect to (a) max. surge constraint and (b) RMS pitch constraint, for scenario B (Location 2, DO LRD). Portions of the design space exceeding the specified constraints are hatched.

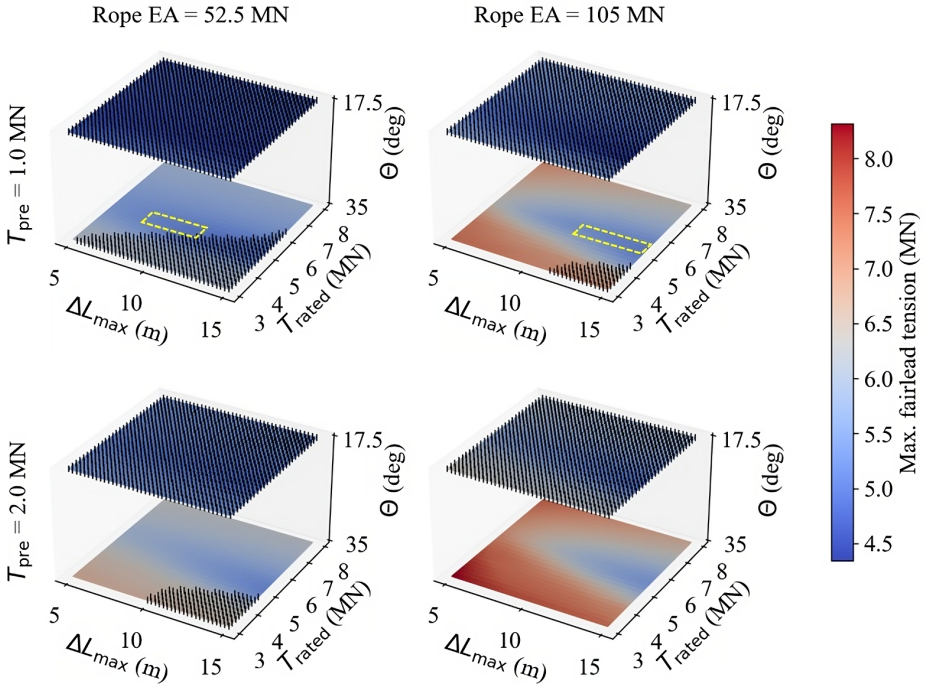

(a) Max. fairlead tension DLCs 6.1

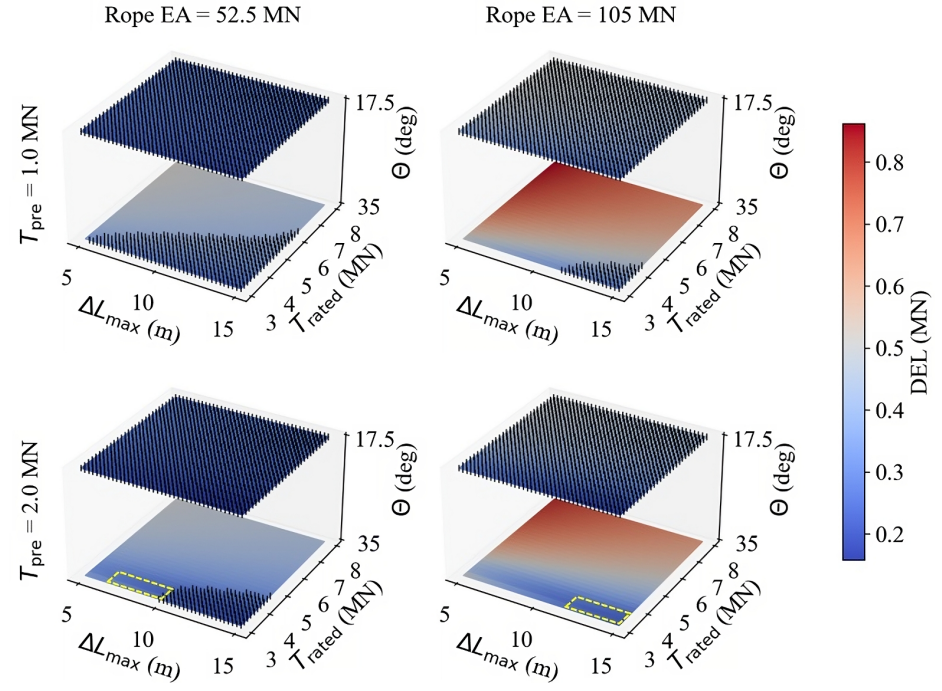

(b) Damage Equivalent Load DLCs 1.1

FIGURE 6.11: Mooring performance with respect to the (a) max. tension reduction and (b) DEL reduction objectives, for scenario A (Location 1, TFI LRD). Portions of the design space which exceeded the specified constraints are hatched, and the optimal regions for max. tension and DEL reduction are marked on (a) and (b) respectively with a dashed yellow box.

lower stiffness, i.e. lower values of rated tension T_{rated}, can lead to higher maximum fairlead tensions for DLC 6.1. This is due to the LRDs with lower rated tensions exceeding their rated tensions in 50-year storms, thus entering their third phase stiffness too early, and not having any compliance remaining to reduce the wave-driven dynamic loads. This is visible on the 3 MN TFI stiffness curve plotted in Figure 6.1a: above 3 MN, the device is 'locked-out' thus bringing no load reduction benefit. Conversely, if its rated tension is too high, the LRD will not extend past its high first-phase stiffness when confronted with dynamic wave loading, thus not providing adequate tension reduction. For all surface plots in Figure 6.11a & b, the optimal ranges of rated tension values are located in the blue/dark blue regions, where the LRD is operating in its second phase stiffness and can provide optimal tension reduction. For maximum tension reduction, i.e. Figure 6.11a, this optimal range is itself dependent on the other mooring line variables: the optimal rated tension is around 4 MN for the low-stiffness combinations of variables (top row, i.e. 17.5°angle and 1 MN pre-tension) and around 6 MN for the highest stiffness combination (bottom row, i.e. 35°angle and 2 MN pre-tension). However, most of the low-stiffness combinations of variables exceed motion constraints (hatched areas). From the available parts of the design space not excluded by the constraints, the areas of lowest maximum fairlead tension, i.e. the solutions to problem sop_1 are marked with a dashed yellow box.

For problem sop_2, which involves minimising the fatigue damage (i.e. DEL) on the mooring system, the optimal areas of the design space are different. As the magnitude of loads expected from normal sea states (DLCs 1.1) is much lower than that expected from extreme sea states (DLCs 6.1), the optimal rated tension to ensure the LRD is in its second phase stiffness is also lower, at around 3 MN for most cases. Higher pretension values (bottom row of Figure 6.11b) increase the base extension of the LRDs into a softer second phase stiffness, providing more DEL reduction. The areas of lowest DEL which also adhere to the motion constraints, i.e. solutions to problem sop_2, are marked with a dashed yellow box. In practice, although these designs would lead to low fatigue damage from normal sea states, they may not be viable as they would lead to high maximum fairlead tensions and lock-out of the LRD in DLCs 6.1. Better solutions could be found by considering both maximum tension and fatigue damage reduction objectives simultaneously, and finding the designs which provide an adequate trade-off between the two objectives.

Results for the design scenario B, i.e. lower intensity location and Dublin Offshore (Location 2, DO LRD), are shown in Figure 6.12. Overall, the lower intensity of environmental loading for extreme sea states (DLCs 6.1) in Location 2 leads to lower overall maximum tension values for scenario B compared to scenario A. As the normal sea states (DLCs 1.1) are similar for both locations, and loads for these sea states are mainly driven by the operational wind thrust on the turbine, the magnitudes of DEL values for scenario B are similar to those of scenario A.

The effect of mooring design variables on maximum tension and DEL follow similar trends as for scenario A, with lower-stiffness designs (i.e. lower pre-tension, lower rope stiffness, lower line angle) generally leading to lower fairlead tension. However, the LRD design space is different, due to the difference in shape of the non-linear stiffness curve for the DO LRD, which

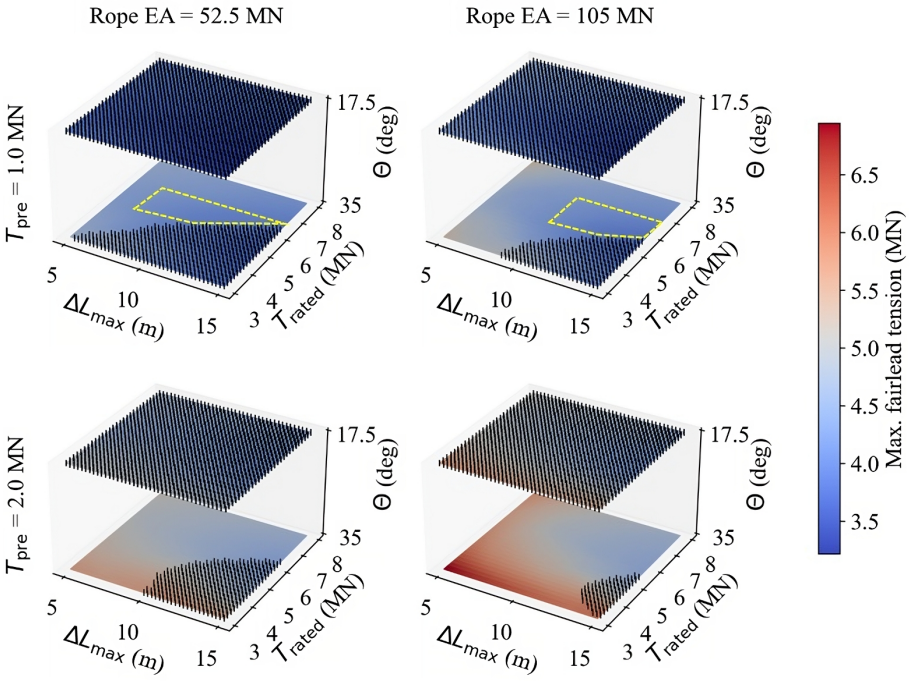

(a) Max. fairlead tension DLCs 6.1

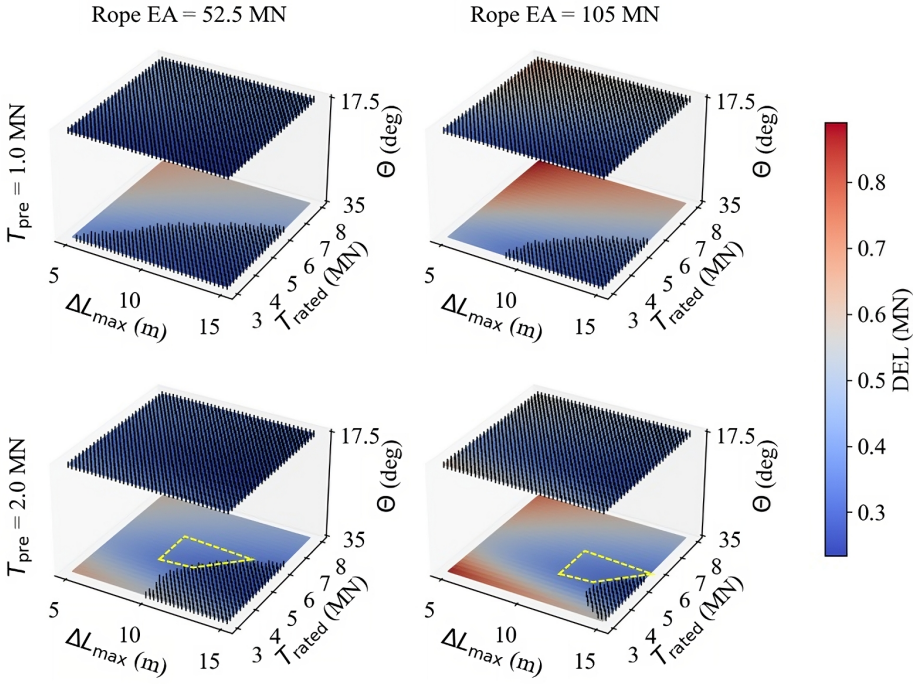

(b) Damage Equivalent Load DLCs 1.1

FIGURE 6.12: Mooring performance with respect to the (a) max tension reduction and (b) DEL reduction objectives, for scenario B (Location 2, DO LRD). Portions of the design space which exceeded the specified constraints are hatched, and the optimal regions for max. tension and DEL reduction are marked on (a) and (b) respectively with a dashed yellow box.

exhibits a longer, and slightly stiffer second-phase than the TFI LRD (see Figure 6.1a). Although the stiffer second-phase of the DO curve can lead to a slight disadvantage with regards to maximum tension reduction [128], it also means the window of optimal rated tensions to ensure the device operates in its second phase stiffness is larger, illustrated by larger regions of blue in the surface plots in Figure 6.12. The optimal regions which satisfy the constraints for both problems sop_1 and sop_2 are marked with dashed yellow boxes in Figure 6.12a and b respectively.

6.4.3 Numerical multi-objective optimisation

6.4.3.1 Optimisation problem definition

Although the graphical approach is useful for understanding the design space and provides good indications for concept design, the wide grid spacing for the non-LRD variables means that some solutions will inevitably be missed, as not all combinations of variables are assessed. For more precision and complete cover of the design space, numerical optimisation should be used. Numerical approaches enable efficient computation of multiple optimisation objectives, which can provide a more complete and versatile optimisation process than single-objective constrained optimisation. In particular, the constrained approach may result in the exclusion of certain solutions for minor violations of constraints, even if these solutions perform significantly better with respect to the objective. For instance, a mooring design that results in a surge slightly above the limit, but with much lower tension, could be rendered viable by adjusting the power cable design, resulting in a cheaper overall solution. In this context, platform motions such as surge, pitch, and nacelle accelerations could be treated as additional objectives, rather than constraints.

The surrogate model and subsequent optimisation routine can be used to define a single or multi-objective problem with any number and combination of objectives, with any cost-function formulation as long as it is a function of the available outputs shown in Figure 6.3. In the context of mooring design optimisation for FOW, all of the following outputs typically require minimisation: Fairlead tension (T), to reduce the size of the mooring line and anchor required; Surge (S), to ensure safety of the power cable; pitch (P), to improve aerodynamic performance of the turbine; and nacelle accelerations (A) to reduce structural damage to the turbine. In a detailed design scenario, some of these objectives will be more design-driving than others, but this ultimately depends on project-specific parameters which may not be fully determined at the time of initial concept design screening. In theory, the surrogate model would allow each objective to be given an individual weight, and combined into a single cost function, but this would output a unique design solution that does not provide insight on the trade-offs between competing objectives. At a concept design level, a versatile multi-objective optimisation tool that outputs a range of possible design solutions will provide more useful insight to design engineers [97] [20]. To demonstrate this versatility, four example multi-objective optimisation

problems were considered (mop_1 to mop_4), each with two objectives relating to the design considerations described in Table 2.4.

All four problems were given a first objective of minimising maximum fairlead tension for DLCs 6.1 ($T_{\text{max, 6.1}}$), and the second objective was assigned as follows: for mop_1 and mop_2, minimising $S_{\text{max, 6.1}}$ and $P_{\text{RMS, 1.6}}$ respectively (i.e. same DLCs and metrics used for constraints in section 6.4.2.4); for mop_3, minimising maximum values of horizontal nacelle acceleration in DLCs 6.1 ($A_{\text{max, 6.1}}$), to minimise damage to the turbine [33]; for mop_4, minimising fatigue damage on the mooring line for all normal operational load cases ($T_{\text{DEL, 1.1}}$). Additionally, two constraints were included in all four optimisation problems to ensure all designs produced by the algorithm are 'safe' for ultimate limit state: the maximum tension in the DCLs 6.2 must be below the rated tension T_{rated} of the LRDs, and below the minimum breaking load (MBL) of the rope MBL_{rope}, with a safety factor of 1.67 [126]. The MBL of the rope is assumed proportional to its stiffness EA_{rope}, according to the datasheets for Bridon MOORLINE polyester ropes [66]. The multi-objective problems mop_1 to mop_4 are expressed in mathematical form as follows:

$$
\begin{aligned}
&mop_1: \\
&\min_{\mathbf{x}} \quad (T_{\text{max, 6.1}}(\mathbf{x}), S_{\text{max, 6.1}}(\mathbf{x})) \\
&\text{s.t.} \quad T_{\text{max, 6.1}}(\mathbf{x}) \leq T_{\text{rated}} \\
&\qquad\quad T_{\text{max, 6.1}}(\mathbf{x}) \leq 0.6 * MBL_{\text{rope}} \\
&\qquad\quad \mathbf{x} \in \mathcal{X}
\end{aligned}
\tag{6.3}
$$

$$
\begin{aligned}
&mop_2: \\
&\min_{\mathbf{x}} \quad (T_{\text{max, 6.1}}(\mathbf{x}), P_{\text{RMS, 1.6}}(\mathbf{x})) \\
&\text{s.t.} \quad T_{\text{max, 6.1}}(\mathbf{x}) \leq T_{\text{rated}} \\
&\qquad\quad T_{\text{max, 6.1}}(\mathbf{x}) \leq 0.6 * MBL_{\text{rope}} \\
&\qquad\quad \mathbf{x} \in \mathcal{X}
\end{aligned}
\tag{6.4}
$$

$$
\begin{aligned}
&mop_3: \\
&\min_{\mathbf{x}} \quad (T_{\text{max, 6.1}}(\mathbf{x}), A_{\text{max, 6.1}}(\mathbf{x})) \\
&\text{s.t.} \quad T_{\text{max, 6.1}}(\mathbf{x}) \leq T_{\text{rated}} \\
&\qquad\quad T_{\text{max, 6.1}}(\mathbf{x}) \leq 0.6 * MBL_{\text{rope}} \\
&\qquad\quad \mathbf{x} \in \mathcal{X}
\end{aligned}
\tag{6.5}
$$

$$
\begin{aligned}
& mop_4 : \\
& \min_{\mathbf{x}} \quad (T_{\text{max, 6.1}}(\mathbf{x}), T_{\text{DEL, 1.1}}(\mathbf{x})) \\
& \text{s.t.} \quad T_{\text{max, 6.1}}(\mathbf{x}) \leq T_{\text{rated}} \\
& \qquad T_{\text{max, 6.1}}(\mathbf{x}) \leq 0.6 * MBL_{\text{rope}} \\
& \qquad \mathbf{x} \in \mathcal{X}
\end{aligned}
\tag{6.6}
$$

The surrogate model enables the efficient use of complex numerical or heuristic approaches to solve this problem, such as Genetic Algorithms (GAs), which typically need to assess thousands of designs to provide optimal solutions. In particular, for multi-objective problems, GA variants such as the non-dominated sorting genetic algorithms (NSGA, NSGA-II, NSGA-III) [131] are most suitable. These evolutionary algorithms evaluate solutions based on non-dominance, i.e., whether a solution is superior across one or more objectives without being inferior in others, and iteratively evolve a population of solutions toward optimal trade-offs between objectives.

The original NSGA algorithm employs non-dominated sorting but suffers from high computational complexity. NSGA-II improves this with fast non-dominated sorting, an elitist approach to preserve high-quality solutions, and a crowding distance mechanism to maintain solution diversity. It is particularly well-suited to problems with 2–3 objectives. NSGA-III further enhances performance for many-objective problems (four or more objectives) by using reference points to guide population evolution and maintain diversity in high-dimensional objective spaces [131]. However, since the optimisation problem in this study involves a limited number of objectives, NSGA-II is the most appropriate choice. It offers better performance and computational efficiency than NSGA or NSGA-III, providing solutions closer to the true Pareto front more quickly without the additional complexity of reference points.

In contrast to the single-objective optimisation approach, that provides a unique solution, the multi-objective optimisation results in many possible solutions, where each solution maximises trade-offs between specific objectives. These solutions are typically visualised through a 'Pareto front', where each point on the Pareto front represents a solution where no objective can be improved without worsening another (see Figure 2.25 section 2.4).

6.4.3.2 Optimisation results

The NSGA-II algorithm was applied to all multi-objective optimisation problems mop_1 to mop_4, with an initial population size of 100 individuals, and was run for 50 generations (i.e. iterations). The resulting Pareto fronts for each of the multi-objective problems mop_1 to mop_4 are shown for scenarios A and B in Figures 6.13 and 6.14 respectively. The blue scattered points represent individuals (i.e. designs) from the final population of the NSGA-II, which are Pareto-optimal with respect to the two objectives, and grey points represent the initial random individuals

which are 'dominated'. For multi-objective problem mop_4 (Figure 6.13 (d) and Figure 6.14 (d)) the non-dominated solutions do not form a classical Pareto front, and are clustered in a single group. This phenomenon is typical of objectives that are not conflicting, and leads to a convergence in the solution space. This contrasts with the results of section 6.4.2.4, which found the DEL and max tension reduction to be conflicting, especially for the TFI LRD. However, this was due to the presence of the surge constraint; if this is omitted, the low-stiffness combinations of mooring design variables (i.e. low angle, low rope stiffness, low pre-tension) can be used, which simultaneously provide optimal tension reduction and DEL reduction (see the top surfaces of Figures 6.11 and 6.12).

Although all solutions on the Pareto fronts are optimal in theory, some provide higher utility than others. To obtain marginal gains in performance with respect to one objective can mean considerable losses with respect to the other. For instance, in the surge vs. tension Pareto front for scenario A (Figure 6.13a), restricting maximum surge to 15 m leads to very high maximum tensions. Similarly, to get pitch values from 5 degrees to 4.4 degrees for scenario A can almost double maximum fairlead tension (Figure 6.13b). In theory, if both objectives are given equal importance, the solutions which maximise utility are located at the 'knee point' of the Pareto front. The 'knee point' represents the point in the Pareto front with the shortest distance to the 'utopia solution', i.e. the imaginary solution which has the optimal value for each objective (e.g., for Figure 6.13 (a), this would be 4 MN max. fairlead tension and 10 m max. surge). For each of the sub-figures in Figure 6.13 and 6.14, the knee point solution is marked in orange, and the design variables associated with that solution are displayed on the plot.

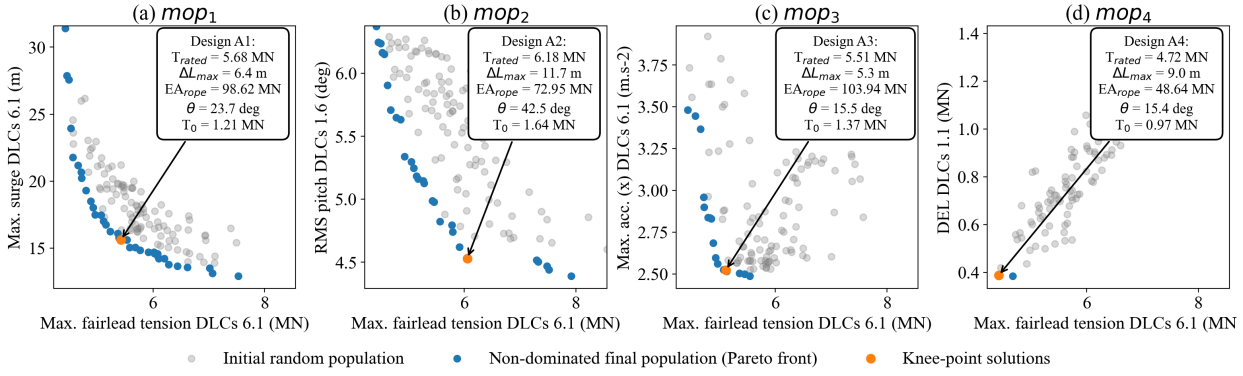

FIGURE 6.13: Results of multi-objective problems, showing trade-offs between 4 key objective pairs, for scenario A (Location 1, TFI LRD). For each multi-objective problem, the non-dominated solutions are shown in blue, and the 'knee-point', i.e. maximum utility solution, is shown in orange.

The combinations of design variables which lead to knee-point solutions follow the same general trends as the solutions found in the graphical optimisation approach (section 6.4.2.4). For all optimisation problems with the TFI LRD (scenario A, Figure 6.13), the knee-point solutions exhibit LRD rated tensions which are approximately equal to the maximum tension, which mean the TFI LRD is operating in the softest part of the second-phase of its non-linear stiffness curve to reduce extreme loads. This is not as apparent for the DO LRD (scenario B,

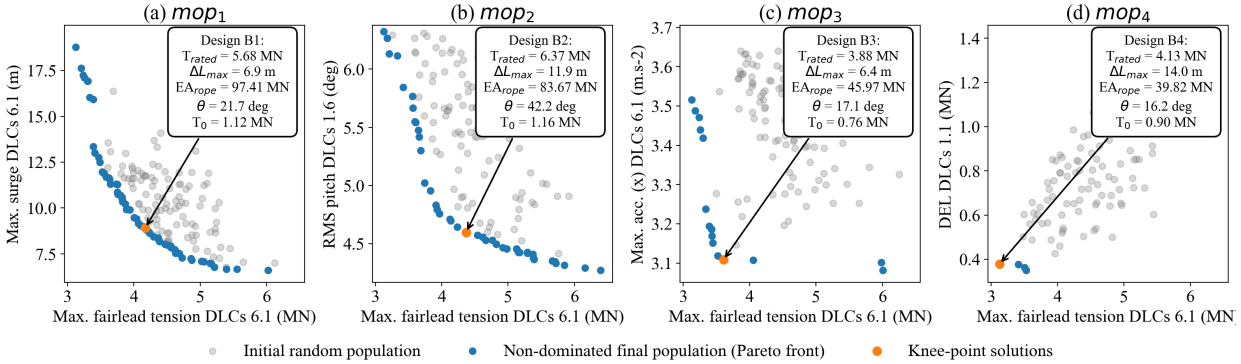

FIGURE 6.14: Results of multi-objective problems, showing trade-offs between 4 key objective pairs, for scenario B (Location 2, DO LRD). For each multi-objective problem, the non-dominated solutions are shown in blue, and the 'knee-point', i.e. maximum utility solution, is shown in orange.

Figure 6.14), due to its longer, constant second phase stiffness, as discussed in section 6.4.2.4. The knee-point solutions which enable low RMS pitch angles (figures 6.13b and 6.14b), as discussed in section 6.4.2.3, require the highest values of mooring line angle to ensure maximal vertical restoring force, combined with high maximum LRD extension to ensure good performance with respect to the maximum tension objective. In contrast, solutions which reduce horizontal acceleration at the nacelle (Figures 6.13c and 6.14c) require lowest values values of mooring line angle to ensure maximal horizontal restoring force. Solutions which minimise both DEL and maximum tension (Figures 6.13d and 6.14d) have the highest levels of compliance and would not be viable in practice, as these would lead to extremely high values of surge.

Whether the knee-point solutions would be optimal for a specific project will then depend on other variables such as cost and availability of various components and installation considerations. Crucially, this approach to optimisation allows complete flexibility in the choice of solution. Although knee-point solutions were marked here to illustrate the process, each Pareto front displays multiple other possible solutions which could offer various degrees of utility within, or close to, the 'knee-point' area. The NSGA-II only does the work of filtering the dominated solutions, i.e. those that are objectively worse, and allows flexibility in the remainder of the decision-making.

6.4.3.3 Final design comparison

The surrogate-based optimisation process demonstrated the usage of a genetic algorithm to find the optimal mooring solutions in the design space, which perform better in all objectives than other 'safe' designs (e.g. the grey points in Figures 6.13 and 6.14). In this section, all knee-point solutions found in section 6.4.3.2 are compared to a base-case full chain catenary mooring, to assess the combined advantages of the surrogate-based optimisation process, with advantages of the new design space of taut rope moorings with LRDs. The base-case mooring system parameters are listed in Table 6.5, selected based on previous studies for locations with similar

environmental loads [111] [132], to ensure integrity of the mooring line and no uplift of the anchor in ultimate limit state (ULS) conditions.

TABLE 6.5: Parameters of base-case full-chain catenary mooring systems used to compare the performance of optimised designs found in this chapter. Chain diameters are set based on previous studies [111] [132], ensuring peak tensions are below chain MBL with a safety factor of 1.67 [14], and anchor-fairlead distance and pretension are set to ensure no uplift at the anchor in ULS conditions.

Parameter	**Scenario A**	**Scenario B**
Chain diameter in mm (studless)	185	152
Chain MBL in kN ($P_{\text{RMS, 1.6}}$)	22,526	16,254
Pretension at the fairlead	8% of MBL	8% of MBL
Anchor - fairlead distance (m)	573	494

Each of the four optimal designs selected for scenarios A and B, i.e designs A1 to A4 (Figure 6.13) and designs B1 to B4 (Figure 6.14) respectively, were compared against the base-case mooring for all outputs considered in the optimisation process. Results of the comparison are shown in Figure 6.15.

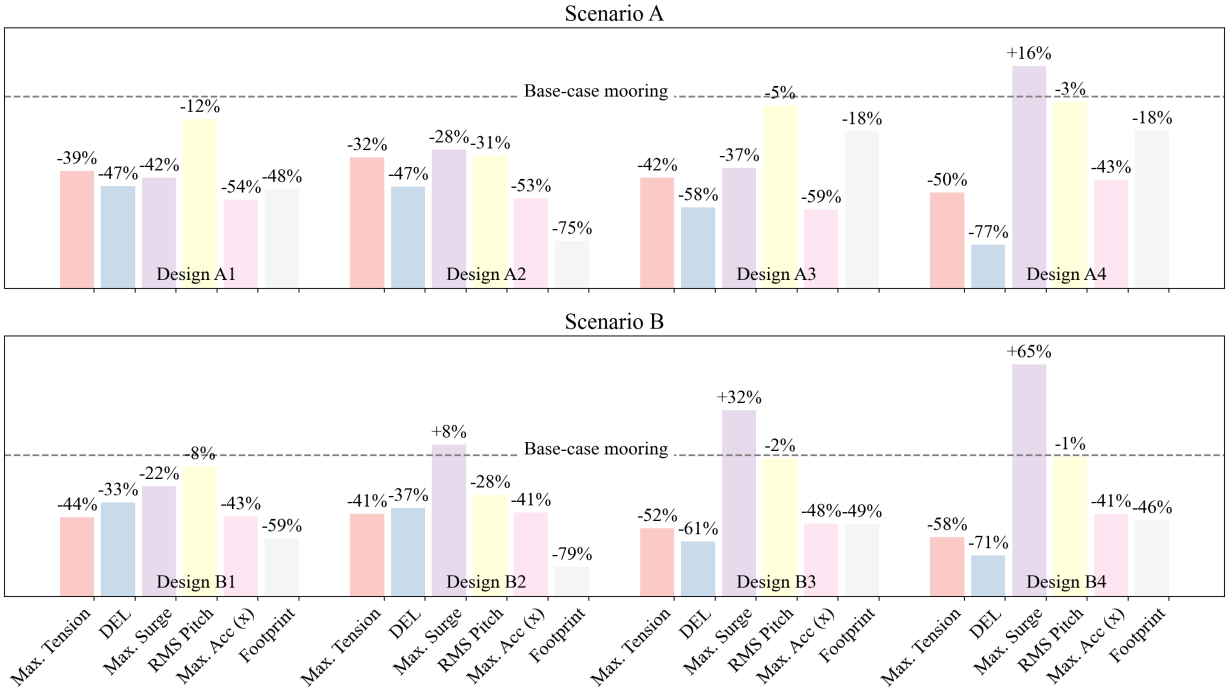

FIGURE 6.15: Comparison of performance of optimal designs found in section 6.4.3.2, i.e. designs A1 to A4 for scenario A (Figure 6.13) and designs B1 to B4 for scenario B (Figure 6.14), against a base-case full-chain catenary mooring system (dashed grey line), for 6 outputs. Each design responds to a different multi-objective problem, from mop_1 to mop_4.

Overall, the designs in Figure 6.15 provide significant improvements in most key outputs compared to the base-case catenary mooring system. All designs provide high maximum tension reduction (32 - 58%), as this was a common objective to all multi-objective problems mop_1 to mop_4. However, each design responds to a different second objective, leading to varying characteristics and system benefits across all 4 designs, which are summarised below:

- mop_1 (surge reduction): Designs A1 and B1 provide an even balance between stiffness and compliance, with an intermediate value of line angle, to limit surge whilst providing adequate tension reduction.
- mop_2 (pitch reduction): Designs A2 and B2 achieve highest pitch reduction through steep mooring line angles, which enable strong restoring moments, whilst also leading to a significant decreases in seabed footprint. However, the reduced footprint also increases the system's stiffness due to shorter rope lengths, which slightly compromises reductions in maximum tension and DEL compared to other designs.
- mop_3 (horz. acc. reduction): Designs A3 and B3 achieve the highest horizontal acceleration reductions due to the lower line angles which alters the horizontal resonant frequency of the mooring. However, the low mooring line angles lead to less seabed footprint reduction and pitch reduction.
- mop_4 (Damage equivalent load (DEL) reduction): Designs A4 and B4 provide the highest compliance, as these were optimised for both DEL and maximum tension reduction objectives, with no consideration for platform motions. This produces the highest values of maximum surge (higher than the base-case catenary moorings).

Overall, Figure 6.15 highlights the versatility of the surrogate-based optimisation methodology, which allows a range of optimisation objectives, metrics, and relevant DLCs to be considered, in turn producing a diverse set of solutions. Although the final choice of solution is up to the designer, this selection can be made from Pareto-optimal designs, i.e. from a set of focused solutions that are guaranteed to maximise the trade-offs with respect to the objectives.

6.5 Conclusion

This chapter proposed a novel approach for holistic optimisation of floating offshore wind (FOW) mooring systems with load reduction devices, using a recurrent neural network-based surrogate model to predict fairlead tension and platform motions. The neural networks were trained with data from fully coupled time-domain finite element analyses of the reference 15 MW FOW turbine, and yielded instantaneous time series results for any combination of mooring design variables, load case and water-depth. The surrogate model could then be used for project-specific optimisation for any locations and design requirements without the need to generate new data and re-train the neural networks. The three key take-aways from this chapter can be summarised as follows:

1. Recurrent neural networks can create an acceptable surrogate model for time series predictions of FOW platform outputs and fairlead tensions, with a mean absolute error of 0.5% and a maximum absolute error of less than 5%.

2. The efficiency of the resulting surrogate model, which is approximately 100,000 times faster than the original FEA model, enables the usage of intensive optimisation methods, including graphical and numerical genetic algorithm which require modelling thousands of designs.

3. The surrogate-based optimisation can be applied to any location and optimisation problem without re-training the neural networks, to produce a diverse set of optimised mooring designs, where each design provides different system benefits.

Chapter 7

Conclusions and future work

7.1 Conclusions

This thesis has addressed design optimisation of mooring systems with load reduction devices for floating offshore wind (FOW), through application of analytical, numerical and machine learning methods. FOW presents a unique challenge for mooring design: it involves mooring multiple structures in shallow water, unlike offshore oil and gas, which involves mooring a single structure in deep water. The shallow water, combined with high wind loading experienced by a FOW turbine, leads to extreme loads on moorings and anchors. The current approach to resisting these loads is to employ large, heavy moorings and anchors, but this is an expensive approach which cannot be delivered at scale. Non-linear extensible mooring components, known as load reduction devices (LRDs), can reduce loads and therefore cost of a FOW project, but introduce several design variables that must be optimised. Current modelling methods are not suited for quickly assessing these variables, making it difficult for developers to evaluate the benefits of LRDs.

The overarching aim of this research was to address these challenges by developing an efficient framework for designing FOW mooring systems with LRDs, adaptable to any project-specific parameters and objectives. The research outcomes reflect the objectives: 1) Development of a quasi-static analytical model for initial sizing of mooring systems including non-linear load reduction devices (chapter 4); 2) Comparison of mooring configurations and non-linear LRD stiffness curves using commercial dynamic analysis software (chapter 5); and 3) Development of a neural network surrogate model, based on dynamic analyses, for holistic optimisation of FOW mooring systems with LRDs according to project-specific platform motion constraints, loads, and water-depths (chapter 6).

From the achievement of these objectives, key conclusions that can be drawn are:

- *Conclusion 1*: Mathematical expressions of non-linear LRD stiffness curves can be combined with established quasi-static mooring equations, to create a quasi-static model

of the full system. This allows for the rapid assessment of optimal LRD length and stiffness, for any mooring configuration, water depth, and expected platform offsets. This approach was demonstrated and validated against finite element modelling with less than 1% error, and was implemented into a graphical design tool for easy visualisation of mooring system geometry and tension-offset profiles. The design tool was demonstrated for a concept design scenario, enabling efficient sizing of an LRD mooring system, as a basis for dynamic finite element analysis.

- *Conclusion 2*: Through comparative dynamic finite element analysis, LRDs with three-phase stiffness curves (i.e. high-stiffness, low-stiffness, high-stiffness), were shown to provide greater peak tension reduction and fatigue damage reduction than two-phase stiffness curves (i.e. low-stiffness, high-stiffness) without increasing platform motions. Combining 3-phase LRDs with high-modulus taut moorings enables especially high load reduction performance, whilst also enabling smaller seabed footprints and lighter mooring lines.

- *Conclusion 3*: Recurrent neural-networks, trained from dynamic finite element analyses, can successfully capture time-domain FOW responses, across a comprehensive set of load cases and design parameters, quasi-instantaneously. A surrogate model was created from these recurrent neural-networks, which allowed optimisation for a variety of locations and objectives without needing new data or retraining. This approach demonstrated significant reductions in maximum tension, nacelle accelerations, fatigue damage, and seabed footprint compared to traditional designs.

  Ultimately, these optimised mooring designs can provide significant reductions to the overall cost of a FOW project, and reduce the carbon footprint and capacity pressures of its supply chain. Additionally, the framework of the method presented is applicable to other design spaces, including alternative mooring configurations, with or without LRDs, or other design problems altogether (e.g. platform design, or turbine controller design).

7.2 Web-apps

While the research presented in this thesis contributes to the academic understanding of FOW mooring system design optimisation, it also offers practical web-based tools for industry application. These tools will make it easier for FOW mooring designers to identify the benefits of employing LRDs and optimising mooring system compliance, and to explore more cost-effective areas of the mooring design space.

Two web-apps have been developed as part of this research, one hosting the quasi-static tool developed in Chapter 4, and one hosting the surrogate model developed in Chapter 6. Screenshots of these apps are shown in Figures 7.1a and 7.1b respectively. These apps can be freely accessed on the WebAppsForEngineers server https://www.webappsforengineers.com/).

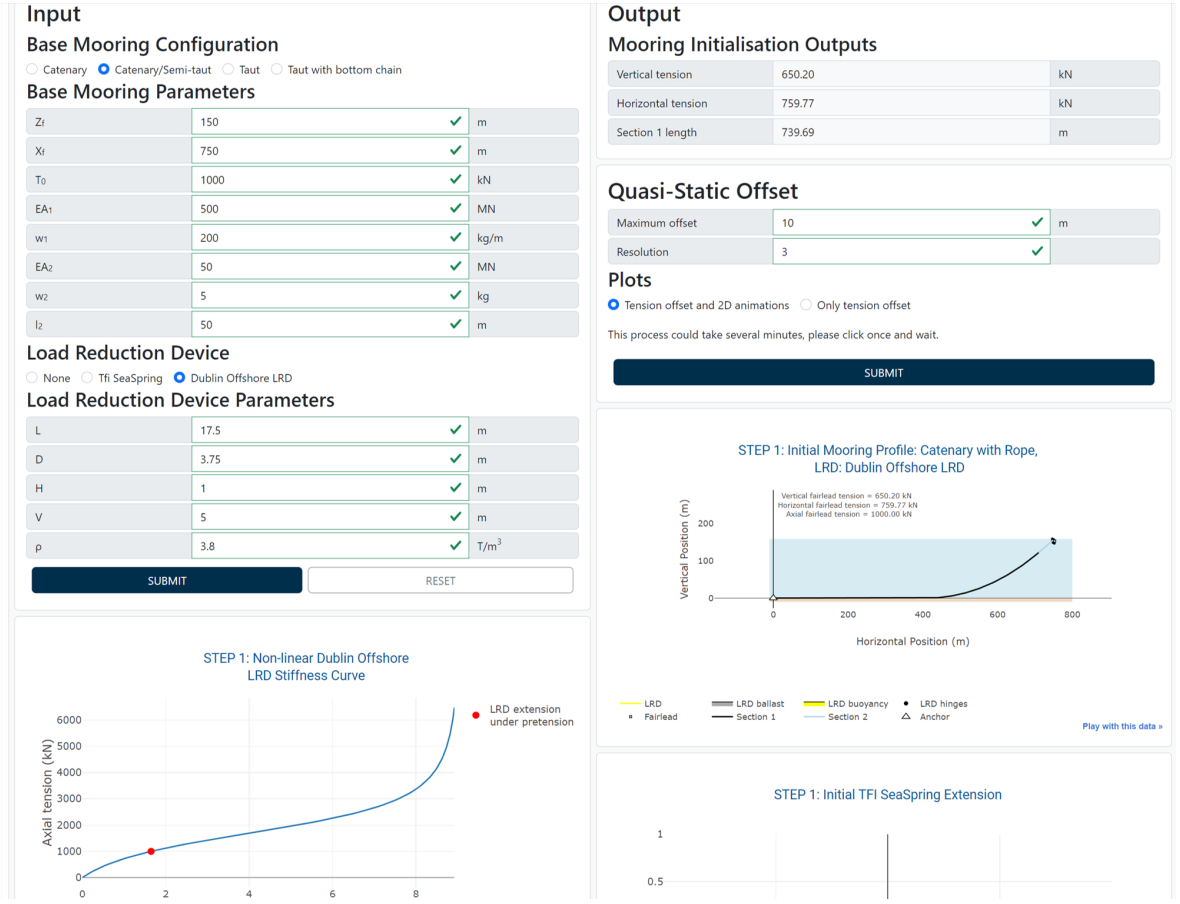

(a) Quasi-static mooring analysis tool, based on the analytical model developed in Chapter 4.

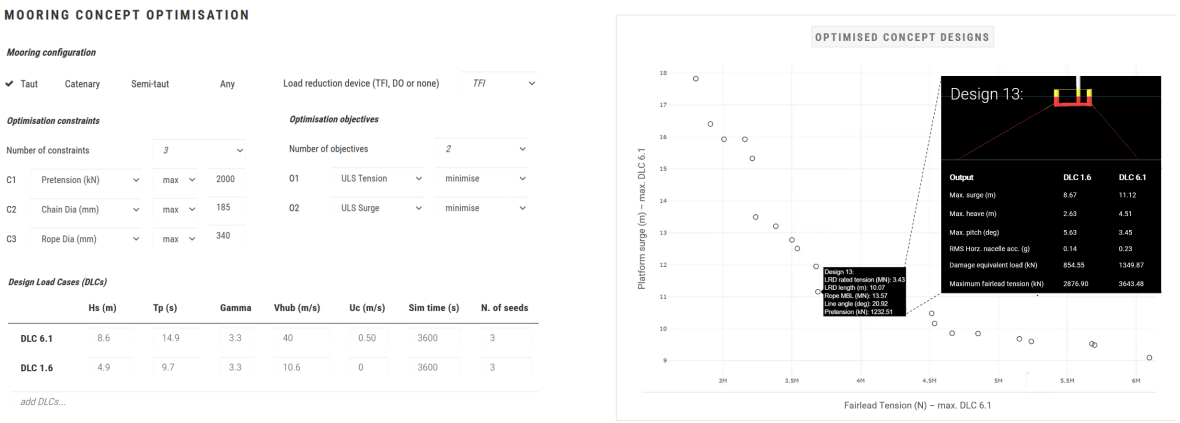

(b) Dynamic time-series analysis tool, based on the surrogate model developed in Chapter 5.

FIGURE 7.1: User interfaces of the two web-apps produced as part of this research, available on the WebAppsForEngineers server https://www.webappsforengineers.com/)

7.3 Limitations

This research contains methodological limitations, which primarily stemmed from simplifications made in the modelling approach. These simplifications were necessary to keep the scope manageable but could be refined in future research. The main limitations are:

- *LRD modelling*: In the dynamic modelling, standardised non-linear spring elements with different non-linear stiffness curves were used to model all LRD concepts, to isolate the impact of the LRD stiffness curve on the system. While effective for this study, this approach limits the ability of the model to capture additional damping or stiffness characteristics dependent on the geometry of the devices (see sections 4.3.3 and 5.2.2 for further discussion). Future studies could employ more detailed, geometrically accurate LRD models to address this limitation.
- *FOW modelling*: Simulations were conducted with full aero-hydro-servo coupling, using irregular JONSWAP waves, constant uniform wind, and co-linear current to simplify the model. The use of constant uniform wind can lead to underestimation of platform motions, fairlead tensions and nacelle accelerations, as it does not account for the peaks in wind loading that would be captured by a full 3D wind field varying in time and space. This simplification was deemed acceptable for concept design, as extreme tensions in the fairlead, which drive LRD design, are primarily caused by extreme wave events rather than wind turbulence. For detailed design, the framework could be adapted to incorporate time-varying wind inputs.
- *Surrogate modelling*: The development of the surrogate model relied on a 'grid-search' parametric analysis to identify the optimal RNN training and architecture hyperparameters, and error analyses on test data to assess the surrogate model performance. The grid search and error analyses effectively identified the optimal RNN hyperparameters for the specific problem, but this is an empirical approach which does not provide transparency regarding how well the model captures the relevant features. To investigate the relative importance of the input features and if the input-output dependencies (within the black box) conform with the problem mechanics, future research could incorporate AI explanatory algorithms like SHAP and LIME, which would offer further insights into model performance and provide a basis for further improvements to the surrogate model.

7.4 Future work

This research provides a basis for further advancements in the field of optimisation of mooring systems with load reduction devices. In particular, the following topics have been identified, which could add value to each of the three main developments presented in this thesis:

- *Quasi-static modelling of a full 3-dimensional mooring system with LRDs*. The quasi-static model developed in chapter 4 is 2-dimensional, meaning it enables optimisation of a windward (i.e. 'front') mooring line, which is the most important mooring line to consider for optimisation. The quasi-static model could be expanded to accommodate lateral 'sway' movement of the fairlead, which would enable modelling of a full multi-line 3D mooring system, in view of optimising the designs of the leeward (i.e. 'rear') mooring lines.

- *Parametric analysis of LRDs for semi-taut moorings*. To build upon the comparative analysis presented in chapter 5, it would be interesting to consider additional mooring configurations, such as the semi-taut configuration, to compare its performance against the taut and catenary configurations considered in this thesis.
- *Surrogate-based optimisation of dynamic cables*. The surrogate-based optimisation methodology presented in chapter 6 is applicable to a wide range of design optimisation problems in offshore engineering. Dynamic cable design for FOW would be particularly well suited to this methodology, as the design space is complex (see Figure 2.8), and modelling with traditional methods is extremely slow, since the design is mainly fatigue-driven and requires assessment of 1000s of load cases [36].

Appendix A

Appendix

A.1 Comparative analysis of load reduction device stiffness curves for floating offshore wind moorings

Ocean Engineering 298 (2024) 117266

Contents lists available at ScienceDirect

Ocean Engineering

journal homepage: www.elsevier.com/locate/oceaneng

Comparative analysis of load reduction device stiffness curves for floating offshore wind moorings

Oscar Festa [a,*], Susan Gourvenec [a], Adam Sobey [a,b]

[a] Faculty of Engineering and Physical Sciences, University of Southampton, Southampton, SO16 7QF, UK
[b] Data-Centric Engineering, The Alan Turing Institute, London, NW1 2DB, UK

ARTICLE INFO

Keywords:
Load reduction devices
Floating wind turbines
Compliant moorings
Mooring system design
Taut moorings

ABSTRACT

Traditional mooring systems can be unsuitable and uneconomical for floating offshore wind turbines. Load reduction devices, which are extensible components installed along mooring lines, have been shown to reduce loads on anchors and mooring lines. This enables the use of smaller and lighter anchors and mooring components and reduces fatigue damage on the mooring system. Load reduction devices come in various forms, including ballasted pendulums, polymer springs, and hydraulic dampers, each with unique non-linear stiffness curves. These non-linear curves typically consist of either a progressively-increasing 'single-phase' stiffness, or a 'three-phase' stiffness which exhibit stiff first and third-phase responses with a low-stiffness second phase. Selecting the correct shape of stiffness curve is key to ensure optimal load reduction performance from the device. This study compares the impact of 4 different non-linear stiffness curves, including 2 single-phase curves and 2 three-phase curves, on tension reduction and platform motions through finite element modelling. Taut and catenary mooring configurations, in both shallow (75 m) and intermediate (150 m) water depths, during 50-year parked and 50-year operational load cases are considered. The IEA 15 MW reference turbine, on the reference Voluturn-US semi-submersible platform are adopted for the analyses. Of the 4 non-linear stiffness curves considered, those with three-phase stiffness offer the maximum load reduction compared to a base mooring with no load reduction device, and are most effective in reducing fatigue damage. All load reduction device stiffness curve types have little effect on out-of-plane motions of the platform and acceleration at the nacelle, but lead to an increase in horizontal offset, or surge, of the floating offshore wind turbine when compared to the base mooring system. The increase in surge is similar regardless of the load reduction device stiffness curve shape, and is shown to be mainly driven by the length and rated tension of the device.

1. Introduction

1.1. Motivation

Up to 80% of worldwide offshore wind resources are located in water depths greater than 60 m (WindEurope, 2017), where traditional fixed-bottom wind turbines become less economically viable. In these water depths, offshore wind turbines must be deployed on floating structures, which are connected to the seabed via mooring systems composed of mooring lines and anchors. Current floating offshore wind turbine (FOWT) mooring system designs are derived from decades of oil and gas practices, and typically employ heavy steel components (Ma et al., 2021) which are expensive and carbon-intensive to manufacture, transport and install. As FOWT farms require large numbers of structures to be moored to the seabed, reducing mooring system material costs per unit has the potential to provide significant reductions to the overall cost of a FOWT project, reducing the carbon footprint and capacity pressures of its supply chain.

The material cost of a mooring system is typically driven by the minimum breaking load (MBL) of mooring line components and the maximum holding capacity of the anchor, both of which must be designed to withstand the extreme loading experienced over the system's lifetime. A typical approach to reducing loads on a mooring system involves increasing the compliance of the mooring system, i.e., reducing its stiffness (Ma et al., 2019). All spread mooring systems exhibit some form of compliance, which can be either geometric or elastic. Geometric compliance describes the ability of the mooring to change shape under loading, e.g. a catenary mooring line lifting off the seabed, while elastic compliance determines the capacity of the mooring line to extend axially, e.g. elastic stretch of a section of polymer rope. By

* Corresponding author.
E-mail address: ogf1n20@soton.ac.uk (O. Festa).

https://doi.org/10.1016/j.oceaneng.2024.117266
Received 22 September 2023; Received in revised form 12 February 2024; Accepted 21 February 2024
Available online 28 February 2024

maximising the compliance of the system to fit the displacement criteria (primarily governed by the allowable range of the electrical power cable), loads on the system can be reduced, thus enabling the safe usage of more cost-efficient anchors and mooring line components.

In deep waters, taut and catenary mooring systems are inherently compliant due to the length of suspended line, which provides more elastic or geometric compliance. However, a significant portion of European floating wind to the mid-century is forecast to be in relatively shallow water depths, i.e., 50–150 m, where designing compliant mooring systems is challenging. Catenary configurations require heavier lines to achieve a reasonable pretension in shallower waters, which, combined with the fact more line gets lifted off the seabed for a given offset, leads to excessively stiff mooring systems and large footprints (Xu et al., 2020). For taut configurations, which typically employ polymer ropes, shallower waters lead to shorter lines for the same inclination angle, which means less available extension of the polymer rope, i.e. elastic compliance. More extension can be obtained by using a line angle closer to horizontal, which increases the length of rope, however this leads to larger footprints and higher material costs.

Load reduction devices (LRDs) are a nascent technology which introduce customisable compliance into a mooring system, so that the mooring system stiffness is not constrained by its physical and geometric properties (e.g. weight of chain, angle of mooring line, MBL of rope). This 'targeted' compliance provides a solution to the challenge of achieving a compliant mooring system in shallower water depths, without resorting to excessively large seabed footprints. LRDs, typically located close to the fairlead, act as non-linear springs that can safely operate at high levels of extension, i.e., 50% of the length of component compared to 5%–10% for traditional polymer rope. The key design parameter of an LRD is its non-linear stiffness curve, which effectively governs the stiffness of the mooring system. The non-linear stiffness curve is highly customisable by LRD manufacturers to provide greatest possible tension reduction whilst adhering to platform motion criteria. The devices can be tailored to a specific project environment and can be incorporated into catenary or taut mooring lines. The effect of the shape of the LRD non-linear stiffness curve on tension reduction and platform motions has not yet been comprehensively assessed for FOWT applications, and is the object of this research.

1.2. Background on LRDs

Current LRD concepts include the Technology for Ideas Seaspring (TFI), Dublin Offshore LRD (DO), and Exeter Intelligent Mooring System (IMS). The TFI device (Fig. 1a) is formed of a compressive polymer spring, which provides a low-stiffness, regressive response up until the steel flanges meet and the device 'locks-out'. The DO device (Fig. 1b) is formed of a part-weighted, part-buoyant cylinder which rotates under axial load to provide extension, counteracted by the restoring moments created by the weighted and buoyant sections. The IMS device (Fig. 1c) is composed of a hollow braided rope containing a water-filled pressurised bladder which resists reduction in the rope's diameter. The adjustable bladder pressure means the stiffness response of the device can be tuned in operation. Existing research around these LRD technologies has been highly driven by physical testing, and all three have been shown to successfully withstand the offshore environment (Harrold et al., 2020; OffshoreWind.biz, 2021; Offshore-mag.com, 2021).

Although the exact non-linear stiffness responses are customisable, each LRD concept has a characteristic curve shape, shown in Fig. 1, with two different curves chosen to represent different stiffness profiles achievable with the IMS device. Overall, the curves can be divided into two categories: '3-phase' curves (TFI, DO), or 'single-phase' curves (IMS 1, IMS 2). 3-phase curves have a high initial stiffness, then a low stiffness range over which the LRD is intended to operate, and a high third stage stiffness once compliance is exhausted. The single phase curves have a gradually increasing stiffness throughout.

Numerical modelling of the whole FOWT and mooring system is key at the design stage to ensure the optimal stiffness curve and length (or maximum extension) of the device are found for the specific application. Various studies, from the LRD developers, have provided such numerical modelling and assessed the performance of their LRD for a specific set of mooring and environmental input conditions. These studies provide little opportunity for comparison across LRDs, as variations in input conditions lead to vastly different results, ranging from 10% peak load reduction for the IMS (Harrold et al., 2020) to 59% reduction in peak load for the TFI (Lozon et al., 2022). Some further studies from the developers of the IMS have compared the performance of a specific LRD in different water depths, showing that tension reductions can be up to three times higher in 100 m water depth compared to 200 m (Khalid et al., 2020). Research by TFI developers has provided parametric analyses on LRD length, showing that longer LRDs provide increased tension reduction up to a certain point, with diminishing returns once sufficient compliance is reached (McEvoy and Johnston, 2019). The effect of various stiffness curve shapes for the TFI device has been compared (McEvoy and Kim, 2017), but this was for a tidal energy converter application rather than a FOWT. No existing study in the public domain has compared the stiffness curves for each of these devices, across constant sets of input conditions, for catenary and taut FOWT moorings. A summary of all numerical studies on LRDs for FOWTs, wave energy converters (WECs), and tidal energy converters (TECs) is given in Table 1.

1.3. Comparative analysis workflow

This paper presents a comparative analysis on the effect of different non-linear LRD stiffness curve shapes, each representative of a specific LRD concept, on tension reduction and platform motions for FOWT. To provide a comprehensive assessment with a broad range of applicability, the LRD stiffness curves were considered across a matrix of 8 different mooring scenarios and load cases:

- 4 mooring scenarios: 150 m depth catenary, 150 m depth taut, 75 m depth catenary, 75 m depth taut
- 2 load cases: parked 50-year extreme, operational 50-year extreme

The results were obtained from numerical modelling on a reference 15 MW wind turbine and semi-submersible platform. The model, mooring system, LRD modelling approach and load cases are described in the methodology. The results are then divided into three sections. The first two sections consider a fixed LRD length, and study the effect of the LRD curve shape on fairlead tension reduction and FOWT motions respectively. The third section compares the effect of varying the LRD length on fairlead tension and platform motions, for different LRD curve shapes.

2. Methodology

2.1. FOWT model description

The numerical modelling of the floater, turbine and mooring system was performed using Flexcom, a commercial finite element (FE) software. Flexcom offers fully-coupled aero-hydro-servo modelling using

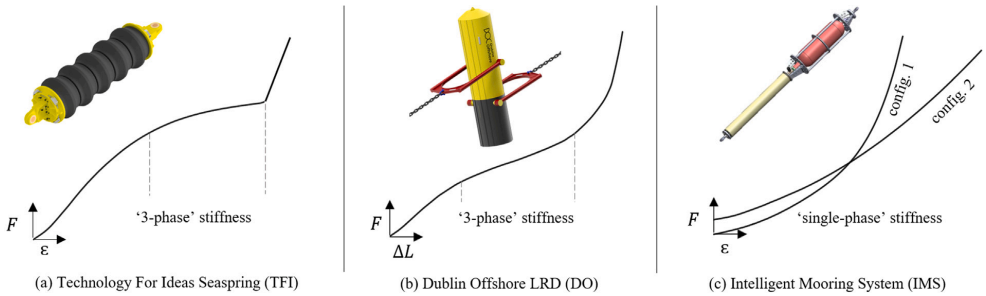

(a) Technology For Ideas Seaspring (TFI) (b) Dublin Offshore LRD (DO) (c) Intelligent Mooring System (IMS)

Fig. 1. Visualisation of the three different LRD concepts along with their characteristic stiffness curves: (a) Technology for Ideas Seaspring (TFI), (b) Dublin Offshore LRD (DO), (c) Intelligent Mooring System (IMS).

Table 1
Summary of publicly available numerical studies on LRDs, categorised by the parameterised variable(s).

Parameterised variable	Load case	Water depth	LRD length	Mooring configuration	LRD stiffness curve shape
Studies for WECs/TECs	Luxmoore et al. (2016)	Luxmoore et al. (2016)	McEvoy and Kim (2017)	Luxmoore et al. (2016)	McEvoy and Kim (2017)
Studies for FOWTs	Lozon et al. (2022), Khalid et al. (2020), Festa et al. (2022)	Khalid et al. (2020)	McEvoy and Johnston (2019), Harrold et al. (2020) Festa et al. (2022)	McEvoy et al. (2021), Pillai et al. (2022)	*no studies in public domain*

FAST plug-ins INFLOWWIND, AERODYN and SERVODYN, and has been validated against other commercial and academic software for a 5 MW turbine as part of an offshore code collaboration project (Robertson et al., 2020). The FOWT model used in this study is composed of the International Energy Agency (IEA) reference 15 MW wind turbine on the Volturn-US semi-submersible floating platform, and has been validated against the FAST model in Flexcom documentation (FLEXCOM, 2022). The full platform and turbine characteristics are described in detail in publications from the National Renewable Energy Laboratory (NREL) (Gaertner et al., 2020; Allen et al., 2020).

2.2. Base mooring description

Two conventional symmetric mooring configurations were studied, both composed of three evenly-spaced lines: a full-chain catenary mooring and a taut mooring composed of polyester rope with chain ends. Each mooring configuration was modelled in two water depths, 75 m and 150 m, resulting in a total of 4 mooring scenarios. Each scenario is shown in Fig. 2, annotated with the direction of wind and wave loading. All mooring components for both configurations (i.e. chain, polyester, and chain links) were given the same MBL of 15 MN for consistency in the comparative analysis. This corresponds to an R3 Studlink chain with a diameter of 143 mm, and Brydon–Bekaert MoorLine polyester rope diameter of 234 mm (Brydon, 2022). Pretension was also kept constant across all configurations and water depths, at 12.5% of MBL. The taut mooring was set at an inclined angle of 35 degrees with respect to horizontal, for both the shallow and intermediate water depth moorings, based on a previous study for taut FOWT systems (Bach-Gansmo et al., 2020). The mooring parameters are summarised for both mooring configurations in Table 2.

2.3. LRD modelling

To model the LRD mooring systems, the base mooring configurations were modified by substituting a non-linear spring element, representing the LRD, for a section of the line at each fairlead. No damping was attributed to the LRDs, aside from the mass damping of the whole mooring line included in the base Volturn-US Flexcom model (which was calibrated with the NREL model). This approach is in keeping with the numerical modelling from the various studies listed in Table 1. As the aim of this study is to compare different non-linear stiffness curves rather than the physical LRDs designs, physical properties such as diameter, linear mass and LRD length were equalised to provide a meaningful comparison. In practice, these parameters vary depending on the LRD concept considered, but also on the desired stiffness curve of the LRD. For the two spring-like devices, values of diameter and dry linear mass ranging from 0.3 m and 71 kg/m for IMS (Khalid et al., 2020), to 1.43 m and 1759 kg/m for TFI (Lozon et al., 2022) have been quoted in literature. The diameter of the cylindrical DO device, Fig. 1(b), typically ranges from 2.9–5.1 m, and the buoyant section is designed such that the full device is neutrally buoyant in water (Dublin Offshore, 2020). For this study, the LRD spring sections were all given a diameter of 1 m, and the dry linear mass was then set to 785 kg/m for neutral buoyancy in seawater. The lengths of LRDs considered also vary across different studies, ranging from 4 m (Harrold et al., 2020) to 30 m (McEvoy and Johnston, 2019). A length of 20 m was taken as the reference length for the LRD spring sections in this study, with subsequent comparison of additional lengths from 10 m to 30 m. By using standardised physical properties for all LRD concepts, the impact of the LRD stiffness curve on the system was isolated, which is key for this study. For more advanced studies on a specific LRD, a detailed, geometrically accurate LRD model should be employed to capture additional hydrodynamic or mechanical characteristics.

Non-linear stiffness curves for each LRD concept were reproduced from developer documentation, and normalised such that all LRDs exhibit the same tension at 0.5 strain (i.e. 10 m extension for the 20 m spring sections considered). For each of the 4 curve shapes, shown in Fig. 1 for the 3 devices, the stiffness is scaled depending on its 'rated tension', which is defined in this study as the tension in the device at 0.5 strain. DO and TFI refer to the rated tension as the 'Safe Working Load'

Table 2
Mooring parameters of the base mooring system. See Appendix for stiffness of the full mooring systems.

Mooring configuration	Taut inclined (35 deg)	Catenary
Pretension	1.875 MN	1.875 MN
Material type	Brydon Moorline Polyester	R3 Studlink Chain
MBL	15 MN	15 MN
Diameter	234 mm	143 mm
Stiffness (EA)	100 MN	3750 MN
Mooring radius (m)	252 (150 m depth); 145 (75 m depth)	640

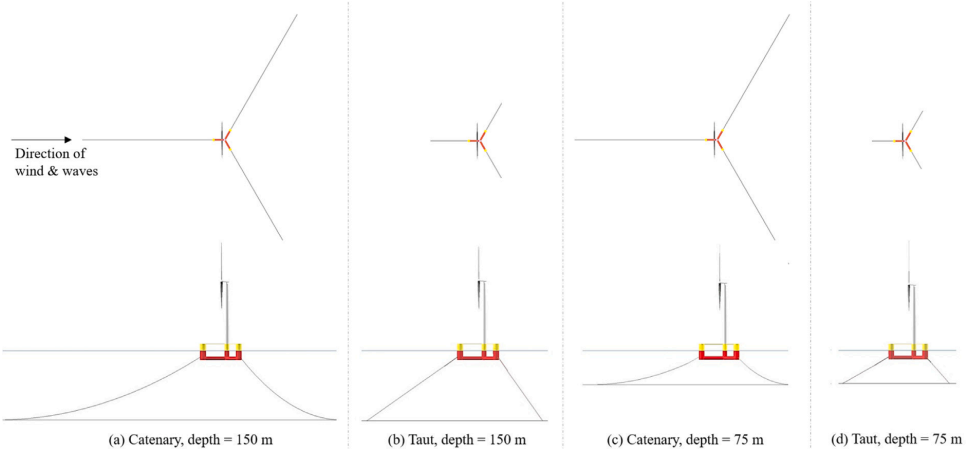

Fig. 2. Top-down and side views of the 3D Flexcom model of the IEA 15 MW wind turbine on the Volturn US platform, for the four mooring scenarios considered in this paper.

and 'Target Load' respectively. In practice, these different rated tensions are obtainable by changing the dimensions and/or material properties of the LRD. Higher rated tensions often apply to locations with more severe environmental loading, which typically require higher MBLs, but the LRD's MBL and rated tension are not inherently coupled. The MBL of the LRD can be can be adjusted to whichever value meets safety requirements, whereas the rated tension is a separate design variable which drives performance of the device. In this study, selected rated tensions range from 2.5 MN, which is just above the mooring pretension, to 7 MN, which is just below the maximum expected tension with no LRD, determined from an analysis on the base-case mooring system. The 10 rated tensions considered in this study are shown for each of the 4 stiffness curve shapes in Fig. 3. Each combination of LRD stiffness curve shape, rated tension and mooring scenario then leads to a different stiffness curve of the mooring system as a whole. Full mooring stiffness curves are shown for each combination in the Appendix.

2.4. Design load cases

The load cases applied in the model are representative of the New York Bight area (Lozon et al., 2022). Two load cases were considered: a 50-year return period load case for an operational wind turbine, and a 50-year return period load case for a parked turbine, i.e., with feathered blades to reduce wind loading. For the operational load case, the wind speed equals the turbine's rated wind speed of 10.59 m/s, generating the highest amount of wind thrust on the system (Gaertner et al., 2020). This scenario can sometimes cause higher tensions on the mooring system than more extreme conditions with a parked turbine, hence both load cases require consideration as potential design driving scenarios. The parameters of each load case are summarised in Table 3.

Table 3
Operational and parked load cases used in this study (Lozon et al., 2022).

Load case	50-yr operational	50-yr parked
IEC load case reference	IEC 1.6	IEC 6.1
Wind speed (m/s)	10.59	41.10
Turbulence intensity	0.085	0.154
Significant wave height (m)	4.72	8.70
Peak wave period (s)	10.03	12.73
Peak shape parameter	2.02	2.03
Current	not considered	not considered

The two load cases were run on all 4 base mooring scenarios for the IEC-recommended duration of 3600 s (International Electrotechnical Commission, 2019), with wind and waves acting in the direction shown in Fig. 2. For the irregular wind and wave seeds considered, the highest loads on the windward mooring line occurred in the first 1200 s of the simulation. The resulting time-series of fairlead tension and surge (i.e. horizontal platform offset), were cropped to the first 1200 s and are shown in Fig. 4.

The fairlead tensions are highest for the taut moorings in 75 m water depth (Fig. 4d), due to the lowest compliance in the mooring system. These high fairlead tensions, which are essentially restoring forces maintaining the platform in position, translate to much lower surge of the platform (see Fig. A.1 in Appendix for additional discussion). Conversely, the catenary mooring in 150 m depth (Fig. 4c), is the

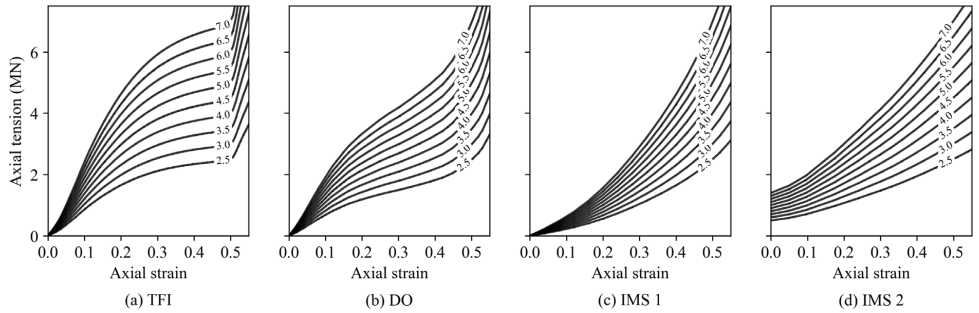

Fig. 3. : Tension–strain plots for the 4 non-linear curve shapes considered in the study, which are attributed to the spring elements representing the LRDs in the FE model. 10 different rated tensions are modelled for each curve shape, from 2.5 MN to 7 MN, which determine the tension at 0.5 strain (i.e., at 10 m extension for the 20 m spring length).

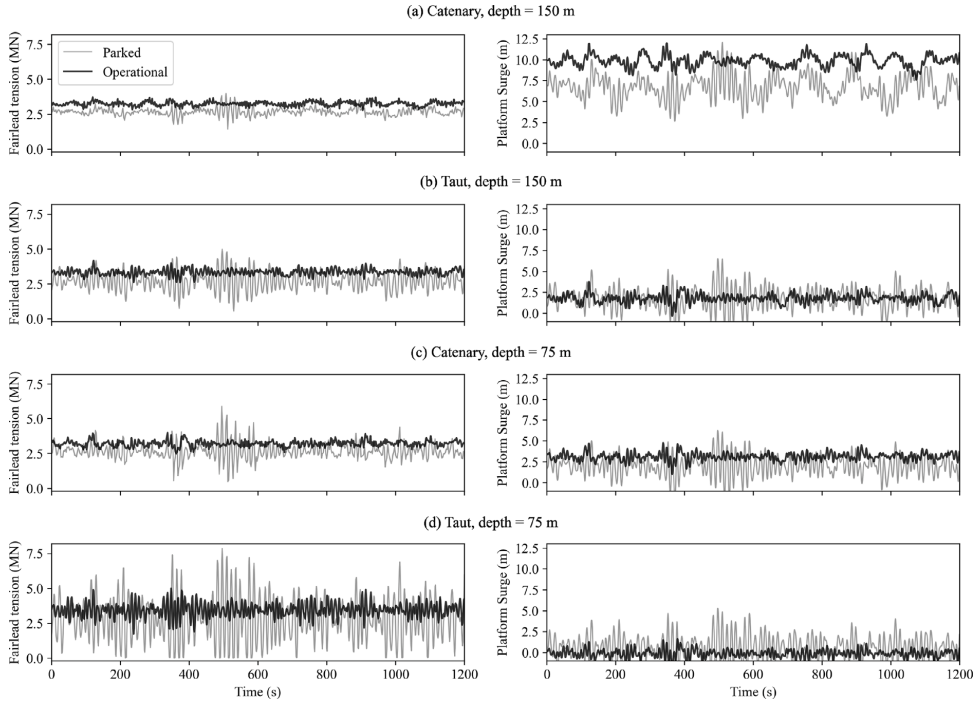

Fig. 4. Time-series of fairlead tensions and platform surge for the four base-case mooring scenarios, for parked and operational load cases.

most compliant and shows the highest surge and lowest tensions at the fairlead. Under the 50-year parked load case, the shallow taut configuration also exhibits numerous 'slack' events, where the fairlead tension momentarily reaches zero. These events can potentially be damaging to the mooring system. In practice, this mooring system would not be viable without an LRD for the given conditions, and a line angle much closer to horizontal would have to be considered to increase the line length and deliver more compliance. However, this steep line angle was maintained for the taut-line model as it provides two advantages for this study: 1. The taut-line angle is similar to the catenary line hang-off angle at the fairlead, leading to comparable ratios of vertical to horizontal forces across both configurations; 2. Less contribution of synthetic rope towards the compliance of the system puts more emphasis on the behaviour of the LRDs.

3. Effect of the LRD stiffness curves on tension reduction

3.1. Significance of the LRD rated tension in stiffness curve comparison

To compare the LRD stiffness curves, the loading time-series shown in Fig. 4 are applied to the LRD mooring system, for each of the 4 different stiffness curve shapes and 10 rated tensions shown in Fig. 3.

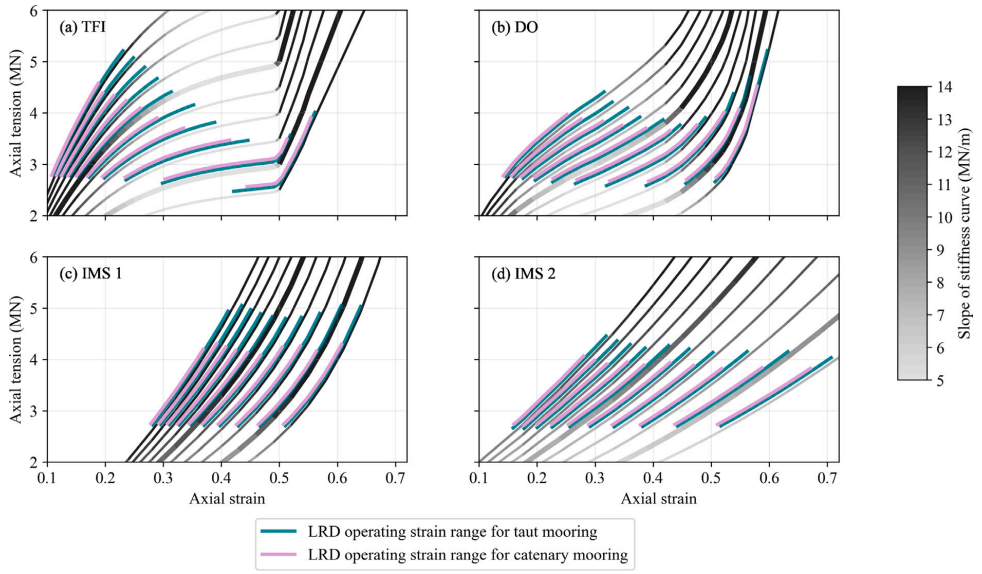

Fig. 5. Stiffness curves plotted for each rated tension and curve type, and colour graded according to the slope of the stiffness curve. The operating strain region of the LRD, for the 75 m water depth and parked load case, is plotted on top of each curve. The 3 MN and 5 MN rated tension curves are shown with thick lines.

For the 3-phase curves, the rated tension defines the point at which the LRD enters its third-phase stiffness. However, in a more general sense, the rated tension defines the overall steepness of the non-linear stiffness curve, i.e. its slope $dT/d\varepsilon$. This impacts the performance of the LRD, by affecting the phase of the stiffness curve over which it operates and is effective in reducing tension. This is depicted in Fig. 5, which shows the span between the mean LRD strain and the maximum LRD strain over the course of the time-series, defined as the 'operating strain region'. For brevity, the operating strain regions are shown only for the highest load conditions, i.e. 75 m water depth and parked load case.

For all 4 stiffness curve shapes, the lower rated tensions lead the LRD to operate in higher strain regions. For the two single-phase curve shapes (Figs. 5c & 5d) this has limited significance, as the slope of the stiffness curve is similar regardless of the operating strain region. However, for the 3-phase curve shapes (Figs. 5a & 5b), the slope of the stiffness curves varies considerably depending on the operating strain region. The lowest maximum tensions, i.e. tension at maximum strain, are found when the LRD operates in the second phase stiffness, which has the lowest stiffness curve slope. Thus, to obtain the full benefit of the LRD in extreme 50-year conditions, the rated tension of 3-phase curves must be low enough for the LRD to stretch past its first-phase stiffness, but high enough such that it doesn't exceed its rated tension and operate in its stiff, third phase.

To visualise the effect of different LRD stiffness curve shapes and rated tensions on the system, Fig. 6 shows a time-series of fairlead tension for the LRD moorings plotted against the base-case mooring, for all 4 mooring scenarios in the parked load case. For each of the stiffness curve shapes, 2 rated tensions are considered, 3 MN and 5 MN. The time-series are cropped to capture the peak loading events, which occur between 450 s and 550 s in the parked load case, for the wind and wave seeds considered (see Fig. 4). For the conditions considered, all LRDs offer peak tension reduction, and eliminate slack line events in the taut mooring configurations. Greater tension reduction is apparent in mooring scenarios with less inherent compliance in the base-case mooring configuration, i.e. in the taut line and shallow water moorings (Fig. 6d).

As expected, LRDs with 3-phase stiffness curves, TFI and DO, show different fairlead tension responses depending on their rated tension, whereas the single-phase stiffness curve LRDs show similar responses for the two rated tensions considered. For the DO device, the 3 MN rated tension LRD is too soft, thus operating in the third phase stiffness and not reducing tension as much as the stiffer 5 MN LRD which operates in the second phase as intended. Conversely, the 5 MN TFI device is too stiff, thus operating in the first phase of its stiffness curve and not reducing tension as much as the 3 MN device. However, as shown by the operating strain region of the 3 MN TFI curve (Fig. 5a) the device momentarily exceeds its rated tension and enters its third phase stiffness at the maximum load for the 75 m water depth case. This is visible in the time-series of the TFI device (Fig. 6d, at 490 s and 510 s), where a secondary peak in tension appears, caused by the device 'locking-out' at 50% strain as it suddenly enters the high-stiffness third phase.

3.2. Maximum fairlead tension reduction

In the following results, the maximum fairlead tension reduction provided by different LRD curve shapes is compared across all rated tensions, to ensure the optimal rated tension is captured for each curve shape. Maximum fairlead tension is recorded over the full time-series for each LRD curve shape, and compared to the tensions in the base mooring for the same conditions (Fig. 7).

Across all 8 sets of input conditions, the 3-phase stiffness curves (TFI, DO) show better maximum tension reduction than the single-phase curves (IMS 1, IMS 2), as long as a suitable rated tension is selected. The window of suitable rated tensions, which allow the LRDs to operate in their second phase stiffness, is smaller for the TFI curve (3–4 MN) than for the DO curve (4–6.5 MN). This is due to the low, regressive slope of the TFI stiffness curve in its second phase (less

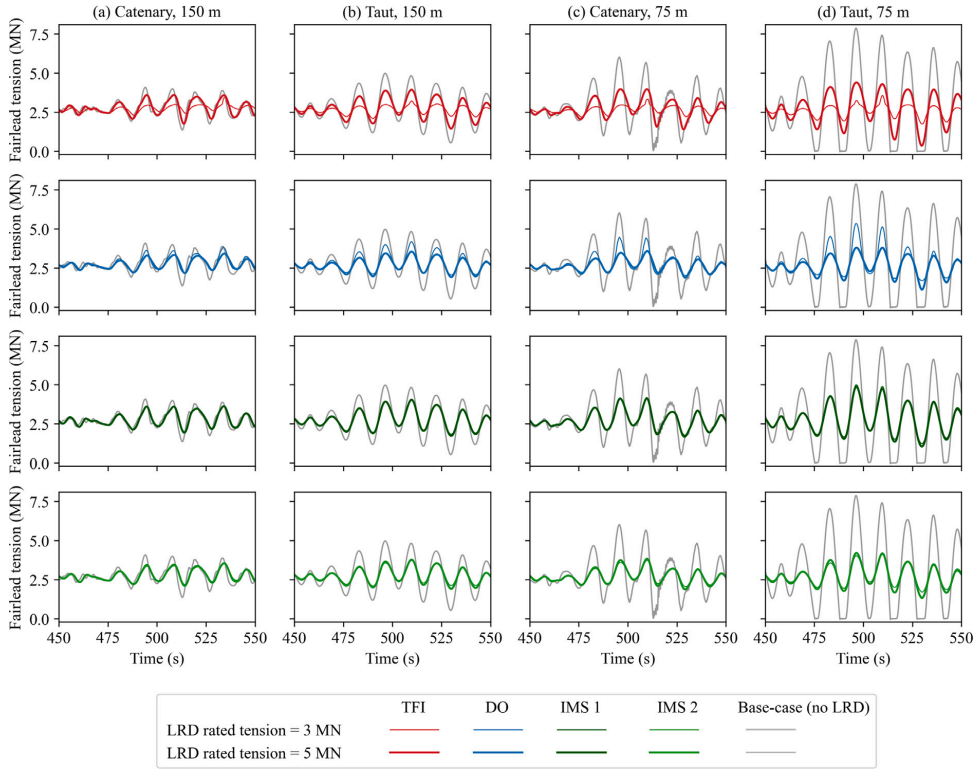

Fig. 6. Peak fairlead tension event in parked turbine load case. Time-series for each LRD is plotted against no LRD case, for two values of rated tension.

than 5 MN/m), which is highly effective at reducing tension, but also translates to rapid extension of the device the as it approaches its rated tension. The DO curve has a stiffer second-phase response, leading to slightly lower tension reduction, but enabling a greater range of rated tensions to operate within the second phase.

In the scenario where peak loads are design-driving, the rated tension which provides the highest tension reduction would theoretically be the most advantageous. However, in some cases, selecting this rated tension could lead to the LRD exhausting its compliance and exceeding its rated tension. For instance, with the TFI LRD in the taut 150 m case (Fig. 7b), a rated tension of 3 MN provides the highest tension reduction. However, the maximum fairlead tension when using this device is of 3.2 MN, meaning the LRD has exceeded its rated tension and entered its third-phase, 'lock-out' stiffness. If the 'optimal' rated tension for the specific application is defined as that which provides the highest tension reduction without the LRD exceeding its rated tension, a rated tension of 3.5 MN should be chosen for the TFI curve. Similarly, the 'optimal' rated tensions for this application would be taken as 4.5 MN for the IMS and DO LRDs.

In general, all curves offer better tension reduction in the parked load case than in the operational load case. This can be put down to two factors: 1. The higher waves in the parked case create more dynamic tension, which in turn increases the effectiveness of the LRDs (Festa et al., 2022); 2. the lower wind thrust in the parked case leads to a lower effective strain range in the LRD, meaning more compliance is left to reduce the peak wave-induced loading. The wind thrust in the operating case causes a constant, 'background' load, which displaces floater from its reference position, stiffening the mooring system in the process. This offset increases the mean strain of the LRD, meaning less compliance is available to reduce peak dynamic wave loads. This is especially apparent with lower rated tensions on the 3-phase curves, where the LRD has exhausted its compliance under the background load, leading to an increase in maximum tension.

3.3. Fatigue damage reduction

In addition to reducing the tension caused by the maximum loading event, which can lower the required material cost of a FOWT moorings and anchors, LRDs also reduce the tension on the mooring system caused by other, lesser, loading events. The damage caused by these lesser loads can accumulate over the structure's lifetime, causing fatigue in the mooring components which constitutes the leading cause of chain failure for permanent moorings (Fontaine et al., 2014). The reduction in lower-amplitude loads is apparent in the time-series shown in Fig. 6, where 'smaller' peaks in tension occurring at 450 s and 475 s are reduced by the LRDs. This tension reduction reduces the overall damage caused on the chains, ropes, and mooring components, which can extend their fatigue life and reduce the risk of failure. To portray this, the magnitude and timestamp of every fairlead tension peak were measured from the original time-series of the base-case moorings, for each of the time-series shown in Fig. 4. For each peak, the resulting tension reduction for the LRD moorings is measured and scattered

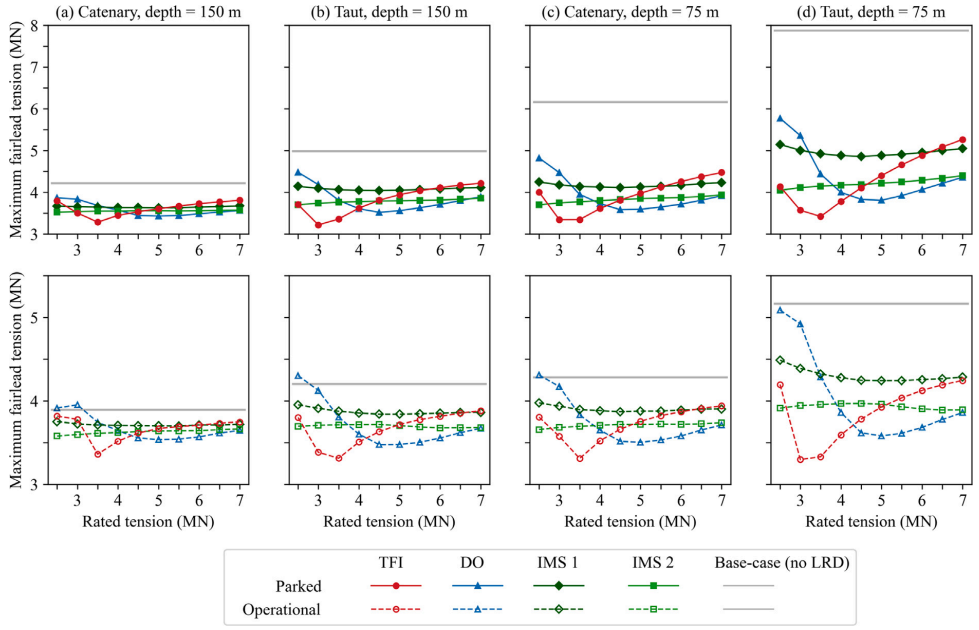

Fig. 7. Maximum fairlead tension for each of the 4 LRD curve types across a range of rated tensions. Each of the 8 subplots represents a same set of input conditions, covering all 4 mooring scenarios and 2 load cases.

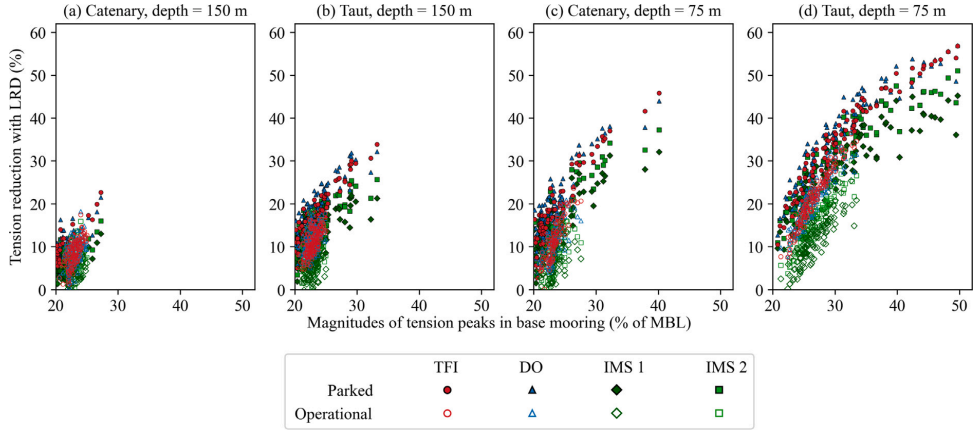

Fig. 8. Reduction in tension provided by each LRD (with rated tensions of 3.5 MN for TFI, and 4.5 MN for DO, IMS1, and IMS2) for individual fairlead tension peaks across the time series, plotted against magnitude of the peak in the base-case mooring scenario, i.e. without LRD.

against the magnitude of the original peaks (Fig. 8), using the optimal rated tensions determined in Section 3.2.

These results show a strong correlation between peak load magnitude in the base-case mooring, and the resulting tension reduction provided by the LRD. The moorings with more inherent compliance (Fig. 8 a & b) do not experience loads above 35% MBL, thus do not obtain the full benefit of the LRDs. Peak load reductions in the operational load case follows the same correlation, albeit with slightly lower reductions due to more of the LRD compliance being consumed by the background wind load. The 3-phase stiffness curves, TFI and DO, are shown to offer the best tension reduction across all load magnitudes above 20% MBL, regardless of the mooring scenario or load case, which suggests they provide the highest damage reduction.

The total fatigue damage caused over a specific duration can be estimated by a metric known as the damage equivalent load (DEL). For a given irregular loading time-series, the DEL represents the amplitude of a constant cyclic load that results in the same cumulative fatigue damage as the irregular loading time-series itself (ASTM International, 2011). This was calculated using a rainflow counting algorithm, with a fatigue slope of 5 (Lozon et al., 2022), for each full time-series. The

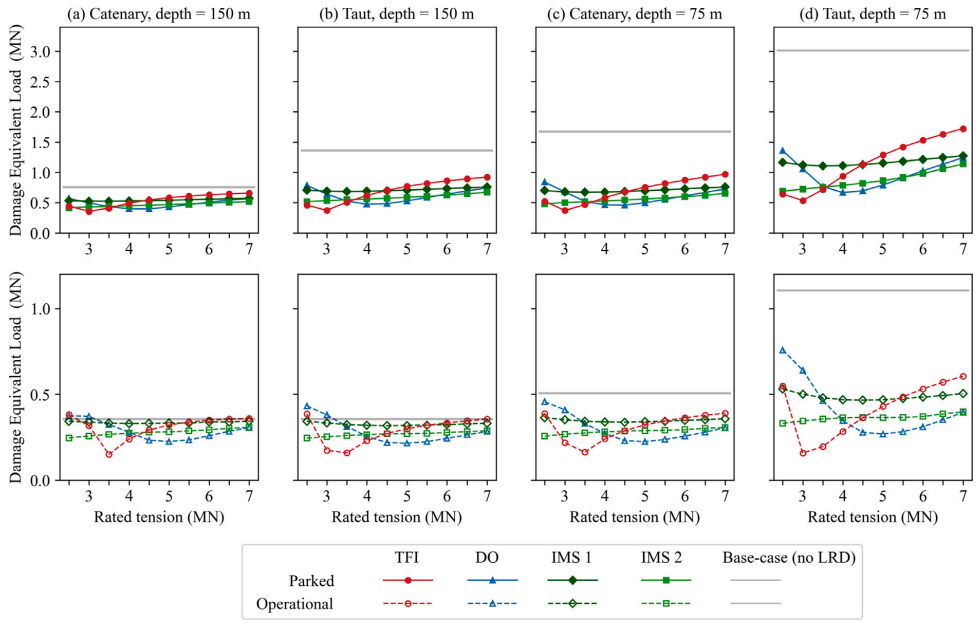

Fig. 9. Damage equivalent load over the full time-series for each of the 4 LRD curve types and 10 rated tensions considered. Each of the 8 subplots represents a same set of input conditions, covering all 4 mooring scenarios and 2 load cases.

resulting DEL is shown in Fig. 9 for each rated tension and stiffness curve type.

As with maximum load reduction, the DEL reduction is highest in the taut moorings and shallower waters, where there is less inherent compliance in the base-case mooring system. The effect of the LRD stiffness curve shape on the DEL follows a similar pattern to its effect on the maximum tension, with the three-stage stiffness curves offering the most DEL reduction, as long as suitable rated tensions are selected. However, the rated tensions which provide highest DEL reduction are slightly lower than the rated tensions which provide highest maximum load reduction, as the lower stiffness can better reduce the impact of lesser loads. In the taut 75 m case for instance (Fig. 9d), the 3 MN TFI and 4 MN DO curves provide highest DEL reduction, whereas the 3.5 MN and 4.5–5 MN curves provide highest maximum load reduction (see Fig. 7d). In the scenario where fatigue is design driving, the lower rated tension could be considered, at the cost of the device potentially exceeding its rated tension and entering its third phase stiffness under the maximum load. Whether this trade-off is acceptable would depend on the type of LRD and developer guidance.

4. Effect of LRD stiffness curves on platform motions

4.1. Significance of platform motions

In the offshore environment, the FOWT platform exhibits motions in 6 degrees of freedom (DOFs), as depicted in Fig. 10. When altering the stiffness response of a mooring system, such as by introducing an LRD, it is crucial to consider the subsequent impact on the motions of the platform. Since the wind and wave loads considered in this study are acting along the same axis (surge axis in Fig. 10), only the DOFs in the plane parallel to this axis are considered, i.e. only the surge, pitch and heave DOFs. FOWT projects typically have strict

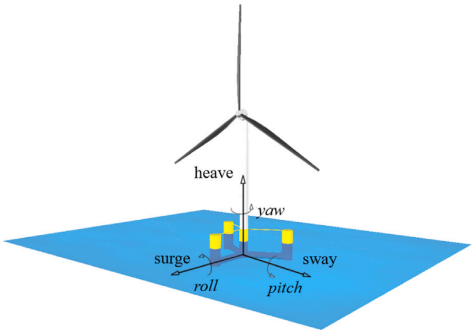

Fig. 10. Visualisation of the 6 DOFs of the FOWT platform. Rotational motions are shown in italics.

criteria regarding the maximum allowable motions in these 3 DOFs, as they can cause undesirable effects to the system: surge (i.e. horizontal platform offset) can damage the power cable if its allowable range is exceeded; pitch affects the efficiency of energy production; and high nacelle accelerations can cause structural and mechanical damage to turbine components (Taboada et al., 2020).

Mooring designs for FOWTs must allow the system to safely operate within the maximum motion criteria. This is particularly important for surge, as the maximum surge under a given set of environmental loads is directly dependent on the stiffness of the mooring system (see Appendix). Motions and accelerations outside of the water plane such as heave and pitch are typically more influenced by the hydrodynamics of the platform than by the mooring system, but must be considered in mooring design nonetheless. This section studies the effect of LRD

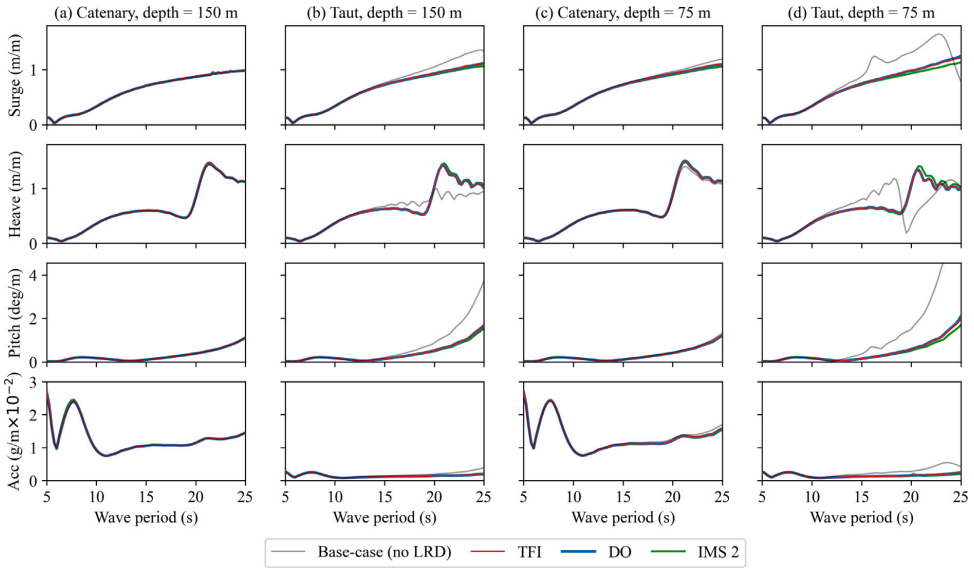

Fig. 11. Effect of regular wave-only loading on platform surge, heave, pitch and nacelle accelerations.

stiffness curves on platform motions and nacelle accelerations. For brevity, IMS 1 is omitted, and one rated tension is selected for the 3 other LRDs, which correspond to the 'optimal' rated tensions described in Section 3.2: 3.5 MN for TFI and 4.5 MN for DO and IMS 2.

4.2. Wave-induced motions

To isolate the effect of the LRDs on wave-induced motions of the structure, wind loading was disabled, and the full FOWT and mooring system were subjected to a set of regular Airy waves with varying frequency and fixed amplitude of 2.36 m. The amplitude of motion was measured, normalised with respect to the wave amplitude, and plotted against the frequency of the waves. The resulting statistic forms the Response Amplitude Operator (RAO). RAOs for the 4 key motions are shown in Fig. 11, for each mooring scenario and LRD stiffness curve type.

For the catenary configurations, the RAOs of the LRD moorings are near identical to those of the base moorings. This is in agreement with the full mooring system stiffness curves shown in Appendix, which suggest that at low offset, the base moorings and LRD moorings have the same stiffness (i.e., same gradient of tension–offset curve). This is not the case for the taut moorings, which are much stiffer without the LRD, and hence highly sensitive to the introduction of an LRD, leading to a more visible effect of the LRD on the RAO curve.

These results show that the addition of the LRDs does not introduce problematic frequencies for wave-induced motions, irrespective of the LRD stiffness curve shape. In fact, for the taut moorings, surge, heave and pitch motions are slightly reduced across key wave periods, 10–15 s. This reduction is higher in the shallow water scenario. Heave response is increased by LRDs at very high wave periods, 20–25 s, but these are typically not experienced in realistic sea states so should not be of concern.

4.3. Wind-induced motions

To isolate the effect of the LRDs on wind-induced motions of the structure, the full FOWT and mooring system were subjected to the same irregular wind conditions used in Section 2.4, but without waves. Resulting time-series of surge (i.e. horizontal platform offset), heave, and horizontal nacelle accelerations are shown in Fig. 12, cropped to show the peak loading event, which occurs at different timestamps for the parked and operational cases. Only 75 m water depth mooring scenarios are displayed, as these are most sensitive to LRDs as shown in Fig. 11. The vertical degrees of freedom (heave, vertical acceleration) are omitted as the absence of waves means loading is purely horizontal.

The wind generates a constant 'background' load on the structure, especially in the operational case where the thrust on the turbine is at its highest. The subsequent moment on the turbine also leads to high mean pitch (Fig. 12 c & d). During the parked case (Fig. 12 a & b), the blades are feathered to shed load, but the wind speed is much higher (41.10 m/s vs. 10.59 m/s for operational) and less regular, leading to a more varying response for both surge and pitch. In both parked and operational cases, the negligible dynamic loading means nacelle accelerations are low.

In both cases, with the absence of waves, the relationship between fairlead tension and platform surge is essentially quasi-static: the platform finds an equilibrium position, which is determined by the stiffness of the mooring system. Hence, the presence of an LRD, which reduces the mooring stiffness, increases the mean surge (or horizontal offset) of the platform. However, the mean pitch, which is mostly influenced by platform design rather than mooring stiffness, is not increased by the LRD. Overall, when similar rated tensions are considered, these trends do not depend on the shape of the LRD stiffness curve.

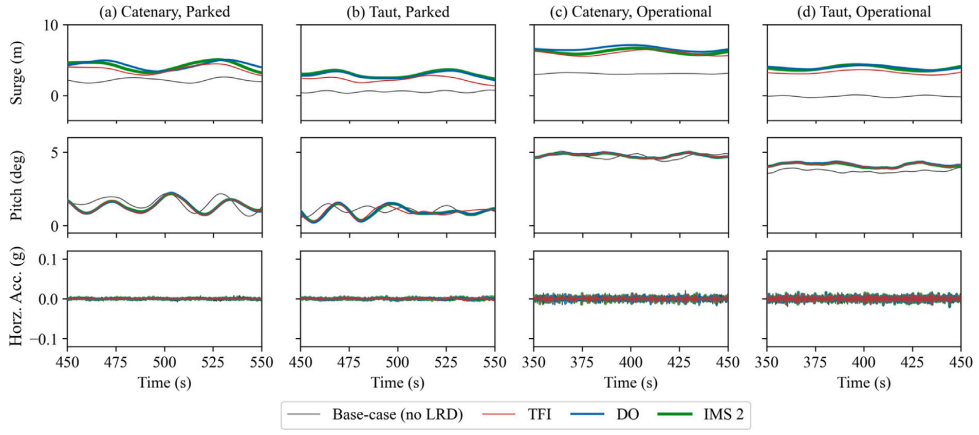

Fig. 12. Effect of wind-only loading on platform surge, pitch and horizontal nacelle accelerations, for 75 m water depth.

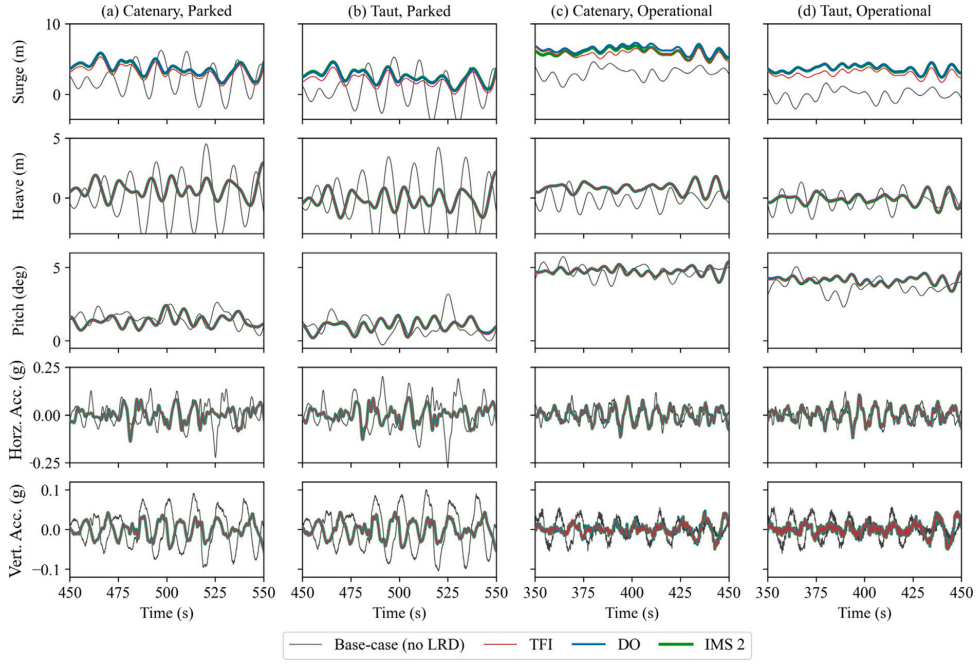

Fig. 13. Effect of combined wind and waves on platform motions in 3 DOF and nacelle accelerations in 2 DOF (vertical and horizontal), for 75 m water depths.

4.4. Combined wind and wave motions

Having studied the effect of LRDs on the motion response to wind and wave loading individually, the next step is to analyse the response to combined wind and wave loading. The same design load cases as described in Section 2.4 are considered, and time-series of the relevant platform motions in the wind/wave plane are recorded for each LRD curve type. Resulting time-series of platform motions are shown in Fig. 13, cropped to show the peak event. For brevity, only the 75 m water depth mooring scenarios are displayed, as these are the most sensitive to LRDs.

The general effect of the LRDs on platform motions and nacelle accelerations, regardless of stiffness curve shape, can be summarised as follows:

- Although the wind-induced surge component is increased by LRDs (as shown in Section 4.3), the damping effect from the LRDs results in a lower wave-induced dynamic surge response. This leads to a higher increase in surge in the operational case with higher wind loading (Fig. 13 b and c) than in the parked case with

higher wave loading (Fig. 13 a and b). Thus, the governing design case, i.e. case of maximum surge, can become the operational case when incorporating an LRD.
- Heave motions caused by the lower frequency waves, occurring at 500 s in the parked condition, are reduced by the LRDs, which is consistent with the RAO results. As the heave motion is driven by wave height, amplitudes are higher in parked condition with a higher significant wave height.
- Pitch oscillations are due to wave loads, whereas the mean pitch is caused by the moment from the wind thrust on the rotor, leading to much higher mean pitch in the operational load cases compared to the parked load cases. The wave-induced pitch oscillations are reduced by the LRDs, but the mean pitch is not affected, as was shown in Section 4.3.
- Wave-induced accelerations at the nacelle are reduced by LRDs for both the horizontal and vertical components, especially in the parked load case.

Overall, as was shown in the RAOs, the variation in stiffness curve shape of an LRD has very little effect on the motion response of the platform when compared to the response with the base-case mooring, i.e. without the LRD. All LRD curve shapes reduce oscillatory motions for pitch, heave and nacelle accelerations, but increase maximum surge (i.e. horizontal platform offset) of the platform. The surge motion is the only case where slight differences could be noted between the three LRD curve shapes. This is due to differences in the extension of the LRDs, which are minimal as the rated tensions considered across the 3 devices (3.5 MN, 4.5 MN, 4.5 MN) were similar.

5. Sensitivity analysis of LRD length

5.1. Significance of LRD length in stiffness curve comparison

Previous analyses in this paper have considered two LRD design parameters: stiffness curve shape and rated tension. Another key design parameter is the maximum extension of the LRD, which is defined by the length of the LRD section in the FE model. This determines the amount of compliance introduced by the LRD, and can make a significant difference to the overall tension–offset profile of the mooring system (Festa et al., 2023). The LRD length has been fixed at 20 m in the results presented so far, i.e., a maximum extension of 10 m when the LRD reaches its rated tension at 50% strain. In practice, the 'length' of the LRD section, or its maximum extension, would be increased by combining multiple devices in series, or in the case of the mechanical DO device, by increasing the distance between its hinge points.

5.2. Influence of LRD length on tension reduction

Fig. 14 shows the effect of varying the length of the LRD section on the maximum tension reduction, in the parked load case, for two rated tensions. For each curve shape, one rated tension is set 0.5 MN below the 'optimal' rated tension defined in Section 3.2, the other is set 0.5 MN above.

For all stiffness curve shapes, increase in LRD length leads to higher reductions in maximum tension. The gains in tension reduction tend to be greater in the scenarios where the base-case mooring has little compliance (Fig. 14d). However, these benefits are regressive: once sufficient compliance is reached, increasing the length of the LRD has less effect on the tension reduction.

These trends also vary across the three curve shapes considered. In particular, for the 3-phase stiffness curves, varying the LRD lengths can change the optimal rated tension of the LRD. This has significant implications for LRD design: using shorter LRDs, which provide less compliance, requires higher rated tensions to avoid extending into the third-phase stiffness. Conversely, with longer LRDs, the lower rated tensions can provide greater tension reduction. This benefit is especially significant for the 3 MN TFI curve, which is operating in its stiff, third phase stiffness when the LRD is too short, thus not providing adequate compliance, but can provide much higher tension reduction when the length of the device is increased.

5.3. Influence of LRD length on maximum platform surge

The wind-induced surge (i.e. horizontal platform offset) increase introduced by LRDs, which constitutes additional 'quasi-static' platform offset along the axis of loading, is expected to be driven by the extension of the LRD (see Fig. 12). The extension of the LRD, as was shown in Fig. 15, is itself dependent on both its length and rated tension. Thus, to get a better idea of the effect of the LRD stiffness curves on surge, multiple combinations of lengths and rated tensions should be considered. Fig. 14 shows the effect of varying the length of the LRD section on the added surge, in the operational load case, for two rated tensions. For each curve shape, one rated tension is set 0.5 MN below the 'optimal' rated tension defined in Section 3.2, the other is set 0.5 MN above.

As expected, the increased length of LRDs leads to more surge of the operational turbine, across all 4 mooring scenarios. However, Fig. 15 also shows that the increased surge can be mitigated by using a stiffer LRD, i.e., with a higher rated tension. This is especially true for the 3-phase stiffness curves, where a 1 MN higher rated load can lead to over 60% reduction in additional surge. This is due to the slightly stiffer LRD not fully entering its second phase stiffness when in operation, and consequently extending much less, which can come at the cost of sightly lower tension reduction (see Fig. 14). For the three-phase stiffness curves, this trade off is not linear, and using the stiffer LRDs can be beneficial as it significantly reduces surge for only small increase in tension. For instance, in the taut 75 m depth case with a 20 m TFI device, using a 4 MN curve instead of 3 MN leads to 45% less surge increase (Fig. 15d), at the cost of only 5% less tension reduction benefit (Fig. 14d).

The underlying principle here is the coupling between variables: the rated tensions which provide optimal tension reduction for a 20 m LRD, as defined in Section 3.2, may not be optimal for other LRD lengths. Similarly, the LRD lengths which provide acceptable surge (i.e. horizontal platform offset) increase for a given rated tension and stiffness curve shape, may not be acceptable for other rated tensions. Hence, LRD design should be attempted holistically, where different combinations of LRD length, stiffness curve shape, and rated tension are assessed in parallel, to obtain the required reduction in fairlead tension which fits platform motion constraints.

6. Conclusion

The LRDs with 3-phase non-linear stiffness curves, featuring a high initial and final stiffness with a low-stiffness second phase, performed better than 'single-phase' curves both in terms of maximum tension and DEL reduction. This was true regardless of the water depth, mooring configuration, and load case. However, optimal tension reduction for 3-phase curves is highly dependent on finding the right rated tension, to ensure the LRD operates in the second phase of the curve. The single-phase stiffness curves were shown to offer similar tension reduction performance regardless of rated tension. In terms of platform motions,

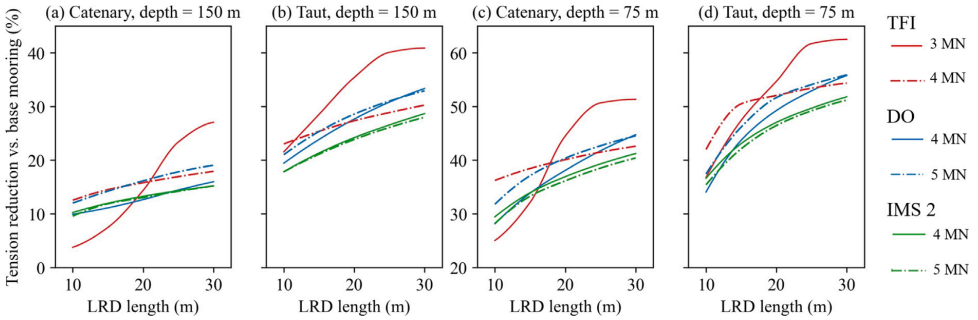

Fig. 14. Effect of varying the LRD length on maximum tension reduction compared to the base-case mooring, for the parked load case. Two rated tensions are considered, either side of the optimal rated tensions defined in Section 3.2.

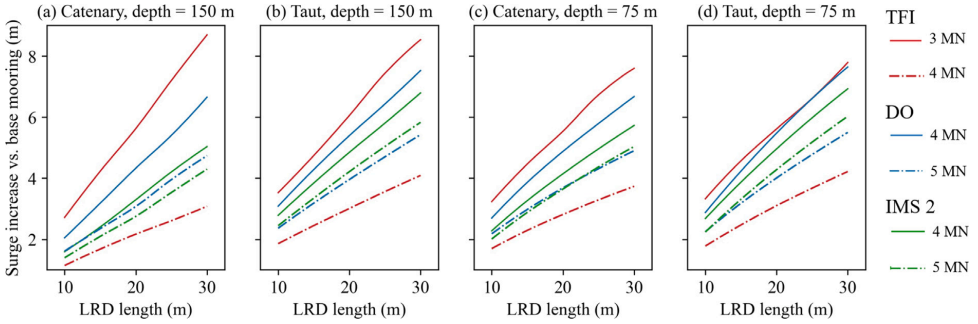

Fig. 15. Effect of varying the LRD length on surge increase (i.e. horizontal platform offset difference) compared to the base-case mooring, for the operational load case. Two rated tensions are considered, either side of the optimal rated tensions defined in Section 3.2.

all LRD curve shapes had similar effects on the system. Amplitudes of wave-induced surge (i.e. horizontal platform offset), heave, pitch and nacelle accelerations were reduced. Wind-induced surge was increased, especially in the operational load case, and was shown to be mainly affected by LRD length rather than curve shape.

Finding the optimal LRD design for a specific application involves determining the combination of rated tension and device length that provide suitable tension reduction whilst maintaining allowable platform surge. For 3-phase stiffness curves, there will typically be an interval of rated tensions that provide highest tension reduction. This interval is dependent on the length (or maximum extension) of the LRD, and thus must be determined with a multivariate analysis.

Two further conclusions can be drawn, valid across all LRD curves for the specific set of input conditions considered in this study: 1. LRDs provided more tension reduction in mooring systems with lower compliance, i.e. high modulus taut moorings, and shallower waters; and 2. LRDs provided more tension reduction in extreme parked conditions than extreme operational conditions. In future work, investigating a wider range of environmental conditions could be beneficial, to further assess how the LRD's performance and optimal design parameters vary depending on the expected wave height and wind speed.

CRediT authorship contribution statement

Oscar Festa: Writing – original draft, Visualization, Validation, Software, Methodology, Formal analysis, Conceptualization. **Susan Gourvenec:** Writing – review & editing, Supervision, Resources, Methodology, Funding acquisition, Conceptualization. **Adam Sobey:** Writing – review & editing, Resources, Conceptualization.

Declaration of competing interest

The authors declare that they have no known competing financial interests or personal relationships that could have appeared to influence the work reported in this paper.

Data availability

Data will be made available on request.

Acknowledgments

This work forms part of the activities of the Royal Academy of Engineering Chair in Emerging Technologies Centre of Excellence for Intelligent & Resilient Ocean Engineering (www.southampton.ac.uk/iroe), based at the University of Southampton. Susan Gourvenec is supported by the Royal Academy of Engineering, UK under the Chairs in Emerging Technologies scheme. Adam Sobey is supported by the Lloyd's Register Foundation, UK. The authors thank Aengus Connolly for his advice on Flexcom.

Appendix. Stiffness of full mooring systems

The stiffness of a full mooring system, including all of its components (in this case, LRD and rope or chain) is defined as the relationship between the position of the platform and the subsequent restoring force imparted on the platform (i.e. fairlead tension). The mooring stiffness dictates the equilibrium position of the platform for a given mean load,

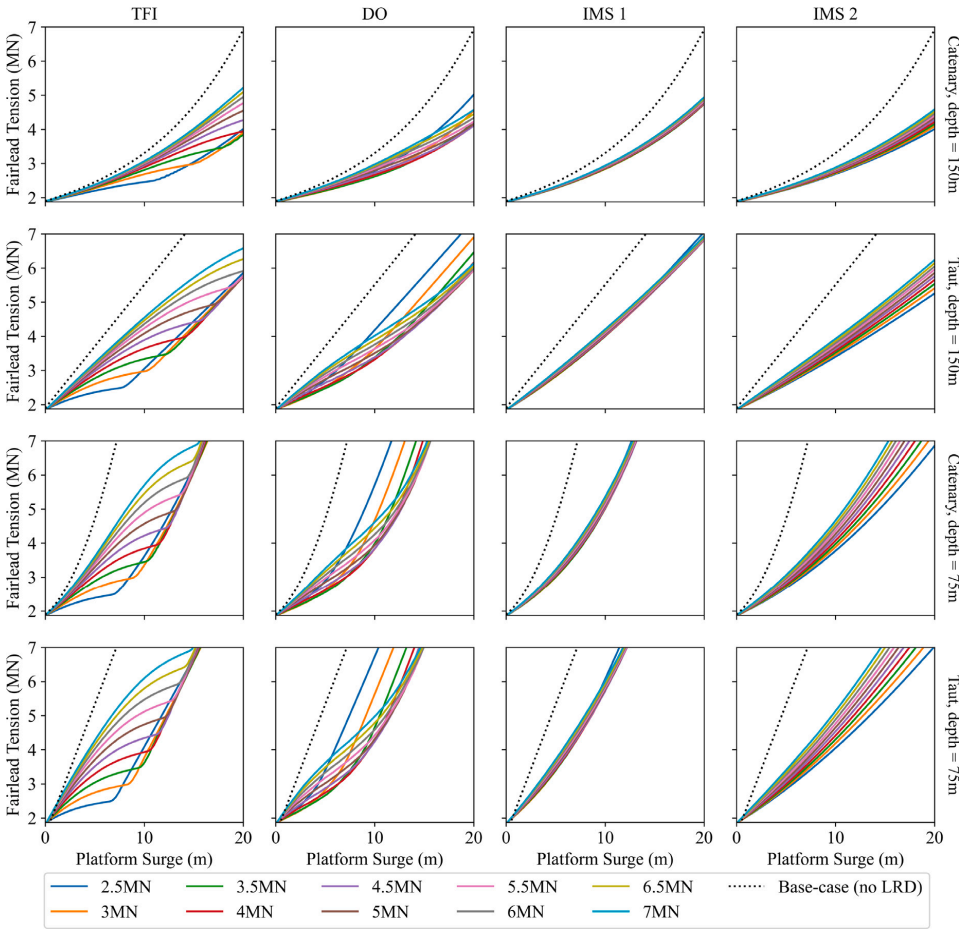

Fig. A.1. Stiffness curves of the full mooring system (i.e., mooring line + LRD) for all combinations of mooring scenarios, LRD curve shapes, and LRD rated tensions.

and the slope of the stiffness curve about this mean load then affects the dynamic response of the mooring.

The full mooring system stiffness is highly dependent on the stiffness of the LRD, but is also driven by the response of the catenary chain or taut rope which forms the rest of the mooring line. To obtain the stiffness profile of the full system, the platform was slowly displaced along the surge axis, and the fairlead tension required for static equilibrium was calculated at every step. Resulting plots of fairlead tension against surge (i.e. horizontal platform offset) are shown in Fig. A.1. These plots illustrate some useful concepts:

- The shallower and taut mooring systems exhibit higher stiffness, which translates to lower surge (i.e. horizontal platform offset) for the same value of fairlead tension.
- The taut moorings are generally less compliant than the catenary mooring, and their stiffness is more dominated by the stiffness of the LRD. In other words, the stiffness curve of the taut mooring system is very similar to that of the LRD, as the rope does not contribute much to the compliance.
- In the case of a 3-phase LRD stiffness curve (TFI, DO), low rated tensions can actually lead to much stiffer mooring systems once a certain value of surge is reached, as the LRD compliance is rapidly exhausted, leading to operation in the stiff, third-phase of the curve.

References

Allen, C., Viscelli, A., Dagher, H., Goupee, A., Gaertner, E., Abbas, N., Hall, M., Barter, G., 2020. Definition of the UMaine volturnUS-S reference platform developed for the IEA wind 15-megawatt offshore reference wind turbine. http://dx.doi.org/10.2172/1660012, URL: https://www.osti.gov/biblio/1660012.

ASTM International, 2011. Standard practice for cycle counting in fatigue analysis. ASTM E1049-85.

Bach-Gansmo, M., Garvik, S., Thomsen, J., Andersen, M., 2020. Parametric study of a taut compliant mooring system for a FOWT compared to a catenary mooring. J. Mar. Sci. Eng. 8, http://dx.doi.org/10.3390/jmse8060431.

Brydon, 2022. Moorline polyester [Datasheet]. URL: https://www.brydon.com/products/moorline-polyester.

Dublin Offshore, 2020. Load reduction device (LRD) – how it works. URL: https://www.dublinoffshore.ie/media/pages/technology/6f4e7419f6-1635594571/how-it-works.pdf.

Festa, O., Gourvenec, S., Sobey, A., 2022. Proxy model for the design of extensible floating offshore wind turbine mooring systems. In: International Ocean and Polar Engineering Conference. URL: https://eprints.soton.ac.uk/457472/1/2022_Festa_et_al_ISOPE.pdf.

Festa, O., Gourvenec, S., Sobey, A., 2023. Analytical model of non-linear load reduction devices for catenary moorings. In: International Conference on Offshore Mechanics and Arctic Engineering. URL: https://eprints.soton.ac.uk/457472/1/2022_Festa_et_al_ISOPE.pdf.

FLEXCOM, 2022. Flexcom comparison to FAST results for 15 MW Volturn-US FOWT. URL: https://flexcom.fea.solutions/l04---umaine-volturnus-s-iea15.html.

Fontaine, E., Kilner, A., Carra, C., Washington, D., Ma, K., Phadke, A., Laskowski, D., Kusinski, G., 2014. Industry survey of past failures, pre-emptive replacements and reported degradations for mooring systems of floating production units. In: OTC Offshore Technology Conference. http://dx.doi.org/10.4043/25273-MS, arXiv:https://onepetro.org/OTCONF/proceedings-pdf/14OTC/4-14OTC/D041S047R002/1505598/otc-25273-ms.pdf.

Gaertner, E., Rinker, J., Sethuraman, L., Zahle, F., Anderson, B., Barter, G., Abbas, N., Meng, F., Bortolotti, P., Skrzypinski, W., Scott, G., Feil, R., Bredmose, H., Shields, M., Dykes, K., Allen, C., Viselli, A., 2020. IEA wind TCP task 37: Definition of the IEA 15-megawatt offshore reference wind turbine. http://dx.doi.org/10.2172/1603478, URL: https://www.osti.gov/biblio/1603478.

Harrold, M., Thies, P., Newsam, D., Ferreira, C., Johanning, L., 2020. Large-scale testing of a hydraulic non-linear mooring system for floating offshore wind turbines. Ocean Eng. 206, 107386. http://dx.doi.org/10.1016/j.oceaneng.2020.107386, URL: https://www.sciencedirect.com/science/article/pii/S0029801820304145.

International Electrotechnical Commission, 2019. IEC 61400-3:2019 - Wind energy generation systems - Part 3: Design requirements for offshore wind turbines. URL: https://www.iso.org/standard/72447.html. (Accessed 24 March 2023).

Khalid, F., Johanning, L., Thies, P., Newsam, D., 2020. Assessment of Potential Sites for a Non-Linear Mooring System in Floating Offshore Wind Applications. pp. 650–656. http://dx.doi.org/10.1201/9781003134572-74.

Lozon, E., Hall, M., McEvoy, P., Kim, S., Ling, B., 2022. Design and analysis of a floating-wind shallow-water mooring system featuring polymer springs. In: International Offshore Wind Technical Conference. Vol. 486.

Luxmoore, J., Grey, S., Newsam, D., Johanning, L., 2016. Analytical performance assessment of a novel active mooring system for load reduction in marine energy converters. Ocean Eng. 124, 215–225. http://dx.doi.org/10.1016/j.oceaneng.2016.07.047, URL: https://www.sciencedirect.com/science/article/pii/S0029801816302955.

Ma, K., Luo, Y., Kwan, T., Wu, Y., 2019. Chapter 4 - Mooring design. In: Mooring System Engineering for Offshore Structures. Gulf Professional Publishing, pp. 63–83. http://dx.doi.org/10.1016/B978-0-12-818551-3.00004-1.

Ma, K., Wu, Y., Stolen, S.F., Bello, L., ver der Horst, M., Luo, Y., 2021. Mooring designs for floating offshore wind turbines leveraging experience from the oil & gas industry. In: International Conference on Offshore Mechanics and Arctic Engineering. Vol. 1, http://dx.doi.org/10.1115/OMAE2021-60739.

McEvoy, P., Johnston, E., 2019. Polymer mooring component for offshore renewable energy. In: OTC Offshore Technology Conference. http://dx.doi.org/10.4043/29587-MS.

McEvoy, P., Kim, S., 2017. Mooring load management for SR2000 floating tidal device using non-linear polymer components. In: 12th European Wave and Tidal Energy Conference. URL: https://uploads-ssl.webflow.com/5f8964a5a533790d6cc8820a/5f96cb7a8ba32845a778cb9e_EWTEC-2017.pdf.

McEvoy, P., Kim, S., Haynes, M., 2021. Fibre spring mooring solution for mooring floating offshore wind turbines in shallow water. In: International Conference on Offshore Mechanics and Arctic Engineering. http://dx.doi.org/10.1115/OMAE2021-62892, V009T09A029.

Offshore-mag.com, 2021. Floating wind load suppression system completes prototype trials. URL: https://www.offshore-mag.com/renewable-energy/article/14205082/floating-wind-load-suppression-system-completes-prototype-trials.

OffshoreWind.biz, 2021. EMEC verifies Dublin Offshore's floating wind mooring component. URL: https://www.offshorewind.biz/2021/03/12/emec-verifies-dublin-offshores-floating-wind-mooring-component/.

Pillai, A., Gordelier, T., Thies, P., Cuthill, D., Johanning, L., 2022. Anchor loads for shallow water mooring of a 15 MW floating wind turbine—Part II: Synthetic and novel mooring systems. Ocean Eng. 266, 112619. http://dx.doi.org/10.1016/j.oceaneng.2022.112619, URL: https://www.sciencedirect.com/science/article/pii/S0029801822019023.

Robertson, A., Gueydon, S., Bachynski-Polić, E., Wang, L., Jonkman, J., Alarcon Fernandez, D., Amet, E., Beardsell, A., Bonnet, P., Boudet, B., Brun, C., Chen, Z., Féron, M., Forbush, D., Galinos, C., Galvan, J., Gilbert, P., Gómez, J., Harnois, V., Wohlfahrt-Laymann, S., 2020. OC6 Phase I: Investigating the underprediction of low-frequency hydrodynamic loads and responses of a floating wind turbine. J. Phys. Conf. Ser. 1618, 032033. http://dx.doi.org/10.1088/1742-6596/1618/3/032033.

Taboada, M., Ortega, A., Martín, R., Pombo, A., Moreu, J., 2020. An evaluation of the effect that motions at the nacelle have on the cost of floating offshore wind turbines. In: OTC Offshore Technology Conference. http://dx.doi.org/10.4043/30632-MS.

WindEurope, 2017. Floating offshore wind vision statement. URL: https://windeurope.org/wp-content/uploads/files/policy/position-papers/Floating-offshore-wind-energy-a-policy-blueprint-for-Europe.pdf.

Xu, K., Larsen, K., Shao, Y., Zhang, M., Gao, Z., Moan, T., 2020. Design and comparative analysis of alternative mooring systems for floating wind turbines in shallow water with emphasis on ultimate limit state design. Ocean Eng. 219, http://dx.doi.org/10.1016/j.oceaneng.2020.108377, URL: https://www.sciencedirect.com/science/article/pii/S0029801820312841.

A.2 Analytical model of non-linear load reduction devices for catenary moorings

Proceedings of the ASME 2023 42nd International Conference on Ocean, Offshore and Arctic Engineering
OMAE2023
June 11–June 16, 2022, Melbourne, AU

OMAE2023-100845

ANALYTICAL MODEL OF NON-LINEAR LOAD REDUCTION DEVICES FOR CATENARY MOORINGS

Oscar Festa[1], Susan Gourvenec[1], Adam Sobey[1,2]

[1] Faculty of Engineering and Physical Sciences, University of Southampton, UK
[2]Data-Centric Engineering, The Alan Turing Institute, UK

ABSTRACT

Load reduction devices are extensible components which can be installed along mooring lines to reduce peak loads and fatigue damage in the mooring system. This has the potential to reduce risk of failure for Floating Offshore Wind Turbine (FOWT) mooring systems, and can provide significant reductions to the overall material, handling and installation costs of a FOWT project. Various load reduction device concepts exist, including ballasted pendulums, thermoplastic springs and hydraulic dampers, all of which are designed to exhibit a non-linear load-extension behaviour: lower stiffness in the operational strain range to reduce loads, and higher stiffness at high strain. These devices are becoming an increasingly common consideration for FOWT mooring systems, and are pushing traditional analysis and design methods to readily incorporate non-linearity. Well-established static catenary equations, used to define mooring tension-offset profiles, only account for linear elasticity such that capturing non-linear response typically requires finite element modelling. This paper presents an alternative through parameterising equations for three different non-linear load-extension curves and incorporating them into the existing catenary equations. For a given non-linear load-extension curve and length of load reduction device, the resulting analytical model can be solved quasi-instantaneously using Newton-Raphson or Newton-Krylov iterations to give vertical and horizontal mooring line tensions and thus strain of the device. Results from the new analytical model are compared with finite element predictions showing agreement to within 1%. The analytical model can be solved for any two unknowns, such that optimal load reduction device length and stiffness can be determined instantaneously given maximum environmental load and allowable offset. The new analytical equations are implemented into a graphical app, which allows the user to input any load reduction device parameters and visualise the resulting mooring system's geometry and tension-offset profile.

Documentation for `asmeconf.cls`: Version 1.31, July 4, 2023.

1. INTRODUCTION

1.1 Motivation for compliant FOWT mooring design

Up to 80% of worldwide offshore wind resources are in water depths greater than 60 m [1], where traditional fixed-bottom wind farms are not economically viable. In these deeper waters, offshore wind turbines must be deployed on floating structures, connected to the seabed via mooring lines and anchors. Mooring systems are designed to ensure station-keeping of the floating structure: they maintain the structure within an acceptable distance from its reference position. Station-keeping requirements for Floating Offshore Wind Turbines (FOWTs) are often more lenient than for oil & gas installations [2] and are primarily constrained by the motion of the electrical power cable [3].

Designing a mooring system involves finding a balance between stiffness and compliance to fit the station-keeping requirements [4]. A stiffer mooring system will maintain the floating structure closer to its reference position, at the expense of high loads on the mooring lines and anchors. A compliant mooring system will allow more motion of the floating structure in response to environmental loads, reducing forces in the mooring line and anchor, in turn allowing for smaller, cheaper anchors and a reduced chance of mooring line failure (Table 1). As FOWT farms require large amounts of structures to be moored to the seabed, reducing mooring and anchoring costs per unit through compliant moorings can lead to significant overall savings.

TABLE 1: EFFECT OF COMPLIANCE ON FOWT SYSTEM

Mooring design:	stiff	compliant
Platform displacements	–	+
Mooring and anchor loads	+	–
Mooring and anchor cost	+	–

In response to the incentive to reduce the cost of FOWT moorings, various means of adding compliance to mooring systems have been developed, in particular in the form of load reduction devices (LRDs). Current concepts include the Exeter Intelligent

Mooring System (IMS), (Fig.1a) [5], the Dublin Offshore LRD (DO), (Fig.1b) [6], and the Technology for Ideas Seaspring (TFI), (Fig.1c) [7]. These devices are incorporated into a mooring line, typically close to the fairlead, and can provide high levels of compliance (extensibility) without compromising breaking strength [8]. For the same breaking strength, typical synthetic ropes cannot achieve such low elastic stiffness. The DO and TFI devices are passive, whereas the IMS is 'active' as it can change stiffness curve in operation. Thus, two curves are considered for the IMS device, which correspond to the upper and lower bound stiffness for the given configuration.

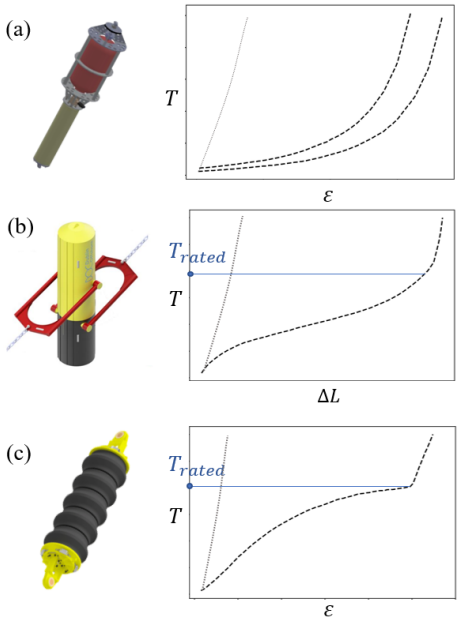

FIGURE 1: LRD TECHNOLOGIES AND ASSOCIATED STIFFNESS CURVES: (A) IMS [5], (B) DO [6], (C) TFI [7] . POLYESTER ROPE STIFFNESS SHOWN WITH GRAY DOTTED LINE FOR COMPARISON

These devices have highly non-linear stiffness curves, which can be tailored to fit the specific loading conditions and mooring arrangement (Fig. 1). These non-linear stiffness curves have a compliant range over which the LRD is intended to operate to effectively reduce mooring line tension. The curves then exhibit higher stiffness at high strain when they reach their rated tension T_{rated}, i.e., once all the compliance has been exhausted. Graphical representation of the rated tension is shown for DO and TFI in Figure 1. The key to designing a mooring system with a LRD is to ensure the device operates in its compliant range as much as possible, meaning the LRD is generally designed such that the maximum tension in the device stays below T_{rated}. The optimal length of the LRD should then be determined to ensure the extension provided does not exceed station-keeping constraints. Current approaches to finding this optimal length and rated tension involve time-consuming iterations of Finite Element (FE) analyses. The aim of this paper is to propose an analytical model of catenary moorings with LRDs, which can be used for efficient quasi-static design of an LRD mooring system.

1.2 Quasi-static mooring system design

If all dynamic mooring effects (damping, inertia) are ignored, and the system is assumed to be static at a given instant t, the geometry of the mooring line can be solved analytically as a function of the fairlead coordinates and the physical parameters of the mooring line. This constitutes the quasi-static mooring analysis, which is typically the first step in mooring system design [9]. The quasi-static analysis is useful for determining the tension-offset response of a mooring system, which informs designers of the restoring force provided by the system in response to displacement of the fairlead.

For neutrally buoyant taut moorings, the relationship between fairlead coordinates and restoring forces is trivial: the mooring line adopts a straight line between the fairlead and anchor, and the tension-offset of the system corresponds directly to the material stiffness of the mooring line [10]. This relationship is more complex for catenary moorings, as the catenary configuration (i.e., weight of suspended line) is controlled by tension, leading to a non-linear tension-offset profile. This is captured by the catenary mooring equations, which define the fairlead coordinates x_f and z_f as a function of the fairlead restoring forces H_f and V_f [11] and the mooring line length L, stiffness EA and unit weight w (Fig. 4). For a line partially resting on a friction-less seabed:

$$x_f(H_f, V_f) = L - \frac{V_f}{w} + \frac{H_f}{w} \cdot \ln\left[\frac{V_f}{H_f} + \sqrt{1 + \left(\frac{V_f}{H_f}\right)^2}\right] + \frac{H_f L}{EA} \tag{1a}$$

$$z_f(H_f, V_f) = \frac{H_f}{w} \cdot \left[\sqrt{1 + \left(\frac{V_f}{H_f}\right)^2} - 1\right] + \frac{V_f^2}{2EAw} \tag{1b}$$

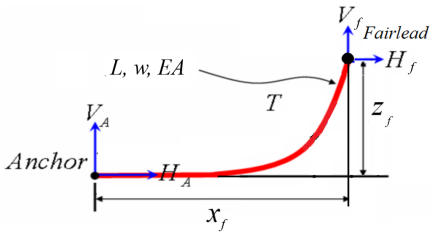

FIGURE 2: PROFILE VIEW OF SIMPLE CATENARY MOORING LINE

The system of equations 1a & 1b can then be solved for any two unknowns. However, this is only valid for a homogeneous mooring line (i.e. full chain), and the stiffness term EA must be linear. As such, these equations cannot be used for analysis of a mooring system with a non-linear LRD. Other publications have presented equations for multi-segmented catenary mooring lines with a non-linear stiffness segment, in particular for polymer rope applications [10]. The non-linear stiffness is expressed in simple

power law form, where the strain ε is given as a function of axial load T and constants p and q :

$$\varepsilon = pT^q \tag{2}$$

The power law form offers a good fit for material stiffness of typical synthetic polymer ropes, but this does not match the LRD stiffness curves as shown in Figure 1.

Since no analytical solution is available, current approaches to modelling moorings with LRDs include discretisation of the mooring lines and/or piece-wise linear interpolation of the non-linear stiffness curves. Commercial software such as Orcaflex is typically used for dynamic modelling of LRDs [12], which uses linear interpolation between consecutive points of the user-defined non-linear stiffness curve. LRDs have also been modelled with the open-source lumped-mass modelling software Moordyn, which also uses linear interpolation of the stiffness curve [7].

This paper presents continuous functions which model the non-linear stiffness curves of the LRD devices shown in Figure 1. These functions are then combined with the existing equations for catenary moorings, to create a static analytical model of catenary moorings with LRDs. This requires no discretisation or stiffness interpolation, and as such provides a quicker approach to obtain the mooring geometry and restoring forces based on any input mooring properties and LRD parameters (rated tension, curve shape, LRD length). The analytical model can then be used to find optimal LRD parameters for a given water-depth, mean environmental load, and offset constraint.

2. METHOD

This paper employs an analytical approach to mooring systems modelling. Firstly, a 2-segment formulation for a catenary mooring line with a linear-stiffness LRD at the fairlead is presented based on established equations. This formulation is then adapted with various non-linear stiffness functions, to form a set of equations for a chain catenary line with non-linear LRDs. These are solved using numerical root-finding methods, in particular the Newton-Raphson method [13], implemented in Python. Commercial FE software Flexcom is then used to validate the results obtained from the analytical equations. The validated analytical model is then applied to initial quasi-static design of an LRD. A structural overview of the methodology of the paper is shown in Fig 3.

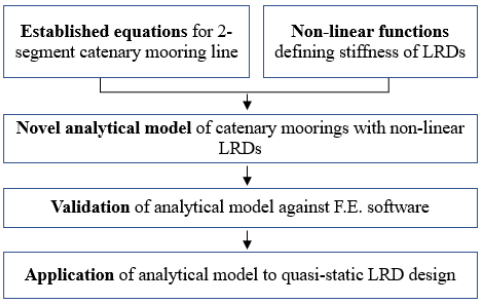

FIGURE 3: METHODOLOGY FOR THE ANALYTICAL SOLUTION

3. DEVELOPMENT OF ANALYTICAL MODEL

3.1 Catenary equations for linear-stiffness LRDs

The static catenary equations 1a & 1b apply to a catenary line formed of a unique, homogeneous segment, with material properties defined by a single value of stiffness EA and apparent weight in water per unit length w. This section presents an adapted formulation for a mooring line with two distinct segments: one segment for the chain catenary line and one segment for a linear stiffness LRD at the fairlead (Fig. 4). This linear LRD formulation is then used as the starting point for the next section, which presents the equation for non-linear stiffness LRDs.

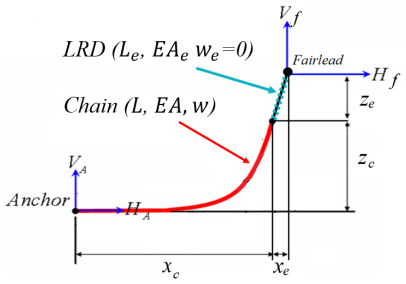

FIGURE 4: PROFILE VIEW OF THE MULTISEGMENT LINE

The static multi-segment mooring analysis approach is well-documented in literature [10]. For a catenary line composed of n segments of line, the fairlead coordinates (x_f, z_f) are given as a sum of the horizontal and vertical components of each segment:

$$x_f = \sum_{i=1}^{n} x_i \tag{3a}$$

$$z_f = \sum_{i=1}^{n} z_i \tag{3b}$$

Where the coordinates of the extremities of the i^{th} segment x_i and z_i are each defined by the catenary equations in their own coordinate system, with the origin at the start of the segment (starting from the anchor).

If the LRD is modelled as a simple non-linear spring segment, and assumed to be near-neutrally buoyant in water, which is typically the case of the IMS and DO technologies [5][6], this means the spring is subjected to constant tension throughout its length, thus adopting a straight line rather than a catenary shape. For a linear stiffness LRD, its extension ΔL_e is based on Hooke's law, where the tension-strain profile is a straight line passing through the origin and a single point EA. The coordinates of the horizontal and vertical extremities of the LRD segment (x_e, z_e) are then given by:

$$x_e = \frac{H_f l_e}{\sqrt{H_f^2 + V_f^2}} + \frac{H_f L_e}{EA_e} \tag{4a}$$

$$z_e = \frac{V_f l_e}{\sqrt{H_f^2 + V_f^2}} + \frac{V_f L_e}{EA_e} \tag{4b}$$

Where the left-hand terms represent the horizontal (4a) or vertical (4b) projections of the unstretched length L_e of the LRD, and the right-hand term represents the elongation of the LRD, obeying Hooke's law.

According to the multisegment theory from equations 3a & 3b, equations 4a & 4b can be added to the chain catenary equations to give the coordinates of the fairlead (x_f, z_f) as a function of the restoring forces (H_f, V_f):

$$x_f(H_f,V_f) = L - \frac{V_f}{w} + \frac{H_f}{w}\cdot\ln\left[\frac{V_f}{H_f} + \sqrt{1+\left(\frac{V_f}{H_f}\right)^2}\right] + \frac{H_f L}{EA} + \frac{H_f L_e}{\sqrt{H_f^2+V_f^2}} + \frac{H_f L_e}{EA_e} \tag{5a}$$

$$z_f(H_f,V_f) = \frac{H_f}{w}\cdot\left[\sqrt{1+\left(\frac{V_f}{H_f}\right)^2} - 1\right] + \frac{V_f^2}{2EAw} + \frac{V_f L_e}{\sqrt{H_f^2+V_f^2}} + \frac{V_f L_e}{EA_e} \tag{5b}$$

3.2 Catenary equations for non-linear stiffness LRDs

To replace the Hookean extension term in equations 4a & 4b, the non-linear extension of the LRD must be defined as a function of the force applied at its extremities. This means determining the function ε which gives the LRD strain for any value of axial mooring line tension T, where T is the resultant of the horizontal and vertical mooring line forces H_f and V_f :

$$\varepsilon(T) = \varepsilon(\sqrt{H_f^2+V_f^2}) = \frac{\Delta L_e}{L_e} \tag{6}$$

Equations analogous to 5a and 5b can be obtained by substituting the Hookean extension term (the final term in equations 5a & 5b) with the non-linear strain function ε, giving:

$$x_f(H_f,V_f) = L - \frac{V_f}{w} + \frac{H_f}{w}\cdot\ln\left[\frac{V_f}{H_f} + \sqrt{1+\left(\frac{V_f}{H_f}\right)^2}\right] + \frac{H_f L}{EA} + \frac{H_f L_e}{\sqrt{H_f^2+V_f^2}}(1+\varepsilon(T)) \tag{7a}$$

$$z_f(H_f,V_f) = \frac{H_f}{w}\cdot\left[\sqrt{1+\left(\frac{V_f}{H_f}\right)^2} - 1\right] + \frac{V_f^2}{2EAw} + \frac{V_f L_e}{\sqrt{H_f^2+V_f^2}}(1+\varepsilon(T)) \tag{7b}$$

These equations are valid for an extensible section located at the fairlead, attached to a homogeneous catenary mooring line with a portion resting on the seabed (i.e. no vertical loading on the anchor), where seabed friction is neglected. An analogous expression can also be derived for non-buoyant taut and semi-taut moorings where vertical anchor loading is non-zero, based on the equations for a fully-suspended line [11].

Equations 4a & 4b assume that the extensible section is neutrally buoyant in seawater. This is a valid assumption for the IMS and DO devices, but the TFI device has a non-negligible weight in water [7]. This means the upper extremity of the LRD is subjected to additional tension due to self-weight of the device, with a difference in vertical tension between the two extremities equal to $L_e w_e$ where L_e is the length of the device and w_e is its wet weight per unit length. Due to this difference in tension, the strain of the LRD is not constant along its length, and requires an integral to compute analytically. As a simpler approximation, the tension can be assumed to be constant throughout the LRD, taking the value of the tension at its midpoint, which is subjected to half of the self weight of the LRD: $\frac{1}{2}L_e w_e$. With this assumption, the strain in the device given by Equation 6 can be redefined as:

$$\varepsilon(T) = \varepsilon\left(\sqrt{H_f^2 + (V_f - \frac{1}{2}L_e w_e)^2}\right) \tag{8}$$

The chain section of the line, which is below the LRD, is not subjected to the additional vertical tension component. Thus, we define the component of vertical tension at the top chain as V_{tc} which does not include the self weight, and is given by $V_{tc} = V_f - L_e w_e$. The full expression is then given by:

$$x_f(H_f,V_f) = L - \frac{V_{tc}}{w} + \frac{H_f}{w}\cdot\ln\left[\frac{V_{tc}}{H_f} + \sqrt{1+\left(\frac{V_{tc}}{H_f}\right)^2}\right] + \frac{H_f L}{EA} + \frac{H_f L_e}{\sqrt{H_f^2+(V_f-\frac{1}{2}L_e w_e)^2}}(1+\varepsilon(T)) \tag{9a}$$

$$z_f(H_f,V_f) = \frac{H_f}{w}\cdot\left[\sqrt{1+\left(\frac{V_f}{H_f}\right)^2} - 1\right] + \frac{V_f^2}{2EAw} + \frac{(V_f-\frac{1}{2}L_e w_e)L_e}{\sqrt{H_f^2+(V_f-\frac{1}{2}L_e w_e)^2}}(1+\varepsilon(T)) \tag{9b}$$

3.3 Continuous functions for LRD stiffness curves

Adapting the general-form equations 7a & 7b or 9a & 9b to a specific LRD technology requires determining the function $\varepsilon(T)$which gives LRD strain as a function of axial tension T. In this section, functions have been derived for the three curve types shown in Figure 1. These functions are mostly based on the Ramberg-Osgood model, which is typically used to define non-linear stress-strain relationships. The original model defines stress as a function of strain and 3 parameters [14]. In this case, the model is used only in its mathematical sense, and the form is reversed to define strain ε as a function of axial tension T such that it can be incorporated into the catenary equations. This adaptation of the basic-form Ramberg-Osgood model can be given as:

$$\varepsilon(T) = \frac{aT}{(1+(\frac{aT}{c})^n)^{\frac{1}{n}}} \tag{10}$$

Where a, c and define the shape of the curve (Fig. 5).

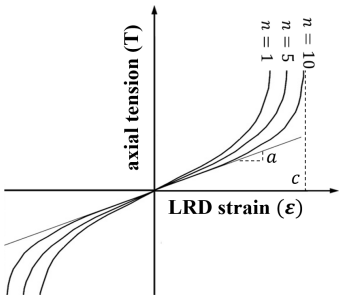

FIGURE 5: BASIC-FORM RAMBERG-OSGOOD CURVE

The basic form equation of the Ramberg-Osgood model given in Equation 10, does not directly fit all of the LRD devices identified in Figure 1, in particular the TFI and DO LRDs which require additional terms and parameters. These variations of the basic form equation are described in the following subsections.

Exeter IMS

The curve of the IMS is the closest fit to the Ramberg-Osgood model, with the exception of the curve not passing through the origin due to variable pre-load in the device [5]. An additional parameter b is introduced, which shifts the curve along the x-axis from the origin, such that the overall equation is given by:

$$\varepsilon_{IMS}(T) = \frac{aT - b}{(1 + (\frac{aT-b}{c})^n)^{\frac{1}{n}}} \tag{11}$$

Where b/a is the pre-tension, c is the asymptotic strain, and n is a parameter defining the rate at which the curve reaches its asymptotic strain, as shown in Figure 5. The value of n can be found if the rated tension required at a specific value of strain is known. The parameters of Equation 11 are fitted to two example supplier curves [5], using a simple linear regression algorithm, and the resulting curve fits are plotted in Figure 6. The values of each fitted parameter are given in Table 2, for curves A and B.

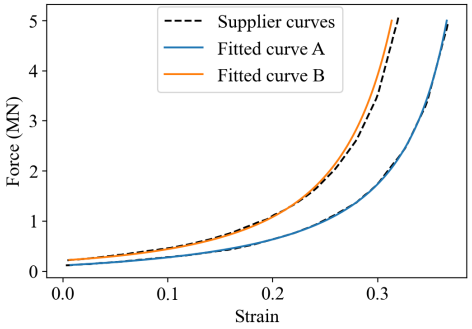

FIGURE 6: IMS STIFFNESS CURVES FROM SUPPLIER PUBLICATION [5], AGAINST FITTED CURVE FROM EQ. 11

TABLE 2: IMS FITTED PARAMETERS FOR EQ. 11

Parameter	fitted value (A)	fitted value (B)
a	0.958	0.837
b	0.113	0.183
c	0.426	0.396
n	0.834	0.728

Dublin Offshore LRD

To obtain an expression of the DO curve, the base curve from Figure 5 is translated with an additional parameter b, as with the IMS fit. However, the curve must pass through the origin, which is not the case of the IMS curve in Eq. 11, which passes through the point $[0, \varepsilon(0)]$, where $\varepsilon(0)$ given by:

$$\varepsilon_{IMS}(0) = \frac{-b}{(1 + (\frac{b}{c})^n)^{\frac{1}{n}}} \tag{12}$$

To ensure that the DO curve passes through the origin, the term shown in Eq. 12 is subtracted from Eq. 11, giving an expression of $\Delta L_{Dublin}(T)$ (Eq. 13). The shape factor n, which defines the rate at at which the function reaches its asymptote, is fixed to $n = 2$. The parameters a, b and c of Equation 13 are fitted to the example curve from supplier documentation [6] using linear regression, resulting in the curve fit shown in Figure 7. The values of each fitted parameter for this curve are given in Table 3.

$$\Delta L_{Dublin}(T) = \frac{aT - b}{(1 + (\frac{aT-b}{c})^2)^{\frac{1}{2}}} + \frac{b}{(1 + (\frac{b}{c})^2)^{\frac{1}{2}}} \tag{13}$$

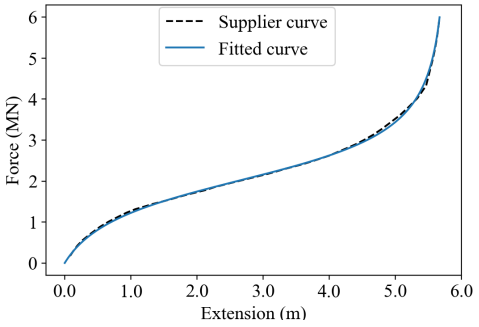

FIGURE 7: DO STIFFNESS CURVE FROM SUPPLIER PUBLICATION [6], AGAINST FITTED CURVE FROM EQ. 13

In Eq. 13, parameter a is related to the rated tension of the device and c is related to the asymptotic extension of the device. These parameters can also be linked to physical dimensions of the device, based on supplier documentation [6]. As opposed to the IMS and TFI devices which are spring-like, the DO LRD extends by rotating under loading (Fig. 1b). Thus, extension $\Delta L(T)$ is used rather than the strain term $\varepsilon(T)$. When incorporated into the final system of static equations 7a & 7b, the

TABLE 3: DO FITTED PARAMETERS FOR EQ. 13

Parameter	fitted value
a	7.500
b	7.432
c	2.568

length of device Le can then be based on the starting distance between the two hinge points. It should also be noted that Eq 13 is only valid for a fixed mooring line angle. The line angle affects the magnitude of the moment generated by the mooring line on the LRD hinges, in turn changing the shape of the stiffness curve. A more complete expression is given in the published code [15], which captures the effect of the line angle, and relates the curve parameters to physical dimensions of the LRD.

TFI Seaspring

The TFI stiffness curve (Fig. 1b) is complex to model with a continuous function due to the sudden stiffness increase at $T = T_{rated}$. The required function deviates more significantly from the base Ramberg-Osgood model, in three ways: 1. Parameter c is subtracted to the denominator of the first term to create the sudden gradient change; 2. An additional parameter k is introduced to factorise the whole expression, such that the rated strain of the curve can be directly adjusted without changing the other parameters; 3. An additional term is introduced, function of a new parameter d, in an attempt to better match the final phase stiffness. The resulting expression is given in Eq. 14, with the associated curve fit is shown in Figure 8, and the fitted parameter values given in Table 4.

$$\varepsilon_{TFI}(T) = k \cdot \left(\frac{a(eT - f) - b}{1 + [a(eT - f) - b - c]^2} + \frac{af + b}{1 + [-af - b - c]^2} + d\sqrt{a(eT - f)} - d\sqrt{-af} \right) \tag{14}$$

The fit is accurate up to, and including, the sudden increase in stiffness at $T = T_{rated}$. . Accurate modelling of the response past this point is not crucial, as in practice the device should not be operating above T_{rated}. Although the expression is complex, only parameters k and e are required to parameterise the rated tension and strain. Any value of rated tension T_{rated} can be obtained by varying parameter e, and any value of rated strain $\varepsilon(T_{rated})$ can be obtained by varying parameter k.

For each LRD, the derived non-linear stiffness function is substituted for the $\varepsilon(T)$ term in the general form equations (7a & 7b, 9a & 9b), with the resulting systems of equations forming the analytical model. This model can be solved for the vertical and horizontal restoring forces H_f and V_f at the fairlead, for any fairlead coordinates x_f and z_f, by employing numerical root-finding methods. All LRD stiffness functions and resulting mooring equations are fully differentiable over their domain. This means the system can be solved with a Newton-Rhapson scheme with analytical Jacobians, providing fast and robust computation.

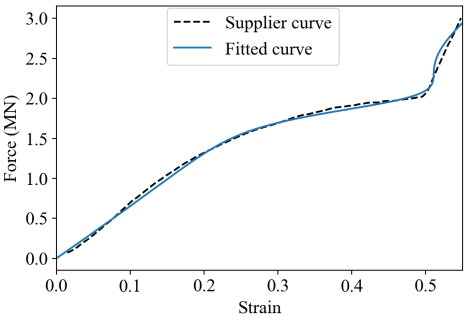

FIGURE 8: TFI STIFFNESS CURVE FROM SUPPLIER PUBLICATION [7], AGAINST FITTED CURVE FROM EQ. 14

TABLE 4: TFI FITTED PARAMETERS FOR EQ. 14

Parameter	fitted value
a	1.238×10^{-2}
b	2.119×10^{2}
c	7.516×10^{-1}
d	1.149×10^{1}
e	2.405×10^{2}
f	-1.672×10^{5}
k	1.379×10^{-1}

4. VALIDATION OF ANALYTICAL MODEL

The analytical model was then validated against results obtained from the commercial FE software Flexcom, which discretises the mooring line and interpolates the stiffness from a set of force-strain points. The validation was performed by comparing quasi-static tension-offset profiles for each of the LRD concepts. To obtain the quasi-static tension-offset profile, the horizontal fairlead coordinate x_t is gradually displaced along the horizontal axis parallel to the mooring line, and the analytical model is used to calculate the resultant fairlead tension T from the fairlead forces H_f and V_f at every step. This is depicted graphically in Figure 9. This figure was obtained using a graphical app built on Python, based on the analytical model, which enables visualisation of the geometry of a mooring system with any LRD parameters [15].

The properties of the mooring system used are identical to those of the OC4 Phase II mooring system [16], with the exception of the water depth which is set to 150 m rather than 200 m, to make the mooring system more sensitive to the LRD. These properties are summarised in Table 5. For each LRD concept, the stiffness curve parameters are taken from the curve fits shown in section 3.3 and the LRD lengths are set such that they all exhibit 5 m of extension at $T_{rated} = 2MN$. This rated tension was chosen arbitrarily for this illustration, but the LRDs can be designed for any value of T_{rated}. The IMS and DO devices were modelled using Eq. 7a & 7b, which are valid for neutrally buoyant devices, whereas the TFI device was modelled using Eq. 9a & 9b. The wet weight of the TFI device was set to 8 kN/m, which corresponds to the weight of a 1m-diameter device with rated tension of 2 MN.

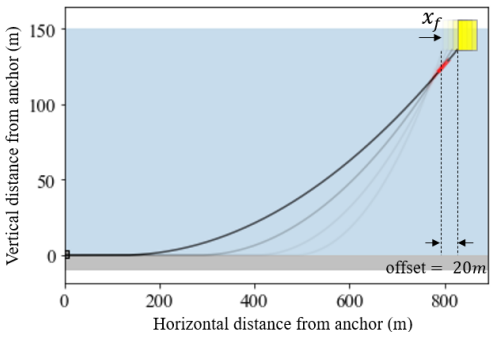

FIGURE 9: 2D PLOT OF MOORING LINE, WITH FAIRLEAD DISPLACED ALONG HORIZONTAL AXIS UP TO AN OFFSET OF 20M

TABLE 5: MOORING SYSTEM PARAMETERS, BASED ON OC4 [16]

Mooring system parameter	Value
Fairlead-seabed vertical dist.	136 m
Unstretched mooring line length inc. LRD	825.35 m
Initial anchor-fairlead distance	796.7 m
Chain mass per unit length	145 kg/m
Chain EA	750 MN

The resulting tension-offset plots are shown in Figures 10, 11 and 12. These are displayed alongside the equivalent full-chain mooring system tension-offset, i.e. a catenary mooring with the same overall line length but no LRD. These show close alignment between the analytical and FE results, with a mean error $< 0.1\%$ and a maximum error across all curves of 0.4%. The maximum error occurs at the gradient change point of the TFI curve, where the fitted stiffness curve does not perfectly match the interpolated curve (Fig. 8). Other general take-away points from the tension-offset profiles are listed below:

- All three LRD moorings show significantly more compliance than the full-chain catenary (i.e. lower gradient of tension-offset), especially at lower offsets where the LRDs operate in their low-stiffness regions. As a result of this increased compliance, the LRD moorings display higher horizontal offsets than the full-chain mooring for the same fairlead tension.
- All three LRDs have exhausted all their extensibility once the fairlead tension is above the rated tension of the device. In practice, this would mean no extension is left to reduce dynamic loads. If these high loads/offsets are expected, an LRD with higher rated tension should be used.
- The extension of the LRDs under the weight of the chain at zero-offset leads to reduced pre-tension of the mooring system. In practice, this could be compensated for by reducing the overall length of line. Due to its self-weight, the TFI device (Fig. 12) shows higher pre-tension than the other LRDs for the same mooring line length.

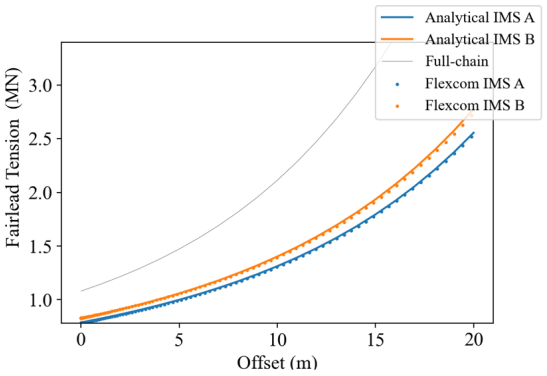

FIGURE 10: TENSION-OFFSET PROFILE FROM ANALYTICAL SOLUTION AND FE SOFTWARE FOR IMS CURVES (CONFIGURATIONS A & B)

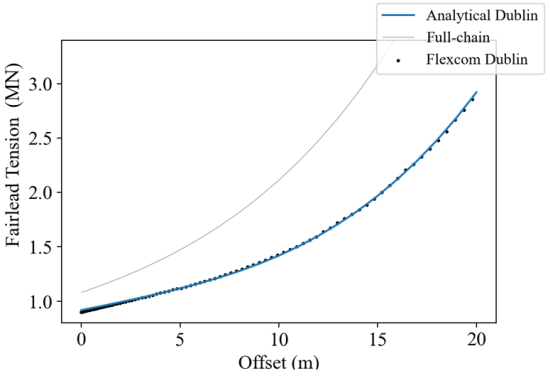

FIGURE 11: TENSION-OFFSET PROFILE FROM ANALYTICAL SOLUTION AND FE SOFTWARE FOR DO CURVE

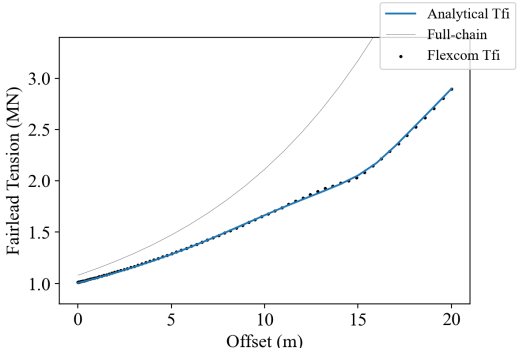

FIGURE 12: TENSION-OFFSET PROFILE FROM ANALYTICAL SOLUTION AND FE SOFTWARE FOR TFI CURVE

5. APPLICATION OF ANALYTICAL MODEL TO LRD DESIGN

5.1 Quasi-static design scenario

Quasi-static design typically involves approximating a mean horizontal environmental force from met-ocean data [9]. This force is applied at the fairlead, and the analytical model can be used to find the fairlead tension and platform offset such that the system is in static equilibrium. For this example, the 50-year horizontal force was set as $F_{env} = 2MN$. Knowing the horizontal fairlead force $H_f = F_{env}$, the vertical force V_f and resulting offset x_f were obtained from eq. 9a & 9b. The 50-year quasi-static fairlead tension $T_{50yr,QS}$ was then calculated from the horizontal and vertical forces. The LRD design parameters could then be adjusted based on the quasi-static offset and fairlead tension.

In particular, two key LRD parameters should be determined at the initial design stage: 1. The rated tension of the device, determined based on the maximum expected load; 2. The maximum extension of the device (i.e., length of the device for spring-like LRDs), determined based on the maximum allowable offset. These parameters are typically found based on iterative dynamic analyses [7], which can be computationally-intensive. This section demonstrates how the analytical model can be used to find a fast initial approximation of the optimal LRD parameters at the quasi-static design stage. This example design scenario is applied to the TFI Seaspring LRD in a catenary mooring system with the physical properties listed in table 5.

5.2 Determining the LRD rated tension

The aim is to determine the suitable T_{rated} for the LRD such that it is not only above the 50-year quasi-static fairlead tension, but also above the 50-year dynamic tensions, to ensure the device can safely operate in the compliant range throughout its design life. Typical quasi-static mooring design approaches require application of a safety factor to the 50-year quasi-static tension to obtain the design tension, with values typically ranging from 1.4 to 2 in relevant design codes [17]. As the LRD is expected to significantly reduce dynamic loads, a low safety factor of 1.4 is used for this example, such that:

$$T_{rated} \geq 1.4 * T_{50yr,QS} \tag{15}$$

To solve this, the analytical model was used to iterate through values of the TFI curve parameter e which is inversely related to T_{rated} (see Eq. 14), starting from a high value of e such that the starting rated tension T_{rated} is equal to the horizontal force F_{env}. All the other curve parameters were fixed to the values shown in Table 4. The fairlead tension, mooring configuration and resulting tension-offset profiles were then computed for each value of e, for the given environmental load until the value of T_{rated} that fits the criterion (Eq. 15) was reached. In this case, the 50-year quasi-static (QS) tension was found to be $T_{50yr,QS} = 2.217MN$, which gives $T_{rated} \geq 3.10MN$ when including the safety factor (Eq. 15). This is depicted graphically in Figure 13. In this case, the value of $T_{50yr,QS}$ is only slightly above the horizontal environmental force F_{env}. This is due to the chain being relatively light, meaning the additional vertical restoring force component at the fairlead is small.

The curve with the lowest rated tension is operating above its rated tension when subjected to the 50-year horizontal load.

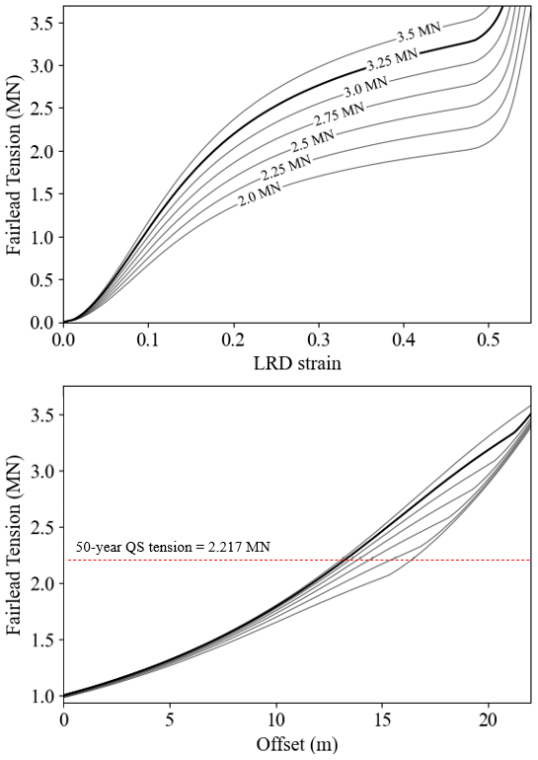

FIGURE 13: TOP: LRD TENSION-STRAIN CURVES FOR 7 VALUES OF T_{rated}; BOTTOM: RESULTING MOORING SYSTEM TENSION-OFFSET PROFILE FOR EACH CURVE. THE CURVE SATISFYING THE DESIGN CRITERION IS SHOWN IN BOLD.

This is visible on the tension-offset profile, with the dashed red line located above the 'kink' in the curve. The curve which satisfies the criterion is operating safely below its rated tension when subjected to the same load, meaning the LRD would be operating in its compliant range as intended. While an even higher rated tension would also be suitable in theory (e.g. 3.5 MN), the resulting tension-offset of the mooring system is stiffer overall, and less effective at reducing loads.

5.3 Determining the LRD length

In the case of a spring-like LRD (e.g. TFI), the length of the device determines its maximum extension, which in turn affects the load reduction potential [18] as well as the resulting platform offset. In the study thus far, LRDs lengths were set such that they exhibit 5 m of extension at the rated strain, i.e. $L_e = 10m$ for the TFI device. For the curve with a rated tension of $T_{rated} = 3.25MN$, the resulting 50-year quasi-static offset is of $T_{50yr,X} = 13.35m$ (can be deduced graphically from Fig. 13). If this is below the maximum quasi-static offset criterion, a longer LRD could be used, for added compliance. As an example, the maximum allowable quasi-static offset is set to 20m. The model was then used to iterate values of L_e, and resulting tension-

offset plots were generated. The optimal length of the LRD is selected by finding the tension-offset profile which is just below the maximum offset for the 50-year tension. This process is depicted in Figure 14, and yields $L_e = 15m$.

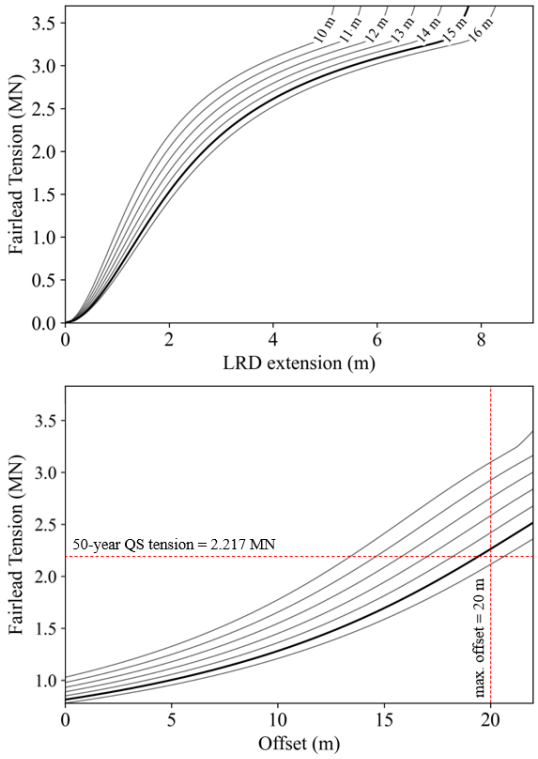

FIGURE 14: TOP: LRD TENSION-EXTENSION CURVES FOR 7 VALUES OF L_e; BOTTOM: RESULTING MOORING SYSTEM TENSION-OFFSET PROFILE FOR EACH CURVE. THE CURVE SATISFYING THE MAXIMUM OFFSET CRITERION IS SHOWN IN BOLD.

6. CONCLUSION

This paper presented an analytical quasi-static tension-offset model of catenary moorings with LRDs with three different non-linear stiffness curves. The model is applicable to any catenary mooring scenario, and is of particular interest for initial FOWT mooring design and analysis. Continuous parameterised equations, defined for the stiffness curves of three different LRDs, were incorporated into the static equations for a multi-segmented catenary mooring. Results from the analytical model, using the continuous equations for the LRD stiffness, match closely with results of a commercial FE model, which uses piece-wise interpolation of user-defined LRD stiffness cruves. The analytical model has been packaged into an executable function as well as an associated web application, which enables visualisation of the mooring geometry and tension-offset profiles for any input LRD and mooring design parameters [15].

The effectiveness of the analytical model has also been demonstrated here through an example quasi-static design scenario, and was used to find an initial LRD design for a given 50-year environmental load. By determining the optimal stiffness curve, the LRD was ensured to operate below its rated tension, and by finding the optimal LRD length, it satisfied the maximum offset criterion while maintaining maximum compliance. This design approach yields quasi-instantaneous results, and could provide an efficient starting point for subsequent dynamic analyses.

ACKNOWLEDGMENTS

This work forms part of the activities of the Royal Academy of Engineering Chair in Emerging Technologies Centre of Excellence for Intelligent & Resilient Ocean Engineering (www.southampton.ac.uk/iroe), based at the University of Southampton. Susan Gourvenec is supported by the Royal Academy of Engineering under the Chairs in Emerging Technologies scheme. Adam Sobey is supported by the Alan Turing institute.

REFERENCES

[1] Burges Salmon. "Floating Wind – Challenges and Opportunities for a Buoyant Technology,." *Burges Salmon - News & Insight* URL https://www.burges-salmon.com/news-and-insight?Sector+expertise=Energy+Power+and+Utilities.

[2] COREWIND. "D1.2 Design basis." URL https://corewind.eu/wp-content/uploads/files/publications/COREWIND-D1.2-03-Design-Basis.pdf.

[3] COREWIND. "D3.1 Review of the state of the art of dynamic cable system design." URL https://ec.europa.eu/research/participants/documents/downloadPublic?documentIds=080166e5cca0f37e&appId=PPGMSl.

[4] Cruz, J. and Mairead, A. "Floating Offshore Wind Energy : The Next Generation of Wind Energy." *Green Energy and Technology*. 2016. Springer. URL http://search.ebscohost.com/login.aspx?direct=true&db=nlebk&AN=1282129&site=ehost-live.

[5] Harrold, M., Thies, P., Johanning, L., Newsam, D., Checkley, M. and Bittencourt Ferreira, C. "Dynamic load reduction and station keeping mooring system for floating offshore wind." *ASME 2018 1st International Offshore Wind Technical Conference*. 2018. American Society of Mechanical Engineers Digital Collection.

[6] Dublin Offshore. "Load Reduction Device (LRD) – How it works." URL https://www.dublinoffshore.ie/media/pages/technology/6f4e7419f6-1635594571/how-it-works.pdf.

[7] Lozon, E., Hall, M., McEvoy, P., Kim, S. and Ling, B. "Design and Analysis of a Floating-Wind Shallow-Water Mooring System Featuring Polymer Springs." *International Offshore Wind Technical Conference (IOWTC2022)*. 2022.

[8] WFO. "Mooring Systems for Floating Offshore Wind: Integrity Management Concepts, Risks and Mitigation,." *World Forum Offshore Wind 2022 e.v.* URL https://wfo-global.org/?jet_download=5751.

[9] Ma, K., Luo, Y., Kwan, T. and Wu, Y. "Mooring System Engineering for Offshore Structures." Ma, K., Luo, Y., Kwan, T. and Wu, Y. (eds.). *Chapter 15 - Mooring for floating wind turbines*. Gulf Professional Publishing (2019): pp. 299–315. DOI https://doi.org/10.1016/B978-0-12-818551-3.00015-6. URL https://www.sciencedirect.com/science/article/pii/B9780128185513000156.

[10] Oppenheim, B and Wilson, P. "Static 2-D Solution of a Mooring Line of Arbitrary Composition in the Vertical and Horizontal Operating Modes." *International shipbuilding progress* Vol. 29 (1982): pp. 142–153.

[11] Jonkman, J. "Dynamics modeling and loads analysis of an offshore floating wind turbine." Technical Report No. NREL/TP-500-41958. National Renewable Energy Lab (NREL), Golden, CO (United States). 2007. URL https://www.nrel.gov/docs/fy08osti/41958.pdf.

[12] McEvoy, P. and Johnston, E. "Polymer Mooring Component for Offshore Renewable Energy." *OTC Offshore Technology Conference*, Vol. Day 3 Wed, May 08. 2019. DOI 10.4043/29587-MS. URL https://onepetro.org/OTCONF/proceedings-pdf/19OTC/3-19OTC/D031S033R004/1986721/otc-29587-ms.pdf.

[13] Kelley, C. T. "Solving Nonlinear Equations with Newton's Method.": pp. 57–83. 2003. Society for Industrial and Applied Mathematics. DOI 10.1137/1.9780898718898.ch3. URL https://epubs.siam.org/doi/pdf/10.1137/1.9780898718898.ch3.

[14] Ramberg, W. and Osgood, W. "Description of stress-strain curves by three parameters." Technical Report No. 902. National Advisory Committee for Aeronautics. 1943.

[15] Festa, Oscar. "Quasi-static LRD mooring model." (2023). DOI 10.5281/zenodo.7794703. URL https://doi.org/10.5281/zenodo.7794703.

[16] Robertson, A., Jonkman, J., Vorpahl, F., Popko, J., W.and Qvist, Frøyd, Lars, Chen, X., Azcona, J., Uzunoglu, Emre, Guedes Soares, Carlos, Luan, Chenyu, Yutong, H., Pengcheng, Feng, Yde, Anders, Larsen, Torben, Nichols, James, Builds, R., Lei, L., Nygard, T. and Guerinel, Matthieu. "Phase II Results Regarding a Floating Semisubmersible Wind System." *Offshore Code Comparison Collaboration Continuation Within IEA Wind Task 30*. 2014. DOI 10.13140/2.1.2822.9121. URL https://www.nrel.gov/docs/fy14osti/61154.pdf.

[17] Brevik, S. and Kovesdi, B. "Modifications to DNV Mooring Code (POSMOOR) and Their Consequences." *Proceedings of the 17th International Conference on Offshore Mechanics and Arctic Engineering*, Vol. 1: pp. 169–177. 1998. American Society of Mechanical Engineers.

[18] Festa, O., Gourvenec, S. and Sobey, A. "Proxy model for the design of extensible floating offshore wind turbine mooring systems." *In Proc. 32nd International Symposium on Ocean and Polar Engineering (ISOPE), June 5 – 10 (virtual)*. 2022. URL https://eprints.soton.ac.uk/457473/.

[19] Davidson, J. and Ringwood, J. "Mathematical Modelling of Mooring Systems for Wave Energy Converters—A Review." *Energies* Vol. 10 No. 5. DOI 10.3390/en10050666. URL https://www.mdpi.com/1996-1073/10/5/666.

[20] Festa, O., Gourvenec, S. and Sobey, A. "Comparative parametric analysis of extensible catenary moorings for floating offshore wind turbines." *2021 CORE - Glasgow*. 2021. URL https://eprints.soton.ac.uk/457472/.

[21] Kwan, C.T. and Bruen, F.J. "Mooring Line Dynamics: Comparison of Time Domain, Frequency Domain, and Quasi-Static Analyses." *OTC Offshore Technology Conference*. 1991. DOI 10.4043/6657-MS. URL https://onepetro.org/OTCONF/proceedings-pdf/91OTC/All-91OTC/OTC-6657-MS/1997242/otc-6657-ms.pdf. OTC-6657-MS.

A.3 Proxy model for the design of extensible floating offshore wind turbine mooring systems

Proxy model for the design of extensible floating offshore wind turbine mooring systems

Oscar Festa[1], Susan Gourvenec[1] and Adam Sobey[2]
[1]Department of Civil, Maritime and Environmental Engineering, University of Southampton, Southampton, UK
[2]Marine and Maritime Group, Data-Centric Engineering, The Alan Turing Institute, The British Library, London, NW1 2DB

ABSTRACT

Mooring systems for floating offshore wind turbines (FOWTs) are designed to resist extreme loads, employing heavy mooring lines and large anchors which contribute to high capital expenditure. Incorporating extensible sections to mooring lines reduces peak dynamic loading, enabling the use of smaller, easier to install and therefore cheaper anchors. Finite element (F.E.) modelling of extensible mooring lines is time consuming and is not well suited to optimization since all the mooring line variables must be defined a priori. This paper presents a quick and versatile approach to exploring the effect of linear and non-linear stiffness extensible moorings on the FOWT system, which can be used for automated optimization of one variable for given constraints in the others. The proxy model was based on data from fully-coupled F.E. analyses of the DeepCwind semi-submersible FOWT. The proxy model is formed of numerical relationships between environmental loads, fairlead tension, platform surge, and extensible section design parameters (length *L*, axial stiffness *EA*). From these relationships, the model can determine optimal extensible section parameters which minimise fairlead tension for a given surge criterion, or minimise surge for a given maximum tension criterion. When applied to an example design scenario, results from the proxy model show good agreement with F.E. results, with a maximum error of 1.2% for linear stiffness results and 4.3% for non-linear stiffness section properties.

KEY WORDS: Floating offshore wind turbines (FOWT); Extensible moorings; FEA; Proxy modelling; System optimisation.

INTRODUCTION

Significance of FOWT mooring design

To maintain a 1.5°C global warming pathway, the International Energy Agency (IEA) is calling for a sevenfold increase in global offshore wind capacity by 2030 (GWEC, 2021). Up to 80% of worldwide offshore wind resources are located in water depths greater than 60 m (Burges Salmon, 2021) where traditional fixed-bottom wind turbines are not economically viable. In these deeper waters, offshore wind turbines must be deployed on floating platforms, which are connected to the seabed via mooring lines and anchors to maintain their position. Various fixed and floating offshore wind concepts are shown in Fig. 1.

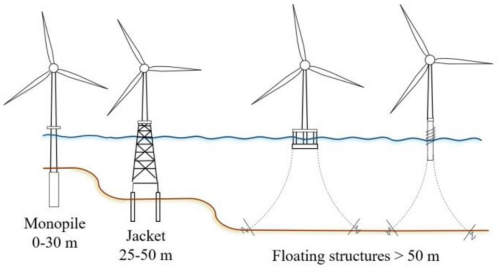

Fig. 1 Fixed and floating offshore wind concepts

Mooring system design involves striking a balance between stiffness and compliance. Stiff mooring systems provide high restoring forces to the platform, while compliant designs reduce loads transferred to the mooring line and anchor at the cost of additional platform motions. Current FOWT mooring designs are derived from oil and gas practices and typically employ heavy, inextensible chain catenary lines (QuestFWE, 2020) which provide high stiffness to keep the platform on station in extreme conditions. FOWT station-keeping requirements are often more lenient than those of oil and gas installations (Dumont, 2016), meaning that more compliant designs could be employed to avoid over-designed mooring lines and anchors. Avoiding over-design is important from an economical perspective, as mooring and anchoring systems can account for over 15% of overall FOWT costs (Reuters, 2021).

This paper presents a method of tailoring mooring designs to project-specific station-keeping requirements, ensuring an optimal level of compliance in the mooring system. This will reduce the loads transferred to the anchor, enabling smaller anchoring systems that are more cost-effective. Such reductions in costs are necessary to improve the scalability of FOWTs, in turn facilitating commercialization and allowing floating wind energy to play a key role in meeting net zero targets.

Review of current extensible mooring systems

Compliance in catenary moorings can be geometric and/or elastic. Geometric compliance comes from the change in shape of the mooring profile, whereas elastic compliance comes from change in length (i.e. extension) of the line. There are various approaches to increasing the extensibility of mooring systems. Low-modulus synthetics such as nylon and polyester have been used in deep water oil and gas moorings for decades, although to reduce weight rather than for extensibility. More recently, elastic tethers, sections of highly extensible line that usually employ elastomeric materials, have been developed for mooring load reduction in marine renewable energy applications. These include the Exeter Tether, Tfi Seaspring, and Exeter Itelligent Mooring System (IMS), all of which can provide much higher levels of compliance than typical polymer ropes without compromising breaking strength (Parish, 2016; Luxmoore et al., 2016; Thies et al., 2014). Parametric analyses have been performed on tether dimensions and stiffness to compare load reduction performance for various load cases and applications for the Tfi Seaspring (McEvoy, 2019) and the IMS (Harold, 2018). Results from commercial software simulations in these studies show that the extensible tethers can offer peak mooring load reductions of up to 50% compared to full-chain (inextensible) lines. However, the reduction in mooring load comes at the cost of increased platform displacements, notably surge, and this trade-off has not yet been comprehensively explored. Maximum surge is an important design constraint for FOWT mooring systems, and is typically dictated by the range of the dynamic power cables connected to the FOWT (Corewind, 2020).

Motivation for proxy model-based design

The aim of the study presented in this paper was to derive numerical relationships between platform displacements, fairlead tension, environmental loads, and extensible section parameters (Fig. 2), in the form of a proxy model based on a data set generated from F.E. analyses. The proxy model can estimate fairlead tension reduction (T_{red}) and platform surge increase (S_{inc}) compared to an inextensible line, for given extensible section lengths (L) and stiffness values (EA), and for various combinations of wave height (H_s) and wind speed (U) in parked turbine states (i.e. extreme conditions). The proxy model is derived for both linear and non-linear extensible section stiffness values.

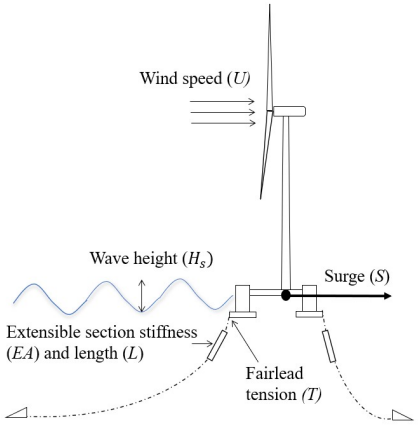

Fig. 2 Key system variables considered in analyses

The derived numerical relationships between key system variables can then be used to improve the design process of extensible mooring systems. In the public domain, no existing research has documented an approach to designing extensible moorings to fit project-specific displacement constraints. Typical mooring design approaches would involve running commercial software simulations iteratively until output parameters such as surge and tension meet the design requirements. Design input parameters are restricted to environmental loads and mooring line parameters. The aim of the numerical proxy model is to allow the project-specific constraints such as surge and fairlead tension to be used as input parameters, with the extensible mooring line parameters EA and L to meet the design requirements as outputs. This is a more computationally efficient approach and directly determines the design parameters which give the closest fit to project constraints.

Structure of paper

The first part of this paper describes the F.E. model and Flexcom analysis routine used to develop the database, along with the numerical approach taken to derive the proxy model from the database. The proxy model is presented in the next section as a selection of surface fits representing the relationships between variables. The model is then applied to a specific load case scenario and maximum platform surge constraint from the Hywind demonstrator, to illustrate use of the proxy model. Results are discussed, comparing extensible section performance for both linear and non-linear stiffness.

METHOD

Floating Offshore Wind Turbine F.E. model

The FOWT model used in this study is based on the DeepCwind semi-submersible floating platform and 5-MW reference turbine, from the Offshore Code Collaboration project (OC4), led by the National Renewable Energy Laboratory (NREL). The full platform and mooring geometry are described in detail in the OC4 publication (Robertson, 2014), along with the basic parameters of the wind turbine system. A top-down view of the catenary arrangement is shown in Fig. 3. The model was previously used to verify Flexcom against other commercial and open-source FOWT simulation codes that participated in the OC4 initiative, and the results of the verification showed good alignment with the other software for the load cases considered (Festa et al., 2021).

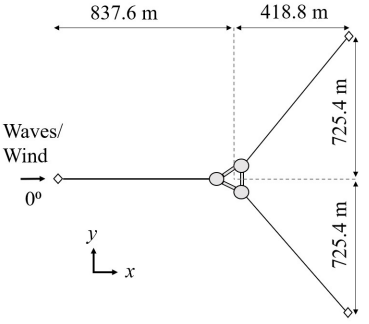

Fig. 3 Top-down view of the OC4 mooring system. The surge motion of the platform is defined as horizontal displacement along the x-axis.

For the analyses in this study, all platform and turbine geometry were left unchanged from the OC4 DeepCWind model. The focus was on the mooring lines, which were partly modified to include extensible sections. Mooring lines are modelled in Flexcom as a succession of beam elements. To create extensible sections, elements in these sections were assigned a reduced axial stiffness, while other element properties such as density and diameter were kept constant. A side-on view of a catenary mooring system in static equilibrium is shown in Fig. 4, with and without extensible sections. Water depth, anchor to fairlead distance and unstretched line length are unchanged, although the shape of the catenary is more slack due to the stretch of the extensible section under the weight of the chain. This means a lower restoring force on the floating platform, due to less weight of suspended chain.

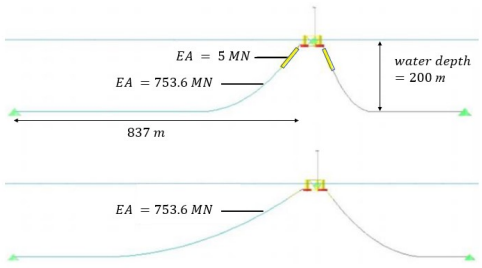

Fig. 4 Side-on view of the mooring system, including an extensible section (top) and a full-chain catenary line (bottom)

When defined by a single value of stiffness EA, the extensible section adopts a linear stiffness, with a force-strain curve defined by a straight line through the origin and the single point EA. In practice, few compliant materials used in offshore moorings have a fully linear stiffness profile. Existing elastic tether technologies are specifically designed with a non-linear stiffness to improve their performance. For instance, the Tfi Seaspring combines thermoplastic and elastomeric elements to obtain a 'stepped' stiffness response. This ensures a high initial stiffness to limit extension of the spring under static loading, and a reduced stiffness in the operational strain range to effectively reduce variable wind and wave loads. For the parametric analyses in this study, both linear and non-linear stiffness extensible sections are considered to determine the importance of this non-linearity in the design phase.

Variables for parametric F.E. analyses

The parametric analyses were run on Flexcom with various combinations of extensible section parameters and load cases, and the maximum platform surge and fairlead tension were recorded for each simulation. The analyses were fully-coupled dynamic simulations in the time-domain, thus the fairlead tension combines both static and dynamic components, and the surge accounts for wind loads as well as wave induced drift forces.

A total of 42 combinations of EA and L were considered, with 9 different combinations of wind speed (U) and wave height (H_s), representing a total of 378 simulations. Wave period (T_p) is scaled to the wave height with a linear relationship rather than considered as an independent variable to improve efficiency of the proxy model by minimizing the number of variables. In practice, wave height and wave period are frequently correlated (Mackay, 2012). The load cases (LC) are numbered from 1 to 9 for each combination of wind speed and wave height, with LC1 being the least severe ($U = 25mps$, $H_s = 6m$, $T_p = 10m$) and LC9 the most severe ($U = 45mps$, $H_s = 14m$, $T_p = 13m$). All load cases considered in this study are extreme cases, with wind speeds above the turbine cut-off point (i.e. $U > 25mps$) meaning the turbine is always in the parked condition ($rotorspeed = 0$) with feathered blades. The full design space of extensible section variables and load case parameters is shown in Table 1.

Table 1 Variables considered in parametric analyses

	Parameterised variables	Values
Extensible section	L (m)	10, 20, 30, 40, 50, 60
	EA (MN)	1.5, 2, 3, 4.5, 6, 7.5, 9
Load cases	U (mps)	25, 35, 45
	[H_s (m); T_p (s)]	[6; 10], [10; 11.5], [14; 13]

The same set of parametric analyses was repeated analogously for the non-linear extensible sections (i.e. an additional 378 simulations). The stiffness values described in Table 1 were used to define both the linear and non-linear stiffness curves. For non-linear stiffness, these values represent the axial force at 100% strain. The shape of the non-linear stiffness curves is based on stiffness of the Tfi Seaspring [11], and is maintained for all the different values of target stiffness. The set of curves used in the parametric analyses is shown in Fig. 5.

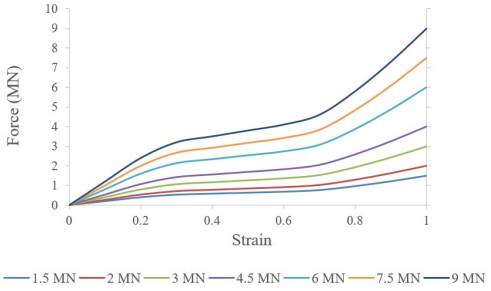

Fig. 5 Non-linear stiffness curves considered in parametric analyses, with force at 100% strain equal to that of the linear stiffness curves

Proxy modelling workflow

The proxy model presented in this paper belongs to the category of reduced-order models (ROMs), a large family of numerical methods aiming to reduce the complexity of numerical simulations (Schilders, 2008). In particular, proxy models are characterised by a combination of mathematically defined functions that approximate the response of the full-scale simulation model output for selected input parameters (Deeney, 2010). In this case, the proxy model combines 5^{th} order polynomial regression and cubic spline modelling methods, which can accurately capture non-linear relationships. However, these methods cannot accurately be used for extrapolation, notably due to the piecewise nature of cubic spline interpolation (Hahn, 1977), meaning that model inputs are limited to the bounds of the F.E. data set.

For each wave height and wind speed combination n, a polynomial fit was carried out for surge (S_n) and tension (T_n). These functions determine the maximum surge increase and tension reduction respectively from input variables of the extensible section properties, stiffness (EA)

and length (L). For the proxy model to cover all relevant combinations of wave height and wind speed, a surface fit is then completed for each polynomial coefficient of the set of polynomials S_n and T_n. Thus, each polynomial coefficient can be determined for any load case input H_s and U. The polynomials used were of degree 5 in EA and 3 in L, leading to a total of 18 polynomial coefficients to be fitted for both S_n and T_n. These fits were achieved using cubic interpolation rather than the polynomial surface fits used for EA and L. The combination of polynomial and cubic interpolated fits results in two overall functions which determine the increase in surge and reduction in fairlead tension from inputs EA, L, H_s, U. This process is depicted in the flowchart in Fig. 6.

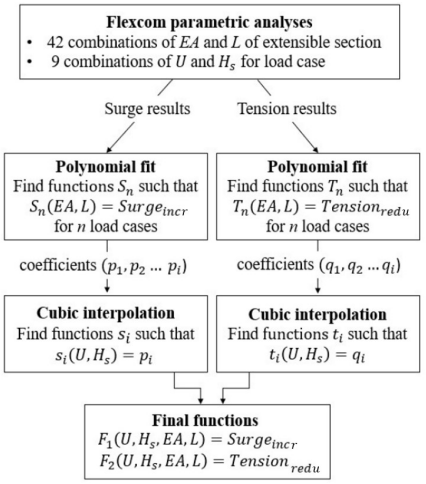

Fig. 6 Process to determine surge and tension functions

PROXY MODEL

Overview

Outcomes of the proxy model, which consists of the polynomial and cubic interpolation fits based on the F.E. data set as described in the methodology, are presented in this section. For brevity, polynomial fits are shown only for LC1 which is the least severe ($U = 25mps$; $H_s = 6m$) and LC9 which is the most severe ($U = 45mps$; $H_s = 14m$). The cubic interpolated polynomial coefficient fits are then shown for the first coefficient (i.e. the most significant). This modelling process is repeated for both linear and non-linear EA, with results split into two analogous subsections. The resulting trends between variables are only briefly discussed, as a more in-depth commentary on the inter-relationships between variables is presented in Festa et al. (2021). The intention here is to demonstrate the suitability of the proxy model to capture those relationships.

Linear stiffness proxy model

Effect of extensible section length and stiffness on platform surge

The first set of polynomials estimate the increase in platform surge compared to an inextensible line for any combination of extensible section stiffness and length in the design space. The surface fits for the linear proxy model are shown for LC1 and LC9 in Fig. 7, alongside the original F.E. results (points).

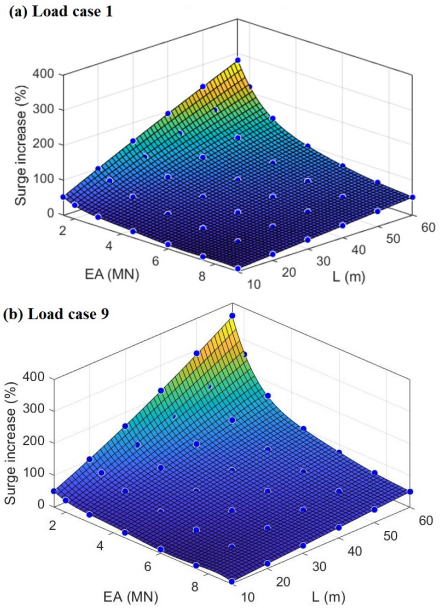

Fig. 7 Polynomial surface fits of platform surge increase for (a) least severe and (b) most severe load cases

As expected, higher section length and lower stiffness lead to a significant increase in platform surge compared to an inextensible mooring line. Increases in section length have a roughly linear relationship with surge increase, which is not the case for increases in stiffness. This explains the lower order polynomial being sufficient to fit the L variable, whereas the EA variable requires higher order terms. The overall profile for both load cases is similar, with the most severe load case (LC9) leading to higher increases in surge compared to the least severe load case (LC1).

Effect of extensible section length and stiffness on fairlead tension

The polynomial surface plots for the reduction in fairlead tension for any combination of EA and L in the design space are shown in Fig. 8, alongside the original F.E. results (points). In contrast to the surge, there is a notable difference in surface shape between the two load cases for tension response. The stiffer and shorter extensible sections provide limited compliance under lower loads, but can be elongated by higher values of wind and wave, in turn providing more tension reduction.

Assessment of polynomial fitting

Overall, the polynomials provide a close fit for both tension increase and surge reduction to the F.E. results, with consistently low root mean square error (RMSE) values across all load cases (Table 2). In theory, a lower degree polynomial would provide sufficient goodness of fit for these linear stiffness plots, but the higher order polynomial was used as it did not significantly increase computational time, and allowed the use of the same proxy model framework as for the non-linear stiffness.

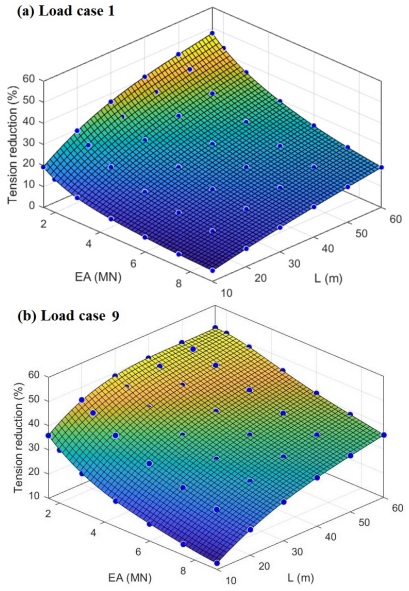

Fig. 8 Polynomial surface fits of fairlead tension reduction for (a) least severe and (b) most severe load cases

Table 2 RMSE of tension and surge polynomial fits for linear *EA*

Load case	1	2	3	4	5	6	7	8	9
Surge inc. fit RMSE	1.10	1.26	1.36	1.30	1.55	1.82	1.88	2.63	2.47
Tension red. fit RMSE	0.08	0.07	0.07	0.11	0.11	0.11	0.18	0.19	0.18

Effect of wind speed and wave height on polynomial coefficients

The coefficients of each polynomial are then extrapolated across the 9 different combinations of load case parameters H_s and U using a cubic interpolated fit. The surface fits are shown for the first of the 18 coefficients for both surge and tension in Fig. 9 (a) and (b) respectively. Fig.9 (a) shows that wind speed is the main factor affecting surge, and Fig.9 (b) shows that tension reduction is primarily influenced by wave height.

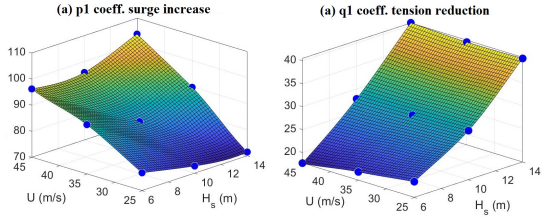

Fig. 9 Cubic interpolated fit of 1st polynomial coeff. for (a) surge increase and (b) tension reduction for linear stiffness

Non-Linear stiffness proxy model

Effect of extensible section length and stiffness on platform surge

The same parametric analysis and curve fitting procedure was then repeated, replacing the single values of *EA* by the non-linear force-strain curves shown in Fig. 5. Polynomial fits of platform surge increase are presented in Fig. 10 for the least and most extreme load cases (LC1 and LC9). These results are similar to those of the linear stiffness section for LC9, but display a greater non-linearity between variables for LC1. This is due to the extreme load case (LC9) causing the extensible section to operate in strain ranges above 70%, where the stiffness curves shown in Fig. 5 display a more linear behaviour.

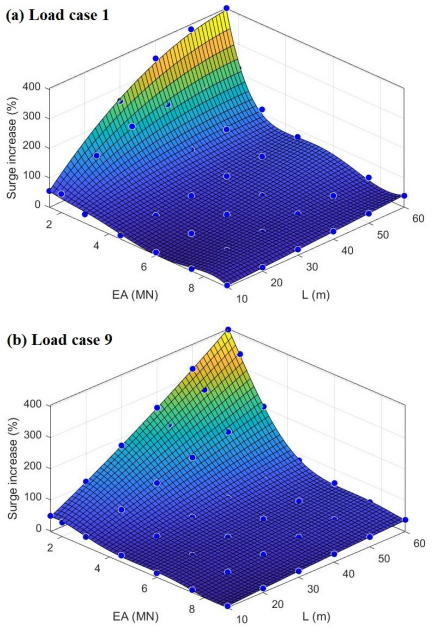

Fig. 10 Polynomial surface fits of platform surge increase for (a) least severe and (b) most severe load cases

Effect of extensible section length and stiffness on fairlead tension

Further non-linear behaviour is apparent for the tension reduction surface fits (Fig. 11), notably for the most extreme load case (LC9). This is of particular interest, as it means improved trade-offs between tension reduction and surge increase emerge for specific combinations of *EA* and *L*. For instance, Fig. 11 (b) shows an increase in fairlead tension when reducing the target stiffness from 4 MN to 2 MN, which seems counter-intuitive. This is due to the lower stiffness extensible section undergoing higher strains and therefore acting in the high stiffness range and not providing as much elongation under the transient wave loads. Such an observation reinforces the value of the proxy modelling and holistic design approach, the optimal and sub-optimal configurations of non-linear *EA* and *L* would be difficult to determine from simple iterative trial-and-error F.E simulations.

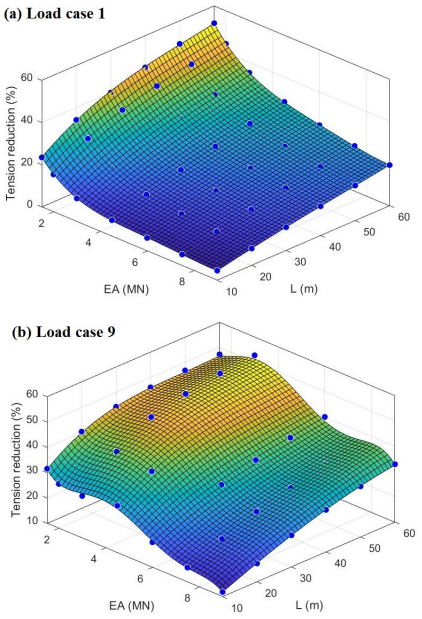

Fig. 11 Polynomial surface fits of fairlead tension reduction for (a) least severe and (b) most severe load cases

Assessment of polynomial fitting

As expected, the relationships between variables for non-linear stiffness are less consistent over the design space compared to the linear stiffness surface plots. While the linear stiffness means constant EA regardless of loads, the stiffness of the non-linear section is dictated by the strain in operation. The operating strain range of the extensible section is affected by the environmental loads, notably the wind thrust, which leads to an initial 'background' elongation, but also by the initial length of the extensible section where a longer section leads to a lower value of strain under the same load. The variation in operating strain range across each configuration results in different sensitivities to wind and wave loads, leading to highly non-linear system behaviour which is complex to predict. As such, the polynomials do not achieve the same goodness of fit as with linear stiffness, despite the high number of coefficients (Table 3).

Table 3 RMSE of tension and surge fit for non-linear stiffness

Load case	1	2	3	4	5	6	7	8	9
Surge inc. fit RMSE	12.62	9.93	10.02	8.74	9.54	7.59	8.14	9.16	3.26
Tension red. fit RMSE	0.39	0.55	0.63	0.79	1.03	1.09	1.28	1.45	1.26

Effect of wind speed and wave height on polynomial coefficients

The first polynomial coefficients for surge increase and tension reduction polynomials are shown in Fig.12 (a) and (b) respectively, for comparison with those of linear stiffness shown in Fig. 9. Whereas the linear stiffness coefficients could have been effectively modelled with a polynomial, these plots justify the use of a cubic interpolation which captures the non-linear variations effectively.

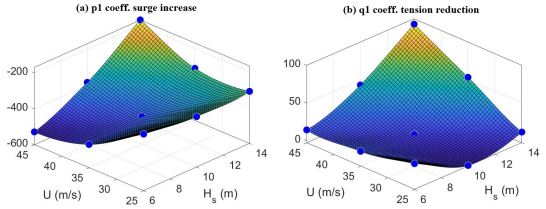

Fig. 12 Cubic interpolated fit of 1st polynomial coeff. for (a) surge increase and (b) tension reduction for non-linear stiffness

DESIGN APPLICATION

Process

Application of the proxy model to a given load case and specific set of design requirements is presented in this section, showing how the method can be used effectively as part of the extensible mooring design process, removing the need for iterative 'trial-and-error' F.E. simluations. Fig. 13 outlines the process for applying the proxy model to a particular design scenario .

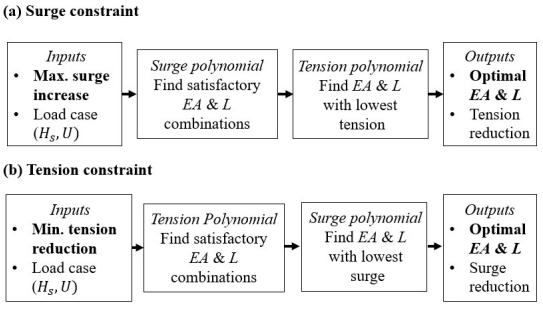

Fig. 13 Inverted proxy model-based design approach for (a) surge increase constraint and (b) tension reduction requirement

The first set of inputs to the proxy model are the wind speed and significant wave height parameters U and H_s. From these inputs, the polynomial coefficients can be interpolated to obtain the full surface plots of tension reduction and surge increase for EA vs L. After setting the maximum surge increase constraint S_{max}, all pairs of EA and L which exactly satisfy the surge constraint are determined by finding the roots of the following expression f:

$$f(EA, L) = S_{U,H_s}(EA, L) - S_{max} \tag{1}$$

where S_{U,H_s} is the surge increase polynomial based on the specific load case parameters U and H_s. The resulting combinations of EA and L which satisfy the surge constraint are then used as inputs to the tension reduction polynomial, to determine whether some configurations offer more tension reduction than others. This process can be completed with the minimum required tension reduction T_{min} as an input parameter rather than surge constraint, i.e. finding which design parameters offer the desired tension reduction, whilst minimising surge increase. This involves

finding the roots of the following expression g, where T_{U,H_s} is the tension reduction polynomial:

$$g(EA, L) = T_{U,H_s}(EA, L) - T_{min} \tag{2}$$

Field example

The design load for the case study is taken from the 50-year storm conditions at the Hywind demo site (Onstad et al., 2016), with $U = 30.5mps$ and $H_s = 13.3m$. The maximum surge constraint was arbitrarily taken as $S_{max} = 60\%$ increase compared to an inextensible line, which equals a total surge displacement of 20 metres. The resulting multivariate plots derived by the proxy model for the specific load case are shown in Fig. 14, highlighting the combinations of design parameters which satisfy the surge constraint.

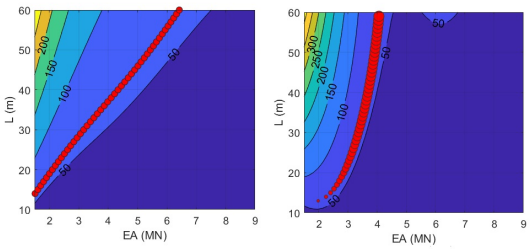

Min. tension reduction = 37%
Max. tension reduction = 38%

Min. tension reduction = 33%
Max. tension reduction = 45%

Fig. 14 Estimated surge increase contour plot for the specific load case based on the proxy model; for linear stiffness (left) and non-linear stuffness (right). Each EA and L pair that satisfies the maximum surge constraint is shown with a red marker, with bigger markers signifying a higher reduction in tension.

The combinations of design parameters that satisfy the surge constraint for linear EA are all approximately equivalent for tension reduction, i.e. all configurations offer a similar trade-off, indicated by all the red markers having the same size (Fig. 14). This is not the case for the non-linear EA, with some combinations of design parameters proving more viable than others, shown by some red markers being bigger than others. For the same amount of surge, the shorter non-linear extensible sections operate in a higher strain region on the non-linear force-strain curve than the longer sections (above 70%), thus making them stiffer (Fig. 5, due to thermoplastic element) and less effective at reducing dynamic loads from the waves. The most and least effective configurations are shown in Tables 4 and 5, along with the actual results from bespoke F.E. simulations to compare accuracy. The full F.E. dataset is publicly available online (Festa, 2022).

For the same load conditions, the proxy model can also be used to find design parameters which satisfy a tension reduction constraint. For this example, a required tension reduction of 30% is specified. The proxy model determines which configurations of EA and L meet this requirement for the given load conditions design, and which of these configurations is most effective for minimising surge. The configurations that meet the prescribed constraints are shown in Fig. 15, Table 4 and Table 5, along with the actual results from F.E. to compare accuracy. Significant disparities in surge increase can be noted between the different configurations for the non-linear stiffness, with the most effective configuration reducing surge by over 30% for the same value of tension reduction.

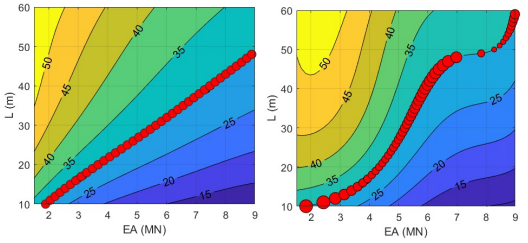

Max. surge increase = 35%
Min. surge increase = 32%

Max. surge increase = 45%
Min. surge increase = 17%

Fig. 15 Estimated tension reduction contour plot for the specific load case based on the proxy model; for linear stiffness (left) and non-linear stiffness (right). Each EA and L pair satisfying the min. tension reduction is shown with a red marker, with bigger markers signifying a higher surge.

The linear proxy model results show very good agreement with the F.E. results (Table 4), especially for tension reduction prediction. This follows the RMSE trends displayed in Tables 2 and 3, with tension results on average more accurate than surge results by a factor of 10. Non-linear results are slightly less accurate (Table 5), with the proxy model underestimating surge increase compared to the F.E. results, by approximately 4%. The design application of the proxy model clearly demonstrates the value of the approach in finding configurations with improved trade-offs between surge increase and tension reduction for the given design constraint. Another key strength of the proxy model lies in the ability to reverse the design question, and predict required extensible mooring line properties, EA and L, to achieve the prescribed design constraint on either platform surge or fairlead tension reduction.

Table 4 Summary of linear stiffness proxy model results for load case application

Design constraint	Optimal config. based on proxy	Comparison with F.E results
Surge increase = 60 %	Tension reduction = 38.47% EA = 2.73 MN, L = 26 m	Surge increase = 61.18% Tension reduction = 38.27%
Tension reduction = 30 %	Surge increase = 32.08% EA = 6.57 MN, L = 36 m	Surge increase = 33.22% Tension reduction = 30.12%

Table 5 Summary of non-linear stiffness proxy model results for load case application

Design constraint	Optimal config. based on proxy	Comparison with F.E results
Surge increase = 60 %	Tension reduction = 44.91% EA = 4.06 MN, L = 57 m	Surge increase = 64.11% Tension reduction = 46.13%
Tension reduction = 30 %	Surge increase = 17.48% EA = 8.47 MN, L = 52 m	Surge increase = 21.79% Tension reduction =33.04%

Future work will involve replicating the F.E. dataset and proxy model for composite and taut mooring lines, in view of developing a fully-generalisable design framework.

CONCLUSION

This paper presents an approach to determine optimal extensible tether parameters *EA* and *L* to fit project-specific surge or tension requirements, for both linear and non-linear tether stiffness profiles. This was achieved using a proxy model based on a data set created with results from a commercial F.E. software.

The main take-away points from this study are:

- Polynomials proved adequate to describe relationships between mooring loads, platform surge and extensible section design parameters *EA* and *L*. The goodness of fit was better for linear stiffness than for non-linear stiffness extensible sections, as the inter-variable relationships were more consistent.
- The simple proxy model not only enables computationally efficient modelling of extensible moorings, it also allows design constraints, i.e fairlead tension and platform surge, to be used as inputs in the design problem, returning the required extensible section parameters. This is a more efficient workflow than direct F.E. analyses where extensible section parameters are prescribed as input, with analyses returning fairlead tension and surge. This approach simplifies the task of finding a bespoke extensible section design to fit station-keeping criteria.
- A holistic design approach, as demonstrated here, is especially beneficial for non-linear stiffness extensible tethers. Different combinations of *EA* and *L* that satisfy the prescribed design requirement can vary significantly in terms of their impact on either platform surge or fairlead tension. The proxy model can help to determine which combinations of non-linear stiffness curves and tether length maximise the trade-off between surge increase and tension reduction for any given load case.

ACKNOWLEDGMENTS

This work forms part of the activities of the Royal Academy of Engineering Chair in Emerging Technologies Centre of Excellence for Intelligent & Resilient Ocean Engineering (www.southampton.ac.uk/iroe), based at the University of Southampton. Susan Gourvenec is supported by the Royal Academy of Engineering under the Chairs in Emerging Technologies scheme. Adam Sobey is supported by the Lloyd's Register Foundation.

REFERENCES

Burges Salmon (2021). "Floating Wind – Challenges and Opportunities for a Buoyant Technology", *Burges Salmon - News & Insight*, URL: https://www.burges-salmon.com/news-and-insight/legal-updates/energy-power-utilities/floating-wind-challenges-and-opportunities-for-a-buoyant-technology#_ftn1

Corewind (2020). "Review of the state of the art of dynamic cable system design", *Corewind D3.1* , URL: https://corewind.eu/wp-content/uploads/files/publications/COREWIND-D3.1-Review-of-the-state-of-the-art-of-dynamic-cable-system-design.pdf

Denney, D (2010). "Pros and Cons of Applying a Proxy Model as a Substitute for Full Reservoir Simulations", *Journal of Petroleum Technology*, 62.07, p. 41:42.

Dumont, M (2016). "Critical Issues in the Design of FOWT Mooring Systems when Comparing to Oil & Gas Industry Standards", *SNAME 21st Offshore Symposium*, Houston, SNAME-TOS-2016-008.

Festa, O, Gourvenec, S, Sobey, A (2021). "Comparative parametric analysis of extensible catenary moorings for floating offshore wind turbines", *CORE 2021*, Glasgow

Festa, O (2022). "Flexcom extensible tether parametric analysis data", doi = "10.6084/m9.figshare.19403513.v1"

GWEC (2021). "Global wind report 2021", *Global Wind Energy Council*, URL: https://gwec.net/wp-content/uploads/2021/03/GWEC-Global-Wind-Report-2021.pdf

Hahn, G (1977). "The Hazards of Extrapolation in Regression Analysis", *Journal of Quality Technology*, 9.04, p. 159:165

Harrold, M, Thies, P, Newsham, D (2018). "Dynamic load reduction and station keeping mooring system for floating offshore wind", *ASME 2018 1st International Offshore Wind Technical Conference*, San Francisco, V001T01A018

Luxmoore, J, Grey, S, Newsham, D, and Johanning, L (2016). "Analytical performance analytical performance assessment of a novel active mooring system for load reduction in marine energy converters", *Ocean Engineering*, p. 124:215–225

Mackay, E (2012). "Resource Assessment for Wave Energy", *Comprehensive Renewable Energy*, 8.03, 11-77

McEvoy, P, Johnston, E (2019). "Polymer Mooring Component for Offshore Renewable Energy", *OTC Offshore Technology Conference*, Houston, Vol.1 Session 33.

Onstad, A, Stokke, M, Saetran, L (2016). "Site Assessment of the Floating Wind Turbine Hywind Demo", *Energy Procedia*, 94, 409 – 416.

Parish, D (2015). "A novel mooring tether for highly dynamic offshore applications ", *PhD Thesis*, URL: https://ore.exeter.ac.uk/repository/handle/10871/21337

Quest FWE (2020). "The definitive guide to floating wind energy concepts.", URL: https://questfwe.com/definitive-guide-to-floating-wind-concepts/

Reuters Events (2021). "Shared anchors slice cost of floating wind parts", URL: reutersevents.com/renewables/wind/shared-anchors-slice-cost-floating-wind-parts-vessels

Robertson, A, Jonkman, J (2014). "Offshore code comparison collaboration continuation within IEA wind task 30: Phase ii results regarding a floating semisubmersible wind system.", *ASME 2014 33rd International Conference on Ocean, Offshore and Arctic Engineering.*, San Francisco, V09BT09A012

Schilders, W (2008). "Introduction to Model Order Reduction", *Model Order Reduction: Theory, Research Aspects and Applications*, Vol. 13, p. 3-32

Thies, P, Johanning, L, and McEvoy, P (2014). "A novel mooring tether for peak load mitigation: Initial performance and service simulation testing", *International Journal of Marine Energy*, Vol. 7

A.4 Design benefits for plate anchors for floating offshore wind through coupling floater, mooring and geotechnical responses

Design benefits for plate anchors for floating offshore wind through coupling floater, mooring and geotechnical responses

K.A. Kwa, O. Festa, D.J White, S. Gourvenec,
University of Southampton, Southampton, UK

A. Sobey
The Alan Turing Institute, British Library, UK
University of Southampton, Southampton, UK

ABSTRACT: This study presents analysis of a floating offshore wind system to illustrate methodologies for reducing the mooring loads transmitted to the anchor and the required anchor size. These design efficiencies support acceleration of the development of floating offshore wind, to help meet the growth required for 2050 net zero targets. The anchor loading and size reductions are achieved by combining techniques that i) reduce the anchor loads by considering load reduction devices (LRD) in the mooring line configuration, and ii) mobilise additional seabed resistance by considering beneficial seabed effects due to inertia and changing strength. This study demonstrates the benefits of combining these effects through an integrated floater-mooring and anchor-seabed analysis approach. The method is applied to an example whole-life application spanning the operating life of a floating offshore wind (FOW) system. This analysis indicates a potential 50% reduction in the required anchor size for the same system reliability.

1 **Introduction**

1.1 *The need for floating offshore wind (FOW)*

To meet net zero targets by 2050, decarbonisation of global energy supply will require a rapid expansion of offshore wind. The global offshore wind energy compact proposes a global ambition of 2000 GW by 2050 to meet the aims of the Paris Agreement (GWEC, 2022). Much of this growth will be provided by floating offshore wind (FOW) technology, which can be installed further from shore, where there is more available ocean space, high energy wind resources are located and conventional fixed offshore wind is not practical. Among the challenges of upscaling the production and installation of FOW systems is the need for efficient and reliable mooring and anchoring systems (Cerfontaine et al., 2023).

1.2 *Opportunities for more efficient mooring and anchor systems*

FOW infrastructure is subjected to a wide range of actions from metocean (e.g. wind and wave) and operational conditions, which are transmitted by mooring lines to the anchors that are typically embedded in the seabed. Taut mooring arrangements are attractive for FOW turbines as they require less length and lighter synthetic mooring line than traditional heavy chain catenary mooring arrangements. Taut moorings also transmit significantly higher mean and peak uplift tensions to the anchor compared to catenary moorings, where much of the mooring load is transmitted laterally and much of the load is taken by the weight of the chain. Further improvements to taut mooring configurations are currently being explored to reduce peak mooring uplift loads on the anchor through the development of load reduction devices (LRD) that achieve a non-linear stiffness profile with an initial compliant phase for operating conditions and a stiffer response at higher extensions to deal with extreme events (Gordelier et al., 2015; Dublin Offshore, 2021; Pillai et al., 2022; Lozon et al., 2022).

The seabed surrounding an embedded anchor also has potential to offer extra anchor capacity enhancements depending on the loads that are transmitted via the mooring lines to the anchoring system and surrounding seabed. For long-term cyclic loads that vary due to sea state and season during the whole-life or lifetime of the facility (e.g. 20 years), seabed strength, s_u, and therefore anchor capacity can evolve with time due to shearing and consolidation of the soil during sustained and variable low amplitude cyclic uplift loads (Blake et al., 2011; Cocjin et al., 2014; Smith & White, 2014; O'Loughlin et al., 2020; Zhou et al. 2020;; Gourvenec, 2020; Da Silva et al., 2021; Laham et al., 2021, Kwa et al., 2023a, c) . This can result in increases in the long-term embedded plate anchor capacity, Q_s, as defined below

$$Q_s = f(\{s_u\}) = N_c s_u A \quad (1)$$

where N_c is a bearing capacity factor (e.g. 13.11 for a rough circular plate anchor (Martin & Randolph 2001)) and A is the cross sectional area the anchor.

The strength $\{s_u\}$ can vary between the initial value, s_{u0}, the cyclically remoulded minimum s_{ur} and hardened maximum s_{uh} as a result of remolding and consolidation as defined in White et al. (2021). However, these long-term or whole-life increases in capacity are not typically considered in conventional geotechnical foundation capacity analysis. Under dynamic, high-amplitude loads, e.g. during a storm event, soil viscous rate effects can have a positive effect on the shear strength of the soil, depending on the strain rate as defined, for example, by eqn 2. (Randolph 2004).

$$s_u = s_{u0}\, max\left[1, 1 + \mu'\, sinh^{-1}\frac{\dot{\gamma}}{\dot{\gamma}_{ref}}\right] \quad (2)$$

where s_{u0} is the undrained soil shear strength defined at a slow or static strain rate as typically used in laboratory testing to evaluate s_u, μ' is a rate parameter, typically found to be ~0.1 (i.e. 10% extra strength per increment of strain), $\dot{\gamma}$ is a representative strain rate in the failing soil and $\dot{\gamma}_{ref}$ is a reference strain rate associated with the selected value of s_{u0}.

Wave-structure interaction can cause rapid, high amplitude snatch loads, which can have time periods ~10 times shorter than the wave itself (Hann et al., 2015). In this case extra dynamic anchor capacity is also created from mobilising the mass of the soil surrounding the plate (Kwa et al., 2021). This added soil mass can be described by the hydrodynamics 'added mass' term, which is well recognised in fluid mechanics and is routinely considered in the dynamic motion of floating structures and mooring lines, but is not considered in conventional geotechnical capacity analysis. The added mass for a geotechnical failure mechanism is typically double that for fluid flow around the same object (Kwa et al. 2021).

Allowing for this multiscale hierarchy of mooring-anchor-seabed load-time processes, which span from snatch loads (~10^0 s) to wave loading periods (~10^1 s), through to seabed consolidation durations (~$10^{4\text{-}6}$ s), over the full facility life (~10^{12} s) can have a beneficial design outcome, offering opportunities for reductions in anchor size and therefore, more efficient anchoring systems for FOW infrastructure. However, typical fluid-structure interaction models capture the response of floaters and mooring lines in the time-domain over relatively short time periods (i.e. up to 3 hours) rather than over a whole-life operational lifetime. They also model the connection of the mooring system to the seabed as a pin connection and so beneficial connected mooring-anchor-seabed interactions are not generally considered.

1.3 *Aim and outline of paper*

The aim of this study is to explore the benefits from connecting FOW mooring analyses of taut mooring line configurations with and without LRDs with anchor-seabed response. This is achieved through coupling a developing anchor macro model, *Ancmac*, with a Flexcom Finite Element Model (FEM) mooring-floater analysis of an International Energy Agency (IEA) 15 MW UMaine reference turbine in an idealised example design lifetime application.

2 Method: Anchor and floating system models

2.1 *Geotechnical anchor macro model*

Anchor macro models can be used to efficiently simulate the response of an anchor in terms of the resultant forces and displacements at the anchor, as an idealisation of the integrated effect of the surrounding elements of soil. This approach was formalised in the 1990s by Nova & Montrasio (1991), Houlsby et al., (1992) and Schotman (1989) by using a plasticity framework. The *Ancmac* model captures the anchor capacity as a time-varying function of the applied loads, reflecting short term processes of softening and pore pressure generation, u, and long-term processes of consolidation. Consolidation and pore pressure dissipation leads to hardening and strength gain over the anchor life time (Kwa et al., 2022, 2023c). A similar approach has also been implemented in an anchor macro model developed in Da silva (2021) and could be incorporated into other multi-directional anchor macro models (e.g. Yang et al. 2012; Cassidy et al., 2012).

The overall whole-life anchor simulation process is summarised in Figure 1 and is carried out using two software elements; *Ancmac* and a wrapper program, referred to as K^2M^2.

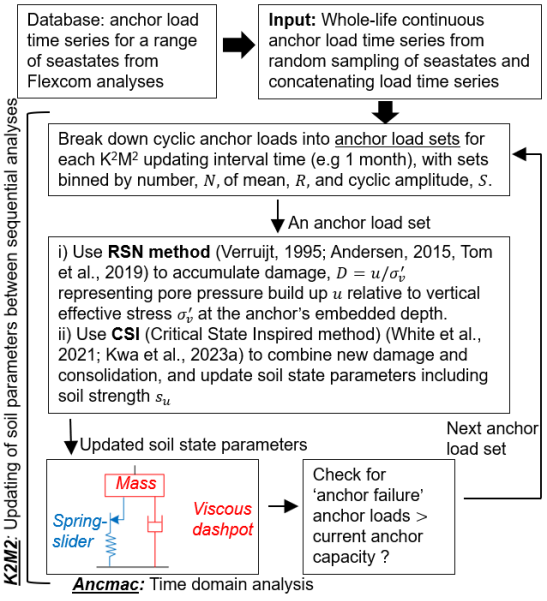

Figure 1: Flow chart of the anchor macro model routine

Ancmac represents the geotechnical anchor response using a one-dimensional parallel Iwan model (Iwan, 1967), in which the spring-sliders incorporate viscous rate effects, in combination with an added mass component. The detailed formulation of *Ancmac* and K^2M^2 can be found in Kwa et al., (2023a,b). The simulation routine of *Ancmac* when it is coupled with a separate numerical analysis package can be found in Kwa et al (2022).

2.2 *Hydrodynamic floating system model*

A hydrodynamic mooring-floater FEM in the commercially available software numerical analysis package Flexcom was used to model an International Energy Agency (IEA) 15 MW wind turbine and the Umaine Volturn-US semi-submersible FOW turbine. The full FOW turbine platform and turbine characteristics are described in detail in NREL publications (Evan et al, 2020; Allen et al., 2020). Flexcom FAST plug-ins AERODYN and SERVODYN were used to model the fully-coupled aero-hydro-servo response.

This modelling methodology has been validated against other software as part of an offshore code collaboration project OC6 (Robertson et al. 2020). Two taut mooring configurations were considered (a) a conventional taut mooring system, composed of high modulus synthetic polyester rope; (b) a taut mooring system, composed of the same polyester rope, with the addition of a polymer spring load reduction device (LRD) at each fairlead. This LRD is based on the Tfi Seaspring (Lozon et al., 2022) and can operate at high strain (20-50%), thus providing high levels of elongation to reduce dynamic loads on mooring lines and anchors. The LRD is modelled with a 3-phase nonlinear stiffness curve, to match the curve of the Tfi Seaspring The unstretched length of the LRD is modelled as 25 m, with a stretched length of 37.5 m at 4MN load. The general mooring parameters are shown in Table 1, with profile views of both mooring configurations shown in Figure 2.

Table 1: General mooring parameters of taut mooring system, applicable to both (a) conventional base case and (b) with LRD

Parameter	Value
Water depth, z_w	150 m
Number of mooring lines	3
Anchor radius from platform centerline	260 m
Seabed-mooring line angle, θ_m	34 deg
Polymer rope stiffness, $(EA)_{rope}$	7 MN
Polymer rope linear density ρ_{rope}	8.5 kg/m
Fairlead pre-tension, $T_{m,PT}$ *	2 MN

* with no applied wind or wave loads

Stochastic load cases were applied to the FOW turbine model based on the IEC design load case (DLC) matrix. From the matrix of load cases, two 'operational' load cases were selected, as well as two parked FOW turbine case for a storm and 1 in 50-year storm, as summarised in Table 2. All environmental loads are applied in the same direction, and each simulation was run for 10800s (3 hours). The resulting force time-series, T_m, was measured at the anchor point of the windward mooring line. The range (i.e. minimum, maximum and mean) values of T_m are summarised in Figure 3 for the taut conventional mooring and mooring with LRD cases. A typical comparison between the load-time series at the anchor point for the taut conventional mooring and mooring with LRD cases is summarised in Figure 4.

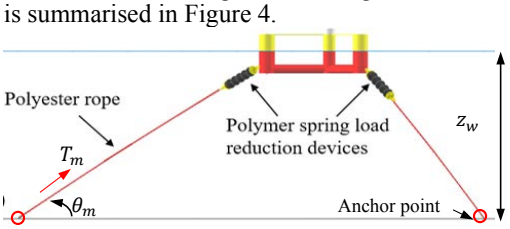

Figure 2: Profile view of taut mooring with load reduction devices (LRDs). The model of the conventional mooring system does not have the LRDs in the mooring lines.

Table 2: Summary of 3 load cases used in this study, selected from UMaine design matrix (Allen et al., 2020)

IEC DLC ref.	Load case description	Wind Speed (v_w) (m/s)	Sig. wave height (H_s)	Peak wave period (T_p)	Shape factor
1.1.4	Operational	4	1.1 m	8.52 s	1.00
1.1.12	Operational	12	1.84 m	7.44 s	1.00
6.3.38	Parked storm	38	6.98 m	11.70 s	2.75
6.1.47	Parked 1 in 50-yr storm	47.5	10.70 m	14.20 s	2.75

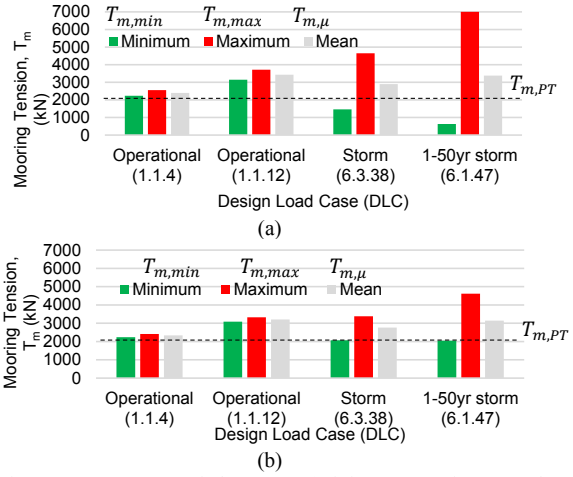

Figure 3: Summary of the range (minimum, maximum and mean) of loads at the anchor point for design load cases (DLCs as shown applied to (a) conventional taut mooring and (b) taut mooring with load reduction systems (LRD).

In both taut mooring cases, the mean loads, $T_{m,\mu}$ were higher than the pre-tensioned value, $T_{m,PT}$

($T_{m,\mu}$=2.3 to 3.4 MN), and there was an increasing variation between the minimum and maximum loads for the DLCs associated with higher windspeed. Including an LRD in the mooring configuration resulted in reduction in the maximum loads and load amplitudes transmitted to the anchor. This load reduction was particularly significant in the more severe storm loading cases; up to 37% reduction in the parked regular storm case and 50% in the 1-in-50-year storm case. Smaller reductions of 5 to 11% were observed in the operational cases as a result of including LRDs in the mooring configuration.

These load-time-series were used to build synthetic yearly realisations reflecting seasonality in anchor loads in the example whole-life application as described and discussed in Section 3.

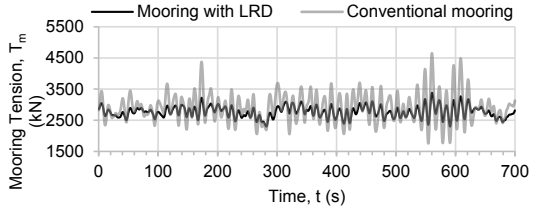

Figure 4: Example comparison between loads transmitted to the anchor for taut mooring configurations with and without LRD (for DLC 6.3.38)

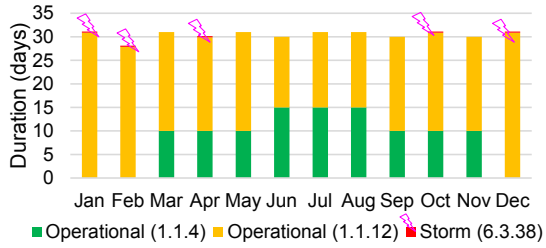

Figure 5: Selected seasonal variations in metocean conditions.

2.3 *Applied whole-life metocean conditions and initial seabed conditions*

To build the synthetic seasonally-varying yearly realisations of whole-life anchor loads, illustrative combinations of the DLCs were chosen to artificially reflect seasonally-varying metocean conditions within a year (i.e. calmer in summer and more severe in winter) as shown in Figure 5. This combination of DLCs was repeated over 20-years to idealise a design lifetime of a FOW turbine. To investigate the response of the system under an extreme loading event, a 1 in-50-year storm was additionally applied for a period of 3 hours in the 15th year of the design lifetime.

It is assumed that these loads are transmitted directly to the anchor, whereas in reality, additional geotechnical resistance would be mobilised from interactions between the embedded section of mooring line and the seabed. Based on analytical solutions for the frictional capacity of embedded anchor chains (Neubecker & Randolph 1995), this decrease in load would be less than ~10% and is neglected in this analysis.

An illustrative set of seabed input parameters to *Ancmac* and K^2M^2 were selected to be representative of lightly over consolidated clay around a circular plate anchor embedded at a depth of ~20m. The selected seabed values were an initial undrained strength s_{u0}=80kPa, coefficient of consolidation base case value of c_v=6m^2/s and a variation case of 12m^2/s, and a sensitivity S_t=2.5 at the anchor point. These selected seabed values were similar to those in centrifuge tests performed by O'Loughlin et al., (2020) and Zhou et al., (2020).

Two sets of simulations were also considered; one where seabed strengthening or hardening was disabled and another set where seabed hardening was enabled. When seabed hardening was disabled, seabed strength, s_u, is limited to vary between the initial value, s_{u0}, and a cyclically remoulded minimum, s_{ur}. When seabed hardening is enabled, both seabed softening and beneficial whole-life seabed strengthening effects from consolidation were considered in the analysis, and as a result, s_u is allowed to vary between s_{ur} and hardened maximum s_{uh} from consolidation. This change in s_u affects the through-life available anchor capacity Q_s according to Equation 1, which is compared with T_m to find the required anchor sizes.

3 Results and discussion: An integrated whole-life geotechnical-hydrodynamic application

3.1 *Basis for defining required anchor size*

Results are presented for the 15MW taut-moored FOW turbine, with and without an LRD in the mooring line, with a deeply-embedded circular plate anchor. Anchor capacity is updated on a monthly basis, so a monthly factor of safety (FoS) is calculated based on eqn 3.

$$FoS = Q_s/T_{m,max} \quad (3)$$

To determine the required anchor size for each case, a minimum factor of safety, FoS ≥1 is set over the 20-year design lifetime in the simulations. The analysis of the anchor response throughout the design lifetime was repeated, iterating the anchor size each time, to find the minimum anchor size that meets this condition. For deeply-embedded circular plate anchors, the capacity is proportional to the cross sectional anchor area.

This adopted criteria of FoS ≥1 is a lower FoS than could be accepted according to conventional design practice, but is used here to provide a simple consistent basis to compare different modelling cases (with and without LRD, with and without seabed hardening). A change in the required FoS would not affect the relative performance for different cases, only the absolute results (i.e. the required anchor

size). The minimum required anchor sizes for each of the four simulation cases are summarised in Figure 6.

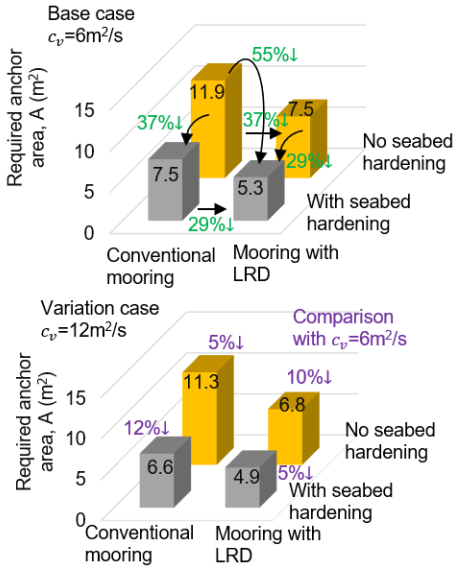

Figure 6: Comparison of required anchor sizes for FoS ≥ 1

The differences in required anchor size are created by two effects. Firstly, the use of a LRD in the mooring line reduces the loading at the anchor. Secondly, the anchor capacity varies through the design life depending on (i) the applied loading, (ii) whether seabed hardening is modelled and (iii) the consolidation coefficient of the seabed, which controls the rate of strength regain. These effects are illustrated by the time evolution of the key loading (Q_s and $T_{m.max}$) and soil parameters (s_u, H and D), which are shown in Figure 7 and 9 for the conventional mooring case and the mooring with LRD case. The resulting variation in FoS over the design life for each case is shown in Figure 8 and 10.

3.2 *Results for conventional mooring*

In the conventional mooring case, $T_{m,max}$ varied between 3.7 to 4.6 MN as a result of the selected yearly metocean conditions (Figure 5). As a result of these loads, the anchor capacities reduced significantly to a minimum value of approximately 0.6× the initial anchor capacity Q_{s0} and undrained seabed strength, s_{u0} within the first year of the simulated design lifetime as shown in Figure 7a and b. This initial drop in anchor capacity also corresponded to a decrease in the through-life FoS as shown in Figure 8.

This initial drop in anchor capacity during the first year, was a result of the seabed softening under cyclic loading and because insufficient time has passed to allow consolidation and dissipation of damage or pore pressure generated by the applied anchor loads.

For the no-hardening case, this seabed softening response dominated and the available anchor capacity remained at $0.6 \times s_{u0}$ and Q_{s0} (as shown by the dotted lines in Figure 7. Consequently, the anchor size is set by the requirement to resist the higher applied anchor loads from the 1 in 50-year storm in year 15 to achieve a FoS ≥ 1, as marked by F' in Figure 7a and 8b.

If hardening was enabled in the simulations, the required anchor size is instead controlled by the initial drop in anchor capacity and the requirement for FoS ≥ 1 (marked as F in Figure 7a and 8a) during the initial year. After year 1, seabed strengthening eclipsed the effect of damage from the applied loads resulting in an increase in capacity towards $1.3\times s_{u0}$ and Q_{s0}, as shown by the solid lines in Figure 7a to c. This increase in available anchor capacity resulted in FoS >1 when the 1 in 50-year storm was applied at year 15 and corresponded to 37% decrease in the required anchor size (i.e. 7.5 vs. 11.9 m^2) as shown in Figure 5.

3.3 *Results for mooring with LRD*

When LRDs were present in the mooring lines, smaller anchor loads were applied. $T_{m,max}$ varied between 3.3 to 3.4 MN and reached a peak of 4.6 MN during the 1 in 50 year storm as summarised in Figure 4. Compared to the no-LRD case, this resulted in less seabed damage, D, as well as smaller and more gradual increases in hardening, H, undrained strength, s_u, and anchor capacity, Q_s, as shown in Figure 9. The final values of seabed strength, s_u, and anchor capacity, Q_s, were similar in the cases with or without LRDs. Therefore, with soil hardening, it is possible to have a 29% decrease in the required anchor size (i.e. 5.3 vs 7.5 m^2) if LRDs are present in the mooring configuration compared to the no-LRD case.

When seabed hardening was enabled the required anchor sizes were determined based on the initial drop in anchor capacity, Q_s and FoS in the first year, FoS≤1 (marked as F in Figure 9a and 10a), the same as for the no-LRD case. This is because the seabed strengthened and hardened in subsequent years such that FoS >1 when the 1 in 50 year storm was applied in year 15.

When hardening was not enabled, the anchor size depended on the anchor capacity when the 1 in 50 year storm was applied in year 15 (marked as F' in Figure 9a and 10b). This anchor size was larger than when hardening was enabled (7.5 vs 5.3 m^2).

When both LRD and whole-life seabed effects are considered together, the required anchor size is reduced by 55% compared to the case where conventional mooring is used and no seabed hardening is considered (i.e. 5.3 vs 11.9m^2), as shown in Figure 6.

3.4 *Variation: higher consolidation coefficient, c_v*

Increasing the coefficient of consolidation from c_v=6 to 12 m^2/s increases the rate of seabed hardening H, and recovery of applied damage, D, as shown by the green and blue lines in Figure 7 and 9.This increase in c_v resulted in a 5 to 12% decrease in anchor size for all cases as shown in Figure 6.

3.5 *Full coupling of anchor and mooring response*

This analysis uses a FoS limit on the static anchor capacity to define the required anchor size. It does not consider movement of the anchor, and the loads come from a mooring analysis in which the anchor is represented as a fixed pin. Further design efficiencies could result from considering anchor ductility, where the anchor can move beyond its installed position and also mobilise seabed added mass. This is explored in more detail in Kwa et al. (2022; 2023d).

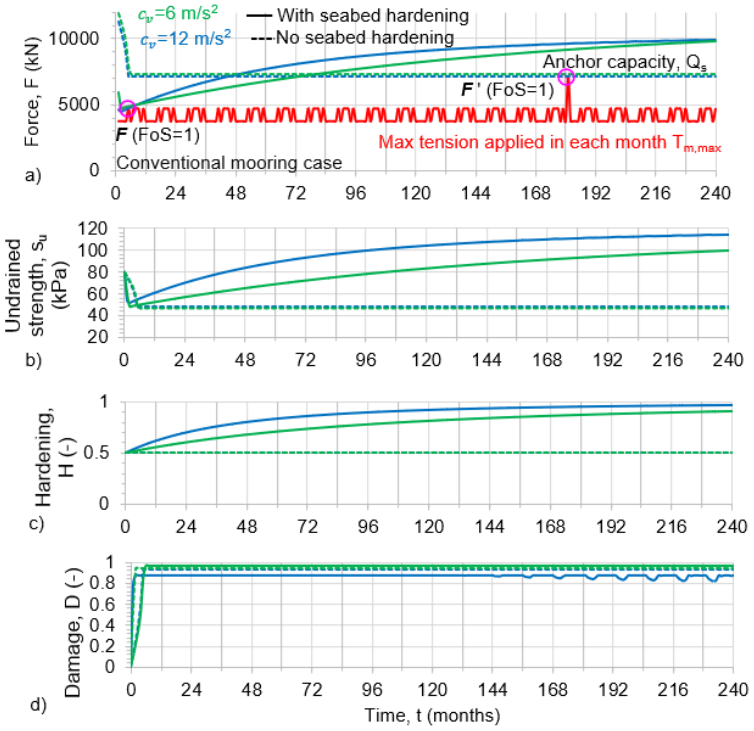

Figure 7: Summary of (a) anchor capacity relative to applied tension loads (b) changes in seabed undrained strength, (c) hardening and (d) damage for conventional taut mooring case

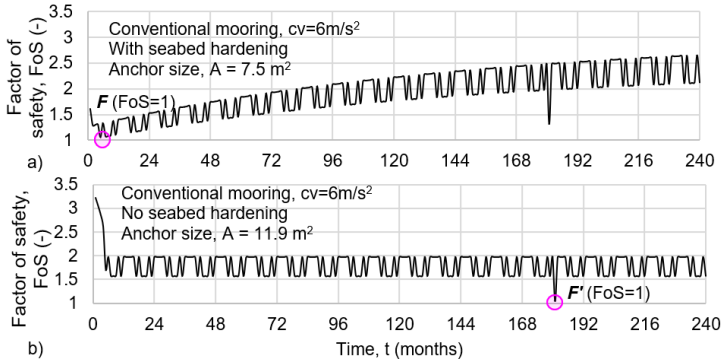

Figure 8: Changes in through-life factor of safety (FoS) (a) with seabed hardening and (b) without seabed hardening for the conventional taut mooring case

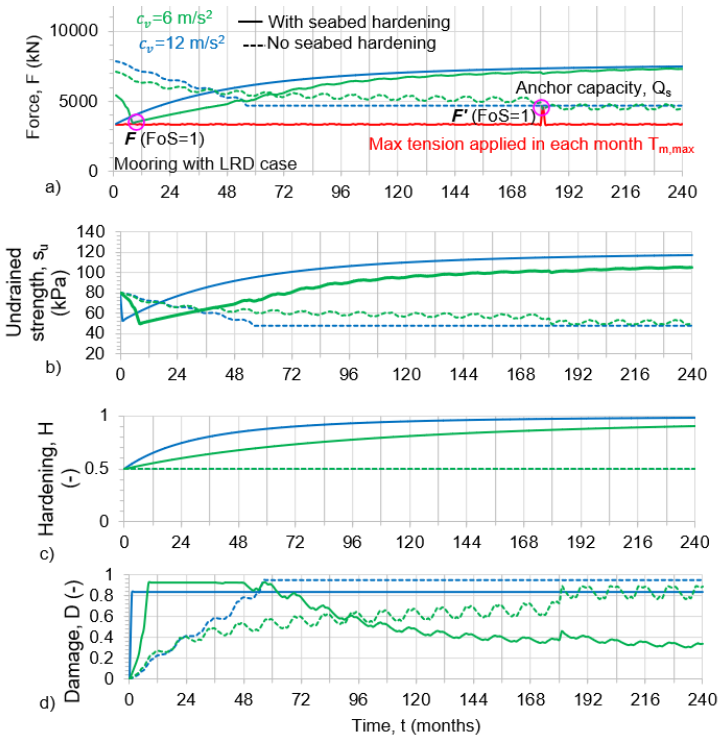

Figure 9: Summary of (a) anchor capacity relative to applied tension loads (b) changes in seabed undrained strength, (c) hardening and (d) damage for mooring with LRD case

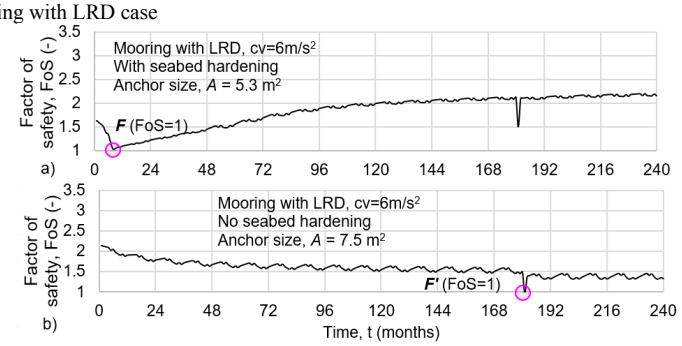

Figure 10: Changes in through-life factor of safety (FoS) (a) with seabed hardening and (b) without seabed hardening for the taut mooring with LRD case

4 Conclusions

Coupling floater-mooring analyses with whole-life anchor-seabed response uncovers opportunities for more efficient mooring and anchoring systems for floating offshore wind. Results from an example whole-life analysis show that if load reduction devices (LRDs) are included in the mooring configuration when deriving anchor loads, this can result in a 29 to 37% decrease in required anchor size. If beneficial whole-life anchor-seabed effects are considered separately, this can result in a similar decrease in anchor size. If both factors (LRDs and whole-life seabed are considered together, it is possible to approximately halve the required anchor size. The coupling between the floater-mooring and whole-life anchor-seabed response can be achieved efficiently via a developing anchor macro model, *Ancmac* that simply and practically connects with floater-mooring analyses, to assess through-life changes in anchor capacity and seabed response during the full operational lifetime of FOW infrastructure.

5 Acknowledgements

This work forms part of research supported by the Royal Academy of Engineering under the Research Fellowship Programme, RAEng Chair in Emerging Technologes Centre of Excellence in Intelligent & Resilient Ocean Engineering (IROE), and Supergen ORE Hub (Grant EPSRC EP/S000747/1). Katherine

Kwa is supported by the RAEng Research Fellowship Scheme, David White is supported by the Supergen ORE Hub, Susan Gourvenec is supported by the Royal Academy of Engineering through the Chair in Emerging Technologies scheme, and Adam Sobey is supported by The Lloyd‘s Register Foundation.

6 References

Allen, C. et al. (2020) Definition of the UMaine VolturnUS-S Reference Platform Developed for the IEA Wind 15MW Offshore Reference Wind Turbine. NREL/TP-5000-76773

Andersen, K.H. (2015). Cyclic soil parameters for offshore foundation design. Front. in offshore geotech. III 5-82.

Bransby, M.F. (2002) The undrained inclined load capacity of shallow foundations after consolidation under vertical loads. Num models in geom. NUMOG VIII, 431-437

Blake et al., (2011) Setup following keying of plate anchors assessed through centrifuge tests in kaolin clay. In Proc. ISFOG 2011, Perth, Australia (pp. 8-10).

Cassidy M.J. et al. (2012). A plasticity model to assess the keying of plate anchors. Géot., 62(9): 825–836

Cerfontaine, B., et al. (2023) Anchor geotechnics for floating offshore wind: current technologies and future innovations, J. Ocean Eng. 279, p. 114327

Cocjin M., et al. (2014). Tolerably mobile subsea foundations – Observations of performance. Géot. 64(11): 895-909.

Crown Estate (2020. Broad horizons: Key resource areas for offshore wind. Summary report

Deeks, A., et al. (2014) Design of direct on-seabed sliding foundations, OMAE2014-24393, V003T10A024

DNV (2002). DNG-RP-E02: Recommended practices: design and installation of plate anchors in clay. DNV

Dublin Offshore (2021) Executive Summary-Load Reduction Device, Dublin Offshore.

Evan, G. et al. 2020. Definition of the IEA 15-Megawatt Offshore Reference Wind. Golden, CO: National Renewable Energy Laboratory. NREL/TP-5000-75698.

Gordelier, T et al. (2015). A novel mooring tether for highly-dynamic offshore applications; mitigating peak and fatigue loads via selectable axial stiffness. J. of Marine Sc. and Eng., 3(4), pp.1287-1310.

Gourvenec S. (2020) Whole-life geotechnical design: What is it? What’s it for? So what? & what next? Proc. 4th ISFOG. 2021, Austin, Texas, USA, ASCE Geo-Institute & DFI

Hann, M., et al. (2015). Snatch loading of a single taut moored floating wave energy converter due to focussed wave groups. J. Ocean Eng., 96, pp.258-271.

Houlsby, G. T., & Wroth, C. P. (1991). The variation of shear modulus of a clay with pressure and overconsolidation ratio. Soils & Found., 31(3), 138-143.

Iwan, W. D. (1967). On a class of models for the yielding behavior of continuous & composite systems.

Kwa, K.A., et al. (2021a). Analysis of the added mass term in soil bearing capacity problems, Geot. Let. 11, pp. 80-87

Kwa, K.A. et al. (2022) A numerical macro model to simulate the whole life response of anchors for floating offshore renewable energy systems. OMAE 2022-81101

Kwa, K.A., et al. (2023a) The RSN-CSI model: A whole life geotechnical anchor macro model for floating offshore systems (under review)

Kwa, K.A., et al. (2023b) A whole-life macro model of anchor capacity for floating offshore renewable energy systems, NUMGE, London, UK

Kwa, K. A., & White, D. J. (2023c). Numerical modelling of plate anchors under sustained load: the enhancement of capacity from consolidation. Comp. & Geot., 158, 105367.

Kwa et al., (2023d) Dynamic seabed-anchor capacity enhancements for taut-moored floating offshore wind. SEG 2023, Delft (Extended abstract under review)

Laham, N. I., et al. (2021). Episodic simple shear tests to measure strength changes for whole-life geotechnical design. Géot. Let., 11, 103-111.

Lozon. E et al. (2022). Design and Analysis of a Floating-Wind Shallow-Water Mooring System Featuring Polymer Springs: Golden, CO: NREL/CP-5000- 83342.

Martin, C. M. & Randolph, M. F. (2001). Applications of the lower and upper bound theorems of plasticity to collapse of circular foundations. In Proc. 10th Int. Conf. on Computer Methods and Advances in Geomechanics,

Neubecker, S.R. & Randolph, M.F., 1995. Profile and frictional capacity of embedded anchor chains. Journal of geotechnical engineering, 121(11), pp.797-803.

Nova R. & Montrasio L (1991) Settlements of shallow foundations on sand. Geot.,41(2): 243-256.

Pillai AC, et al. (2022) Anchor loads for shallow water mooring of a 15 MW floating wind turbine — Part I: Chain catenary moorings for single and shared anchor scenarios, Ocean Engineering, vol 266, 111816.

O'Loughlin, C. D., et al. (2020). Load-controlled cyclic T-bar tests: a new method to assess effects of cyclic loading & consolidation Géot. Let., 10(1), 7-15.

Da Silva, A.P. et al. (2021a). A non-associative macro-element model for vertical plate anchors in clay. Can. Geo. J 58(11), p.1703-1715

Da Silva, A.P. et al., (2021b). A cyclic macro-element framework for consolidation dependent three dimensional capacity of plate anchors, J. Mar. Sc & Eng. ((2), 199

Da Silva, A. P. (2021c). Macro-element modelling of plate anchors for floating offshore structures accounting for capacity changes during operational conditions PhD Thesis.

Randolph, M., (2004). Characterisation of soft sediments for offshore applications, In Proc. Geot.& Geophys. Site Charac., Portugal, p.209-232

Robertson, A. N., et al. (2020). OC6 Phase I: Investigating the underprediction of low-frequency hydrodynamic loads and responses of a floating wind turbine. In J. of Physics: Conference Series (Vol. 1618, No. 3, p. 032033).

Schotman, G.J.M. (1989). The effects of displacements on the stability of jackup spudcan foundations'. Proc. 21st Offshore Tech. Conf., Houston, Texas, OTC 6026.

Smith V. B. & White D. J. (2014) Volumetric hardening in axial pipe soil interaction. In Proc. Offshore Tech. Conf. Asia, OTC ASIA 2014 (Vol. 2, pp. 1611-1621).

Stanier, S.A. & White, D.J., (2018). Enhancement of bearing capacity from consolidation: due to changing strength or failure mechanism?. Géot, 69(2), pp.166-173.

Tom, J.G., et al., 2019, June. Fluid-structure-soil interaction of a moored wave energy device. In International Conference on OMAE (Vol. 58899, p. V010T09A024). ASME

Verruijt, A. (1995). Computational geomechanics (Vol. 7). Springer Science & Business Media.

White, D. J., et al. (2021). A cyclic py model for the whole-life response of piles in soft clay. Comp. & Geot., 141, 104519.

Yang, M. et al., (2012). Behaviour of suction embedded plate anchors during keying process. J. Geot. & Geoenv. Eng. 138(2), pp.174-183.

Zhou, Z., et al. (2020). Improvements in plate anchor capacity due to cyclic and maintained loads combined with consolidation. Géotechnique, 70(8), pp. 732-749.

A.5 Dynamic seabed-anchor capacity enhancements for taut-moored floating offshore wind

Symposium on Energy Geotechnics
Accelerating the energy transition
3-5 October 2023, Delft, the Netherlands

Peer-reviewed Conference Contribution

Dynamic seabed-anchor capacity enhancements for taut-moored floating offshore wind

Katherine Kwa[1,*], David White[1], Oscar Festa[1] and Susan Gourvenec[1]

[1] University of Southampton
* Corresponding author: k.a.kwa@soton.ac.uk

Decarbonisation of global energy supply to meet Net Zero targets by 2050 requires rapid expansion of offshore wind [4]. Much of this growth will come from floating offshore wind (FOW) technology where seabeds are less congested, high energy wind resources are located and conventional fixed offshore wind is not practical [1]. The required scale of FOW requires a step change in mooring and anchoring technology compared to existing hydrocarbon solutions. New, efficient and reliable mooring and anchoring systems are essential to economically deliver the necessary FOW [1]. Taut mooring arrangements can be attractive for FOW turbines as they require less length and lighter synthetic mooring line than traditional chain catenary mooring arrangements. However, taut moorings transmit significantly higher mean and peak tensions to the anchor compared to catenary moorings. It is therefore important to fully quantify the capacity available from anchors during typical FOW load conditions, including dynamic effects.

This study focuses on how a numerical anchor macro model, *Ancmac* [6], can be used to capture and quantify dynamic anchor-seabed capacity benefits such as from seabed added mass, F_{am} [5] and viscous soil strength effects. These effects can enhance the dynamic anchor capacity and are not typically considered in anchor design. Typical mooring-floater fluid-structure interaction analyses also model the connection of the mooring lines to the seabed as a fixed pin connection and so seabed-anchor-mooring interactions are not typically considered. *Ancmac* can replace this fixed pin connection node at the seabed as it uses mechanical analogue components (e.g. spring-viscous-slider and mass) to simply and practically link forces on the anchor with anchor and chain movements in the time domain to determine the seabed response and the current available anchor capacity. This study presents an example case where *Ancmac* is used to model the response of an embedded plate anchor that is subjected to a high amplitude, short period (T= 6 and 10 s) high mean load event (Figure 1a). The anchor loads , F_m, are derived from applying a 1-50 year storm design loading event on a 15MW FOW turbine [3] with a taut mooring line configuration composed of high modulus synthetic polyester rope [8].

Results show that if dynamic seabed benefits are not considered (purple line in Figure 1a), then a static anchor capacity of $Q_{ult,stat}$= 4.15 MN and corresponding anchor size of $A_{p,stat}$= 11.13 m^2 is required (for an anchor buried in slightly overconsolidated soft clay s_u=30 kPa and bearing capacity factor N_c=12.42). If beneficial dynamic seabed enhancements are considered (shown by red lines $F_g = f(v)$), then a lower initial static anchor capacity can be adopted Q_0=3.13 MN, which corresponds to a ~25% decrease in the required anchor size ($A_{p,dyn}$=8.41 m^2). During the design loading event, as the applied anchor load, F_m increases above the available static capacity, towards the maximum applied value, the anchor begins to move (Figure 1b) generating dynamic resistance from mobilising the non-linear viscous slider and added mass resistance components. The resistance in the viscous slider component is based on a model for the change in undrained strength with increasing equivalent strain rate (γ'=v/D, where D is anchor diameter), as shown in Figure 1c. The resistance from the viscous slider component reaches a maximum at the time marked V slightly after the peak of the applied mooring line loads, at time M, as shown in Figure 1a-c. Reducing the period of the applied load (T=10 s to 6 s) increased the added mass resistance as the anchor is subjected to higher accelerations. As a result, the anchor experienced significantly smaller (~50% less) maximum displacement and reduced velocities. This comparison is also evident in Figure 1d, which compares the contributions of resistance forces from the spring-viscous-slider and added mass components.

DOI: https://doi.org/10.59490/seg23.2023.619

Ancmac can also capture the long-term enhancements in seabed strength and anchor capacity as a time-varying function of the life-cycle of seasonally varying, operational applied loads. This could, for example, further reduce the required anchor sizes, as s_u can increase from beneficial long-term seabed consolidation effects [7]-[10]. These short and long-term seabed benefits that occur over the range of different loading timescales, and result in enhanced anchor capacities for loads that are relevant to FOW taut mooring configurations, will be further discussed during the presentation.

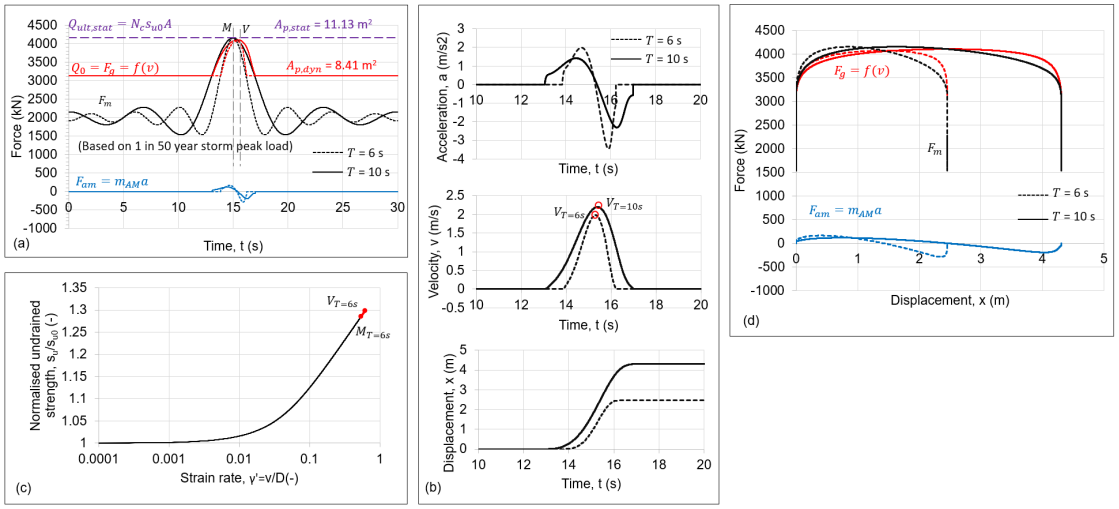

Figure 1: Summary results showing capacity enhancement during dynamic loading using numerical anchor macro model *Ancmac*

Contributor statement: Katherine Kwa: Conceptualisation, data curation, formal analysis, funding acquisition, investigation, methodology, writing- original draft, writing- review & editing; David White: Conceptualisation, funding acquisition, writing- review & editing; Oscar Festa: analysis, writing -review & editing; Susan Gourvenec: Conceptualisation, funding acquisition, writing- review & editing.

Acknowledgments

This work forms part of research supported by the Royal Academy of Engineering under the Research Fellowship Programme, RAEng Chair in Emerging Technologes Centre of Excellence in Intelligent & Resilient Ocean Engineering (IROE), and Supergen ORE Hub (Grant EPSRC EP/S000747/1). Katherine Kwa is supported by the RAEng Research Fellowship Scheme, David White is supported by the Supergen ORE Hub and Susan Gourvenec is supported by the Royal Academy of Engineering through the Chair in Emerging Technologies scheme.

References

[1] Cerfontaine, B., White, D., Kwa, K., Gourvenec, S., Knappett, J., & Brown, M. (2023). Anchor geotechnics for floating offshore wind: Current technologies and future innovations. Ocean Engineering, 279, 114327. https://doi.org/10.1016/j.oceaneng.2023.114327
[2] Euro. Tech. & Innov. Platform on Wind Energy (2020) ETIP Wind Roadmap. https://etipwind.eu/files/r ports/ETIPWind-roadmap-2020.pdf
[3] Allen, Viscelli, Dagher, Goupee, Evan, Abbas, Hall, Barter, (2020) Definition of the UMaine VolturnUS-S Reference Platform Developed for the IEA Wind 15-Megawatt Offshore Reference Wind Turbine. Golden, CO: NREL NREL/TP-5000-76773.
[4] GWEC (2022) Global Offshore Wind Report, GWEC, https://gwec.net/gwecs-global-offshore-wind-report/
[5] Kwa, K.A., Weymouth, G.D., White, D.J. & Martin (2021). Analysis of the added mass term in soil bearing capacity problems, Geotechnique Letters (11) 80-87 https://doi.org/10.1680/jgele.20.00097
[6] Kwa, K. A., Sivasithamparam, N., Deeks, A., & White, D. J. (2022). A numerical macro model to simulate the whole life response of anchors for floating offshore renewable energy systems. In Int. Conf. on Off. Mech. & Arctic Eng. (Vol. 85949, p. V009T10A003). ASME.
[7] Kwa, K. A., & White, D. J. (2023). Numerical modelling of plate anchors under sustained load: the enhancement of capacity from consolidation. Computers and Geotechnics, 158, 105367. https://doi.org/10.1016/j.compgeo.2023.105367
[8] Kwa.K.A., Festa, O., White, D., Sobey, A. & Gourvenec, S. (2023) Integrated numerical modelling of soil-anchor-mooring line- floater response for floating offshore wind, Int. Conf. on Numerical Methods in Geomechanics (NUMGE) 2023, London
[9] Kwa, K.A., Tosdevin, T. Jin, S. White, D.J. & Greaves, D. (2023) Whole-life modelling of anchor capacity for floating systems: the RSN-CSI approach (In review).
[10] Laham, N. I., Kwa, K. A., White, D. J., & Gourvenec, S. M. (2021). Episodic simple shear tests to measure strength changes for whole-life geotechnical design. Géotechnique Letters, 11(1), 103-111. https://doi.org/10.1680/jgele.20.00124

A.6 Integrated numerical modelling of soil-anchor-mooring line-floater response for floating offshore wind

Proceedings 10th NUMGE 2023
10th European Conference on Numerical Methods in Geotechnical Engineering
Zdravković L, Konte S, Taborda DMG, Tsiampousi A (eds)
ISSN

doi: 10numge-2023-129

Integrated numerical modelling of soil-anchor-mooring line-floater response for floating offshore wind

K.A.Kwa[1] , O. Festa[1] , D.J. White[1], A.Sobey[1,2] , S. Gourvenec[1]

[1] *Civil, Maritime and Environmental Engineering Department, University of Southampton, Southampton, UK*
[2]*Data-centric Engineering, Alan Turing Institute*

ABSTRACT: This paper presents the development of an anchor macro model and its integration with mooring analyses, for easy coupling of the anchor-seabed-mooring response and full system modelling of a floating offshore wind turbine. The model combines techniques that (i) mobilise additional seabed resistance by considering the added mass and whole-life effects of changing strength of the seabed and (ii) reduce the anchor loads by considering a compliant mooring system, to result in reduced required anchor size. The benefits of combining these approaches lead to reductions of up to 50% in the minimum required anchor size for the same system reliability.
Keywords: Macro-modelling; Anchors; Offshore Geotechnics; Whole-life modelling;

1 INTRODUCTION

1.1 Background and Aim

Floating offshore wind (FOW) infrastructure is subject to a wide range of actions from metocean and operational conditions, which are transmitted via mooring lines to the anchor. These loads can affect the geotechnical properties of the seabed and in turn affect the capacity and response of the infrastructure over its lifetime (Gourvenec, 2020). However, typical mooring-floater fluid-structure interaction analyses model the connection of the mooring lines to the seabed as a fixed pin connection and so seabed-anchor interactions with the mooring and floater analysis are generally not considered. This uncoupled method of analysis can result in potentially overconservative anchor designs.

This challenge is addressed by using a novel anchor macro model, referred to as *Ancmac*, that captures the 'whole-life' geotechnical response of the seabed surrounding the anchor, and simply and practically connects with mooring analyses. In this context, whole-life geotechnics, enables assessment of the through-life changes in seabed response and anchor capacity as a result of variable mooring tensions that are applied to the anchor over the lifetime of the FOW infrastructure. This approach can have beneficial design outcomes over traditional design methods including more accurate predictions of seabed-anchor response, available anchor capacity and required anchor size throughout the FOW design lifetime. This study describes *Ancmac* and its integration with FOW mooring analyses to demonstrate the benefits of considering the coupled seabed-anchor-mooring floater response over an idealised FOW facility lifetime of 20 years.

2 ANCHOR-MOORING-FLOATER MODEL CONFIGURATION

2.1 Geotechnical anchor model

Ancmac is a macro model which simulates the response of an anchor in terms of the resultant forces at the anchor, as an idealisation of the integrated effect of the surrounding elements of soil. The approach was formalised in the 1990s by Nova et al., (1991), Houlsby et al., (1992) and Schotman (1989) by using a plasticity framework. The novel contribution of this study is that the anchor strength is a time-varying function of the applied loads, reflecting short term processes of softening and pore pressure generation, u, and long-term processes of consolidation where the seabed can also recover, harden and strengthen over the whole-life time. This approach could be incorporated into multi-directional anchor macro models (such as those presented in Cassidy et al., 2012; Peccin da Silva, 2021).

Ancmac is explicit, following the terminology of Jostad et al (2022), as a time history of cyclic anchor loading is converted to increments of the model state parameters. These parameters are then translated into spring-sliders, dashpots and added mass mechanical analogue parameter (MAP) components – which define an extended parallel Iwan model (Iwan, 1967) that represents the anchor in a time domain of the next set of cyclic loads. The updating of the MAPs takes place at intervals that are long enough in time so that the whole operating life of an anchor can be modelled efficiently, but also short enough that the anchor capacity does not change significantly during a single simulated set of cycles. 'Failure' of the embedded anchor is identified when any of the anchor loads that are mobilized exceed the current anchor capacity.

The overall simulation process (as summarised in Figure 1) involves two elements; *Ancmac* and a wrapper program K^2M^2. *Ancmac* holds the current MAP components of the anchor model, which do not change in value during a time domain analysis of mooring lines during a certain sea state. For every time domain analysis of the mooring line, *Ancmac* outputs a series of cyclic anchor forces and the corresponding anchor movements (i.e. displacements, x, velocities, v, and accelerations, a) at the anchor point.

The wrapper program, referred to as K^2M^2, uses an acceleration strategy that factors up the number of cyclic loads from *Ancmac* to represent a longer period of time. K^2M^2 then uses the upscaled force time series to accumulate the pore pressures or damage applied to the seabed , D, from the time history of applied loads from RSN curves, which are based on the mean, R, and cyclic amplitude, S, of the applied load cycles, N (Verruijt, 1995, Andersen, 2015 and Tom et al., 2019). K^2M^2 also handles consolidation and the updating of soil strength and other state parmeters using a critical state inspired (CSI) method as described in White et al., (2021). These are used to update the *Ancmac* spring-slider MAPs before before K^2M^2 moves to the next time domain simulation. Therefore, together, *Ancmac* and K^2M^2 predict the through-life changes in anchor capacity and movements of the anchor at the anchor point over different time scales and enable easy coupling with mooring-floater analyses which do not traditionally model these aspects. The following sub sections will briefly describe formulation of the MAP model components. The detailed formulation and benchmarking of the model has been is presented in separate studies (Kwa et al., 2021b, 2022, 2023).

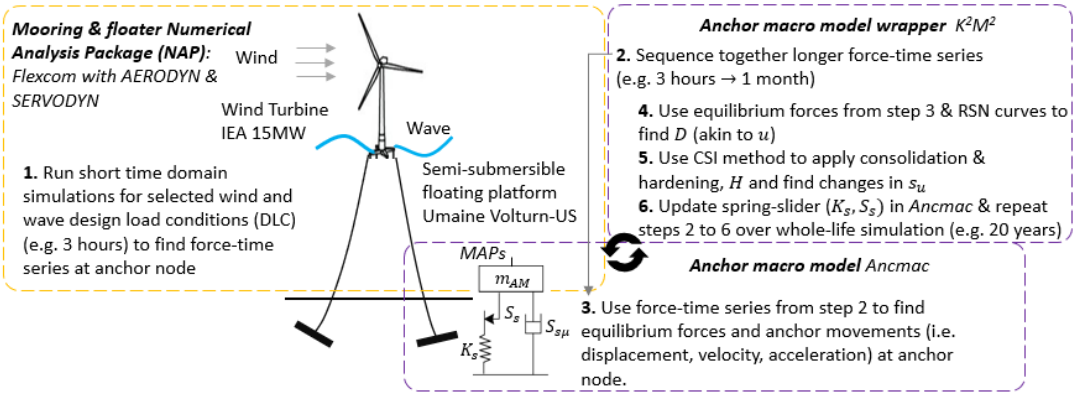

Figure 1: Anchor-mooring-floater model configuration

2.1.1 Spring-slider component

A parallel Iwan (PI) model defines the force-displacement responses in *Ancmac*. This consists of a number of spring-slider elements, connected in parallel and defined by parameters $K_{s,}$ and S_s. The number of spring-slider elements and their initial parameters can be derived from the monotonic backbone curve, as outlined in Kwa et al. (2022, 2023). The force in any spring, $F_{PI,n}$, is the product of the elastic displacement, δ_e, and the spring stiffness, $K_{s.}$ The elastic displacement is the difference between the total displacement, δ, and the plastic displacement, δ_p,

$$F_{PI,i} = K_{s,i}\,(\delta - \delta_p), \tag{1}$$

where if $abs(F_{PI,i}) > K_{s,i}$, the capacity of the slider has been exceeded and the value of the plastic displacement must be incremented by the change in total displacement. Therefore, the resulting force from the spring-sliders is given in equation 2,

$$F_{PI} = \min\left[\sum_{j=1}^{i} S_{s,j}\,, \sum_{j=i+1}^{n} K_{s,j}(\delta_j - \delta_{p,j})\right]. \tag{2}$$

During a whole-life analysis, the values of K_{si} or S_{si} are updated in the K^2M^2 routine to reflect a whole-life soil response where soil strength and therefore anchor capacity, Q_s, can evolve with time due to shearing and consolidation of the soil during sustained and variable low amplitude cyclic loads according to Equation 3;

$$Q_s = f(D, H, \{s_u\}, \tag{3}$$

where D is damage, which leads to a reduction in soil strength and varies by D=0→1. The damage is calculated using the RSN curves. The hardening, H, is also defined such that H=0→1, and is a result of the dissipation of damage. It reflects the progressive gain in soil strength as the soil densifies. Finally, $\{s_u\}$, is the potential range of undrained soil strengths. Defining Q_s in this manner enables the model to capture rises in the long-term capacity of anchor in a similar manner to established approaches for the capacity of surface foundations and pipelines (e.g. Bransby et al., 2002; Gourvenec et al., 2014; Cocjin et al., 2014; O'Loughlin et al., 2020). To update K_{si}, the model uses non-dimensionalised elastic responses and shear modulus vs

over consolidation ratio relationships (Houlsby et al., 1991) as defined in Equation 4;

$$K_{s,i} = G_s \frac{B}{2} K_\nu, \quad (4)$$

where B is anchor diameter, K_ν, is a dimensionless elastic stiffness coefficient dependent on Young's Modulus, ν=0.5, in undrained conditions and the anchor embedment ratio, both of which are assumed to be constant during the analyses. The shear modulus, G_s, is given by Equation 5;

$$G_s = \left(\frac{G_s}{s_u}\right)_{nc} (OCR^{\eta-\Lambda} \times s_u), \quad (5)$$

where $\left(\frac{G_s}{s_u}\right)_{nc}$ is the initial shear modulus to undrained strength of a normally consolidated soil, η is a fitting constant, typically taken as 0.5 in clays, Λ depends on the slopes of the normal compression and unloading/reloading lines λ and κ according to the relationship $\Lambda = \frac{\lambda-\kappa}{\lambda}$ and the over consolidation ratio, OCR, is related to hardening, H. Therefore, K_{si}, changes according to,

$$\frac{K_{s,i}}{K_{s,0}} = \frac{OCR_i^{\eta-\Lambda} \times s_{u.i}}{OCR_0^{\eta-\Lambda} \times s_{u.0}}. \quad (6)$$

The slider value, $S_{s,i}$, is related to changes in undrained strength as,

$$S_{s,i} = N_c \, s_u \left(\frac{B}{2}\right)^2 \pi \quad (7)$$

where N_c is the bearing capacity factor and is 13.11 for a deeply embedded a circular rough plate (Martin et al, 2001). Therefore, changes in the slider component are dependent on variations in the undrained strength as $\frac{S_{s,i}}{S_{s,0}} = \frac{s_{u.i}}{s_{u0}}$.

2.1.2 Dashpot component

Viscous rate effects are defined using a dashpot with a resistance proportional to the inverse hyperbolic sine of the strain rate or velocity as defined in (Randolph 2004). This has been used to find modified slider capacities, $S_{s\mu,i}$ to capture increases in undrained strength due to viscous soil effects as defined below.

$$S_{s\mu,i} = S_s \left(1 + \mu' sin\, h^{-1} \frac{\dot{\gamma}}{\gamma_{\dot{r}ef}}\right) \quad (8)$$

2.1.3 Added mass component

Extra dynamic anchor capacity can also be created from mobilising the mass of the soil surrounding the plate under highly dynamic snatch loading conditions (Kwa et al., 2021a). A lumped mass, m_{AM}, represents the mass of the anchor and soil around the anchor mobilised and a resistance force associated with having to accelerate this added mass according to Newton's 2nd Law. The added mass term can also be defined by a dimensionless added mass coefficient, N_{AM}, which under 2D plane strain and 3D axisymmetric cases are;

$$N_{AM,2D} = \frac{m_{AM}}{\rho B^2}, \; N_{AM,3D} = \frac{m_{AM}}{\rho B^3}, \quad (9)$$

where ρ is the density of the medium. These N_{AM} terms have been analytically determined for plate anchors embedded in soft clays in Kwa et al., (2021a) by using conventional geotechnical collapse mechanisms to derive the geotechnical counterpart to the established added mass solutions derived for fluid flow, and are approximately doubled compared to added mass mobilised in the inviscid fluid case (Table 1).

Table 1: Geotechnical and fluid inviscid added mass coefficients N_{AM} for embedded plate anchors

N_{AM}	Geotechnical	Fluid inviscid flow field
$N_{AM,2D}$	1.678[a], 3.356[b]	0.785
$N_{AM,3D}$	0.548[a], 0.599[b]	0.333

[a] rough, [b] smooth cases

2.2 Mooring-floater model

2.2.1 Flexcom model of a FOW Turbine

The modelling of the floater, turbine and mooring system was performed using Flexcom, a commercial FEM software. Flexcom offers fully-coupled aero-hydro-servo modelling using FAST plug-ins AERODYN and SERVODYN, and has been validated against other software as part of an offshore code collaboration project OC6 (Robertson et al. 2020). The FOW turbine model used in this study is composed of the International Energy Agency (IEA)15 MW wind turbine and the Umaine Volturn-US semi-submersible floating platform. The full platform and turbine characteristics are described in detail in NREL publications (Evan et al, 2020; Allen et al., 2020).

Two taut mooring configurations are considered (i) a conventional taut mooring system composed of high modulus synthetic polyester rope; and (ii) a taut mooring system, composed of the same polyester rope, with the addition of a polymer spring load reduction device (LRD) at each fairlead. This LRD, based on the Tfi Seaspring (Lozon et al., 2022), can safely operate at high strain (20-50%), thus providing high levels of elongation to reduce dynamic loads on mooring lines and anchors. The LRD is modelled with a 3-phase non-linear stiffness curve, to match the curve of the Tfi Seaspring. The general mooring parameters are shown in Table 2, with profile views of both configurations as shown in Figure 3, where the mooring lines are connected to the seafloor via a fixed pin connection.

Table 2: Mooring parameters for taut mooring systems

Parameter	Value
Water depth	150 m
Number of mooring lines	3
Anchor radius from platform centerline	260 m
Seabed-mooring line angle	34 deg
Polymer rope stiffness	7 MN
Polymer rope linear density	8.5 kg/m
Fairlead pre-tension	2000 kN

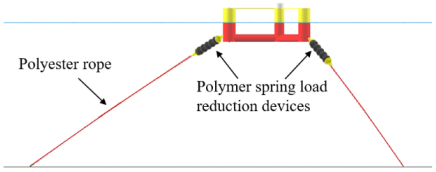

Figure 2: Profile view of taut mooring with load reduction devices (LRDs). The model of the conventional mooring system does not have the LRDs in the mooring lines.

2.2.2 Applied metocean conditions

Stochastic load cases were applied to the FOW model based on the IEA design load case (DLC) matrix. From the matrix of load cases, two operational load cases were selected, one above and below the turbine's rated wind speed, as well as the parked turbine cases for a storm and extreme 1-in-50 year storm, as summarised in Table 3.

Table 3: Summary of design load cases used in this study, selected from UMaine design matrix (Allen et al., 2020)

IEA DLC ref.	Load case description	Wind Speed	Sig. wave height	Peak wave period	Shape factor
1.1	Operational Below-rated	4 m/s	1.1 m	8.52 s	1.00
1.1	Operational Above-rated	12 m/s	1.84 m	7.44 s	1.00
6.3	Parked storm	38 m/s	6.98 m	11.70 s	2.75
6.1	1 in 50 year storm	47.5 m/s	10.70 m	14.20 s	2.75

All environmental loads are applied in the same direction and each simulation is run for 10800s (3 hours). The resulting force time-series was measured at the point where the windward mooring line attaches to the seafloor and these time-series were used to build synthetic yearly realisations reflecting seasonality in anchor loads in the example whole-life application described in Section 3.

3 WHOLE LIFE EXAMPLE APPLICATION

3.1 Applied loads on anchor

In this idealised example application of the anchor-mooring-floater model, the DLC combinations summarised in Table 3 were used to build synthetic anchor load cases, chosen to artificially reflect seasonality of metocean conditions within a year (i.e. calmer in summer and more severe in winter) as shown in Figure 4. This combination of DLCs was repeated over 20-years to idealise a design life time of anchor loads. To investigate the response of the system under an extreme loading event, the 1 in-50-year storm case was applied for a period of 3 hours at year 15 of the design lifetime. It was also assumed that the mooring line tensions were transmitted directly to the anchor. This is a slightly conservative approach as in reality, additional geotechnical resistance from interactions between the embdedded mooring line section and the seabed would reduce the load transmitted to the anchor. Based on analytical solutions for the frictional capacity of embedded anchor chains (Neubecker et al., 1995), this decrease in load would be ~10%.

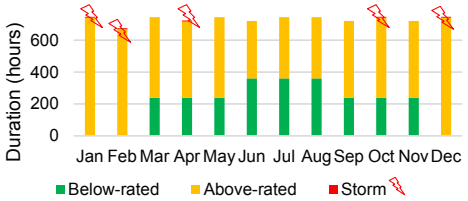

Figure 3: Idealised yearly metocean conditions

3.2 Seabed response and anchor capacity

The seabed input parameters to *Ancmac* and K^2M^2 were selected to be representative of lightly over consolidated clay around a circular plate anchor embedded at a depth of ~20m. The selected seabed values are similar to those reported by O'Loughlin et al., (2020) and Zhou et al., (2020), with an initial undrained strength, s_{u0} =80kPa, coefficient of consolidation, c_v=6m/s^2, and sensitivity, S_t=2.5, at the anchor point. When seabed hardening was enabled, both seabed softening and whole-life seabed strengthening effects were included in the analysis. The required anchor size was determined from running the whole-life simulation and setting a minimum factor of safety, FoS≥ 1, where the FoS is the ratio of the static anchor capacity, $Q_s = N_c s_u A$ to T_{max}, to the maximum applied tension in each simulated month.

The different whole-life seabed responses with and without hardening enabled, are summarised in Figures 4. In the case where a conventional taut mooring was used to generate the input anchor loads, the damage imposed on the seabed increased significantly during the first year (Figure 4a) and this corresponded to a decrease to the minimum through-life undrained strength, anchor capacity (Figure 4c,d) during the whole-life simulation. The damage remained at a maximum, D=1, until year-5, when D started to decrease as the seabed softening effects were eclipsed by consolidation and increases in hardening and undrained strength when hardening was enablled (Figure 4b,c). At year-5, the seabed strength recovered to s_{u0} and subsequently increased to a final normalised value of 1.3× s_{u0} and initial anchor capacity, Q_{s0}. If hardening was not enabled, s_u, decreased and remained at 0.6 × s_{u0} and Q_{s0} and larger anchors were required to achieve a FoS≥ 1 to withstand the 1-in-50 year storm applied at 15 years. In the case where a LRD was incorporated in the mooring and hardening enabeled, the final normalised undrained strength and anchor capacities were similar to the case

where conventional mooring case loads were applied (at $\sim 1.6 \times s_{u0}$ and Q_{s0}). This is a result of the smaller applied anchor loads, which resulted in less seabed damage and therefore smaller and more gradual changes in s_u and Q_s, which are balanced by smaller increases in hardening over the design lifetime. When hardening was disabled, similar to in the conventional mooring case, s_u and Q_s decreased towards a minmum value of $0.6 \times s_{u0}$ and Q_{s0}, and as a result a larger anchor was required and this contributed to a more gradual increase in damage over the design lifetime towards $D \rightarrow 1$.

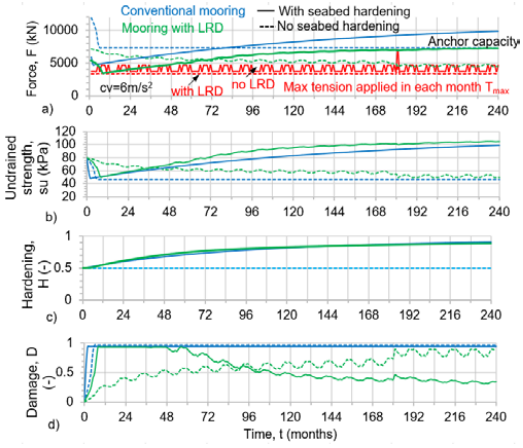

Figure 4 Summary of seabed (a) damage, (b) hardening, (c) changes in undrained strength and (d) anchor capacity relative to applied tension loads

Minimum required anchor sizes for a taut mooring with and without a LRD, and with and without seabed hardening enabled during the simulations are summarised in Table 4. Introducing LRDs into the taut mooring system reduces anchor size by 30%. This is a result of smaller loads being transmitted to the anchor. Separately including beneficial whole-life seabed hardening effects in the analysis reduces anchor size for both conventional taut mooring and mooring with LRD, by 37 and 30% respectively. Finally, when both LRD and whole-life seabed effects are considered together, the minimum required achor size is more than halved.

Table 4: Comparison of minimum required anchor size

Taut mooring case	**Required anchor size, A (m²)**	
	No seabed hardening	**With seabed hardening**
Conventional mooring	11.9	7.5
Mooring with LRD	7.5	5.3

4 CONCLUSIONS

This study presents an anchor macro model, which captures seabed response when coupled with a mooring-floater FEM. Results from an example whole-life application of the anchor-mooring-floater model demonstrate how it can be used to assess the through-life changes in seabed response and anchor capacity. Results show a possible 50% decrease in the required anchor size from combining beneficial effects of LRDs in the mooring lines, and whole-life seabed strenthenging effects, which is more than if either effect were considered separately. If dynamic anchor capacity were also considered and the anchor is permitted to move, rather than be treated as a fixed pin connection in mooring analyses, then this could also lead to further reductions in the required anchor size.

5 ACKNOWLEDGEMENTS

This work forms part of research supported by the Royal Academy of Engineering under the Research Fellowship Programme, RAEng Chair in Emerging Technologes Centre of Excellence in Intelligent & Resilient Ocean Engineering (IROE), and Supergen ORE Hub (Grant EPSRC EP/S000747/1). Katherine Kwa is supported by the RAEng Research Fellowship Scheme, David White is supported by the Supergen ORE Hub, Susan Gourvenec is supported by the Royal Academy of Engineering through the Chair in Emerging Technologies scheme, and Adam Sobey is supported by The Lloyd‘s Register Foundation.

6 REFERENCES

Allen, C. et al. (2020) Definition of the UMaine VolturnUS-S Reference Platform Developed for the IEA Wind 15MW Offshore Reference Wind Turbine. Golden, CO: National Renewable Energy Laboratory. NREL/TP-5000-76773

Andersen, K. H. (2015). Cyclic soil parameters for offshore foundation design. Frontiers in offshore geotechnics III 5.

Bransby, M.F. (2002) The undrained inclined load capacity of shallow foundations after consolidation under vertical loads. In Num. Models in Geomech: 8th Int Symp. Rotterdam, Netherlands, Balkema

Cassidy M.J.,et al. 2012. A plasticity model to assess the keying of plate anchors. Géot., 62(9): 825–836

Cocjin M., et al. (2014) Tolerably mobile subsea foundations –Observations of performance. Géot. 64(11): 895-909.

Deeks, A., et al. (2014) Design of direct on-seabed sliding foundations, OMAE2014-24393, V003T10A024

DNV (2002). DNG-RP-E302: Recommended practices: design &installation of plate anchors in clay. DNV

Evan, G. et al. 2020. Definition of the IEA 15-Megawatt Offshore Reference Wind. Golden, CO: National Renewable Energy Laboratory. NREL/TP-5000-75698.

Gourvenec, S., et al. (2014). A method for predicting the consolidated undrained bearing capacity of shallow foundations. Géot., 64(3), pp.215-225

Gourvenec, S. (2020) Whole-life geotechnical design: What is it? What’s it for? So what? And what next? Proc. 4th International Symposium on Frontiers in Offshore Geotechnics, Austin, Texas, USA, Ed. Westgate, Z., ASCE Geo-Institute and DFI, ISBN: 978-0-9763229-4-8

Heath, J. E. et al. (2017). Applicability of geotechnical approaches & constitutive models for foundation analysis

of marine renewable energy arrays. Renew. & Sust. Energy Reviews, 72, 191-204.
Houlsby, G.T. & Martin, C.M. (1992) Modelling of the behaviour of foundations of jack-up units on clay. Proc. Wroth Memorial Symp. Predictive Soil Mech., Oxford
Houlsby, G. T., & Wroth, C. P. (1991). The variation of shear modulus of a clay with pressure and overconsolidation ratio. Soils & Found., 31(3), 138-143.
Iwan, W. D. (1967). On a class of models for the yielding behavior of continuous & composite systems.
Jostad, H. P., et al. (2020). Evaluation of soil models for improved design of offshore wind turbine foundations in dense sand. Géot., 70(8), 682-699
Kwa, K.A. et al. (2022) A numerical macro model to simulate the whole life response of anchors for floating offshore renewable energy systems. OMAE 2022-81101, V009T10A003 Hamburg, Germany.
Kwa, K.A., et al. (2021a). Analysis of the added mass term in soil bearing capacity problems. Géotech Lett, 11(1):.80-87
Kwa, K. A., & White, D. J. (2021b). Enhanced anchoring systems for MRE infrastructure:'whole life'soil-anchor-floating system interactions. 14th EWTEC, Plymouth, UK
Kwa, K.A., et al. (2023) The RSN-CSI model: A whole life geotechnical anchor macro model for floating offshore systems submitted to Computers and Geotechnics
Martin, C. M. & Randolph, M. F. (2001). Applications of the lower & upper bound theorems of plasticity to collapse of circular foundations. 10th Int. Conf. Computer Methods and Advances in Geomech.
Martin, C. M. & Randolph, M. F. (2001). Applications of the lower &upper bound theorems of plasticity to collapse of circular foundations.10th Int. Conf. Computer Methods and Advances in Geomech.
Nova R. & Montrasio L (1991) Settlements of shallow foundations on sand. Geot.,41(2): 243-256.
Neubecker, S.R. and Randolph, M.F., 1995. Profile and frictional capacity of embedded anchor chains. Journal of geotechnical engineering, 121(11), pp.797-803.
O'Loughlin, C.D., et al. (2017). Plate Anchors for Mooring Floating Facilities–A View Towards Unlocking Cost & Risk Benefits. In Offshore Site Investigation Geotech 8th Int. Conf. Proc, pp. 978-986).
O'Loughlin, C. D., et al. (2020). Load-controlled cyclic T-bar tests: a new method to assess effects of cyclic loading & consolidation Géot. Let., 10(1), 7-15.
Peccin da Silva, A., et al. (2021). A non-associative macro-element model for vertical plate anchors in clay. Canadian Geo. J.
Randolph, M., (2004). Characterisation of soft sediments for offshore applications, Geotech & Geophys. Site Charac., Rotterdam.
Robertson, A. N., et al. (2020). OC6 Phase I: Investigating the underprediction of low-frequency hydrodynamic loads and responses of a floating wind turbine. In Journal of Physics: Conference Series (Vol. 1618, No. 3, p. 032033).
Smith V. B. & White D. J. (2014) Volumetric hardening in axial pipe soil interaction. Offshore Tech. Conf. Asia, OTC ASIA 2014 (Vol. 2, pp. 1611-1621).
Schotman, G.J.M. (1989). The effects of displacements on the stability of jackup spudcan foundations. 21st Offshore Tech. Conf., Houston, Texas, OTC 6026.
Stanier, S.A. & White, D.J., (2018). Enhancement of bearing capacity from consolidation: due to changing strength or failure mechanism?. Géot., 69(2), pp.166-173.
Tom, J.G., et al., 2019, June. Fluid-structure-soil interaction of a moored wave energy device. In International Conference on OMAE (Vol. 58899, p. V010T09A024). ASME
Verruijt, A. (1995).Computational geomechanics (Vol. 7). Springer Science & Business Media.
White, D. J., et al (2021). A cyclic py model for the whole-life response of piles in soft clay. Computers & Geotechnics, 141, 104519.
Zhou, Z., et al. (2020). Improvements in plate anchor capacity due to cyclic and maintained loads combined with consolidation. Géotechnique, 70(8), pp.732-749.

References

[1] H. Putuhena, F. Sturt, and S. Gourvenec. The world needs 200,000 offshore wind turbines by
2050: Mapping the locations, constraints. *Energy Post*, 2023. URL https://energypost.eu/the-world-needs-200000-offshore-wind-turbines-by-2050-mapping-the-locations-constra
Accessed: 2024-08-05.

[2] IEA. Credible pathways to 1.5 , 2023. URL https://iea.blob.core.windows.net/assets/ea6587a0-ea87-4a85-8385-6fa668447f02/Crediblepathwaysto1.5C-Fourpillarsforactioninthe2020s.pdf.

[3] Burges Salmon - News & Insight. Floating wind – challenges and opportunities for a buoyant technology, 2021. URL https://www.burges-salmon.com/news-and-insight/legalupdates/energy-power-utilities/floating-wind-challenges-andopportunities-for-a-buoyant-technology#ftn1.

[4] SBM Offshore. Sbm offshore full year 2023 earnings, 2024. URL https://www.sbmoffshore.com/sites/sbm-offshore/files/PR/2024/SBM%20Offshore%20Full%20Year%202023%20Earnings.pdf.

[5] S. Strivens, E. Northridge, H. Evans, and M. Harvey. Floating wind joint industry project: Phase iii summary report. Technical report, The Carbon Trust, 2021. URL https://www.carbontrust.com/our-work-and-impact/guides-reports-and-tools/floating-wind-joint-industry-project-phase-iii-summary-report. Produced with contributions from ABL Group, Leask Marine, Wood Thilsted, Exeter Consulting, and First Marine Energy.

[6] K. Ma, Y. Wu, S.F. Stolen, L. Bello, M. ver der Horst, and Y. Luo. Mooring designs for floating offshore wind turbines leveraging experience from the oil & gas industry. volume 1 of *International Conference on Offshore Mechanics and Arctic Engineering*, Jun 2021. . URL https://doi.org/10.1115/OMAE2021-60739.

[7] K. Xu, K. Larsen, Y. Shao, M. Zhang, Z. Gao, and T. Moan. Design and comparative analysis of alternative mooring systems for floating wind turbines in shallow water with emphasis on ultimate limit state design. *Ocean Engineering*, 219, Nov 2020. . URL https://www.sciencedirect.com/science/article/pii/S0029801820312841.

[8] J. Cruz and A. Mairead. *Floating Offshore Wind Energy: The Next Generation of Wind Energy*. Green Energy and Technology. Springer, 2016. ISBN 9783319293967. URL http://search.ebscohost.com/login.aspx?direct=true&db=nlebk&AN=1282129&site=ehost-live.

[9] K. Ma, Y. Luo, T. Kwan, and Y. Wu. Chapter 4 - mooring design. In *Mooring System Engineering for Offshore Structures*, pages 63–83. Gulf Professional Publishing, 2019. ISBN 978-0-12-818551-3. . URL https://www.sciencedirect.com/science/article/pii/B9780128185513000041.

[10] Acteon Group. Scaling up for floating wind, 2024. URL https://acteon.com/blog/scaling-up-for-floating-wind/. Accessed: 2024-08-09.

[11] *Polymer Mooring Component for Offshore Renewable Energy*, volume Day 3 Wed, May 08, 2019 of *OTC Offshore Technology Conference*, May 2019. . URL https://doi.org/10.4043/29587-MS. D031S033R004.

[12] P. McEvoy and S. Kim. Mooring load management for sr2000 floating tidal device using non-linear polymer components. 12th European Wave and Tidal Energy Conference, 2017. URL https://uploads-ssl.webflow.com/5f8964a5a533790d6cc8820a/5f96cb7a8ba32845a778cb9e_EWTEC-2017.pdf.

[13] Dublin Offshore. Load reduction device (LRD) – how it works, 2020. URL https://www.dublinoffshore.ie/media/pages/technology/6f4e7419f6-1635594571/how-it-works.pdf.

[14] International Electrotechnical Commission. IEC 61400-3:2019 - wind energy generation systems - part 3: Design requirements for offshore wind turbines, 2019. URL https://www.iso.org/standard/72447.html. Accessed: March 24, 2023.

[15] R.R. Rhinehart. *Engineering Optimization: Applications, Methods and Analysis*. Wiley, 2018. ISBN 9781118936337.

[16] A. Pillai, P. Thies, and L. Johanning. Mooring system design optimization using a surrogate assisted multi-objective genetic algorithm. *Engineering Optimization*, 51(8): 1370–1392, 2019. .

[17] *Mooring Optimization Using ML Techniques*, volume ASME 2022 4th International Offshore Wind Technical Conference of *International Conference on Offshore Mechanics and Arctic Engineering*, Dec 2022. . URL https://doi.org/10.1115/IOWTC2022-98217.

[18] Emma C. Edwards, Anna Holcombe, Scott Brown, Edward Ransley, Martyn Hann, and Deborah Greaves. Trends in floating offshore wind platforms: A review of early-stage devices. *Renewable and Sustainable Energy Reviews*, 193:114271, 2024. ISSN 1364-0321. . URL https://www.sciencedirect.com/science/article/pii/S1364032123011292.

[19] Matti Scheu, Denis Matha, Marie-Antoinette Schwarzkopf, and Athanasios Kolios. Human exposure to motion during maintenance on floating offshore wind turbines.

Ocean Engineering, 165:293–306, 2018. ISSN 0029-8018. . URL https://www.sciencedirect.com/science/article/pii/S002980181831254X.

[20] COREWIND. D2.1: Review of the state of the art of mooring and anchoring designs, technical challenges and identification of relevant dlcs. 2020. URL https://corewind.eu/wp-content/uploads/files/publications/COREWIND-D2.1-Review-of-the-state-of-the-art-of-mooring-and-anchoring-designs.pdf.

[21] M. Randolph and S. Gourvenec. *Offshore Geotechnical Engineering*. 2011. ISBN 9780415477444. .

[22] L. Xiong, D. White, S. Neubecker, W. Zhao, and J. Yang. Anchor loads in taut moorings: The impact of inverse catenary shakedown. *Applied Ocean Research*, 67:225–235, 2017. ISSN 0141-1187. . URL https://www.sciencedirect.com/science/article/pii/S0141118716304540.

[23] QuestFWE. The definitive guide to floating wind energy concepts. 2020. URL https://questfwe.com/definitive-guide-to-floating-wind-concepts/.

[24] T. Choisnet and E. Rogier. Performance and mooring qualification in floatgen: the first french offshore wind turbine project. *16ème Journèes de l'Hydrodynamique*, 1:1–10, 2018.

[25] Windfloat atlantic marks first ever lankhorst dyneema® dm20 mooring. URL https://www.lankhorstoffshore.com/about-us/news-events/windfloat-atlantic-marks-first-ever-lankhorst-dyneema-dm20-mooring.

[26] ORE Catapult and ARUP. Floating offshore wind anchor review. *FOW Centre of Excellence Public Summary Reports*, 2024. URL https://fowcoe.co.uk/wp-content/uploads/2024/03/FOWCoE-Report-Anchor-Review-PN000585-RPT-005-MA03.pdf.

[27] K. Mueller, D. Matha, S. Tidedmann, R. Proskovics, and F. Lemmer. Qualification of innovative floating substructures for 10mw wind turbines and water depths greater than 50m, 2016. URL https://lifes50plus.eu/wp-content/uploads/2015/12/GA_640741_LIFES50plus_D7.1.pdf.

[28] *Design of Mooring Lines of Floating Offshore Wind Turbine in Jeju Offshore Area*, volume Volume 9A: Ocean Renewable Energy of *International Conference on Offshore Mechanics and Arctic Engineering*, Jun 2014. . URL https://doi.org/10.1115/OMAE2014-23772. V09AT09A042.

[29] Principle Power, Inc. Windfloat pacific project, final scientific and technical report. Technical Report DE-EE0005987, Principle Power, Inc., Emeryville, CA (United States), United States, 2016. URL https://www.osti.gov/biblio/1339449.

[30] Atul Agarwal, Vengatesan Venugopal, and Gareth Harrison. The assessment of extreme wave analysis methods applied to potential marine energy sites using numerical model data. *Renewable and Sustainable Energy Reviews*, 27:244–257, Nov 2013. .

[31] DNV-GL. Dnvgl-rp-0286: Coupled analysis of floating wind turbines, 2019. URL https://rules.dnv.com/docs/pdf/DNV/RP/2019-05/DNVGL-RP-0286.pdf.

[32] J. Jonkman. Dynamics modeling and loads analysis of an offshore floating wind turbine. Technical Report NREL/TP-500-41958, National Renewable Energy Lab (NREL), Golden, CO (United States), 2007. URL https://www.nrel.gov/docs/fy08osti/41958.pdf.

[33] M. Taboada, A. Ortega, R. Martín, A. Pombo, and J. Moreu. An evaluation of the effect that motions at the nacelle have on the cost of floating offshore wind turbines. OTC Offshore Technology Conference, May 2020. . URL https://doi.org/10.4043/30632-MS.

[34] K. Ma, Y. Luo, T. Kwan, and Y. Wu. Chapter 15 - mooring for floating wind turbines. In K. Ma, Y. Luo, T. Kwan, and Y. Wu, editors, *Mooring System Engineering for Offshore Structures*, pages 299–315. Gulf Professional Publishing, 2019. ISBN 978-0-12-818551-3. . URL https://www.sciencedirect.com/science/article/pii/B9780128185513000156.

[35] *Critical Issues in the Design of FOWT Mooring Systems when Comparing to Oil & Gas Industry Standards*, volume Day 1 Tue, February 16, 2016 of *SNAME Offshore Symposium*, Feb 2016. D013S003R001.

[36] COREWIND. D3.1 review of the state of the art of dynamic cable system design. 2020. URL https://ec.europa.eu/research/participants/documents/downloadPublic?documentIds=080166e5cca0f37e&appId=PPGMS.

[37] RTE France. College of distinguished experts: The expertise for tomorrow's network. Technical report, RTE France, 2022. URL https://assets.rte-france.com/prod/public/2022-08/College%20of%20distinguished%20experts%2C%20the%20expertise%20for%20tomorrow%E2%80%99s%20network.pdf. Accessed: 2024-08-09.

[38] International Standards Organisation. Iso 19901-7:2013 petroleum and natural gas industries — specific requirements for offshore structures — part 7: Stationkeeping systems for floating offshore structures and mobile offshore units. 2013.

[39] *API RP 2SK 4th Edition - An Updated Stationkeeping Standard for the Global Offshore Environment*, volume Day 1 Mon, April 30, 2018 of *OTC Offshore Technology Conference*, Apr 2018. . URL https://doi.org/10.4043/29024-MS. D011S004R001.

[40] American Bureau of Shipping. Design guideline for stationkeeping systems of floating offshore wind turbines. 2013. URL https://www.bsee.gov/sites/bsee.gov/files/tap-technical-assessment-program/tar705finalreport.pdf.

[41] Det Norske Veritas. Dnv-os-j103: Design of floating wind turbine structures. 2013. URL https://pdf4pro.com/view/dnv-os-j103-design-of-floating-wind-turbine-structures-5b8dfe.html.

[42] Lloyd's Register. Lr-rp-003: Recommended practice for floating offshore wind turbine support structures. 2024. URL https://www.lr.org/en/knowledge/lloyds-register-rules/recommended-practice-for-floating-offshore-wind-turbine-support-structures/.

[43] Bureau Veritas. Ni572: Classification and certification of floating offshore wind turbines. 2015. URL https://marine-offshore.bureauveritas.com/ni572-classification-and-certification-floating-offshore-wind-turbines.

[44] E. Jump. Mooring and anchoring systems - market projections. Technical report, Floating Offshore Wind Centre of Excellence, ORE Catapult, October 2021. URL https://cms.ore.catapult.org.uk/wp-content/uploads/2021/12/PN000413-RPT-003-Rev-2-Mooring-and-Anchoring-Market-Projections_Formatted.pdf. Accessed: 2024-08-09.

[45] L. Méchinaud, M. Chemineau, F. Castillo, M.Y. Mahfouz, Q. Pan, L. Willeke, H. Bredmose, O. Gözcü, and N. Pollini. Exploration of innovations and breakthroughs of station keeping systems for fowt. Technical report, COREWIND, August 2022. URL https://corewind.eu/wp-content/uploads/files/delivery-docs/D2.3.pdf. Deliverable D2.3, Reviewed by Pau Trubat (UPC), Climent Molins (UPC), Tim Habekost (UL), Jean-Christophe Gilloteaux (INNOSEA), Accessed: 2024-08-09.

[46] COREWIND. D1.2 design basis. 2019. URL https://corewind.eu/wp-content/uploads/files/publications/COREWIND-D1.2-03-Design-Basis.pdf.

[47] W. Formosa and T. Sant. Modelling the loads and motions of a floating offshore wind turbine with asymmetric moorings. *Journal of Physics: Conference Series*, 2362:012013, 2022. . URL https://iopscience.iop.org/article/10.1088/1742-6596/2362/1/012013/pdf. EERA DeepWind Offshore Wind R&D Conference.

[48] F. Castillo. Floating offshore wind turbines: Mooring system optimization for lcoe reduction, 2020. URL http://kth.diva-portal.org/smash/get/diva2:1484541/FULLTEXT01.pdf.

[49] S. Banfield, T. Versavel, R.O. Snell, R.V. Ahilan, et al. Fatigue curves for polyester moorings—a state-of-the-art review. In *Offshore Technology Conference*. Offshore Technology Conference, 2000.

[50] E. Lozon, M. Hall, P. McEvoy, S. Kim, and B. Ling. Design and analysis of a floating-wind shallow-water mooring system featuring polymer springs. volume 486 of *International Offshore Wind Technical Conference*, 2022.

[51] *Influence of Mean Tension on Mooring Line Fatigue Life*, volume 2A: Structures, Safety, and Reliability of *International Conference on Offshore Mechanics and Arctic Engineering*, Aug 2020. . URL https://doi.org/10.1115/OMAE2020-18628.

[52] *Mean Load Impact on Mooring Chain Fatigue Capacity: Lessons Learned From Full Scale Fatigue Testing of Used Chains*, volume Volume 3: Structures, Safety, and Reliability of *International Conference on Offshore Mechanics and Arctic Engineering*, Jun 2019. . URL https://doi.org/10.1115/OMAE2019-95083. V003T02A058.

[53] O. Festa, S. Gourvenec, and A. Sobey. Proxy model for the design of extensible floating offshore wind turbine mooring systems. International Ocean and Polar Engineering Conference, Jun 2022. URL https://eprints.soton.ac.uk/457472/1/2022_Festa_et_al_ISOPE.pdf.

[54] K. Xu, K. Larsen, Y. Shao, M. Zhang, Z. Gao, and T. Moan. Design and comparative analysis of alternative mooring systems for floating wind turbines in shallow water with emphasis on ultimate limit state design. *Ocean Engineering*, 219:108377, 2021. ISSN 0029-8018. . URL https://www.sciencedirect.com/science/article/pii/S0029801820312841.

[55] S. Weller, L. Johanning, P. Davies, and S. Banfield. Synthetic mooring ropes for marine renewable energy applications. *Renewable Energy*, 83:1268–1278, 2015. ISSN 0960-1481. . URL https://www.sciencedirect.com/science/article/pii/S0960148115002402.

[56] *Mooring Line Dynamics: Comparison of Time Domain, Frequency Domain, and Quasi-Static Analyses*, volume All Days of *OTC Offshore Technology Conference*, May 1991. . URL https://doi.org/10.4043/6657-MS. OTC-6657-MS.

[57] W. West, A. Goupee, A. Viselli, and H. Dagher. The influence of synthetic mooring line stiffness model type on global floating offshore wind turbine performance. *Journal of Physics: Conference Series*, 1452:012044, Jan 2020. .

[58] Z. Lin and P. Sayer. An enhanced stiffness model for elastic lines and its application to the analysis of a moored floating offshore wind turbine. *Ocean Engineering*, 109:444–453, 2015. ISSN 0029-8018. . URL https://www.sciencedirect.com/science/article/pii/S0029801815004679.

[59] American Bureau of Shipping. Abs-90: Guidance notes on the application of fiber rope for offshore mooring. 2012. URL https://standards.globalspec.com/std/1388545/90.

[60] M. Bach-Gansmo, S. Garvik, J. Thomsen, and M. Andersen. Parametric study of a taut compliant mooring system for a fowt compared to a catenary mooring. *Journal of Marine Science and Engineering*, 8, Jun 2020. .

[61] I. Ridge, S.J. Banfield, and J. Mackay. Nylon fibre rope moorings for wave energy converters. *OCEANS 2010 MTS/IEEE SEATTLE*, pages 1–10, 2010.

[62] M. Wu et al. Experimental study of motion and mooring behavior of a floating oscillating water column wave energy converter. *Coastlab 2018*, pages 1–8, 2018.

[63] A.S. Varney, R. Taylor, and W. Seelig. Evaluation of wire-lay nylon mooring lines in a wave energy device field trial. *2013 OCEANS - San Diego*, pages 1–5, 2013. .

[64] A. Vickers and L. Johanning. Comparison of damping properties for three different mooring arrangements. *Proceedings of the 8th European Wave and Tidal Energy Conference, Uppsala, Sweden, 2009*, 2009. URL http://www.homepages.ed.ac.uk/shs/Wave%20Energy/EWTEC%202009/EWTEC%202009%20(D)/papers/267.pdf.

[65] H. Pham, P. Cartraud, F. Schoefs, T. Soulard, and C. Berhault. Dynamic modeling of nylon mooring lines for a floating wind turbine. *Applied Ocean Research*, 87:1–8, 2019. ISSN 0141-1187. . URL https://www.sciencedirect.com/science/article/pii/S0141118718307296.

[66] Brydon. Moorline polyester [Datasheet], 2022. URL https://www.brydon.com/products/moorline-polyester.

[67] Stian H. Sørum, Nuno Fonseca, Michael Kent, and Rui Pedro Faria. Modelling of synthetic fibre rope mooring for floating offshore wind turbines. *Journal of Marine Science and Engineering*, 11(1), 2023. ISSN 2077-1312. . URL https://www.mdpi.com/2077-1312/11/1/193.

[68] P. McEvoy. Combined elastomeric & thermoplastic mooring tethers. In *Proceedings of the 4th International Conference on Ocean Energy, Dublin, Ireland*, pages 17–19, 2012.

[69] M. Harrold, P. Thies, L. Johanning, D. Newsam, M. Checkley, and C. Bittencourt Ferreira. Dynamic load reduction and station keeping mooring system for floating offshore wind. In *ASME 2018 1st International Offshore Wind Technical Conference*. American Society of Mechanical Engineers Digital Collection, 2018.

[70] D.M. Wyman. Elastic tethering techniques for surface and near-surface buoy systems. *IEEE*, 1982. ISSN 0197-7385.

[71] P. Walter, I. Jim, G. Jason, and G. Mark. Taut elastomeric and chain catenary surface buoy moorings. *Coastal Mooring Design*, Jun 1998.

[72] A. Bowie. Flexible moorings for tidal current turbines. *Sustainable Engineering: Renewable Energy Systems and the Environment*, 2012. URL http://www.esru.strath.ac.uk/Documents/MSc_2012/Bowie.pdf.

[73] P. Thies, L. Johanning, and P. McEvoy. A novel mooring tether for peak load mitigation: Initial performance and service simulation testing. *International Journal of Marine Energy*, 7, Jul 2014. .

[74] D. Parish. A novel mooring tether for highly dynamic offshore applications. 2015. URL https://ore.exeter.ac.uk/repository/handle/10871/21337.

[75] T. Gordelier, D. Parish, P. Thies, and L. Johanning. A novel mooring tether for highly-dynamic offshore applications; mitigating peak and fatigue loads via selectable axial stiffness. *Journal of Marine Science and Engineering*, 3(4):1287–1310, 2015.

[76] T. Gordelier, D. Parish, P. Thies, S. Weller, P. Davies, P.Y. Le Gac, and L. Johanning. Assessing the performance durability of elastomeric moorings: Assembly investigations enhanced by sub-component tests. *Ocean Engineering*, 155:411–424, 2018. ISSN 0029-8018. . URL https://www.sciencedirect.com/science/article/pii/S0029801818301549.

[77] D. Parish, M. Herduin, P. Thies, T. Gordelier, and L. Johanning. Reducing peak & fatigue mooring loads: A validation study for elastomeric moorings. 2017. URL https://ore.exeter.ac.uk/repository/handle/10871/29126.

[78] S. Weller, P. Davies, A.W. Vickers, and L. Johanning. Synthetic rope responses in the context of load history: Operational performance. *Ocean Engineering*, 83:111–124, Jun 2014. .

[79] M. Harrold, P. Thies, D. Newsam, C. Ferreira, and L. Johanning. Large-scale testing of a hydraulic non-linear mooring system for floating offshore wind turbines. *Ocean Engineering*, 206:107386, 2020. ISSN 0029-8018. . URL https://www.sciencedirect.com/science/article/pii/S0029801820304145.

[80] J. Luxmoore, S. Grey, D. Newsam, and L. Johanning. Analytical performance assessment of a novel active mooring system for load reduction in marine energy converters. *Ocean Engineering*, 124:215–225, 2016. . URL https://www.sciencedirect.com/science/article/pii/S0029801816302955.

[81] J. Luxmoore, P. Thies, S. Grey, D. Newsam, and L. Johanning. Performance and reliability testing of an active mooring system for peak load reduction. *Proceedings of the Institution of Mechanical Engineers, Part M: Journal of Engineering for the Maritime Environment*, 232(1): 130–140, 2018.

[82] OffshoreWind.biz. EMEC verifies Dublin Offshore's floating wind mooring component, Mar 2021. URL https://www.offshorewind.biz/2021/03/12/emec-verifies-dublin-offshores-floating-wind-mooring-component/.

[83] D. Hayes, D. Golden, and T. Doyle. Load reduction device: Floating wind technology acceleration competition executive summary. Technical report, Dublin Offshore Consultants Limited, June 2021. URL https://www.dublinoffshore.ie/updates/malin-sea-wind-project. Project funded by the Scottish Government and managed by the Carbon Trust's Floating Wind Joint Industry Project (FLW JIP).

[84] Dublin Offshore. Malin sea wind project, 2024. URL https://www.dublinoffshore.ie/updates/malin-sea-wind-project. Accessed: 2024-08-09.

[85] Wei-Hua Huang and Ray-Yeng Yang. Water depth variation influence on the mooring line design for fowt within shallow water region. *Journal of Marine Science and Engineering*, 9: 409, Apr 2021. .

[86] J. Martins and A. Ning. *Engineering Design Optimization*. Cambridge University Press, 2021. ISBN 9781108833417.

[87] M. Altinakar and H. Qi. Numerical-simulation based multiobjective optimization of agricultural land-use with uncertainty. May 2008. .

[88] R.M. Burkart. Advanced modeling and multi-objective optimization of power electronic converter systems. 2016. URL https://api.semanticscholar.org/CorpusID:54720313.

[89] J. Davidson and J. Ringwood. Mathematical modelling of mooring systems for wave energy converters—a review. *Energies*, 10(5), 2017. ISSN 1996-1073. . URL https://www.mdpi.com/1996-1073/10/5/666.

[90] C. Hand Z. Zhang. The influence of different mooring line models on the stochastic dynamic responses of floating wind turbines. *Journal of Physics: Conference Series*, 1037: 062016, Jun 2018. . URL https://doi.org/10.1088/1742-6596/1037/6/062016.

[91] M. Jameel, A. Ibrahim, S. Ahmad, and Z. Jumaat. Effect of moorings drag and inertia on response of spar platform. *KSCE Journal of Civil Engineering*, 21, Feb 2017. .

[92] G. Benassai, A. Campanile, V. Piscopo, and A. Scamardella. Optimization of mooring systems for floating offshore wind turbines. *Coastal Engineering Journal*, 57:19, Oct 2015. .

[93] M. Brommundt, L. Krause, K. Merz, and M. Muskulus. Mooring system optimization for floating wind turbines using frequency domain analysis. *Energy Procedia*, 24:289–296, 2012. ISSN 1876-6102. . URL https://www.sciencedirect.com/science/article/pii/S1876610212011514. Selected papers from Deep Sea Offshore Wind R&D Conference, Trondheim, Norway, 19-20 January 2012.

[94] M. Masciola, J. Jonkman, and A. Robertson. Extending the capabilities of the mooring analysis program: A survey of dynamic mooring line theories for integration into fast. *Proceedings of the International Conference on Offshore Mechanics and Arctic Engineering - OMAE*, 9, Jun 2014. .

[95] J. Lim, M. Choi, and S. Lee. A bayesian optimization algorithm for the optimization of mooring system design using time-domain analysis. *Journal of Marine Science and Engineering*, 11(3), 2023. ISSN 2077-1312. . URL https://www.mdpi.com/2077-1312/11/3/507.

[96] F.M.G. Ferreira, E.N. Lages, S.M.B. Afonso, and P.R.M. Lyra. Dynamic design optimization of an equivalent truncated mooring system. *Ocean Engineering*, 122:186–201,

2016. ISSN 0029-8018. . URL https://www.sciencedirect.com/science/article/pii/S0029801816302001.

[97] W. West, A. Goupee, S. Hallowell, and A. Viselli. Development of a multi-objective optimization tool for screening designs of taut synthetic mooring systems to minimize mooring component cost and footprint. *Modelling*, 2(4):728–752, 2021. ISSN 2673-3951. . URL https://www.mdpi.com/2673-3951/2/4/39.

[98] FLEXCOM. Flexcom comparison to FAST results for 15 MW Volturn-US FOWT, 2022. URL https://flexcom.fea.solutions/l04---umaine-volturnus-s-iea15.html.

[99] Orcina. Orcaflex - dynamic analysis software for offshore marine systems, 2024. URL https://www.orcina.com/orcaflex/. Accessed: 2024-08-10.

[100] A. Robertson, J. Jonkman, F. Vorpahl, W. Popko, J. Qvist, L. Frøyd, X. Chen, J. Azcona, E. Uzunoglu, C. Guedes Soares, C. Luan, H. Yutong, F. Pengcheng, A. Yde, T. Larsen, J. Nichols, R. Buils, L. Lei, T. Nygard, and M. Guerinel. Offshore code comparison collaboration continuation within iea wind task 30: Phase ii results regarding a floating semisubmersible wind system. Jun 2014. . URL https://www.nrel.gov/docs/fy14osti/61154.pdf.

[101] R. Bergua, W. Wiley, A. Robertson, J. Jonkman, C. Brun, J.-P. Pineau, Q. Qian, W. Maoshi, A. Beardsell, J. Cutler, F. Pierella, C. A. Hansen, W. Shi, J. Fu, L. Hu, P. Vlachogiannis, C. Peyrard, C. S. Wright, D. Friel, Ø. W. Hanssen-Bauer, C. R. dos Santos, E. Frickel, H. Islam, A. Koop, Z. Hu, J. Yang, T. Quideau, V. Harnois, K. Shaler, S. Netzband, D. Alarcón, P. Trubat, A. Connolly, S. B. Leen, and O. Conway. Oc6 project phase iv: validation of numerical models for novel floating offshore wind support structures. *Wind Energy Science*, 9:1025–1051, Feb 2024. . URL https://doi.org/10.5194/wes-9-1025-2024.

[102] A. Pillai, P. Thies, and L. Johanning. Mooring system design optimization using a surrogate assisted multi-objective genetic algorithm. *Engineering Optimization*, 51(8): 1370–1392, 2019. .

[103] M. Cavazzuti. *Deterministic Optimization*, pages 77–102. Springer Berlin Heidelberg, Berlin, Heidelberg, 2013. ISBN 978-3-642-31187-1. . URL https://doi.org/10.1007/978-3-642-31187-1_4.

[104] M. Hall, B. Buckham, and C. Crawford. Evolving offshore wind: A genetic algorithm-based support structure optimization framework for floating wind turbines. In *2013 MTS/IEEE OCEANS - Bergen*, pages 1–10, 2013. .

[105] W. West, A. Goupee, S. Hallowell, and A. Viselli. Development of a multi-objective optimization tool for screening designs of taut synthetic mooring systems to minimize mooring component cost and footprint. *Modelling*, 2(4):728–752, 2021. ISSN 2673-3951. . URL https://www.mdpi.com/2673-3951/2/4/39.

[106] Charles R. Harris, K. Jarrod Millman, Stéfan J. van der Walt, Ralf Gommers, Pauli Virtanen, David Cournapeau, Eric Wieser, Julian Taylor, Sebastian Berg, Nathaniel J. Smith, Robert Kern, Matti Picus, Stephan Hoyer, Marten H. van Kerkwijk, Matthew Brett, Allan Haldane, Jaime Fernández del Río, Mark Wiebe, Pearu Peterson, Pierre Gérard-Marchant, Kevin Sheppard, Tyler Reddy, Warren Weckesser, Hameer Abbasi, Christoph Gohlke, and Travis E. Oliphant. Array programming with NumPy. *Nature*, 585 (7825):357–362, September 2020. . URL https://doi.org/10.1038/s41586-020-2649-2.

[107] Pauli Virtanen, Ralf Gommers, Travis E. Oliphant, Matt Haberland, Tyler Reddy, David Cournapeau, Evgeni Burovski, Pearu Peterson, Warren Weckesser, Jonathan Bright, et al. SciPy 1.0: Fundamental algorithms for scientific computing in python. *Nature Methods*, 17 (3):261–272, 2020.

[108] J. D. Hunter. Matplotlib: A 2d graphics environment. *Computing in Science & Engineering*, 9(3):90–95, 2007. .

[109] A. Robertson, S. Gueydon, E. Bachynski-Polić, L. Wang, J. Jonkman, D. Alarcon Fernandez, E. Amet, A. Beardsell, P. Bonnet, B. Boudet, C. Brun, Z. Chen, M. Féron, D. Forbush, C. Galinos, J. Galvan, P. Gilbert, J. Gómez, V. Harnois, and S. Wohlfahrt-Laymann. OC6 phase i: Investigating the underprediction of low-frequency hydrodynamic loads and responses of a floating wind turbine. *Journal of Physics: Conference Series*, 1618:032033, Sep 2020. .

[110] E. Gaertner, J. Rinker, L. Sethuraman, F. Zahle, B. Anderson, G.E. Barter, N.J. Abbas, F. Meng, P. Bortolotti, W. Skrzypinski, G.N. Scott, R. Feil, H. Bredmose, M. Shields, K. Dykes, C. Allen, and A. Viselli. IEA wind TCP task 37: Definition of the IEA 15-megawatt offshore reference wind turbine. Mar 2020. . URL https://www.osti.gov/biblio/1603478.

[111] C. Allen, A. Viselli, H. Dagher, A. Goupee, E. Gaertner, N. Abbas, M. Hall, and G. Barter. Definition of the UMaine VolturnUS-S reference platform developed for the IEA wind 15-megawatt offshore reference wind turbine. Jul 2020. . URL https://www.osti.gov/biblio/1660012.

[112] Antonio Gulli and Sujit Pal. *Deep learning with Keras*. Packt Publishing Ltd, 2017.

[113] TensorFlow: Large-scale machine learning on heterogeneous systems, 2015. URL https://www.tensorflow.org/. Software available from tensorflow.org.

[114] J. Blank and K. Deb. pymoo: Multi-objective optimization in python. *IEEE Access*, 8: 89497–89509, 2020. .

[115] B. Oppenheim and P. Wilson. Static 2-d solution of a mooring line of arbitrary composition in the vertical and horizontal operating modes. *International Shipbuilding Progress*, 29:142–153, 1982.

[116] J. Jonkman. Dynamics modeling and loads analysis of an offshore floating wind turbine. Technical report, National Renewable Energy Lab. (NREL), Golden, CO (United States), 2007. URL https://www.nrel.gov/docs/fy08osti/41958.pdf.

[117] C. T. Kelley. Solving nonlinear equations with newton's method. In *Society for Industrial and Applied Mathematics*, pages 57–83, 2003. .

[118] W. Ramberg and W. Osgood. Description of stress-strain curves by three parameters. Technical Report 902, National Advisory Committee for Aeronautics, 1943.

[119] Oscar Festa. Quasi-static lrd mooring model, Apr 2023. URL https://doi.org/10.5281/zenodo.7794703.

[120] S. Brevik and B. Kovesdi. Modifications to dnv mooring code (posmoor) and their consequences. In *Proceedings of the 17th International Conference on Offshore Mechanics and Arctic Engineering*, volume 1, pages 169–177. American Society of Mechanical Engineers, 1998.

[121] F. Khalid, L. Johanning, P. Thies, and D. Newsam. *Assessment of potential sites for a non-linear mooring system in floating offshore wind applications*, pages 650–656. Sep 2020. ISBN 9781003134572. .

[122] P. McEvoy, S. Kim, and M. Haynes. Fibre spring mooring solution for mooring floating offshore wind turbines in shallow water. International Conference on Offshore Mechanics and Arctic Engineering, June 2021. . URL https://doi.org/10.1115/OMAE2021-62892. V009T09A029.

[123] A.C. Pillai, T.J. Gordelier, P.R. Thies, D. Cuthill, and L. Johanning. Anchor loads for shallow water mooring of a 15 mw floating wind turbine—part ii: Synthetic and novel mooring systems. *Ocean Engineering*, 266:112619, 2022. ISSN 0029-8018. . URL https://www.sciencedirect.com/science/article/pii/S0029801822019023.

[124] M. Bach-Gansmo, S. Garvik, J. Thomsen, and M. Andersen. Parametric study of a taut compliant mooring system for a fowt compared to a catenary mooring. *Journal of Marine Science and Engineering*, 8, Jun 2020. .

[125] E. Fontaine, A. Kilner, C. Carra, D. Washington, K.T. Ma, A. Phadke, D. Laskowski, and G. Kusinski. Industry survey of past failures, pre-emptive replacements and reported degradations for mooring systems of floating production units. OTC Offshore Technology Conference, May 2014. . URL https://doi.org/10.4043/25273-MS.

[126] ASTM International. Standard practice for cycle counting in fatigue analysis. *ASTM E1049-85*, 2011.

[127] Y. Tian, Y. Zhong, H. Liu, and et al. Effects of turbulent wind and irregular waves on the dynamic characteristics of a floating offshore wind turbine platform. *J Mech Sci Technol*, 37 (8):2921–2931, 2023. . URL https://doi.org/10.1007/s12206-023-0518-2.

[128] O. Festa, S. Gourvenec, and A. Sobey. Comparative analysis of load reduction device stiffness curves for floating offshore wind moorings. *Ocean Engineering*, 250, Mar 2024.

[129] Zachary Lipton. A critical review of recurrent neural networks for sequence learning. May 2015.

[130] Junyoung Chung, Çaglar Gülçehre, KyungHyun Cho, and Yoshua Bengio. Empirical evaluation of gated recurrent neural networks on sequence modeling. *CoRR*, abs/1412.3555, 2014. URL http://arxiv.org/abs/1412.3555.

[131] K. Deb, A. Pratap, S. Agarwal, and T. Meyarivan. A fast and elitist multiobjective genetic algorithm: Nsga-ii. *IEEE Transactions on Evolutionary Computation*, 6(2):182–197, 2002. .

[132] M. Chen, J. Jiang, W. Zhang, C.B. Li, H. Zhou, Y. Jiang, and X. Sun. Study on mooring design of 15 mw floating wind turbines in south china sea. *Journal of Marine Science and Engineering*, 12(1), 2024. . URL https://www.mdpi.com/2077-1312/12/1/33.